

TECHNICAL REPORT

Dipole Models for UXO Discrimination at Live Sites -
Feature Extraction and Classification of EMI Data,
Former Spencer Artillery Range, TN

ESTCP Project MR-201159

JULY 2014

Leonard Pasion
Black Tusk Geophysics Inc.

Distribution Statement A

This document has been cleared for public release



Executive Summary

The demonstration described in this report was conducted at the Former Spencer Artillery Range, Tennessee, under project ESTCP MR-201159 “Dipole Models for UXO Discrimination at Live Sites.” The demonstration was performed under the umbrella of the ESTCP Live-Site Classification Study Program. The objective of the MR-201159 project is to demonstrate the application of feature extraction and statistical classification to the problem of UXO discrimination. At the Spencer Range site, the objective was to discriminate targets of interest (TOI) (including 37 mm, 60 mm, 75 mm, 105mm, 155mm targets and small and medium industry standard objects (ISOs)) from non-hazardous shrapnel, range and cultural debris. In this report, we describe the performance of classification techniques that utilized (1) full coverage, dynamically acquired survey data collected with both the TEMTADS 2x2 and the MetalMapper advanced electromagnetic induction (EMI) sensors, and (2) static, cued interrogation style data acquired with MetalMapper, TEMTADS2x2, and TEMTADS.

The classification techniques applied to the Spencer Range data use dipole model-based features extracted from multi-static, multi-channel EMI data. Single source and multi-source dipole inversions were used to estimate target location, orientation, and principal polarizabilities. From the extracted feature vectors, prioritized dig-lists were created for: (i) the MetalMapper deployed in a dynamic, full coverage mode; (ii) the MetalMapper deployed in a static, cued mode (for 2 unique datasets over identical targets collected by Naeva Geophysics Inc. and URS Corporation); (iii) the TEMTADS 2x2 deployed in a dynamic, full coverage mode; (iv) TEMTADS 2x2 deployed in a static, cued mode; and (v) TEMTADS 5x5 deployed in a static, cued mode.

Anomalies were prioritized based on a match of estimated principal polarizabilities to a polarizability library of known targets of interest, polarizability magnitude, and the rate of decay of polarizabilities. For each dataset, a reference library of polarizabilities was constructed from test pit measurements, site specific training data and polarizabilities derived from data acquired at previous ESTCP demonstration sites. Since dynamic data have higher noise levels than cued data, a more conservative classification algorithm - the Combined Classifier Ranking (CCR) algorithm - was used. The MetalMapper (Naeva) cued data were processed with an automated classification approach that combines multiple ranking rules (e.g. size, decay, etc.) and library matching. Classification parameters for this approach were based on the analysis of ESTCP live site data collected prior to the Spencer Range demonstration, with the only input by the analyst being the reference library of ordnance polarizabilities. All model fits and classification analysis were performed using a classification software suite (UXOLab) that was jointly developed by UBC-GIF and Black Tusk Geophysics.

In order to preserve the integrity of the blind-test, multiple analysts processed the different data sets, with no analyst processing more than one dataset from each of the survey areas (i.e. the Open area, Treed area, or Dynamic area). In this way, ground truth obtained as part of processing data with a particular method would not be shared with a different classification approach. For each dig-list, an objective classification method was applied to the features to construct the dig-list. Analysts were instructed to avoid "expert input" when constructing the dig-list. The dig order was determined automatically, and analysts did not manually change the position of any anomaly within a list based on visual inspection of the polarizabilities (i.e. manual labeling of anomalies as TOI or non-TOI).

Performance metrics defined by the ESTCP program office were calculated for each data set. Application of dipole based classification was successful for all data sets, with 100% of TOI being identified and marked for excavation in each case. The reduction of clutter digs while retaining all TOI, was greater than 80% in all cases. Not surprisingly, the data sets processed with the more conservative CCR algorithm had a higher percentage of false alarms than the data sets processed with a more aggressive approach. The number of "can't analyze" anomalies met the success criteria for all data sets except the MetalMapper (URS) dynamic data acquired in the Dynamic area. For the dynamically acquired data, reliable target parameters were estimated for only 92.1% due to the lack of data coverage at the edges of the survey area. The accuracy with which the data inversion was able to estimate location of each target of interest was not calculated for the cued TEMTADS systems, due to the absence of IMU information. For the cued data sets with IMU information and the dynamically acquired data, the target location estimate error had a standard deviation of less than 10 cm. Data acquired in the Open area and Dynamic area had depth estimate errors with a standard deviation of less than 10 cm. The data acquired in the Treed area by the TEMTADS 2x2 had a depth estimate error standard deviation of 13 cm, which did not meet the success criteria of having a depth estimate error with a standard deviation of less than 10 cm. The survey conditions in the Treed area may have resulted in variation of the ground clearance height of the instrument, whereas we assumed a fixed ground clearance height for all anomalies. It is possible that having a more accurate measure of the ground clearance height for each anomaly would reduce the amount of error in the depth estimates.

This project included a technology transfer and training component. A member of Shaw Environmental's production team attended a one week training session in Vancouver, B.C., Canada with BTG algorithm and software developers. The training session included an overview of UXO inversion and classification theory and software routines. The Shaw geophysicist was responsible for executing all parts of the classification workflow: from data and inversion QC, training data selection, to dig list creation and submittal. The dig list submitted by the Shaw geophysicist successfully identified all TOI and greatly reduced the number of non-TOI digs. A report summarizing the training and processing was prepared by the Shaw geophysicist and is included as an Appendix to this report.

Table of Contents

Executive Summary	i
Table of Contents	iii
List of Tables	vii
List of Figures	ix
Acronyms	xviii
1. INTRODUCTION	19
1.1 BACKGROUND	19
1.2 OBJECTIVE OF THE DEMONSTRATION	20
1.3 REGULATORY DRIVERS	20
2. TECHNOLOGY	21
2.1 Technology Description	21
Anomaly Selection and Feature Extraction	22
Classification of Anomalies	23
2.2 UXOLab Software	24
2.3 Previous Testing of the Technology	24
2.4 Advantages and Limitations of the Technology	27
3. PERFORMANCE OBJECTIVES	28
3.2 OBJECTIVE: MAXIMIZE CORRECT CLASSIFICATION OF TOI	29
3.2.1 Metric	29
3.2.2 Data Requirements	29
3.2.3 Success Criteria	29
3.3 OBJECTIVE: MAXIMIZE CORRECT CLASSIFICATION OF NON-TOI	29
3.3.1 Metric	29
3.3.2 Data Requirements	29

3.3.3 Success Criteria.....	29
3.4 OBJECTIVE: SPECIFICATION OF NO-DIG THRESHOLD	29
3.4.1 Metric.....	29
3.4.2 Data Requirements.....	29
3.4.3 Success Criteria.....	30
3.5 OBJECTIVE: MINIMIZE NUMBER OF ANOMALIES THAT CANNOT BE	30
3.5.1 Metric.....	30
3.5.2 Data Requirements.....	30
3.5.3 Success Criteria.....	30
3.6 OBJECTIVE: CORRECT ESTIMATION OF TARGET PARAMETERS.....	30
3.6.1 Metric.....	30
3.6.2 Data Requirements.....	30
3.6.3 Success Criteria.....	30
4. SITE DESCRIPTION	33
4.1 SITE SELECTION	33
4.2 SITE HISTORY.....	33
4.3 SITE GEOLOGY.....	33
4.4 MUNITIONS CONTAMINATION	33
5. TEST DESIGN	34
6. DATA ANALYSIS AND RESULTS.....	35
6.1 Processing Open Area Datasets	37
URS Cued MetalMapper Results.....	37
NAEVA MetalMapper Results.....	40
TEMTADS 5x5 Results.....	42
6.2 Processing Treed Area Datasets.....	43

TEMTADS 2x2 Cued Data Results	43
6.3 Processing data collected in the Dynamic Area.....	44
URS Cued MetalMapper Results.....	44
URS Dynamic MetalMapper Results.....	45
Cued TEMTADS 2x2 Results	46
Dynamic TEMTADS 2x2 Results	47
6.4 Technology Training and Transfer	48
7. MANAGEMENT AND STAFFING.....	50
REFERENCES	51
APPENDICES	1
Appendix A: Cued MetalMapper Feature Extraction and Classification	1
A.1 MetalMapper-URS Cued Feature Extraction and Classification.....	1
A.2 MetalMapper cued analysis (URS, Dynamic Area).....	19
A.3 NAEVA MetalMapper Cued Feature Extraction and Discrimination	22
Appendix B: Dynamic MetalMapper Feature Extraction and Classification	35
B.1 Analysis of IVS data	35
B.2 Analysis of Field data.....	37
Appendix C: Processing and Classification Analysis of Cued TEMTADS Data.....	45
C.1. TEMTADS 2x2 Classification at the Wooded Area.....	45
C.2. TEMTADS 2x2 Classification at the Dynamic Area.....	51
C.3. TEMTADS 5x5 Classification at the Open Area.....	56
Appendix D: PROCESSING AND CLASSIFICATION ANALYSIS OF DYNAMIC TEMTADS 2x2 DATA.....	64
D.1 Feature extraction.....	64
D.2 Classification.....	66

Appendix E. Polarizability match to Targets of Interest.....	72
Appendix F: Definition of "Skew-ness"	103
Appendix G: Location and depth estimate error distributions.....	105
Appendix H: Summary of Scoring from the Institute of Defense Analysis	111
Appendix I: Technology Transfer.....	121
Appendix J: Points of Contact	125

List of Tables

Table 1: A summary of sites at which classification has been implemented by BTG and UBC-GIF personnel as part of the ESTCP munitions program.	24
Table 2: Examples of inversion and classification testing completed by UBC-GIF and BTG as part of the ESTCP program, prior to the Spencer Range demonstration.....	25
Table 3: Description of performance objectives for the Spencer Range Demonstration	28
Table 4: Summary of performance objectives for the Open and Treed areas of the Spencer Range demonstration.	31
Table 5: Summary of performance objectives for the Dynamic area of the Spencer Range demonstration.....	32
Table 6: Classification Results from Open and Tree areas of Spencer Range.	36
Table 7: Classification Results from Dynamic area of Spencer Range.	37
Table 8. List of ordnance items in the reference library used in creating the final dig list.	12
Table 9: Summary of results from multi-object scenarios.....	15
Table 10: List of ordnance items in the reference library used in creating the final dig list.	29
Table 11: Summary of results from two-object inversion scenarios.	32
Table 12: Ground truth request for the dynamically acquired MetalMapper data	41
Table 13: TEMTADS 2x2 Evaluation at the wooded area.	47
Table 14: Summary of TEMTADS 2x2 cued data classification in the Treed area	49
Table 15: TEMTADS 2x2 Evaluation at the dynamic area.....	52
Table 16: Summary of TEMTADS 2x2 classification at the dynamic area	54
Table 17: TEMTADS 5x5 classification in the Open area.....	56
Table 18: Summary of TEMTADS 5x5 classification at the open area	61
Table 19: MetalMapper URS Cued data collected in the Open area.	77
Table 20: MetalMapper Naeva Cued data collected in the Open area.	83
Table 21: TEMTADS 5x5 cued data from the Open area.	89

Table 22: TEMTADS 2x2 cued data from the Treed area.....	94
Table 23: MetalMapper dynamic data acquired in the Dynamic area.	96
Table 24: MetalMapper URS cued data acquired in the Dynamic area.	98
Table 25: TEMTADS 2x2 dynamic data acquired in the Dynamic area.....	100
Table 26: TEMTADS 2x2 Cued data acquired in the Dynamic area	102

List of Figures

Figure 1: Overview of workflow applied to each dataset from Spencer Range.	36
Figure 2: Polarizabilities for a cluster of self-similar polarizabilities identified with <i>TrainZilla</i> . Colored lines are predicted polarizabilities. Broken grey lines are best fitting reference polarizabilities. Training data were requested for Anomalies 897 and 1097 (stars); ground truth (photos) revealed that both of these anomalies are new TOI (relative to the starting ordnance reference library. Anomaly 897 is 60mm mortar; Anomaly 1097 is a medium ISO. These items were added to the reference library.....	38
Figure 3: Decay versus size feature space plot showing passed models (blue dots) and the location of training data requests (red dots). Stars are library reference items.....	39
Figure 4: Final ROC curve for Spencer cued MetalMapper (URS) for the open area.	39
Figure 5: Polarizabilities for a cluster identified via self-similar poarizabilities. Colored lines are predicted polarizabilities. Broken grey lines are best fitting reference polarizabilities. Training data were requested for Anomalies 1220 and 241; ground truth (photos) revealed that both of these anomalies were 60mm mortars, a new TOI. These items were added to the reference library.....	40
Figure 6: Decay versus size feature space plot showing passed models (blue dots) and the location of training data requests (red dots). Stars are library reference items.....	41
Figure 7: Final ROC curve for Spencer cued MetalMapper (NAEVA) for the open area.	41
Figure 8: ROC curve for the TEMTADS 5x5 data acquired in the Open area.....	42
Figure 9: ROC curve for the TEMTADS 2x2 Cued data analysis in the treed area.....	43
Figure 10: Final ROC curve for Spencer cued MetalMapper (URS) for the dynamic area.	44
Figure 11: Final ROC curve for Spencer Range MetalMapper (URS) data acquired in a dynamic mode.....	46
Figure 12: Final ROC curve for Spencer Range TEMTADS 2x2 cued data acquired in the Dynamic area	47
Figure 13: Decay versus size feature space plot showing passed models (blue dots) and the location of training data requests (red dots). Stars are library reference items.....	48
Figure 14: Final ROC curve for the dynamic TEMTADS 2x2 data from the dynamic survey area at Spencer Range.....	49

Figure 15: ROC curve for the library based classification of MetalMapper (URS) data carried out by a Shaw Environmental geophysicist..... 49

Figure 16: Project management hierarchy showing BTG personnel in grey and UBC-GIF personnel in blue. The hierarchy is split between the development and execution components.. 50

Figure 17: Example of an unrealistic 2OI model (anomaly 1250; frag). The first model of the 2OI (model 2) provides the best fit (i.e., minimum misfit) to the reference polarizabilities (misfit = 0.826), but the predicted depth of 1.2m and location at the edge of the instrument (i.e., at the vertical and horizontal inversion boundaries), and high amplitude and jittery appearance of the polarizabilities are classic signs that this model is an artifact of the multi-object inversion process. Accordingly, this model was failed during QC. Polarizabilities for SOI and 2OI are shown at left. Modeled target locations (X-Y and Z) are shown at the top right (gridded EM61 data is displayed behind the X-Y plot). Gridded observed, predicted and residual data for SOI and 2OI are shown below location maps. Decay versus size feature plot is shown in bottom right. Dots are test data; stars are reference items. Numbered circles are models for this anomaly. 2

Figure 18: Distribution of passed models in decay(t1,t29) versus size(t1) feature space, where size(t1) is the total polarizability measured at the first time channel (t1=0.106ms), and decay(t1,t29) is size(t1)/size(t29) where t29=2.006ms. Some outliers are not shown. Labeled stars represent ordnance library reference items..... 3

Figure 19: Example of use of the training data selection tool (*TrainZilla*). A polygon (solid black line) is drawn in feature space. Clusters of items with self-similar polarizabilities are automatically found based on the specified cluster search parameters. In this case a cluster comprising 7 features is visible (solid feature symbols encompassed by broken line). Polarizabilities for this cluster are shown in Figure 20..... 4

Figure 20: Polarizabilities for the cluster shown in Figure 19. Colored lines are predicted polarizabilities. Broken grey lines are best fitting reference polarizabilities. Training data were requested for Anomalies 897 and 1097 (stars); ground truth (photos) revealed that both of these anomalies are new TOI (relative to our starting ordnance reference library which comprised the four items from the test pit). Anomaly 897 is 60mm mortar; Anomaly 1097 is a medium ISO. These items were added to the reference library. 5

Figure 21: Decay versus size feature space plot showing passed models (blue dots) and the location of training data requests (red dots). Stars are library reference items..... 6

Figure 22: Screen shot of the *DigZilla* graphical user interface. Features in the decay versus size feature plot are color coded according to dig list order. 7

Figure 23: Ordnance library for the MetalMapper URS cued data. Polarizabilities 1 to 13 were used for the Open area. Polarizabilities 14 and 15 were added processing cued data acquired in the Dynamic area. 8

Figure 24: QC Tool display for Anomaly 1063. Large misfits between observed (blue lines in plots at top left) and predicted (green lines) data for most receiver-transmitter combinations for all inversions resulted in this anomaly being classified as cannot analyze..... 10

Figure 25: Partial ROC curve for the stage 1, version 1 dig list. The point at which the dig list switches between order based on matching all three polarizabilities to order based on only the primary polarizability is indicated. 11

Figure 26: Partial ROC curve for the final (stage 3, version) 1 dig list..... 13

Figure 27: Final ROC curve for Spencer cued MetalMapper (URS) for the open area. 14

Figure 28: Comparison of SOI and 2OI inversion results for three two-object scenarios (targets 194, 700 and 873). In all three cases a piece of frag roughly equal in size to a small ISO was seeded with a small ISO. See Table 9 for details..... 16

Figure 29: Polarizabilities for 36 small ISOs in the Spencer Open and Dynamic areas. Colored lines are predicted polarizabilities. Broken grey lines are small ISO reference polarizabilities taken from IVS measurements. Anomaly ID is the number after the “T” in each label. Polarizabilities are sorted by misfit (from best to worst) with respect to the small ISO reference model..... 17

Figure 30: Compilations of polarizabilities for small ISOs from recent Live Site demonstrations. The two Beale and Spencer datasets each comprise the same set of anomalies but the data were collected by two different companies. The Spencer data include small ISOs from both the Open and Dynamic Areas. Misfit values are the mean misfits with respect to the reference polarizabilities calculated over all time channels using all three polarizabilities (L1, L2 and L3). 18

Figure 31: Partial ROC curve for the stage 1, version 1 dig list. The point at which the dig list switches between order based on matching all three polarizabilities to order based on only the primary polarizability is indicated. 21

Figure 32: Final ROC curve for Spencer cued MetalMapper (URS) for the dynamic area. 22

Figure 33: False positives where frag similar in size to a TOI in the reference library results in polarizabilities that are an excellent match to reference items. Reference polarizabilities are indicated by dashed grey line..... 23

Figure 34: Distribution of passed models in decay(t1,t29) versus size(t1) feature space, where size(t1) is the total polarizability measured at the first time channel (t1=0.106ms), and

decay(t_1, t_{29}) is $\text{size}(t_1)/\text{size}(t_{29})$ where $t_{29}=2.006\text{ms}$. Labeled stars represent ordnance library reference items. 24

Figure 35: Example of use of the training data selection tool (*TrainZilla*). A polygon (solid black line) is drawn in feature space. Clusters of items with self-similar polarizabilities are automatically found based on the specified cluster search parameters. In this case a cluster comprising 7 features is visible (solid feature symbols encompassed by broken line). Polarizabilities for this cluster are shown in Figure 4..... 24

Figure 36: Polarizabilities for the cluster shown in Figure 3. Colored lines are predicted polarizabilities. Broken grey lines are best fitting reference polarizabilities. Training data were requested for Anomalies 1220 and 241; ground truth (photos) revealed that both of these anomalies were 60mm mortars, a new TOI (relative to our starting ordnance reference library which comprised the four items from the test pit). These items were added to the reference library..... 25

Figure 37: Decay versus size feature space plot showing passed models (blue dots) and the location of training data requests (red dots). Stars are library reference items..... 26

Figure 38: QC Tool display for Anomaly 571. Large misfits between observed (blue lines in plots at top left) and predicted (green lines) data for most receiver-transmitter combinations for all inversions resulted in this anomaly being classified as cannot analyze..... 27

Figure 39: Partial ROC curve for the stage 1, version 1 dig list..... 29

Figure 40: Ordnance library used when processing the MetalMapper Naeva cued data..... 30

Figure 41: Final ROC curve for Spencer cued MetalMapper (NAEVA) for the open area. 31

Figure 42: Comparison of SOI and 2OI inversion results for three two-object scenarios (targets 194, 700 and 873). In all three cases a piece of frag roughly equal in size to a small ISO was seeded with a small ISO. See Table 9 for details..... 33

Figure 43: Recovered polarizabilities using SOI, 2OI and 3OI for target 308. Neither the SOI or either model of the 2OI produced polarizabilities that matched the 37mm projectile reference (shown as dashed grey). Ground truth revealed the target to be a 37mm projectile. The 3OI produces polarizabilities that match the 37mm reference in the 3OI-1 model. 34

Figure 44: Analysis of Spencer Range dynamic MetalMapper IVS data. The top row show polarizabilities recovered from static, cued data. Multiple soundings acquired over each target, and the polarizabilities estimated from each sounding is plotted for each target. The bottom row plot the recovered polarizabilities when a single pass of dynamic data is collected over the targets. In contrast to operation in the cued mode, only the vertical transmitter is in operation when in dynamic mode. The primary polarizability of the target is poorly constrained for the

IVS data, because each target is oriented with its long axis in an orientation that is poorly illuminated by the dynamic MetalMapper’s transmit field..... 36

Figure 45: A covariance analysis of the L11 component of the polarizability matrix reveals that when passing directly over a target (i.e. x offset = 0), the primary polarizability will be poorly constrained by the data. Interestingly, on a few cms of across track offset from the target will allow for significant improvement in resolving the polarizabilities. 36

Figure 46: Anomaly SR-1520. For this target, the data had a relatively large data misfit, but the anomaly was passed because we considered the recovered polarizabilities to be smaller than the smallest target of interest on the site..... 38

Figure 47: Anomalies categorized as “can’t extract reliable parameters” due to poor data coverage. 39

Figure 48: Example of an automatically identified cluster. In this case, the total polarizability was used to form a cluster. In this cluster, all the targets had similar total polarizabilities. From this cluster, training data was requested for SR-1502 and SR-1661. SR-1661 was a 60 mm mortar. Interestingly SR-1502 turned out to be a multi-target scenario that included an ISO. ... 40

Figure 49: Ground truth photos from the training data request. The target information is summarized in Table 12..... 42

Figure 50: Ordnance library used during classification with the dynamic MetalMapper (URS) data..... 43

Figure 51: Dynamic MetalMapper scoring results from Institute of Defense analysis. 44

Figure 52: Polarizabilities of the last 11 anomalies in the HTOI set. Anomaly SR-2091 (related to the reference item, "rod-tbi") was requested as a training anomaly. 46

Figure 53: Examples of polarizabilities of 12 items from the training set. "Tra" indicates that the time was chose for training data, with the text after "Tra" indicating the ground truth label if the item was categorized as TOI..... 48

Figure 54: ROC curve for the stage 2 (and final) diglist submitted of the TEMTADS 2x2 cued data in the Treed area..... 49

Figure 55: Polarizabilities of 21 TOI anomalies dug in the LTOI and LLTOI sets in stage 1. 50

Figure 56: Polarizabilities of 16 anomalies dug in the HTOI set in stage 1. SR-1525 is a dug non-TOI..... 53

Figure 57: Polarizabilities of 8 anomalies in the training set for the dynamic area..... 54

Figure 58: Polarizabilities of 7 TOI anomalies in the LTOI set for the dynamic area. 55

Figure 59: ROC curve at Stage 1 of TEMTADS 2x2 in the dynamic area.	55
Figure 60: Polarizabilities of 16 training anomalies related to small ISO and rod-tbi (SR-234) in the HTOI set.....	57
Figure 61: QC seeds SR-572 (left) and SR-1160 (right) that were missed in the initial ranked anomaly list.....	58
Figure 62: Recovered polarizabilities (red and blue curves) of the relevant training anomalies and the missed QC seed of SR-572, a 37mm projectile. The closest item to anomaly SR-572 is a small ISO (represented by the gray curves) with $\phi_m = 0.276$. In the initial classification stage, this anomaly was assigned into the Likely TOI (L-TOI) set but not marked to be dug.....	59
Figure 63: Recovered polarizabilities (red and blue curves) of the relevant Training anomalies and the missed QC seed of SR-1160, a small ISO. The closest item to anomaly SR-1160 is a suspicious rod-like object (represented by the gray curves) with $\phi_m = 0.741$. In the initial classification stage, this anomaly was assigned into the Likely Very Low TOI (LVL-TOI) set and not marked to be dug.....	60
Figure 64: Anomaly 1160, the missed QC seed.	60
Figure 65: Polarizabilities of 24 TOI anomalies dug in the LTOI set	62
Figure 66: ROC curve for the Stage 2 dig list based on TEMTADS 5x5 Open Area data	63
Figure 67: Example of dynamic TEMTADS 2x2 data fit and QC interface	65
Figure 68: Distribution of passed (blue) and failed (red) models in decay(t1,t15) versus size(t1) feature space, where size(t1) is the total polarizability measured at the first time channel (t1=0.110ms), and decay(t1,t25) is size(t1)/size(t29) where t29=2.5ms. Some outliers are not shown. Labeled stars represent ordnance library reference items. The polarizability of the smallest training item selected (square symbol) is shown.....	66
Figure 69: Polarizabilities of ground-truth items (first 22 plots) and the three “can’t extract reliable parameters” anomalies and the first 24 anomalies recommended for excavation.	67
Figure 70: Photos of ground-truth items (first 22) and the three “can’t extract reliable parameters” anomalies. Item T1676 was a QC seed that was past the stop-dig point in the first dig-list submission. A yellow label indicates that the item is a TOI.	68
Figure 71: Screen shot of the <i>DigZilla</i> graphical user interface. Features in the decay versus size feature plot are color coded according to dig list order (warmer colors indicate items that are dug first). The first item after the stop-dig point is marked as a square and its feature plot and ground-truth photo are shown.....	69

Figure 72: Polarizability library used for the TEMTADS 2x2 dynamic classification.	69
Figure 73: Size versus time-decay feature space plot with TOI items shown as blue-triangles. The one ISO seed item that occurred after the initial stop-dig point is marked with a square (on-top of the blue triangle).....	70
Figure 74: Final ROC curve for a dynamically deployed TEMTADS 2x2 data acquired in the Spencer Range Dynamic area.	71
Figure 75: MetalMapper URS Cued data collected in the Open area (1/5).....	72
Figure 76: MetalMapper URS Cued data collected in the Open area (2/5).....	73
Figure 77: MetalMapper URS Cued data collected in the Open area (3/5).....	74
Figure 78: MetalMapper URS Cued data collected in the Open area (4/5).....	75
Figure 79: MetalMapper URS Cued data collected in the Open area (5/5).....	76
Figure 80: MetalMapper Naeva Cued data collected in the Open area (1/5).	78
Figure 81: MetalMapper Naeva Cued data collected in the Open area (2/5).	79
Figure 82: MetalMapper Naeva Cued data collected in the Open area (3/5).	80
Figure 83: MetalMapper Naeva Cued data collected in the Open area (4/5).	81
Figure 84: MetalMapper Naeva Cued data collected in the Open area (5/5).	82
Figure 85: TEMTADS 5x5 cued data from the Open area (1/5).	84
Figure 86: TEMTADS 5x5 cued data from the Open area (2/5).	85
Figure 87: TEMTADS 5x5 cued data from the Open area (3/5).	86
Figure 88: TEMTADS 5x5 cued data from the Open area (4/5).	87
Figure 89: TEMTADS 5x5 cued data from the Open area.....	88
Figure 90: TEMTADS 2x2 cued data from the Treed area (1/4)	90
Figure 91: TEMTADS 2x2 cued data from the Treed area (2/4)	91
Figure 92: TEMTADS 2x2 cued data from the Treed area (3/4)	92
Figure 93: TEMTADS 2x2 cued data from the Treed area (4/4)	93
Figure 94: MetalMapper dynamic data acquired in the Dynamic area.....	95

Figure 95: MetalMapper URS cued data acquired in the Dynamic area.	97
Figure 96: TEMTADS 2x2 dynamic data acquired in the Dynamic area.....	99
Figure 97: TEMTADS 2x2 cued data acquired in the Dynamic area.....	101
Figure 98: Examples of the "Skew" metric using Camp Beale data.....	104
Figure 99: Example of the "Skew" metric using Camp Beale data.	104
Figure 100: Location and depth error distributions for the MetalMapper (URS) cued data collected in the Open area.....	105
Figure 101: Location and depth error distributions for the MetalMapper (NAEVA) cued data collected in the Open area.....	106
Figure 102: Depth error distributions for the different cued TEMTADS surveys. Location error information was not calculated due to no IMU information being available.	107
Figure 103: Location and depth error distributions for the MetalMapper (URS) Dynamic data collected in the Dynamic area.....	108
Figure 104: Location and depth error distributions for the MetalMapper (URS) cued data collected in the Dynamic area.....	109
Figure 105: Location and depth error distributions for the TEMTADS 2x2 dynamic data collected in the Dynamic area.....	110
Figure 106: Scoring results for the MetalMapper URS data acquired in cued mode, in the Open area.....	111
Figure 107: Scoring results for the MetalMapper – Naeva cued data acquired in the Open area.	112
Figure 108: IDA scoring summary for TEMTADS 5x5 cued data	113
Figure 109: IDA scoring summary for TEMTADS 2x2 data collected in the Treed area.....	114
Figure 110: IDA scoring summary for TEMTADS 2x2 data collected in dynamic mode in the Dynamic area	115
Figure 111: IDA scoring summary for analysis of TEMTADS 2x2 cued data acquired in the Dynamic area	116
Figure 112: IDA scoring summary for MetalMapper (URS) data collected in dynamic mode in the Dynamic area	117

Figure 113: IDA scoring summary for MetalMapper (URS) data collected in cued mode in the Dynamic area 118

Figure 114: IDA scoring summary for the TETMADS 2x2 cued data acquired in the Treed area 119

Figure 115: IDA scoring summary for the MetalMapper (URS) cued data acquired in the Open area. This summary is based on analysis performed by Shaw geophysicists with UXOLab. ... 120

Figure 116: ROC curve for Shaw processing of MetalMapper (URS) cued data in the Open area. 123

Acronyms

2OI	Two Object Inversion
BTG	Black Tusk Geophysics
BUD	Berkeley UXO Discriminator
CCR	Combined Classifier Ranking
EM	Electromagnetic
EMI	Electromagnetic induction
ESTCP	Environmental Security Technology Certification Program
FAR	False alarm rate
GPS	Global Positioning Systems
IDA	Institute for Defense Analyses
IMU	Inertial Measurement Unit
ISO	Industry standard object
IVS	Instrument verification strip
MEC	Munitions and explosives of concern
MPV	Man Portable Vector
MRS	Munitions Response Site
NAEVA	Naeva Geophysics Inc.
PI	Principal Investigator
QC	Quality Control
ROC	Receiver operating characteristic
SERDP	Strategic Environmental Research and Development Program
SLO	San Luis Obispo
SNR	Signal to noise ratio
SOI	Single object inversion
TEM	Time-domain electromagnetic
TEMTADS	Time Domain Electromagnetic Towed Array Detection System
TOI	Target of interest
UBC-GIF	University of British Columbia – Geophysical Inversion Facility
UBC	University of British Columbia
URS	URS Corporation
USACE ERDC	United States Army Corps of Engineers- Engineering Research and Development Center
UXO	Unexploded ordnance

1. INTRODUCTION

1.1 BACKGROUND

Significant progress has been made in UXO classification technology. To date, testing of these approaches has been primarily limited to test sites with only limited application at live sites. Acceptance of classification technologies requires demonstration of system capabilities at real UXO sites under real world conditions. Any attempt to declare detected anomalies to be harmless and requiring no further investigation will require demonstration to regulators of not only individual technologies, but an entire decision making process.

To demonstrate the viability of advanced detection and discrimination technologies, ESTCP has now conducted multiple UXO classification studies. The results of the first demonstration, at the former Camp Sibert, Alabama were very encouraging. Although conditions were favorable at this site, including a single target-of-interest (4.2-in mortar) and benign topography and geology, all of the demonstrated classification approaches were able to correctly identify a sizable fraction of the anomalies as arising from non-hazardous items that could be safely left in the ground. Of particular note, the contractor EM-61-MK2 cart survey with analysis using commercially available methods correctly identified more than half the targets as non-hazardous.

To build upon the success of this first study, ESTCP expanded the program to include a second study at a site with more challenging topography and a wider mix of targets-of-interest. A range at the former Camp San Luis Obispo (SLO), California, was selected for this demonstration. We again found that, with appropriate use of classification metrics applied to production quality EM-61 data, it was possible to significantly reduce the number of clutter items excavated without missing any targets of interest (TOI). Furthermore, the next generation of EMI sensors, when deployed in a cued-interrogation mode, produced significant additional reductions in the number of clutter items excavated. These sensors could also usually distinguish between different UXO types. A third ESTCP demonstration study was conducted in 2010 at Camp Butner, North Carolina. The site had very little topographic relief but required classification between small targets of interest (37mm projectiles and M48 fuzes) and metallic debris of similar size. Targets were also distributed with a higher density than previously encountered. In 2011, an ESTCP demonstration study was conducted at Camp Beale, California. The site had very little topographic relief but required classification between small targets of interest (37mm projectiles and M48 fuzes) and metallic debris of similar size. Targets were also distributed with a higher density than previously encountered. Also in 2011, a study was conducted at Pole Mountain, Wyoming. The smallest target of interest at this site was a small ISO. Library based classification applied to features derived from cued MetalMapper data resulted in some of the best classification performances to date, with less than 5% of non-TOI requiring excavation before all TOI were recovered.

The latest ESTCP demonstration study was conducted in 2012 at the Former Spencer Artillery Range, Tennessee. The site included both an open area easily accessible by a wide range of sensors and a treed area only accessible with portable sensors. Both full coverage, dynamically acquired data and cued data were acquired. The ranges of targets of interest present included including 37 mm, 60 mm, 75 mm and small and medium ISOs in addition to two large one off items (105mm, 155mm). Multi object targets were also seeded using varying sized pieces of clutter nearby a TOI. This demonstration report describes the data processing, feature extraction and classification that were applied to the Spencer Range data sets

by Black Tusk Geophysics (BTG) and the University of British Columbia Geophysical Inversion Facility (UBC-GIF) personnel.

1.2 OBJECTIVE OF THE DEMONSTRATION

The objectives of this demonstration were to perform data modeling, classification, and classification using electromagnetic (EM) data collected by the various data collection demonstrators participating in the study. Specifically, we processed the following datasets collected at Spencer Range:

- 1) TEMTADS 5x5 cued interrogation data;
- 2) TEMTADS 2x2 dynamic data;
- 3) TEMTADS 2x2 cued interrogation data;
- 4) MetalMapper dynamic data;
- 5) MetalMapper cued interrogation data acquired by URS Corporation; and
- 6) MetalMapper cued interrogation data acquired by Naeva Geophysics Inc.;

Specific processing tasks were as follows:

- 1) *Feature Extraction*: inversion of all electromagnetic data sets with single and multi-source dipole models
- 2) *Classification*: the following ranked dig sheets for the Spencer Range Treed Area were produced :
 - a) Cued TEMTADS 2x2 library match: A dig sheet was produced based on how well the recovered polarizabilities matched the polarizabilities in a library of ordnance items expected at the site.

As well, the following ranked dig sheets were produced for the Spencer Range Open Area:

- b) Cued URS MetalMapper library match: A dig sheet was produced based on how well the recovered polarizabilities matched the polarizabilities in a library of ordnance items expected at the site;
- c) Cued NAEVA MetalMapper automated DigZilla ranking: A dig sheet was produced based on a weighted sum of fit to the library, polarizability size, polarizability decay, and a measure of how "rod-like" the target is based on secondary polarizabilities;
- d) Cued TEMTADS 5x5 library match: As in b) but for TEMTADS 5x5 data;

In addition, the following ranked dig sheets were produced for the Spencer Range Dynamic Area:

- e) Cued URS MetalMapper library match: As in b) but for the dynamic area
- f) Dynamic URS MetalMapper Combined Classifier Ranking (CCR) match: A dig sheet is submitted by combining separate ranked lists based on polarizability misfit, size, and decay;
- g) Cued TEMTADS 2x2 library match: As in e) but for the cued TEMTADS 2x2 data;
- h) Dynamic TEMTADS 2x2 Combined Classifier Ranking (CCR): As in f) but for the dynamic TEMTADS 2x2 data;

Thus we produced a total of eight ranked dig sheets using a variety of different methods and sensor types.

1.3 REGULATORY DRIVERS

Refer to the Program Office demonstration plan for a discussion of regulatory drivers.

2. TECHNOLOGY

2.1 Technology Description

Magnetic and EM methods represent the main sensor types used for detection of UXO. Over the past 15 years, significant research effort has been focused on developing methods to discriminate between hazardous UXO and non-hazardous scrap metal, shrapnel and geology (e.g. Bell et al., 2001; Pasion et al., 2007; Tantom et al., 2008; Liao and Carin, 2009). The most promising classification methods typically proceed by first recovering a set of parameters that specify a physics-based model of the object being interrogated. For example, in time-domain electromagnetic (TEM) data, the parameters comprise the object location and the polarizability tensor which is generally decomposed into orientation and principal polarizabilities. Once the parameters are recovered by inversion, a subset of the parameters is used as feature vectors to guide either a statistical or rule-based classifier.

There are three key elements of the UXO classification process:

1. *Creation of a map of the geophysical sensor data:* This includes all actions required to form an estimate of the geophysical quantity in question (i.e. amplitude of EMI response at a given time-channel) at each of the visited locations. The estimated quantity is dependent on the following:
 - a. Hardware, including the sensor type, deployment platform, position and orientation system and the data acquisition system used to record and time-stamp the different sensors;
 - b. Survey parameters such as line spacing, sampling rate, calibration procedures etc.;
 - c. Data processing such as merging of position/orientation information with sensor data, noise and background filtering applied;
 - d. The background environment including geology, vegetation, topography, cultural features, etc.; and
 - e. Depth and distribution of ordnance and clutter.
2. *Anomaly selection and feature extraction:* This includes the detection of anomalous regions and the subsequent extraction of a polarization tensor model for each anomaly. The reliability of the recovered features is dependent on the quality of the survey data. If the data acquired for creation of the data map is not of sufficient quality to extract reliable parameters, cued data acquired in a static mode is required. Cued data has higher quality data due to having reduced sensor noise by being acquired in a static mode, and by having accurate sensor location information by being acquired with transmitters and receivers in a fixed geometry.
3. *Classification of anomalies:* The final objective of the demonstration is the production of a dig sheet with a ranked list of anomalies. This will be achieved via classification algorithms which will require training data to determine the attributes of the UXO and non-UXO classes.

The focus of this demonstration is on the further testing and validation of the methodologies for 2) and 3) above that have been developed in UXOLab jointly by BTG and the University of British Columbia-Geophysical Inversion Facility (UBC-GIF). We now describe these key elements of the technology as identified above.

Anomaly Selection and Feature Extraction

At this point in the process flow, there is a map of each of the geophysical quantities measured during the survey. The next step in the process is detection of anomalous regions followed by the extraction of features for each of the detected items. For this demonstration, targets have been picked from the EM-61 cart data by the demonstrator, no additional picks were made by BTG/UBC-GIF.

In the EMI method, a time varying field illuminates a buried, conductive target. Currents induced in the target then produce a secondary field that is measured at the surface. EM data inversion involves using the secondary field generated by the target for recovery of the position, orientation, and parameters related to the target's material properties and shape. In the UXO community, the inverse problem is simplified by assuming that the secondary field can be accurately approximated as a dipole. In general, TEM sensors use a step off field to illuminate a buried target. The currents induced in the buried target decay with time, generating a decaying secondary field that is measured at the surface. The time-varying secondary magnetic field $\mathbf{B}(t)$ at a location \mathbf{r} from the dipole $\mathbf{m}(t)$ is computed as:

$$\mathbf{B}(t) = \frac{\mu_o}{4\pi r^3} \mathbf{m}(t) \cdot \left(3\hat{\mathbf{r}}\hat{\mathbf{r}} - \mathbf{I} \right) \quad (1)$$

where $\hat{\mathbf{r}} = \mathbf{r}/|\mathbf{r}|$ is the unit-vector pointing from the dipole to the observation point, \mathbf{I} is the 3 x 3 identity matrix, $\mu_o = 4 \pi \times 10^{-7}$ H/m is the permeability of free space and $r = |\mathbf{r}|$ is the distance between the center of the object and the observation point.

The dipole induced by the interaction of the primary field \mathbf{B}_o and the buried target is given by:

$$\mathbf{m}(t) = \frac{1}{\mu_o} \mathbf{M}(t) \cdot \mathbf{B}_o \quad (2)$$

The induced dipole is the projection of the primary field \mathbf{B}_o onto the target's polarizability tensor $\mathbf{M}(t)$. The polarizability tensor is assumed to be symmetric and positive definite and so can be decomposed as

$$\mathbf{M}(t) = \mathbf{A}^T \mathbf{L}(t) \mathbf{A} \quad (3)$$

with \mathbf{A} an orthogonal matrix which rotates the coordinate system from geographic coordinates to a local, body centered coordinate system. The diagonal eigenvalue matrix $\mathbf{L}(t)$ contains the principal polarizabilities $L_i(t)$ ($i = 1, 2, 3$), which are assumed to be independent of target orientation and location. Features derived from the dipole model, in particular amplitude and decay of the principal polarizabilities, have been successfully used to discriminate between targets of interest and non-hazardous metallic clutter. These parameters are useful because, to first order, a conductor can be modeled as a simple LR loop which is inductively coupled to transmitters and receivers on the surface. The current response of this loop is a decaying exponential which is fully described by an amplitude and time constant (West and Macnae, 1991). The TEM dipole model generalizes this simple circuit model to account for target size and shape. This latter property is represented by the principal polarizabilities, which decay independently in time and are approximately aligned with the semi-major and minor axes of the target.

Equal transverse (secondary and tertiary) polarizabilities indicate an axisymmetric target. Most ordnance can be treated as bodies of revolution (Shubitidze et al., 2002), and so equality of transverse polarizabilities has been proposed as a useful feature for discriminating between TOI and irregularly-shaped clutter. However, in practice it has been difficult to reliably estimate target shape using data from mono-static,

vertical-component sensors conventionally deployed for UXO detection. This is because mono-static data often cannot adequately interrogate the transverse response of buried targets.

Recent advances in TEM sensor technology for UXO detection have helped address these limitations. For example, the MetalMapper sensor is comprised of an array of 7 receivers that measure 3 orthogonal components of the secondary field generated by 3 orthogonal transmitter loops that are fired sequentially. This multi-static, and multi-transmitter configuration provides a very rich data set which is better able to constrain target depth and transverse polarizabilities than a mono-static sensor.

When solving parametric inverse problems, it is usually sufficient to minimize a data norm quantifying the misfit between observed (dobs) and predicted data

$$\phi_d = \left\| V_d^{-1/2} (d^{obs} - d^{pred}) \right\|^2 \quad (4)$$

with $d^{pred} = F(m)$ generally a nonlinear functional of the model m , and $V_d^{-1/2}$ a (usually diagonal) covariance matrix specifying estimated errors on the data. Bound constraints are also typically imposed to ensure that physically reasonable model parameters are obtained (e.g. polarizabilities should be positive). In the case of TEM data, the model is parameterized in terms of target location and orientation, as well as principal polarizabilities at each time channel. Equation 4 is minimized by first estimating the target location, followed by estimating of polarizabilities at each time channel. Decoupling the time channels in this way makes the inversion less sensitive to the specified uncertainties, but produces polarizabilities that are less smooth as a function of time.

Classification of Anomalies

At this stage in the process, we have feature vectors for each anomaly and need to decide which items should be excavated as potential UXO. For this demonstration, we employ Library based classification methods. Library based methods compare the recovered polarizabilities from a target to polarizabilities for a library of targets that may be found at the site. Anomalies are ranked according to the minimum misfit to the library items.

A key part of classification is requesting training data to identify classes of TOI and non-TOI and to determine the variability in recovered polarizabilities. Training data can be selected via visual inspection of estimated features. For example, displaying the features in a space spanned by size and decay parameters can reveal clustering of feature vectors to different target classes (e.g. Billings et al., 2010). Size and decay parameters are defined as

$$Polarizability\ amplitude = \log\left(\sum_{i=1}^M L_{total}(t_i)\right) \quad (5)$$

$$Polarizability\ decay = \frac{L_{total}(t_j)}{L_{total}(t_k)}, \quad (t_j < t_k) \quad (6)$$

Automatic identification of clusters of self-similar feature vectors can be achieved by computing a misfit matrix \mathbf{M} with elements

$$M_{jk} = \sum_{i=1}^N (L_{total}^j(t_i) - L_{total}^k(t_i))^2 \quad (7)$$

where L_{total}^j is the log-transformed total polarizability for the j^{th} feature vector. Feature vectors with mutual misfit less than a pre-defined threshold define a cluster in total polarizability space. This analysis helps to identify clusters that may not be readily evident in size-decay feature space: e.g. targets with consistent polarizabilities that may be hidden in the “cloud” of non-TOI features. Ground truth is

requested for feature vectors which lie between clusters of TOI and non-TOI in order to determine the extent of the distributions of TOI features.

2.2 UXOLab Software

The methodologies for data processing, feature extraction, and statistical classification described above have been implemented within the UXOLab software environment, which was used for this demonstration. UXOLab is a Matlab based software package developed over a six year period at the UBC-GIF, principally through funding by the United States Army Corps of Engineers-Engineering Research and Development Center (USACE ERDC) (DAAD19-00-1-0120). Over the past five seven years, BTG and UBC-GIF have considerably expanded the capabilities of the software. Key modules include *QCZilla* for data and inversion review, *TrainZilla* for identifying training data, and *DigZilla* for applying statistical and library based classification techniques.

2.3 Previous Testing of the Technology

Table 1 provides a list of sites at which classification methods and software developed at the UBC-GIF and BTG were tested and demonstrated as part of the ESTCP program. The list summarizes ESTCP project work until May 2014. The blue text indicate projects that were ongoing at the time this report was being prepared. Green 'X's indicate data sets for which industry geophysicists submitted dig lists following a visit to BTG for training on classification theory and techniques. Table 2 provides additional detail for a selection of classification studies completed prior to the Spencer Range.

Table 1: A summary of sites at which classification has been implemented by BTG and UBC-GIF personnel as part of the ESTCP munitions program.

SITE	PROJECT	1st Generation			Vehicle Mounted			Man Portable			Dynamic		
		MAG	Geonics EM61	Geonics EM63	BUD	MetalMapper	TEMTADS 5x5	BUD-HH	MPV	TEMTADS 2x2	MetalMapper	MPV	TEMTADS 2x2
Former Lowry Bombing and Gunnery Range, CO	MM-0504	X	X	X									
Former Camp Sibert, AL	MM-0504	X	X	X	X								
Former Fort McClellan, AL	MM-0504			X									
San Luis Obispo, CA	MM-0504	X	X		X	X	X						
Former Camp Butner, NC	MR-1004		X			X	X						
Camp Beale, CA	MR-1004		X			X		X	X	X			
Pole Mountain, WY	MR-1159		X			X							
Spencer Range, TN	MR-1158,59					X	X		X	X	X	X	X
Camp Edwards, MMR, MA	MR-1226					X				X			
Camp George West, CO	MR-1228								X			X	
Camp Ellis, IL	MR-1226					X				X			
Ft. Rucker, AL	MR-1226					X							
New Boston, NH	MR-1158,59								X	X		X	
Southwest Proving Grounds, AL	MR-1226					X				X	X		X
Waikaloa, HI	MR-1226					X						X	

Table 2: Examples of inversion and classification testing completed by UBC-GIF and BTG as part of the ESTCP program, prior to the Spencer Range demonstration

Site	Camp Sibert
Inversion/ Classification Test	<p>Geonics EM-61 cart, MTADS EM-61 array, MTADS mag array, and EM-63 single and cooperative inversions. EM-63 cued interrogations were positioned by a Leica TPS 1206 RTS with orientation information provided by a Crossbow AHRS 400 IMU.</p> <p>The objective of the surveys was the classification of a large target (4.2-in mortars). The site was unusual in that the primary munition known to have been used was the 4.2-in mortar, thus providing a site where the classification is a case of identifying a single large target amongst smaller pieces of mortar debris and clutter.</p>
Description	<p>For the EM-61, 3-dipole instantaneous amplitude models were fit to the available 3 time-channels, while for the EM-63, 3-dipole Pasion-Oldenburg models were recovered from the 26 time-channel data. MTADS and EM-63 data were also cooperatively inverted. Parameters of the dipole model were used to guide a statistical classification</p>
Results	<p>The results for all sensor combinations were excellent, with just one false negative for the EM-63 when inverted without cooperative constraints. When inverted cooperatively, the EM-63 cued interrogation was the most effective discriminator. All 33 UXO were recovered with 25 false alarms (16 of these were in the "can't analyze" category). Not counting the "can't analyze" category, the first 33 recommended excavations were all UXO.</p> <p>The MTADS and MTADS cooperatively inverted were also very effective at discrimination, with all UXO recovered very early in the dig list. The MTADS data set suffered from a high number of false alarms due to anomalies with a geological origin. In addition, the operating point was very conservative and many non-UXO were excavated after recovery of the last UXO in the dig list.</p> <p>The results from the EM-61 cart were also very good, although 24 false-positives were required to excavate all 105 UXO. The lower data quality of the EM-61 cart resulted in a larger number of "can't analyze" anomalies over metallic sources than the MTADS</p>
Site	San Luis Obispo
Inversion/ Classification Test	<p>Detection mode surveys were: MTADS magnetometer and EM61 arrays, Geonics EM61 cart and Man-Portable Simultaneous EMI and Magnetometer System (MSEMS) cart. Cued interrogation mode TEMTADS, MetalMapper and Berkeley UXO Discriminator (BUD) surveys were also conducted.</p> <p>At this site the objective was to identify TOI from a number of different target classes: primarily 60 mm, 81 mm, 4.2" mortars, 2.36" rockets, and one each of 37 mm, 3" and 5" projectiles. The site had significant topographic relief.</p>
Description	<p>For all TEM data sets, 3-dipole instantaneous amplitude models were fit to the available time-channels. Single dipoles were fit to targets in magnetics data sets, but cooperative inversion was not used at this site. For detection data sets a threshold on the rate of decay of primary polarizabilities was used to rank targets.</p> <p>Dig sheets for cued interrogation data sets were generated using statistical classifiers trained on size/decay features, as well as with library methods and an "expert" method based on the judgment of an analyst.</p>

Results	<p>Magnetometer detection and classification performance at this site was quite poor. The EM-61 production datasets were much more effective than magnetics. Size estimated from the recovered polarizations was not an effective classification metric due to the small-size of the 60 mm mortars and the inability to accurately constrain depth. However, the time-decay rate estimated from the recovered polarizabilities provided an effective ranking scheme. The EM61 cart performance was marginally better than the MSEMS cart and MTADS EM61 array.</p> <p>For the TEMTADS data the library method was the most effective with 204 of 206 TOI recovered along with 131 of 1076 non-TOI. The two false negatives were the rocket motor pieces declared non-TOI by all cued-interrogation methods and a 60 mm mortar with a target response that overlapped with some nearby clutter. The other classification methods were also effective, generating between 2 to 4 false-negatives.</p> <p>The library method was again most effective for the MetalMapper data with the excavation of 203 of 204 TOI and 175 of 1205 non-TOI. Correct classification of ordnance type was also achieved with up to 99% accuracy achieved with statistical classification.</p>
Site	Camp Butner
Inversion/ Classification Test	<p>Detection surveys with the EM-61 cart and MetalMapper dynamic sensors were conducted. Detected targets from the EM-61 data were revisited with MetalMapper static and TEMTADS cued interrogations.</p> <p>TOI at the site included 105mm HEAT, 37 mm, and M48 fuses. Topographic relief was benign, but there was a significant amount of clutter similar in size and shape to 37 mm.</p>
Description	<p>For all TEM data sets, 3-dipole instantaneous amplitude models were fit to the available time-channels. For detection data sets a threshold on the rate of decay of primary polarizabilities was used to rank targets.</p> <p>Dig sheets for cued interrogation data sets were generated using statistical classifiers trained on size/decay features, as well as with library methods and an "expert" method based on the judgment of an analyst.</p>
Results	<p>Thresholding on time-decay rate of estimated polarizabilities estimated from EM-61 data performed quite poorly, with a 0.92 FAR. This is likely attributable to poor depth estimation for small targets. The MetalMapper dynamic data produced reliable depth estimates, but did not measure sufficiently late in time to provide separation between TOI and non-TOI polarizabilities. FAR was approximately 0.7 for this sensor</p> <p>Excellent classification performance was achieved with the TEMTADS data: all 171 TOI were found with a FAR of only 5%. MetalMapper static performance was similar to TEMTADS, but produced a much higher FAR (78%) owing to outlying TOI attributable to faulty data.</p>
Site	Pole Mountain WY.
Inversion/ Classification Test	<p>Detection mode survey was EM61.</p> <p>Cued interrogation mode MetalMapper survey was also conducted.</p>
Description	Dipole models were fit to the available time-channels. Multi-object inversions

	were also carried out on the MetalMapper data set.
Results	Excellent quality MetalMapper data resulted in near perfect classification results with all TOI recovered with less than 5% non-TOI dug. Detection mode EM61 data had limited detection ability.
Site	Camp Beale
Inversion/ Classification Test	Detection mode survey was EM61. Cued interrogation mode MetalMapper surveys were conducted. Also, the first test of portable sensors including MPV, TEMTADS 2x2, Handheld BUD. The site had magnetic soil present which reduced the SNR of the data relative to previous sites.
Description	For all TEM data sets, dipole polarizabilities were fit to the available time-channels. Multi-object inversions were also carried out on all data sets. For EM-61 detection data, the polarizability rate of decay and size were used to rank targets. Anomalies collected by MetalMapper and portable sensors were ranked using statistical and library-based classification on polarizabilities.
Results	Similar classification performance was achieved for all portable sensors. For each portable sensor excellent classification performance was achieved with no false negatives. MetalMapper diglists also had excellent performance. A diglist featuring no false negatives was submitted for both sets of MetalMapper data.

2.4 Advantages and Limitations of the Technology

The main advantage of the technology is a potential reduction in the number of non-hazardous items that need to be excavated, thus reducing the costs of UXO remediation. Advantages of UXOLab and the algorithms within the package include:

- All the functionality required to process raw geophysical data, detect anomalous regions, and perform geophysical inversion and classification.
- Algorithms for inverting magnetic and TEM data sets both separately and cooperatively using a number of different polarization tensor formulations.
- Extensive set of algorithms for rule-based and statistical classification algorithms.
- Configuration in a modular fashion, so that as new sensor technologies become available (e.g. new TEM systems with multi-component receivers etc), the inversion functionality will be immediately available to those new sensor systems.
- Intuitive design and user-friendly GUIs and workflows

The principal disadvantage is that UXOLab is written in Matlab and has not been configured for general use by contractors and non-specialists. However, as part of ESTCP MR-201004, we transitioned our inversion algorithms to an API that enables access of the algorithms to other software.

3. PERFORMANCE OBJECTIVES

The performance objectives for this demonstration are summarized in Table 3. The first three analysis objectives refer to the classification part of the demonstration with the first two referring to the best results from each approach in a retrospective analysis and the third addressing how well each demonstrator is able to specify the correct threshold in advance. The final two objectives refer to the accuracy of target features extracted from the data.

Table 3: Description of performance objectives for the Spencer Range Demonstration

Performance Objective	Metric	Data Required	Success Criteria
Maximize correct classification of TOI	Number of TOI retained	<ul style="list-style-type: none"> • Prioritized anomaly lists • Scoring reports from Institute for Defense Analysis (IDA) 	Approach correctly classifies all TOI
Maximize correct classification of non-TOI	Number of false alarms eliminated	<ul style="list-style-type: none"> • Ranked anomaly lists • Scoring reports from IDA 	Reduction of clutter digs by > 75% while retaining all TOI
Specification of no-dig threshold	Probability of correct classification of TOI and number of false alarms at demonstrator operating point	<ul style="list-style-type: none"> • Demonstrator -specified threshold • Scoring reports from IDA 	Threshold specified by the demonstrator to achieve criteria above
Minimize number of anomalies that cannot be analyzed	Number of anomalies that must be classified as “Unable to Analyze”	<ul style="list-style-type: none"> • Demonstrator target parameters 	Reliable target parameters can be estimated for > 95% of anomalies on each sensor’s detection list.
Correct estimation of target parameters	Accuracy of estimated target parameters for seed items	<ul style="list-style-type: none"> • Demonstrator target parameters • Results of intrusive investigation 	Polarizabilities $\pm 20\%$ X, Y < 15 cm (1σ) Z < 10 cm (1σ)

3.2 OBJECTIVE: MAXIMIZE CORRECT CLASSIFICATION OF TOI

This is one of the two primary measures of the effectiveness of the classification approach. By collecting high-quality data and analyzing those data with advanced parameter estimation and classification algorithms we expect to be able to classify the targets with high efficiency. This objective concerns the component of the classification problem that involves correct classification of TOI.

3.2.1 Metric

The metric for this objective is the number of items on the anomaly list for a particular sensor that can be correctly classified as TOI by each classification approach.

3.2.2 Data Requirements

We will prepare a ranked anomaly list for the targets on the sensor anomaly list. IDA personnel will use their scoring algorithms to assess the results.

3.2.3 Success Criteria

The objective will be considered to be met if all of the TOI are correctly labeled as TOI on the ranked anomaly list.

3.3 OBJECTIVE: MAXIMIZE CORRECT CLASSIFICATION OF NON-TOI

This is the second of the two primary measures of the effectiveness of the classification approach. By collecting high-quality data and analyzing those data with advanced parameter estimation and classification algorithms we expect to be able to classify the targets with high efficiency. This objective concerns the component of the classification problem that involves false alarm reduction.

3.3.1 Metric

The metric for this objective is the number of items on the sensor dig list that can be correctly classified as non-TOI by each classification approach.

3.3.2 Data Requirements

We will prepare a ranked anomaly list for the targets on the sensor anomaly list. IDA personnel will use their scoring algorithms to assess the results.

3.3.3 Success Criteria

The objective will be considered to be met if more than 75% of the non-TOI items can be correctly labeled as non-TOI while retaining all of the TOI on the dig list.

3.4 OBJECTIVE: SPECIFICATION OF NO-DIG THRESHOLD

In a retrospective analysis as will be performed in this demonstration, it is possible to tell the true classification capabilities of a classification procedure based solely on the ranked anomaly list submitted by each demonstrator. In a real-world scenario, all targets may not be dug so the success of the approach will depend on the ability of an analyst to accurately specify their dig/no-dig threshold.

3.4.1 Metric

The probability of correct classification of TOI, P_{class} , and number of false alarms, N_{fa} , at the demonstrator-specified threshold are the metrics for this objective.

3.4.2 Data Requirements

We will prepare a ranked anomaly list with a dig/no-dig threshold indicated. IDA personnel will use their scoring algorithms to assess the results.

3.4.3 Success Criteria

The objective will be considered to be met if more than 75% of the non-TOI items can be correctly labeled as non-TOI while retaining all of the TOI at the demonstrator-specified threshold.

3.5 OBJECTIVE: MINIMIZE NUMBER OF ANOMALIES THAT CANNOT BE ANALYZED

Anomalies for which reliable parameters cannot be estimated cannot be classified by the classifier. These anomalies must be placed in the dig category and reduce the effectiveness of the classification process.

3.5.1 Metric

The number of anomalies for which reliable parameters cannot be estimated is the metric for this objective.

3.5.2 Data Requirements

We will provide a list of all parameters as part of our results submission along with a list of those anomalies for which parameters could not be reliably estimated.

3.5.3 Success Criteria

The objective will be considered to be met if reliable parameters can be estimated for > 95% of the anomalies on each sensor anomaly list.

3.6 OBJECTIVE: CORRECT ESTIMATION OF TARGET PARAMETERS

This objective involves the accuracy of the target parameters that are estimated in the first phase of the analysis. Successful classification is only possible if the input features are internally consistent. The obvious way to satisfy this condition is to estimate the various target parameters accurately.

3.6.1 Metric

Accuracy of estimation of target parameters is the metric for this objective.

3.6.2 Data Requirements

In our demonstration report, we will compare their estimated parameters for the seed items to those expected.

3.6.3 Success Criteria

The objective will be considered to be met if the estimated polarizabilities are within $\pm 20\%$, the estimated X, Y locations are within 15 cm (1σ), and the estimated depths are within 10 cm (1σ).

Table 4: Summary of performance objectives for the Open and Treed areas of the Spencer Range demonstration.

Performance Objective	Metric	Success Criteria	Data Set			
			Open Area			Treed Area
			Metal- Mapper URS - Cued	Metal- Mapper Naeva - Cued	TEMTADS 5x5 - Cued	TEMTADS 2x2 - Cued
Maximize correct classification of TOI	Number of TOI retained	Approach correctly classifies all TOI	100%	100%	100%	100%
Maximize correct classification of non-TOI	Number of false alarms eliminated	Reduction of clutter digs by > 75% while retaining all TOI	88.5%	84.8%	85.9%	84.7%
Specification of no-dig threshold	Probability of correct classification of TOI and number of false alarms at demonstrator operating point	Threshold specified by the demonstrator to achieve criteria above	$P_{class} = 1$ $N_{fa} = 185$ (18.2%)	$P_{class} = 1$ $N_{fa} = 209$ (20.5%)	$P_{class} = 1$ $N_{fa} = 164$ (16.1%)	$P_{class} = 1$ $N_{fa} = 106$ (17.1%)
Minimize number of anomalies that cannot be analyzed	Number of anomalies that must be classified as “Unable to Analyze”	Reliable target parameters can be estimated for > 95% of anomalies on each sensor’s detection list.	98.8%	99.7%	99.8%	99.2%
Correct estimation of target parameters	Accuracy of estimated target parameters for seed items	Polarizabilities - /+20% X, Y < 15 cm (1 σ) Z < 10 cm (1 σ)	$N(>20\%)=4$ $N(<20\%)=82$ $\sigma_x=0.08m$ $\sigma_y=0.09m$ $\sigma_z=0.05m$	$N(>20\%)=6$ $N(<20\%)=84$ $\sigma_x=0.09m$ $\sigma_y=0.098m$ $\sigma_z=0.05m$	$N(>20\%)=6$ $N(<20\%)=84$ $\sigma_x=NA$ $\sigma_y=NA$ $\sigma_z=0.05m$	$N(>20\%)=4$ $N(<20\%)=70$ $\sigma_x=NA$ $\sigma_y=NA$ $\sigma_z=0.13m$

Table 5: Summary of performance objectives for the Dynamic area of the Spencer Range demonstration.

Performance Objective	Metric	Success Criteria	Data Set			
			Dynamic Area			
			Metal- Mapper URS - Dynamic	TEMTADS 2x2 - Cued	TEMTADS 2x2 - Dynamic	Metal- Mapper URS - Cued
Maximize correct classification of TOI	Number of TOI retained	Approach correctly classifies all TOI	100%	100%	100%	100%
Maximize correct classification of non-TOI	Number of false alarms eliminated	Reduction of clutter digs by > 75% while retaining all TOI	83.5%	91.5%	82.0%	95.3%
Specification of no-dig threshold	Probability of correct classification of TOI and number of false alarms at demonstrator operating point	Threshold specified by the demonstrator to achieve criteria above	$P_{class} = 1$ $N_{fa} = 67$ (21.2%)	$P_{class} = 1$ $N_{fa} = 44$ (13.9%)	$P_{class} = 1$ $N_{fa} = 75$ (23.7%)	$P_{class} = 1$ $N_{fa} = 35$ (11.1%)
Minimize number of anomalies that cannot be analyzed	Number of anomalies that must be classified as “Unable to Analyze”	Reliable target parameters can be estimated for > 95% of anomalies on each sensor’s detection list.	92.1%	100%	100%	100%
Correct estimation of target parameters	Accuracy of estimated target parameters for seed items	Polarizabilities - /+20% X, Y < 15 cm (1 σ) Z < 10 cm (1 σ)	N(>20%)=3 N(<20%)=18 $\sigma_x=0.09m$ $\sigma_y=0.06m$ $\sigma_z=0.03m$	N(>20%)=4 N(<20%)=22 $\sigma_x=NA$ $\sigma_y=NA$ $\sigma_z=0.08m$	N(>20%)=7 N(<20%)=16 $\sigma_x=0.07m$ $\sigma_y=0.07m$ $\sigma_z=0.07m$	N(>20%)=3 N(<20%)=20 $\sigma_x=0.07m$ $\sigma_y=0.07m$ $\sigma_z=0.05m$

4. SITE DESCRIPTION

The former Spencer Artillery Range is a 30,618 acre site located near Spencer, Tennessee. See the Program Office demonstration plan for more details on the site.

4.1 SITE SELECTION

This site was chosen as the next in a progression of increasingly more complex sites for demonstration of the classification process. Spencer Artillery Range was selected because it is more heavily wooded than prior demonstrations and is thought to contain a wide mixture of munitions. These two features increase the site's complexity and both characteristics are likely to be encountered on production sites. The tree cover poses a navigation challenge by increasing the difficulty of obtaining accurate global positioning system (GPS) readings. The survey areas consist of a "Dynamic Area" where all sensors were deployed in dynamic and static mode, and an "Open Area" where MetalMapper and TEMTADS 5x5 were deployed in a cued mode based on target locations picked from detection surveys and the forest survey area (the "Treed Area") where only portable systems were deployed.

4.2 SITE HISTORY

See the Program Office demonstration plan.

4.3 SITE GEOLOGY

See the Program Office demonstration plan.

4.4 MUNITIONS CONTAMINATION

See the Program Office demonstration plan.

5. TEST DESIGN

See the Program Office demonstration plan for a description of the test design for the overall project.

BTG/UBC-GIF processed data and delivered the following three prioritized dig lists for the Spencer Range Open Area:

- 1) Cued URS MetalMapper library match: A dig sheet was produced based on how well the recovered polarizabilities matched the polarizabilities in a library of ordnance items expected at the site;
- 2) Cued NAEVA MetalMapper automated DigZilla ranking: A dig sheet was produced based on a weighted sum of fit to the library, polarizability size, polarizability decay, and a measure of how "rod-like" the target is based on secondary polarizabilities;
- 3) Cued TEMTADS 5x5 library match: As in 1) but for TEMTADS 5x5 data;

BTG/UBC-GIF processed data and delivered the following prioritized dig list for the Spencer Range Tree Area:

- 4) Cued TEMTADS 2x2 library match: A dig sheet was produced based on how well the recovered polarizabilities matched the polarizabilities in a library of ordnance items expected at the site.

BTG/UBC-GIF processed data and delivered the following four prioritized dig lists for the Spencer Range Dynamic Area:

- 5) Cued URS MetalMapper library match: As in 1) but for the dynamic area
- 6) Dynamic URS MetalMapper Combined Classifier Ranking (CCR) match: A dig sheet is submitted by combining separate ranked lists based on polarizability misfit, size, and decay;
- 7) Cued TEMTADS 2x2 library match: As in e) but for the cued TEMTADS 2x2 data;
- 8) Dynamic TEMTADS 2x2 Combined Classifier Ranking (CCR): Same as in 6) but for the dynamic TEMTADS 2x2 data;

6. DATA ANALYSIS AND RESULTS

The Spencer Range demonstration site was divided up into three distinct areas differentiated by the sensors deployed: “Open” area, “Treed” area, and “Dynamic” area. The Open area was surveyed in a cued, static mode by the TEMTADS 5x5 and MetalMapper. Cued MetalMapper data were acquired by Naeva Geophysics Inc. and URS Corporation using the same anomaly list. A more challenging, treed survey area was surveyed by cued portable sensors including the HandHeld BUD, MPV and TEMTADS 2x2. There was also a relatively small dynamic area that was surveyed by the TEMTADS 2x2, MPV and MetalMapper in both cued and dynamic modes to provide cued vs. dynamic deployment comparison for identical targets.

BTG processed multiple datasets in order to test practical UXO classification methods over a range of EMI instruments deployed. BTG processed all the Open area datasets, the TEMTADS 2x2 and MPV data-sets from the Treed area, and all the TEMTADS and MetalMapper URS data from the Dynamic area. All MPV processing was carried out under ESTCP MR-201158, and all MPV results are reported under that project.

The basic data processing workflow was the same for all datasets and is outlined in Figure 1. Classification was performed by BTG or UBC analysts with a strict firewall maintained throughout the analyses. Due to this firewall, information that could aid classification for a particular dataset could NOT be transferred from another dataset (for example, classes of potential targets of interest). Table 6 and Table 7 summarize the classification performance for all of the data sets. The classification metrics were calculated using the ground truth file delivered by the ESTCP program office and the final submitted dig list for each dataset. The model fit statistics (i.e. polarizability percent error, estimated location error, and depth error) were calculated using all anomalies collected. Therefore, if multiple data soundings were acquired over the same target, the resulting best-fit model from each sounding was included in the calculations. The polarizability fit error for each target of interest is presented in Appendix E. Histograms and scatter plots describing the distributions of location and depth estimate errors are found in Appendix G. For the TEMTADS 2x2 and 5x5, the location errors were not recorded due to the absence of IMU information. The IMU information is required for estimating the dipole source location (and therefore target location) in geographic coordinates.

The remainder of this section describe our data analysis procedures in general and summarizes results of the different instruments. A more detailed discussion of the data processing for the datasets summarized here are provided in Appendices A-E.

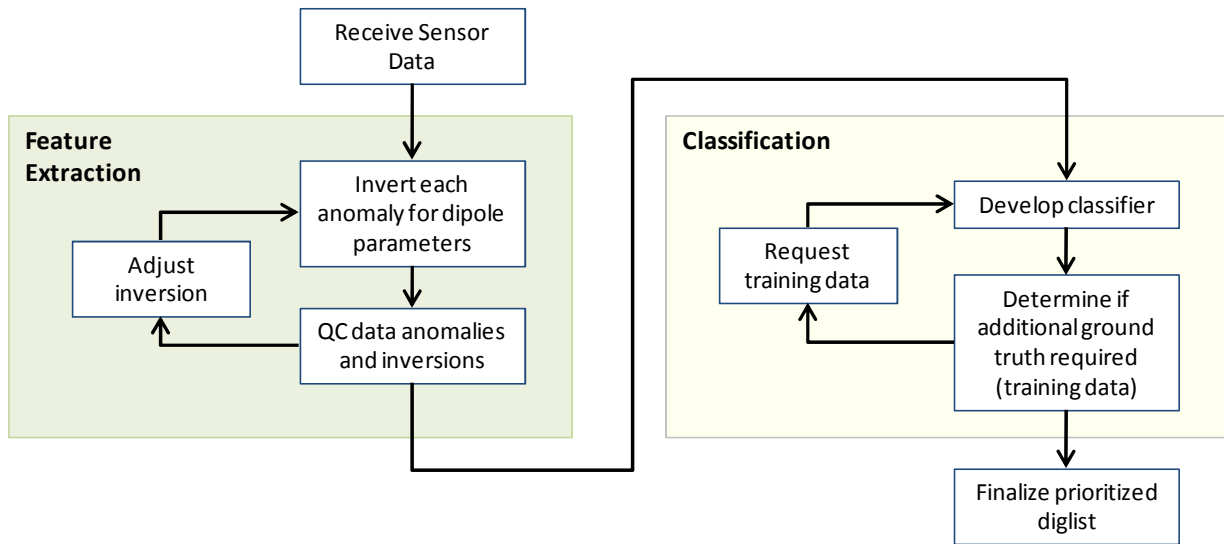


Figure 1: Overview of workflow applied to each dataset from Spencer Range.

Table 6: Classification Results from Open and Tree areas of Spencer Range.

		Open Area			Trees
		Metal Mapper URS	Metal Mapper Naeva	TEMTADS 5x5	TEMTADS 2x2
	Instrument	Metal Mapper URS	Metal Mapper Naeva	TEMTADS 5x5	TEMTADS 2x2
	Site	Open	Open	Open	Trees
	Survey Type	Cued	Cued	Cued	Cued
	Analyst	Zelt	Kingdon	Song	Song
Anomaly Statistics	Total Anomalies	1104	1104	1104	690
	Num TOI	86	86	86	71
	Num Non-TOI	1018	1018	1018	619
False Alarm Rate (FAR)	Percent of Non-TOI	0.115	0.152	0.141	0.153
	Num Non-TOI Dug	117	155	144	95
Stop Dig Point	Digs	271 (24.5%)	295 (26.7%)	250 (22.6%)	177 (25.7%)
	TOI Digs	86 (100.0 %)	86 (100.0 %)	86 (100.0 %)	71 (100.0 %)
	Non-TOI Digs	185 (18.2 %)	209 (20.5 %)	164 (16.1 %)	106 (17.1 %)
Training Data	Digs	51	43	93	63
	TOI	12	8	8	4
	Non-TOI	39	35	85	59
"Cant Analyze" anomalies	Digs	13	3	13	5
	TOI	1	0	0	0
	Non-TOI	12	3	13	5
Polarizability Percent Error	>20%	4	6	6	4
	<20%	82	84	84	70
Position Error	σ (Easting)	0.08	0.09	NA	NA
	σ (Northing)	0.09	0.098	NA	NA
	σ (depth)	0.05	0.05	0.05	0.13

Table 7: Classification Results from Dynamic area of Spencer Range.

	Instrument	Dynamic Area			
		Metal Mapper URS	TEMTADS 2x2	TEMTADS 2x2	Metal Mapper
	Site	Dynamic	Dynamic	Dynamic	Dynamic
	Survey Type	Dynamic	Cued	Dynamic	Cued
	Analyst	Pasion	Song	Billings	Zelt
Anomaly Statistics	Total Anomalies	339	339	339	339
	Num TOI	23	23	23	23
	Num Non-TOI	316	316	316	316
False Alarm Rate (FAR)	Percent of Non-TOI	0.165	0.085	0.18	0.047
	Num Non-Toi Dug	52	27	57	15
Stop Dig Point	Digs	90 (26.5%)	67 (19.8%)	98 (28.9%)	58 (17.1%)
	TOI Digs	23 (100.0 %)	23 (100.0 %)	23 (100.0 %)	23 (100.0 %)
	Non-TOI Digs	67 (21.2 %)	44 (13.9 %)	75 (23.7 %)	35 (11.1 %)
Training Data	Digs	17	20	22	0
	TOI	9	1	5	0
	Non-TOI	8	19	17	0
"Cant Analyze" anomalies	Digs	27	0	0	0
	TOI	3	0	0	0
	Non-TOI	24	0	0	0
Polarizability Percent Error	>20%	3	4	7	3
	<20%	18	22	16	20
Position Error	σ (Easting)	0.09	NA	0.07	0.07
	σ (Northing)	0.06	NA	0.07	0.07
	σ (depth)	0.03	0.08	0.07	0.05

6.1 Processing Open Area Datasets

Cued MetalMapper data were acquired by URS and NAEVA over an identical set of targets using the same instrument. TEMTADS 5x5 cued data were also collected. Three different analysts created ordered dig lists for each MetalMapper dataset and the TEMTADS 5x5 data sets to ensure a firewall was maintained for training data requests and groundtruth. Processing a wide range of sensor data helps reinforce the sensor independent nature of the processing algorithms and classification methodologies. It also provides an opportunity to compare the relative performance of the various sensors as summarized in Table 4.

URS Cued MetalMapper Results

URS MetalMapper data were inverted using both single and two source inversions. *QCZilla* was then used to review the one and two dipole fits and identify the response most similar to a known TOI (and that produced a good fit to the data). In addition, the custom training data selection tool, *TrainZilla* was used to explore feature space and automatically search for clusters of items with self-similar polarizabilities as shown in Figure 2. Training data requests typically focused on: (1) items whose polarizabilities exhibited UXO-like properties distinct from those of items in our reference library; (2) items with polarizabilities similar to items in our reference library, but with degraded quality; and (3) one-off items. Figure 3 shows the location in decay-size feature space of all training requests. Particular

attention was paid to items with polarizabilities suggestive of small objects such as fuzes and small caliber projectiles. All of these turned out to be non-TOI.

The dig list comprised two stages. For the early digs (1-201) the order was based on polarizability misfit using all three polarizabilities. The second stage (digs 202-1104) was based on polarizability misfit using only the primary polarizability. Additional details on the classification approach were provided in our Decision Memo, which is included in Appendix A in its entirety. The final ROC curve for the URS MetalMapper data is shown in Figure 4. At the stop dig point, all TOI were found and greater than 80% of non-TOI were left in the ground.

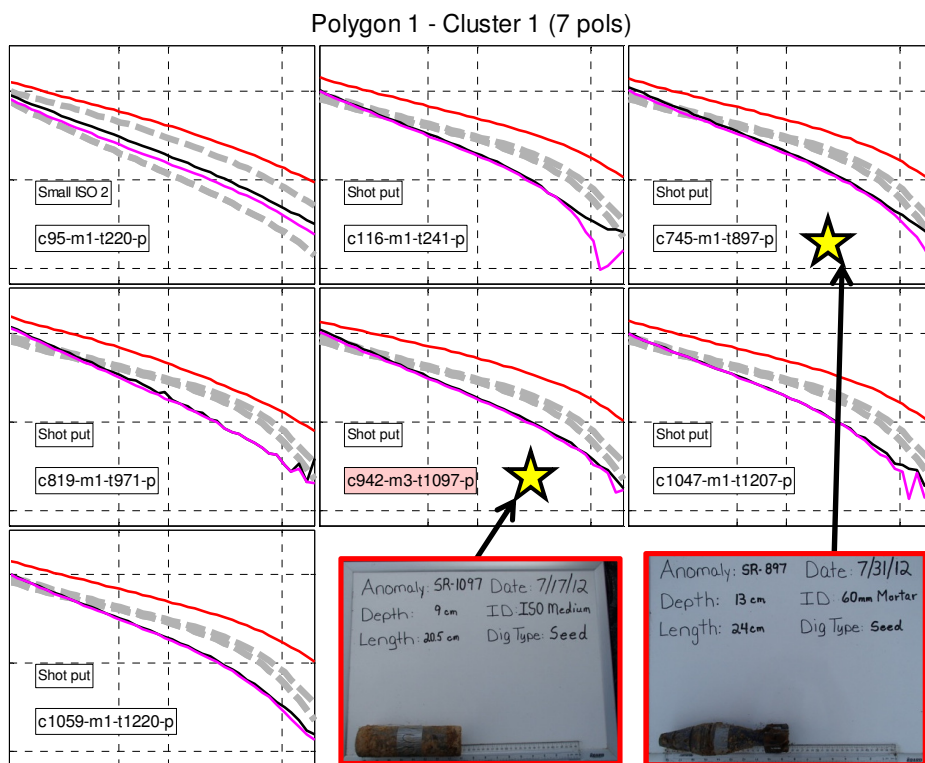


Figure 2: Polarizabilities for a cluster of self-similar polarizabilities identified with *TrainZilla*. Colored lines are predicted polarizabilities. Broken grey lines are best fitting reference polarizabilities. Training data were requested for Anomalies 897 and 1097 (stars); ground truth (photos) revealed that both of these anomalies are new TOI (relative to the starting ordnance reference library). Anomaly 897 is a 60mm mortar; Anomaly 1097 is a medium ISO. These items were added to the reference library.

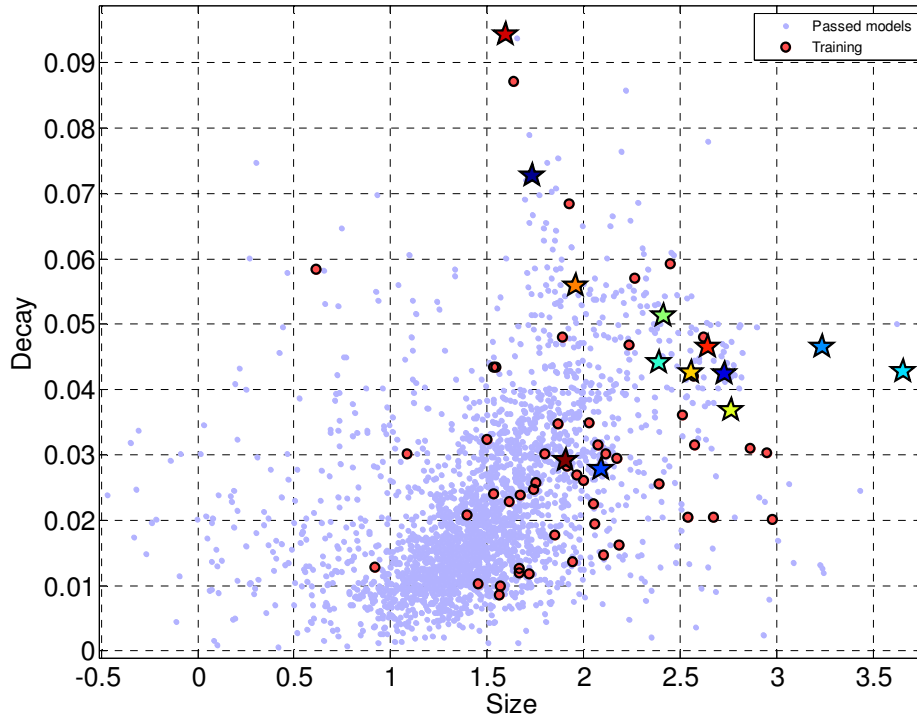


Figure 3: Decay versus size feature space plot showing passed models (blue dots) and the location of training data requests (red dots). Stars are library reference items.

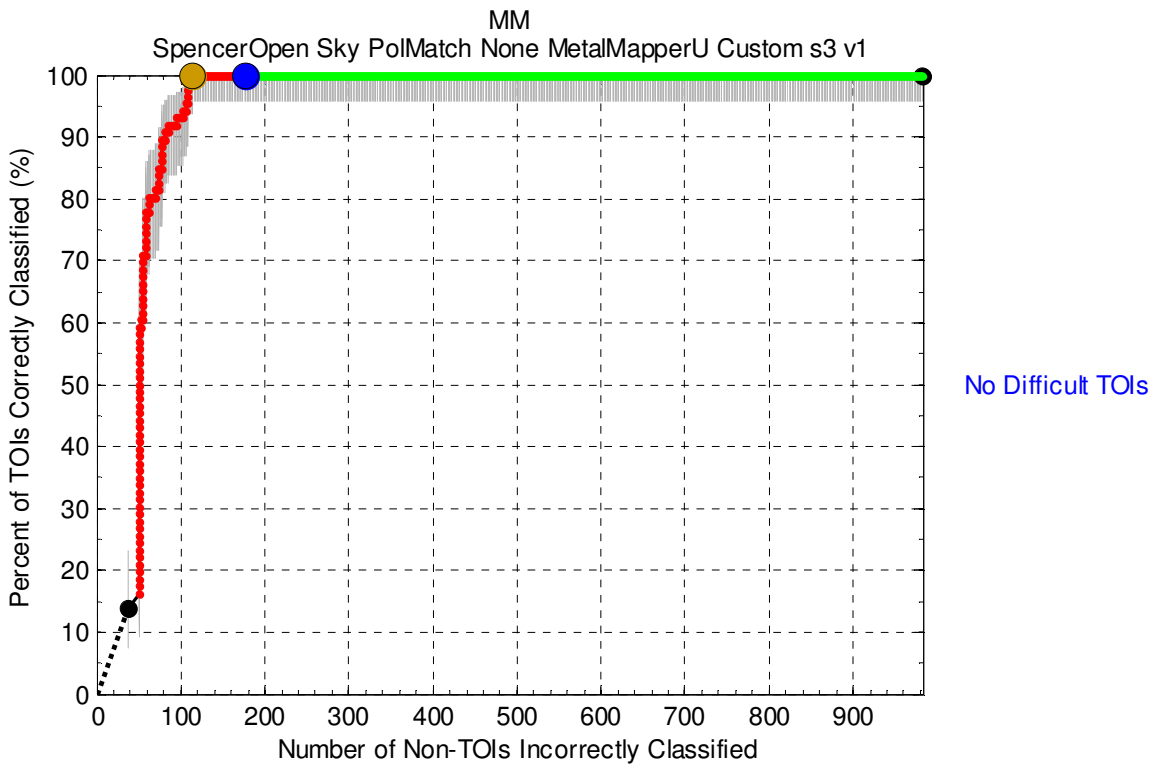


Figure 4: Final ROC curve for Spencer cued MetalMapper (URS) for the open area.

NAEVA MetalMapper Results

NAEVA MetalMapper data was imported, inverted and QC'd in a similar manner as described in the previous section for the URS MetalMapper data. Training data selection involved looking for (1) self-similar polarizabilities, (2) polarizabilities exhibiting UXO-like properties distinct from those of items in our reference library, and (3) polarizabilities that were similar to reference library items but of degraded quality. Figure 5 illustrates a cluster of self-similar polarizabilities that not only revealed a new TOI to add to the reference library (60mm mortar) but also alerted the analyst to the potential of seeded multi object scenarios at the site.

Figure 6 shows the location in decay-size feature space of all training requests. A single stage dig list was generated where targets were ranked based on a combination of misfit using all three polarizabilities (with a weighting of 1) and decay rate (with a weighting of 0.5). The choice of polarizabilities and decay rate and the respective weightings was determined automatically by allowing the *DigZilla* software to search throughout parameter space using a set of starting weights and a bisection approach. The algorithm searches for the set of weights that results in all anomalies that have been flagged as potential/probable TOI being dug as early as possible. A stop dig point was determined by visual inspection of the predicted polarizabilities (in relation to the best fitting reference polarizabilities) of each anomaly plotted in dig list order. The stop dig point was conservatively set to the latest anomaly in the dig list with polarizabilities judged to have a realistic possibility of corresponding to a TOI. Additional details on the classification approach were provided in the Decision Memo, which is included in Appendix A.3 in its entirety. The final ROC curve for the NAEVA MetalMapper data is shown in Figure 7. Although the performance of the non-automated classification was slightly better (Figure 4), all TOI were found and approximately nearly 80% of non-TOI were left in the ground at the stop dig point.

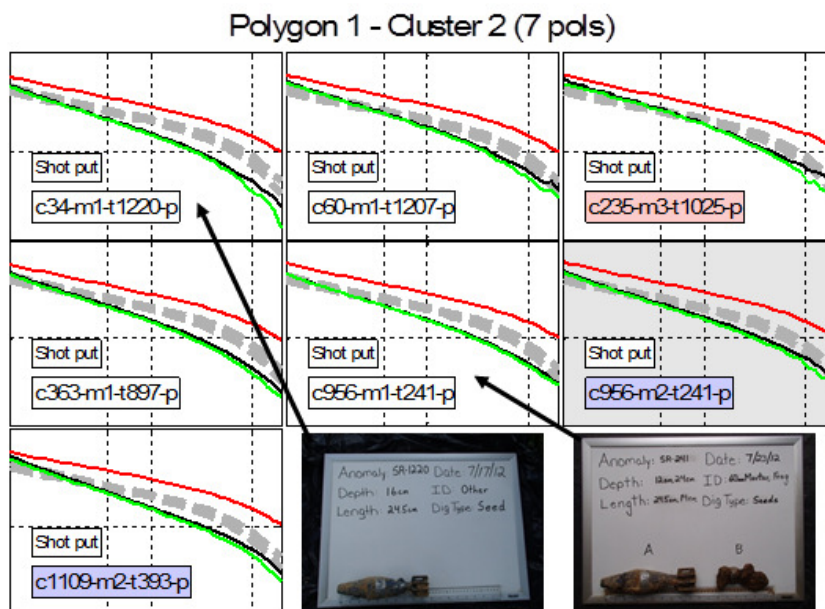


Figure 5: Polarizabilities for a cluster identified via self-similar polarizabilities. Colored lines are predicted polarizabilities. Broken grey lines are best fitting reference polarizabilities. Training data were requested for Anomalies 1220 and 241; ground truth (photos) revealed that both of these anomalies were 60mm mortars, a new TOI. These items were added to the reference library.

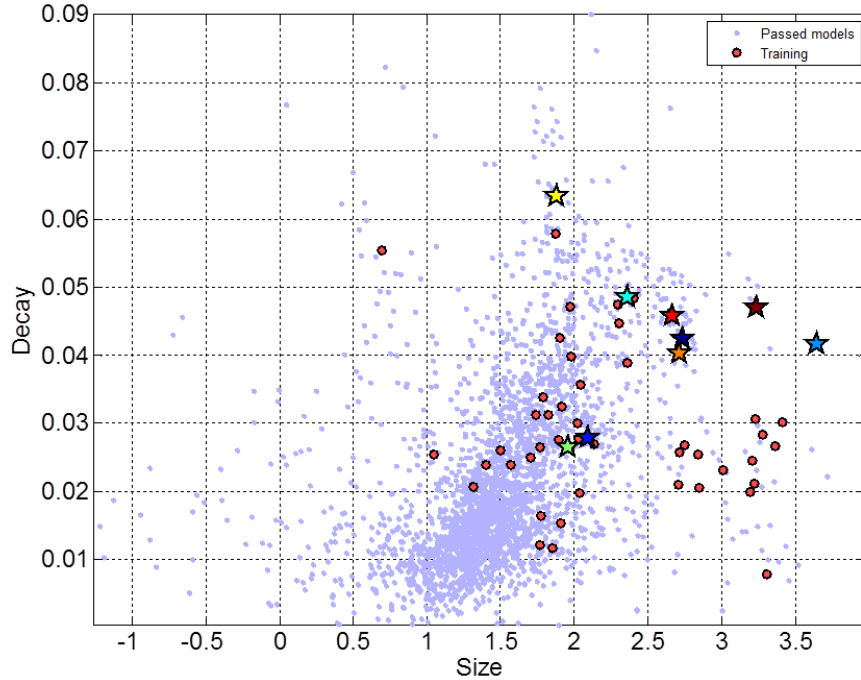


Figure 6: Decay versus size feature space plot showing passed models (blue dots) and the location of training data requests (red dots). Stars are library reference items.

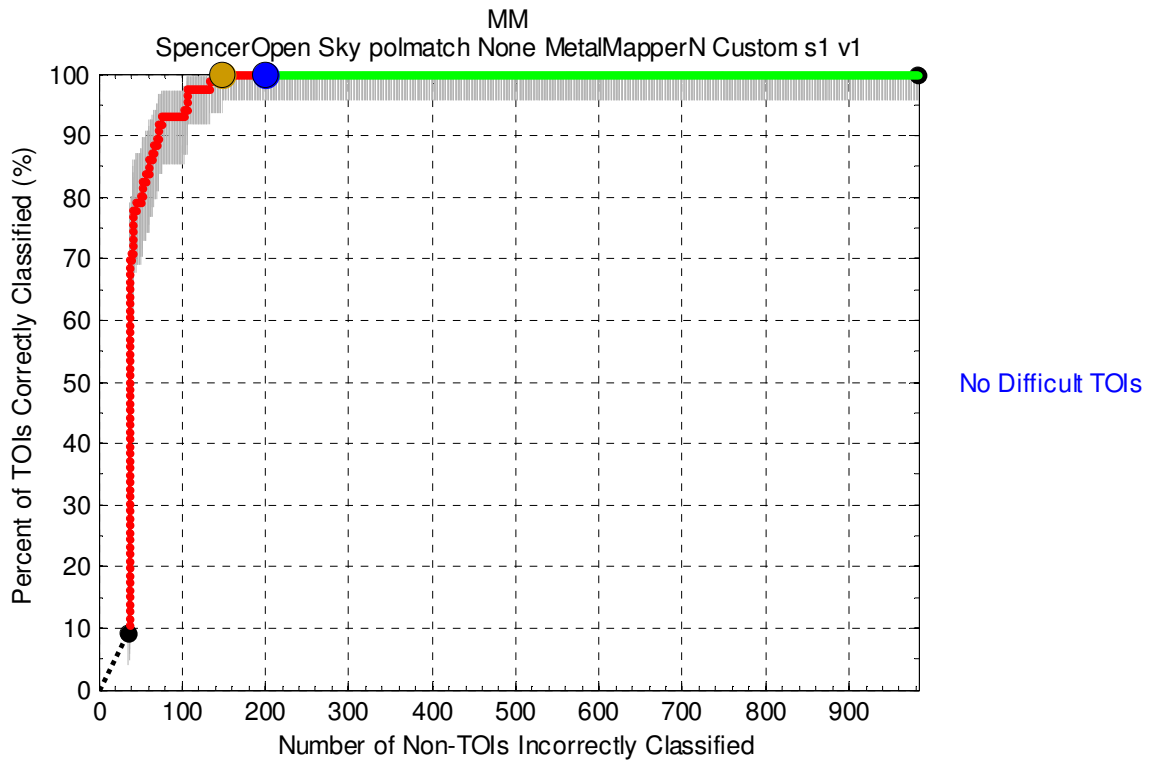


Figure 7: Final ROC curve for Spencer cued MetalMapper (NAEVA) for the open area.

TEMTADS 5x5 Results

Data from each anomaly were inverted using one-, two-, and three-source dipole models. Following the inversions, a data and inversion QC process was completed. This process involved a visual QC, aided by several metrics, including data misfit, data SNR, and properties of the recovered polarizabilities.

A library of reference polarizabilities was built using IVS and test pit measurements, and training data. A number of approaches were used to select training data. A cluster analysis was performed to identify clusters that have distinct features from the existing library members. Training data were chosen to determine the TOI class of each cluster, and the extent of the cluster (i.e. the variability of recovered polarizabilities within the class cluster). Some anomalies with noisy polarizabilities were also chosen for training data. A total of 64 training data anomalies were chosen.

Classification was performed using a library matching method. The library method quantifies how well test polarizabilities agree with a set of reference TOI polarizabilities in the given library. All three principal polarizabilities (i.e. primary, secondary, tertiary) were used to calculate the polarizability misfit (ϕ_m) to a reference (i.e. library) polarizability. The ϕ_m value is used to select which dipole model should be used for a particular anomaly, and the ϕ_m is used to rank all anomalies. The overall classification performance for the TEMTADS 5x5 in the Open area is summarized in Table 4. An initial dig list (Stage 1) missed a pair of QC seeds. Upon receiving ground truth information for these seeds, the polarizability library was modified to include two additional items. To reduce the number of additional targets matching these two additional library items, the late time decay rate was used as an additional classification feature. The stop-dig point chosen for the Stage 2 dig list was dig number 246. At this operating point, 100% of the 86 TOI were identified for excavation. A total of 854 anomalies were left in the ground. At this operating point, 84.2% of the non-TOI items were not dug. Figure 8 shows the ROC curve for the open area. A detailed description of the classification processing can be found in Appendix C.3.

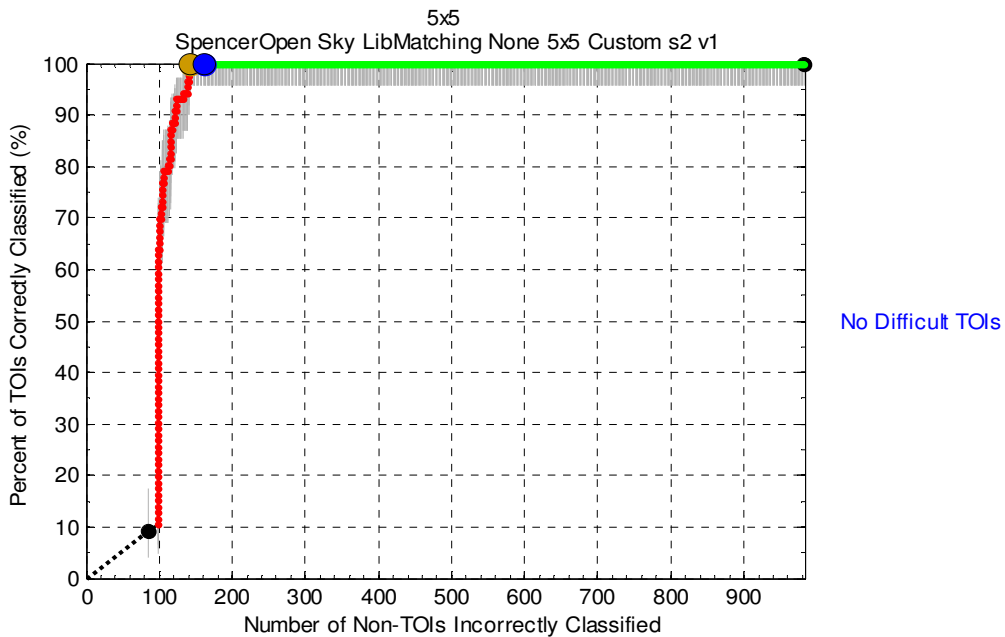


Figure 8: ROC curve for the TEMTADS 5x5 data acquired in the Open area.

6.2 Processing Treed Area Datasets

For this project, BTG generated a dig list for the cued TEMTADS 2x2 in the Portable area at Spencer Range. BTG produced a dig list for the cued MPV as part of ESTCP MR-201158. We refer the reader to the ESTCP MR-201158 Spencer Demonstration report for MPV processing details and results.

TEMTADS 2x2 Cued Data Results

The inversion and classification approach for the TEMTADS 5x5 data (Section 6.1) was applied to the TEMTADS 2x2 cued data. A detailed description of the TEMTADS 2x2 cued data processing approach can be found in Appendix C.1. There were two stages with two submitted dig lists in the classification process. In stage one, 106 anomalies were dug. Of these 106 anomalies, 67 were TOIs. No QC seeds were missed. Based on the ground truth information for stage one, three additional anomalies were dug in stage two. These three anomalies were all non-TOI. A total of 178 items were dug. Five items were assigned to the "Can't extract reliable parameters" class. As a result, all 71 TOI were recovered. 514 anomalies were left in the ground and not dug, i.e. 82.8% of the non-TOI items were correctly labeled as non-TOI; all of the TOI were correctly identified.

Due to an absence of IMU information, metrics related to target location estimate accuracy were not calculated. The depth estimate errors have a standard deviation of 13 cm, which exceeds the success criteria of less than 10 cm. The survey conditions in the Treed area may have resulted in variation of the ground clearance height of the instrument, whereas we assumed a fixed ground clearance height for all anomalies. It is possible that having a more accurate measure of the ground clearance height for each anomaly would reduce the amount of error in the depth estimates.

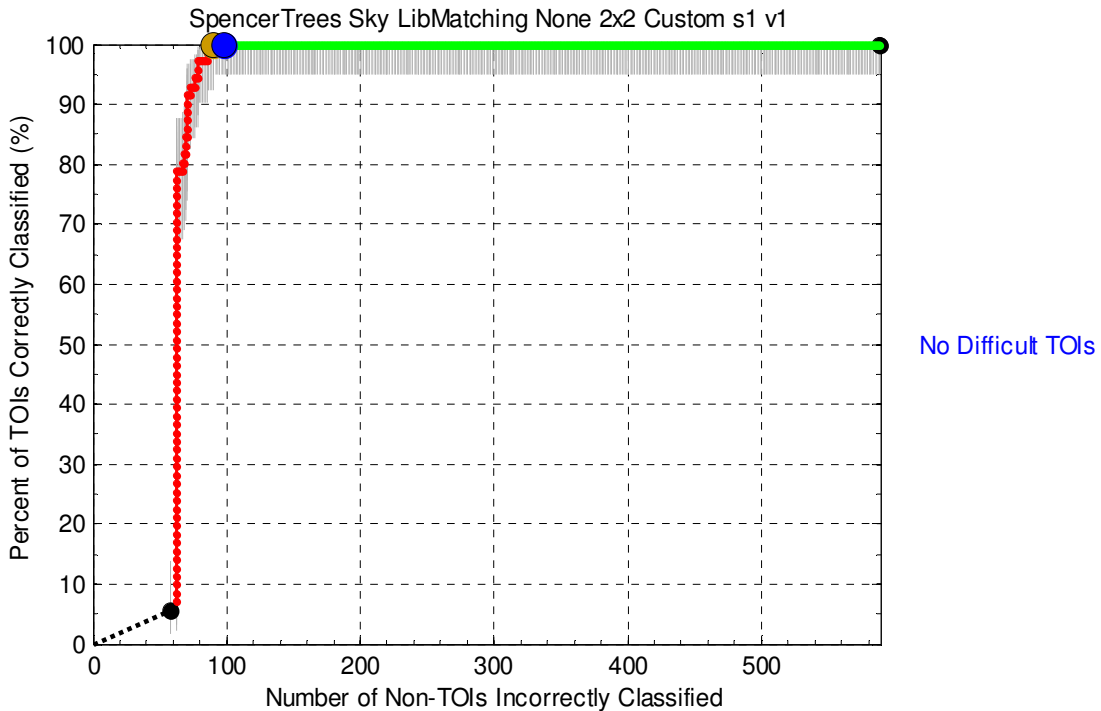


Figure 9: ROC curve for the TEMTADS 2x2 Cued data analysis in the treed area

6.3 Processing data collected in the Dynamic Area

In the Dynamic area at Spencer Range, BTG generated dig lists for the cued TEMTADS 2x2, dynamic TEMTADS 2x2, cued URS MetalMapper and dynamic URS MetalMapper data. We note that BTG also produced a dig list for the cued and dynamically acquired MPV data as part of ESTCP MR-201158. We refer the reader to the ESTCP MR-201158 Spencer Demonstration report for MPV processing details and results.

URS Cued MetalMapper Results

Cued URS MetalMapper data in the Dynamic area were analyzed by the same BTG analyst who previously generated a cued dig list for the URS open area MetalMapper data. A similar approach to the one used for the open area was applied to the dynamic area data. No training data were requested for the dynamic area as it was assumed that the ground truth information that had been received (up to the stop dig point) for the open area was sufficient training data. During visual QC of the data, a new class of suspicious, but unknown, TOI was added to the ordnance library based on the polarizabilities for Anomalies SR-1729 and SR-1550. Both of these turned out to be 37mm TOI. One of these (SR-1729) was a multi-object scenario (i.e. 37mm with four medium to large pieces of frag). The training data tool was used to look for other “hidden” clusters, but none were found.

The classification approach was similar to that used for the open area data. The dig list comprised two stages. For the early digs (1-39) the order was based on polarizability misfit using all three polarizabilities. The second stage (digs 40-339) was based on polarizability misfit using only the primary polarizability. The stop dig point was set at dig number 55. Additional details on the classification approach for the cued MetalMapper data in the open area are provided in the Decision Memo, which is included in its entirety in Appendix A.2.

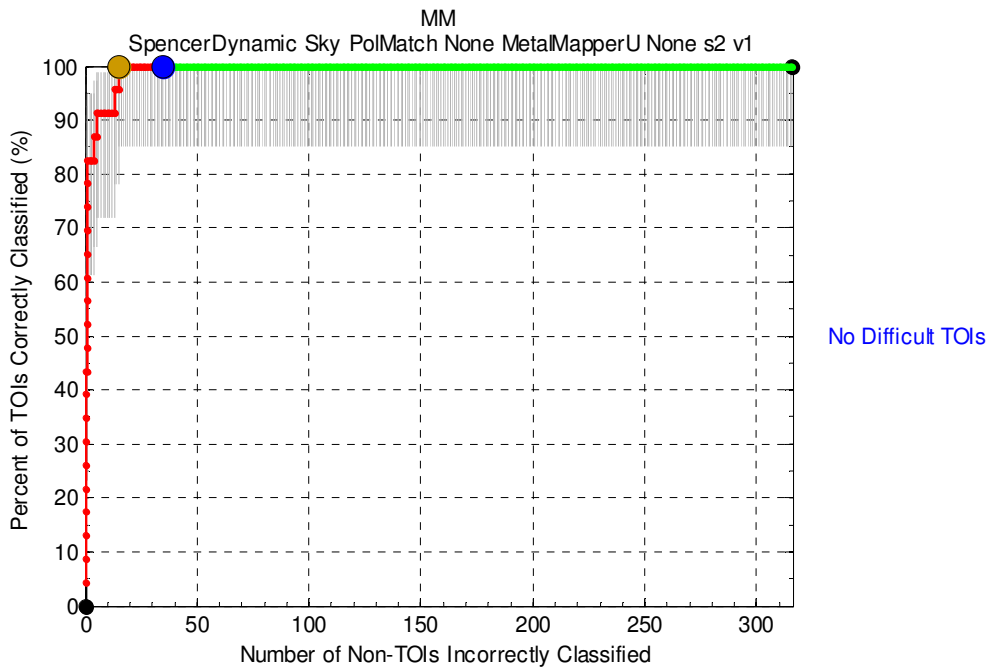


Figure 10: Final ROC curve for Spencer cued MetalMapper (URS) for the dynamic area.

URS Dynamic MetalMapper Results

MetalMapper data acquired in a dynamic, full coverage mode were processed using UXOLab. The data were background corrected by identifying regions in the data that did not contain data anomalies, and then using these anomaly-free regions to estimate background levels which would subsequently be removed from the data.

BTG/UBC-GIF did not carry out any target picking or anomaly selection. An anomaly list was provided by the ESTCP program office. Data within a 1.5m square region surrounding each anomaly flag was extracted from the background corrected dataset, and a one and two dipole source inversion was used to provide location, orientation and dipole polarizability estimates.

We performed a semi-automated cluster analysis to search for clusters of items with self-similar polarizabilities. Clusters were formed in three ways: (1) total polarizability, (2) primary polarizability, and (3) 1st and 2nd largest polarizabilities. Clusters that were judged to be UXO-like or vaguely-UXO like were selected as clusters of interest. From these clusters of interest we typically selected a couple of example items for training data. In addition, anomalies lying on the edge of clusters of very likely UXO-like items would be selected for training data as a means of gauging both the potential variability of a cluster class, and the quality of the data. A single training data request of 17 anomalies was submitted to the program office.

The Combined Classifier Ranking (CCR) algorithm was used for creating a prioritized dig list. Dig list order is based on four metrics: (1) best polarizability misfit relative to a library of reference ordnance items calculated using all three polarizabilities (L_1 , L_2 and L_3); (2) same as (1) but calculated using only the primary (L_1) polarizability; (3) polarizability size; and (4) polarizability decay. The anomalies are sorted according to each metric, creating four lists of ordinals for each anomaly. The final “score” for each anomaly is a weighted sum of the ordinals.

The ROC curve for the submitted list is shown in Figure 11. At the stop-dig point – excluding training data digs and “can’t analyze” digs – there were 90 total digs, of which 23 were TOI and 67 were non-TOI. At this operating point, 100% of the TOI were identified for excavation and 21.2% of the non-TOI anomalies were marked for excavation. The False Alarm Rate (FAR) was 0.165, with 52 of the 316 non-TOI excavated.

All performance metrics related to the accuracy of estimated target location were successfully met (Table 5). A percent error was calculated to quantify the misfit between estimated polarizabilities and the library polarizability corresponding to the ground truth. The percent error is calculated using all three principal polarizabilities. Only three TOI exceeded the 20% threshold for the polarizability percent error metric. Of these three TOI, SR-1502 was identified in the training data stage of the classification, and the other two TOI (SR-1506 and SR-1729) had a low enough primary polarizability misfit to be selected for excavation.

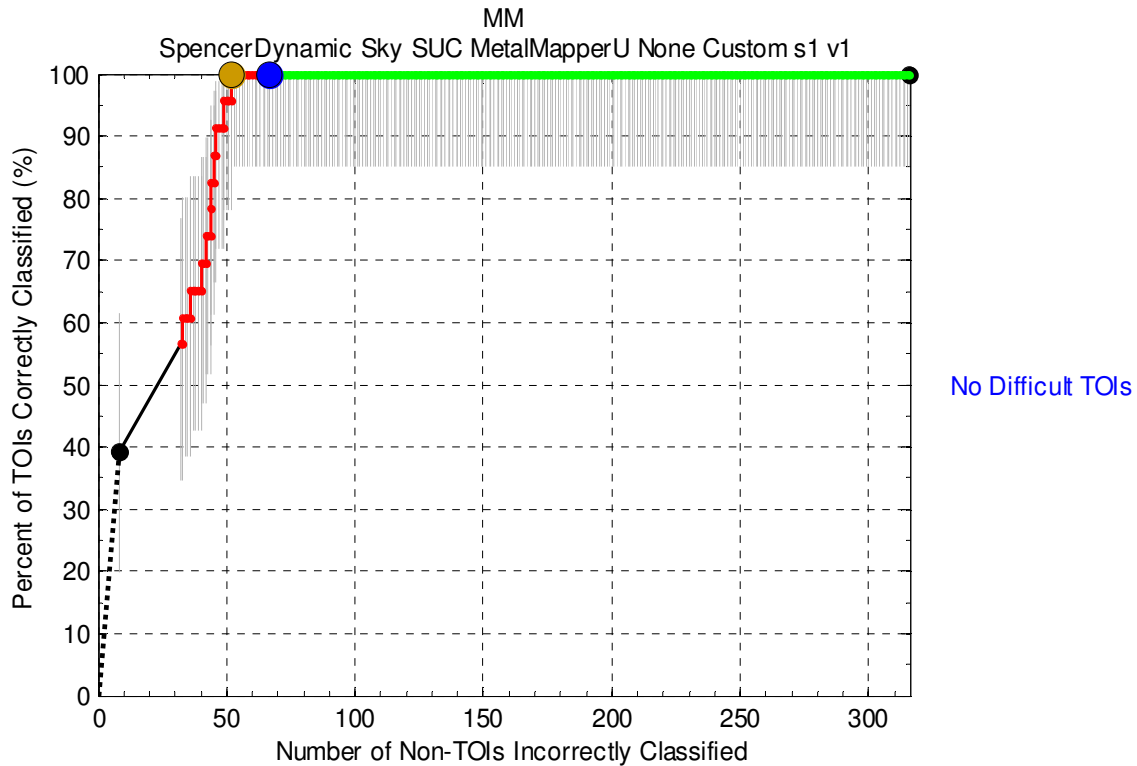


Figure 11: Final ROC curve for Spencer Range MetalMapper (URS) data acquired in a dynamic mode

Cued TEMTADS 2x2 Results

The analyst that processed TEMTADS 2x2 cued data in the Treed area also processed TEMTADS 2x2 data in the Dynamic area. The polarizability library used in the Treed area was used for the dynamic area. The process for requesting training data was similar to that used in the Treed area, and resulted in a total of 20 training anomalies.

A single classification dig list was submitted. No QC seeds were missed in this initial dig list. After reviewing the ground truth information for these anomalies, it was determined that it was unlikely that there would be additional TOI in the remaining anomalies. All 23 TOI are were correctly marked for excavation. 86.9% of the non-TOI items were correctly labeled as non-TOI while retaining all of the TOI on the dig list. Figure 12 shows the final ROC curve provided by IDA.

All performance metrics related to classification of TOI and non-TOI satisfied the success criteria. Location estimates were not calculated, due to the absence of IMU information available for the survey. The standard deviation of the depth estimate error is 0.08 m. A percent error was calculated to quantify the misfit between estimated polarizabilities and the library polarizability corresponding to the ground truth. The percent error is calculated using all three principal polarizabilities. Only 4 TOI exceeded the 20% threshold for the polarizability percent error metric. Of these 4 TOI, SR-1502 was identified in the training data stage of the classification. Two of the 4 TOI (SR-1564 and SR-1576) had data recollected, for which the polarizability fit of the recollected data had a percent error that met the success criteria. Although anomaly SR-1609 had a poor fit to the library item, it was still dug just before the stop-dig point.

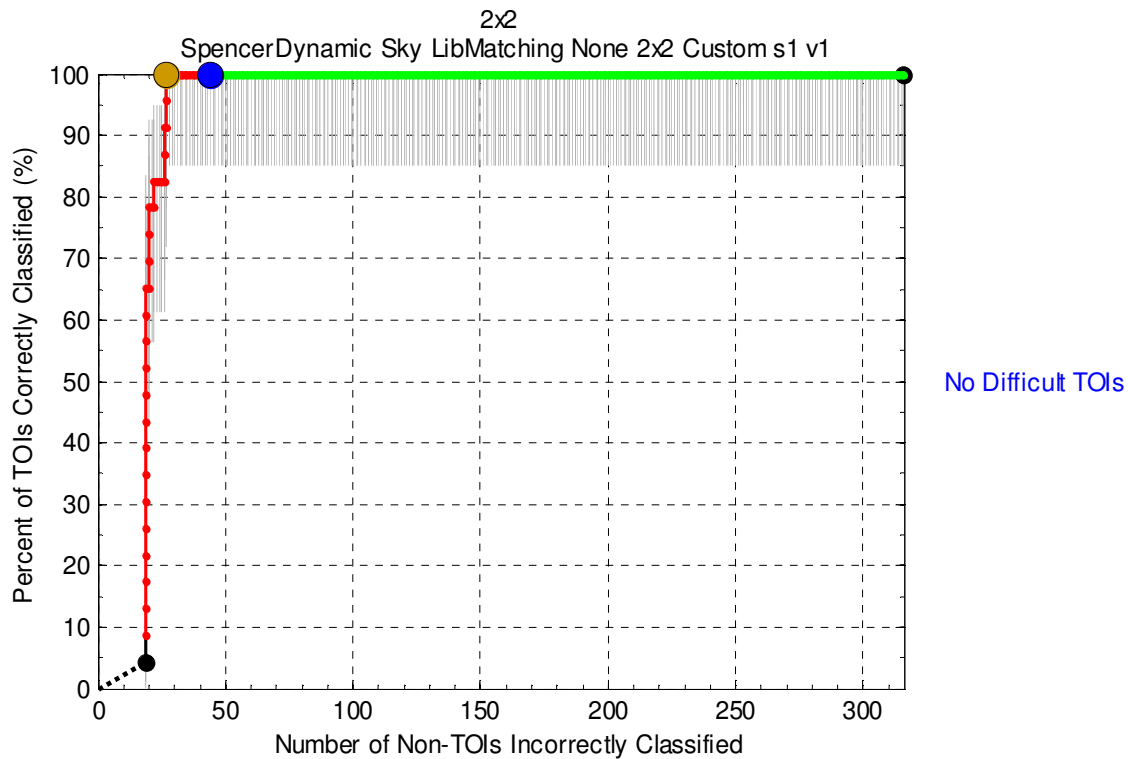


Figure 12: Final ROC curve for Spencer Range TEMTADS 2x2 cued data acquired in the Dynamic area

Dynamic TEMTADS 2x2 Results

The background corrected TEMTADS 2x2 dynamic data collected at Spencer Range were inverted using a sequential inversion approach to estimate target location, depth and principal polarizabilities. Two single-object inversions were performed per anomaly: (1) using all data within 75 cm of the picked target location; and (2) by inverting only the data along the transect that passed closest to the picked target location. Where necessary, the analyst adjusted masks and/or fit a two object inversion model to the data. The best fitting model for any of the inversions performed for a particular anomaly was used to make classification decisions.

Analysis of the data, including visual QC of data and model parameters, selection of training data, and dig list creation, was performed using the UXOLab software suite. Visual QC of the data was performed using *QCZilla*, which allowed us to compare the observed and predicted data, review predicted model parameters, and examine measures of data/model quality. Predicted polarizabilities were compared to reference polarizabilities for various ordnance items initially derived from IVS and test pit measurements. As the analysis proceeded, the library of reference items was augmented with additional items based on ground truth obtained through training data requests.

Training data information was requested for twenty-one items spread across two requests. The training data requests focused on items with similar size and time-decay parameters to the known ordnance items and items that appeared to exhibit axial symmetry. Figure 13 shows the location in decay-size feature space of all training requests.

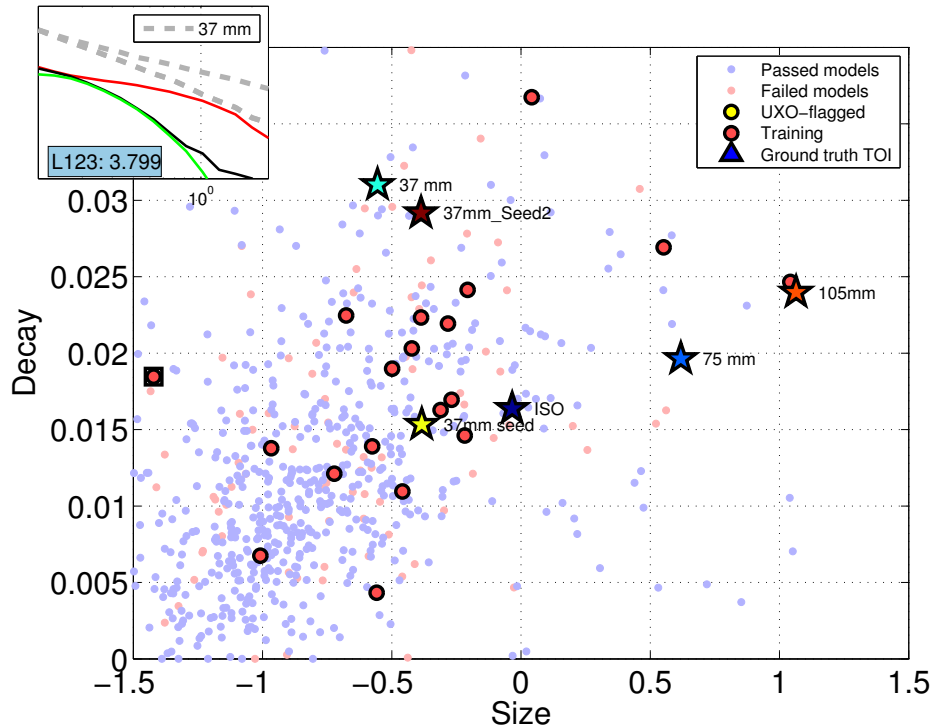


Figure 13: Decay versus size feature space plot showing passed models (blue dots) and the location of training data requests (red dots). Stars are library reference items.

A single stage dig list was generated in which targets were ranked using the Combined Classifier Ranking (CCR) algorithm. In the CCR algorithm we rank anomalies using feature vectors comprising (1) all polarizabilities; (2) primary polarizability; (3) size and (4) decay. Rankings for each of the four sets of feature vectors are obtained by comparison to the equivalent features in the reference library. The Combined Classifier Ranking is obtained by the weighted sum of the rankings in the four separate ranking schemes. Thus a feature vector that ranks high in more than one scheme will rank high in the CCR. The stop dig-point was determined subjectively by the analyst: digging ceased after all items deemed to be high-priority TOI and/or low-confidence non-TOI items were dug. In the original dig-list submission one seed item (SR-1676) occurred past the stop-digging point. This item had a lower than expected time-decay parameter that placed it just past the stop-dig point. The CCR weights were adjusted so that items in the region of feature space below the ISO and 37 mm feature vectors were ranked higher. Additional processing details are found in Appendix D. The final ROC curve for the dynamically acquired TEMTADS2x2 data in the dynamic area is shown in Figure 14. All TOI were identified for excavation and greater than 80% of non-TOI were left in the ground at the stop-dig point.

6.4 Technology Training and Transfer

A member of the Shaw Environmental production team attended a one week training session in Vancouver, B.C., Canada with BTG algorithm and software developers. The training session included an overview of UXO inversion and classification theory and software routines. The Shaw geophysicist was responsible for executing all parts of the classification workflow: from data and inversion QC, training data selection, to diglist creation and submittal. A summary of the approach and results prepared by the Shaw analyst is included in Appendix I. The final ROC curve is shown in Figure 15.

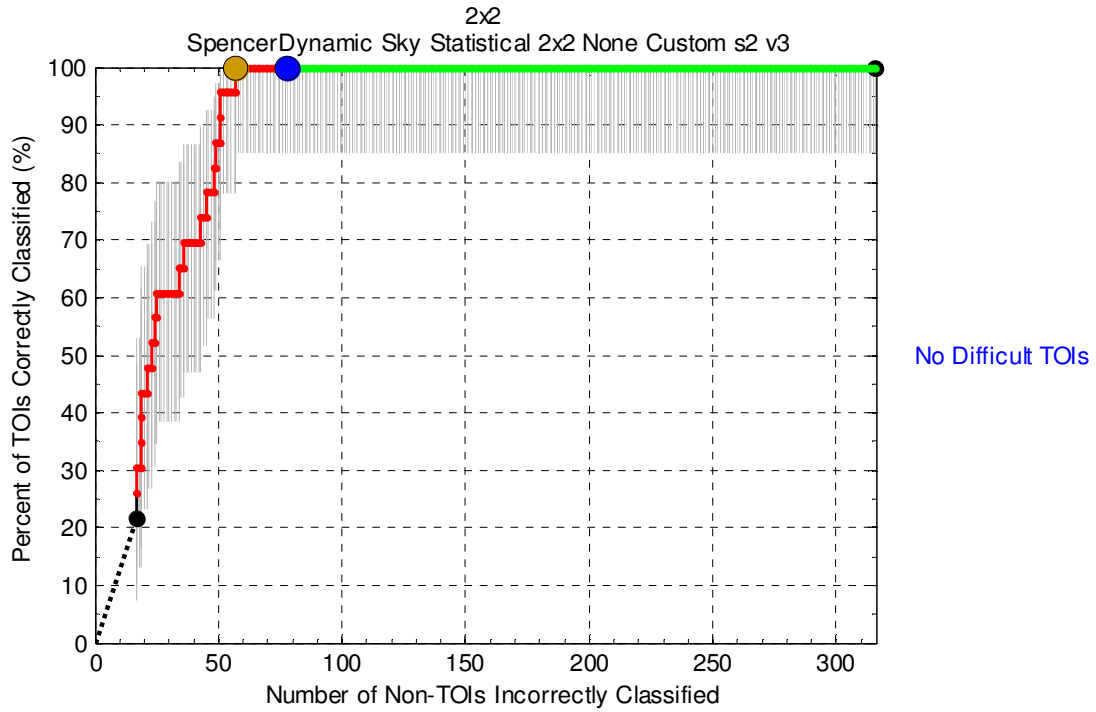


Figure 14: Final ROC curve for the dynamic TEMTADS 2x2 data from the dynamic survey area at Spencer Range.

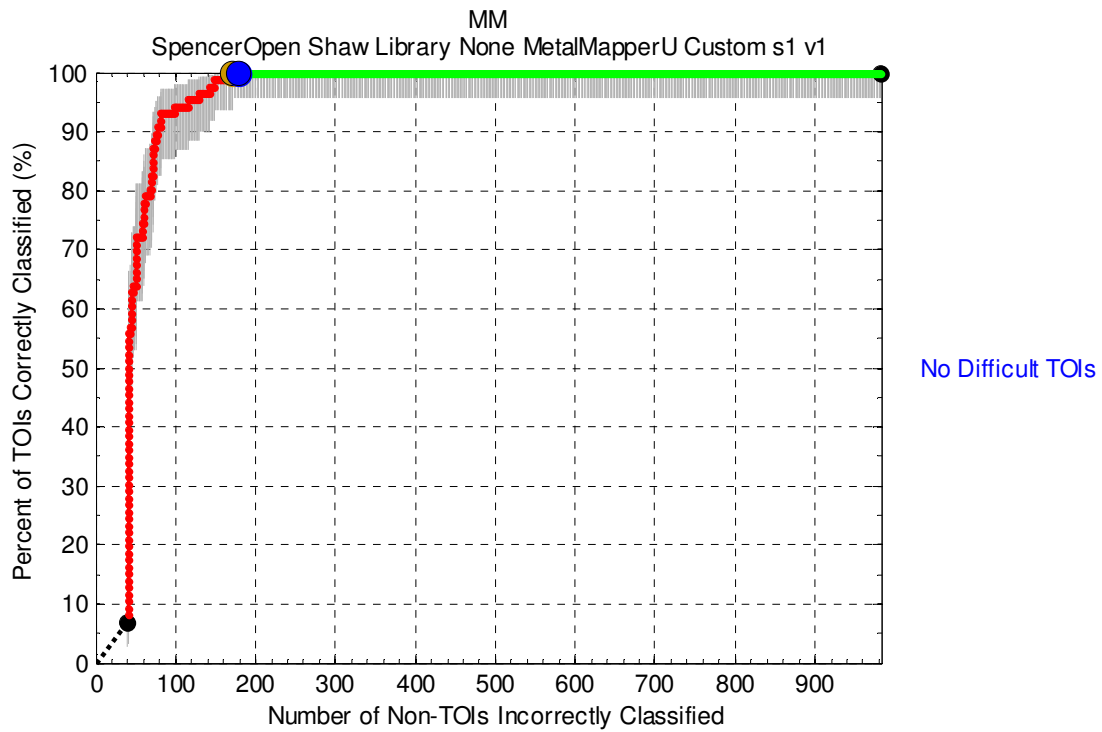


Figure 15: ROC curve for the library based classification of MetalMapper (URS) data carried out by a Shaw Environmental geophysicist.

7. MANAGEMENT AND STAFFING

A flow chart showing the managerial hierarchy and the relationship between the principal investigator (PI) and other personnel is shown in Figure 16.

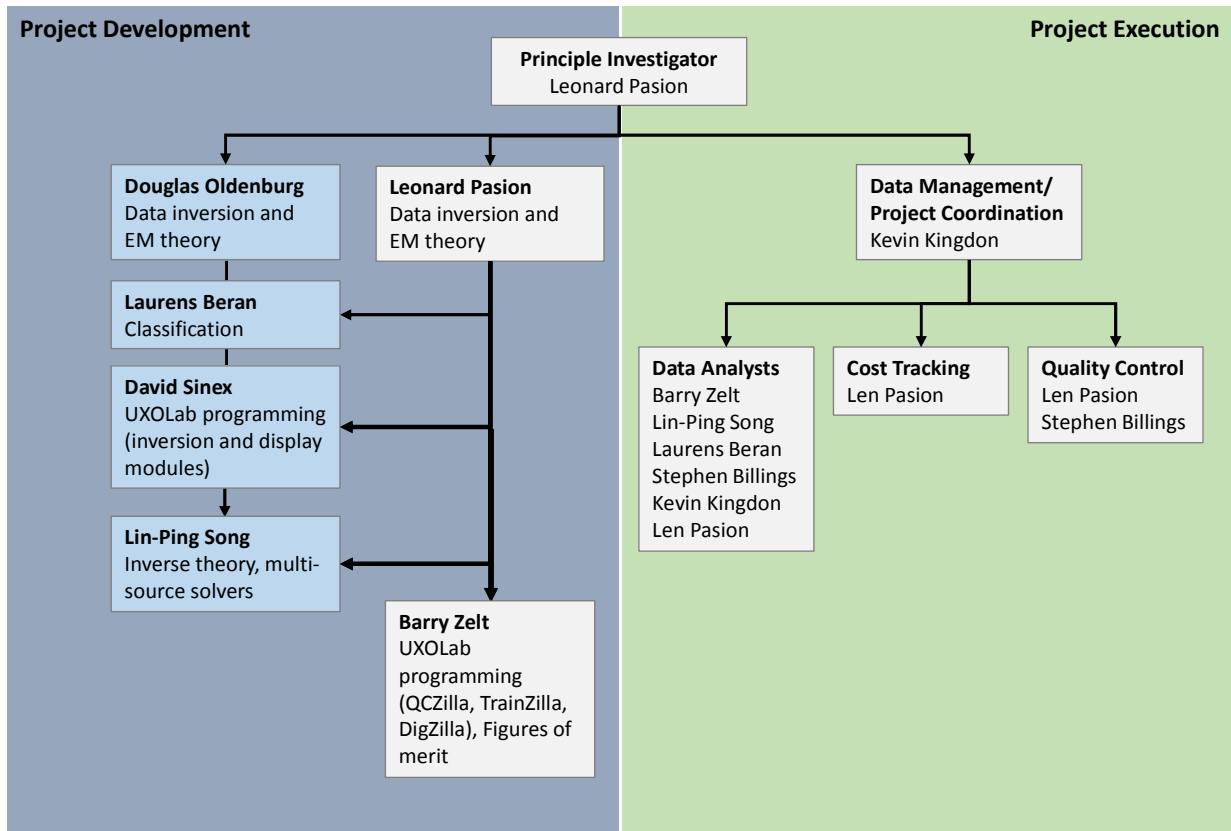


Figure 16: Project management hierarchy showing BTG personnel in grey and UBC-GIF personnel in blue. The hierarchy is split between the development and execution components.

REFERENCES

- T. Bell, B. Barrow, J. Miller, and D. Keiswetter. Time and frequency domain electromagnetic induction signatures of unexploded ordnance. *Subsurface Sensing Technologies and Applications*, 2:153-175, 2001.
- S. D. Billings, L. R. Pasion, L. Beran, N. Lhomme, L. Song, D. W. Oldenburg, K. Kingdon, D. Sinex, and J. Jacobson. Unexploded ordnance discrimination using magnetic and electromagnetic sensors: Case study from a former military site. *Geophysics*, 75:B103-B114, 2010.
- ESTCP. 2010 ESTCP demonstration study, former Camp Butner. Technical report, 2010.
- X. Liao and L. Carin. Migratory logistic regression for learning concept drift between two data sets with application to UXO sensing. *IEEE Trans. Geosci. Remote Sensing*, 47:1454 -1466, 2009.
- L. R. Pasion, S. D. Billings, D. W. Oldenburg, and S. Walker. Application of a library-based method to time domain electromagnetic data for the identification of unexploded ordnance. *Journal of Applied Geophysics*, 61:279-291, 2007.
- F. Shubitidze, K. O' Neill, S. A. Haider, K. Sun, and K. D. Paulsen. Application of the Method of Auxiliary Sources to the Wide-Band Electromagnetic Induction Problem. *IEEE Trans. Geosci. Remote Sensing*, 40:928-942, 2002.
- S. L. Tantom, Y. Li, and L. M. Collins. Bayesian mitigation of sensor position errors to improve unexploded ordnance detection. *IEEE Geosci. Remote Sensing Letters*, 5:103-107, 2008.
- G. F. West and J. C. Macnae. *Electromagnetic methods in applied geophysics*, chapter Physics of the electromagnetic exploration method, pages 5-45. SEG, 1991.
- Y. Zhang, X. Liao, and L. Carin. Detection of buried targets via active selection of labeled data: Application to sensing subsurface UXO. *IEEE Trans. Geosci. Remote Sensing*, 42:2535-2543, 2004.

APPENDICES

Appendix A: Cued MetalMapper Feature Extraction and Classification

There were two MetalMapper datasets acquired over identical anomaly locations by two different contractors at Spencer Range. Two unique BTG analysts processed the respective MetalMapper datasets maintaining a strict firewall throughout the investigation. Barry Zelt processed the MetalMapper data collected by URS and Kevin Kingdon processed the MetalMapper data collected by Naeva Geophysics Inc. Although both analysts utilized a classification approach based on dipole polarizability features and matching, Mr. Kingdon tested a more conservative and automated classification strategy.

A.1 MetalMapper-URS Cued Feature Extraction and Classification

A.1.1 Feature extraction (URS, Open Area)

MetalMapper cued data for all anomalies were received as a set of raw TEM files and two sets of CSV files (with and without background corrections). Our analyses used the background-corrected data. The data were inverted in UXOLab using a sequential inversion approach to estimate target location, depth and principal polarizabilities. Instrument height above the ground was assumed to be 10 cm. Noise standard deviation estimates were not available, so a constant noise value of 1 over all time channels was used. Target location was constrained to lie between ± 0.5 m in both X and Y directions relative to the picked location. Target depth was constrained to lie between -1.2 and 0 m. The initial optimization for target location identified up to three starting models to input into the subsequent estimation of polarizabilities. We performed two inversions per anomaly, solving for (1) a single object (single object inversion: SOI); and (2) two objects (2OI).

Analysis of the data, including visual QC of data and model parameters, selection of training data, and dig list creation, was performed using the UXOLab software suite. Visual QC of the data was performed using *QCZilla*, which provides a thorough overview of the observed and predicted data, predicted model parameters, and measures of data/model quality. Display of the gridded EM61 data at each anomaly provides a useful indicator of the anomaly size and strength. Predicted polarizabilities were compared to reference polarizabilities for various ordnance items initially derived from IVS measurements. The Spencer Artillery Range test pit contained four items: 75, 37mm, Small ISO, and Shot Put. The latter item was not used during the classification process. As the analysis proceeded, the library of reference items was augmented with additional items based on ground truth obtained through training data requests. Each item in the ordnance reference library was assigned a size (diameter) in mm. Each item classified as "likely TOI" in the submitted dig list was assigned a size based on the ordnance item in the reference library with the best matching primary polarizability (L_1).

During data/model QC the primary objectives were to (1) flag high-likelihood TOI; and (2) flag bad models and inversions. Anomalies flagged as high-likelihood TOI were monitored during the dig list creation phase to ensure they were being dug, ideally early in the dig list. Models and inversions were considered to be bad when the inversion failed (i.e., the data misfits are large), or when the recovered model location(s) were on, or near, an inversion boundary. With multi-object inversions it is not uncommon that one of the models is unrealistic (e.g., deep, large in magnitude, sometimes located on or near a horizontal inversion boundary) yet provides the best fit to the reference polarizabilities (e.g., Figure

17). In all of these cases the model was flagged as failed. Models flagged as failed were not used in the classification process. Anomalies with all models from all inversions failed were classified as "can't extract reliable parameters"; these anomalies will be dug. For a given anomaly, if more than one model was passed the classification procedure will consider all passed models and effectively use the one that is "best".

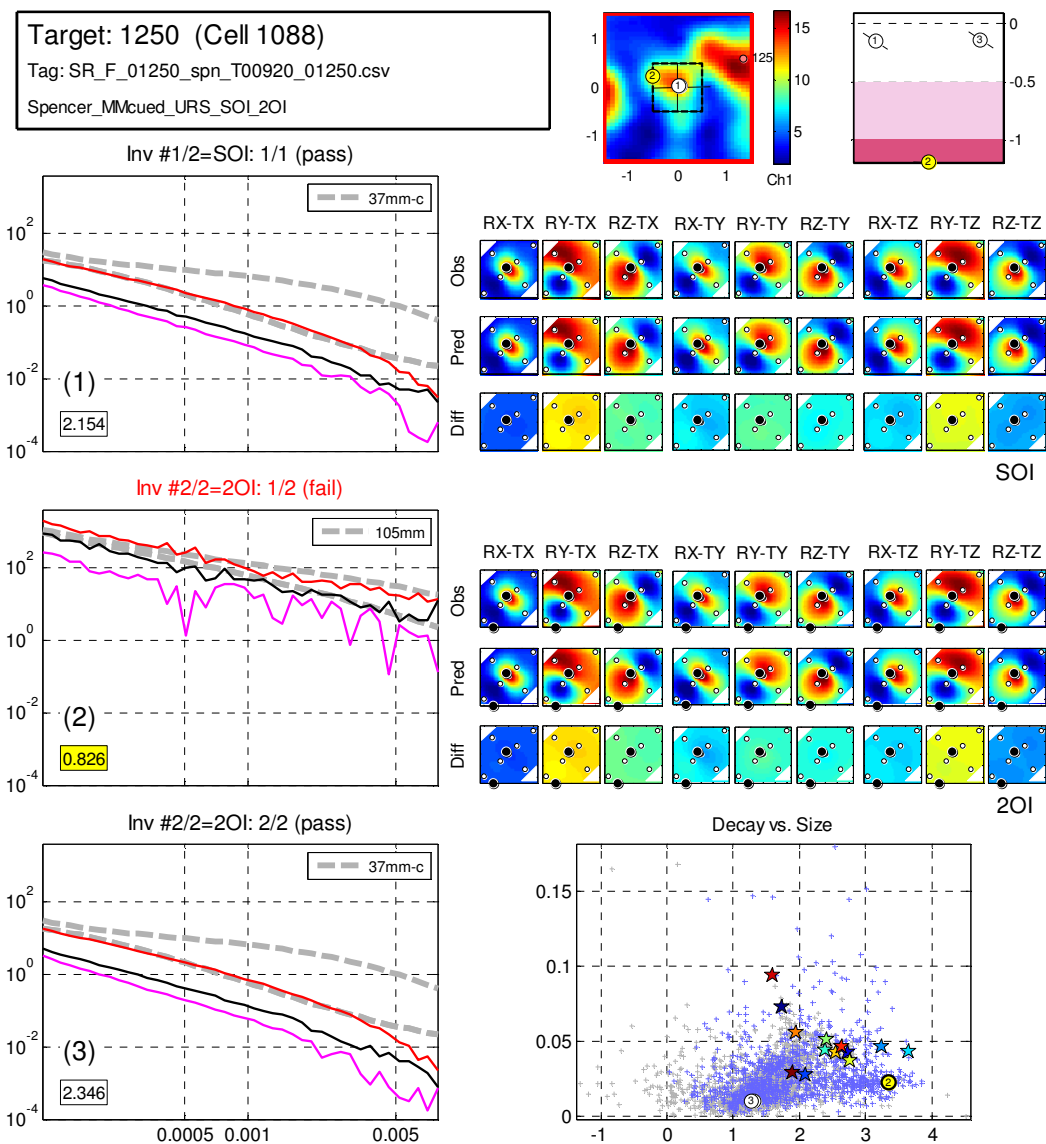


Figure 17: Example of an unrealistic 2OI model (anomaly 1250; frag). The first model of the 2OI (model 2) provides the best fit (i.e., minimum misfit) to the reference polarizabilities (misfit = 0.826), but the predicted depth of 1.2m and location at the edge of the instrument (i.e., at the vertical and horizontal inversion boundaries), and high amplitude and jittery appearance of the polarizabilities are classic signs that this model is an artifact of the multi-object inversion process. Accordingly, this model was failed during QC. Polarizabilities for SOI and 2OI are shown at left. Modeled target locations (X-Y and Z) are shown at the top right (gridded EM61 data is displayed behind the X-Y plot). Gridded observed, predicted and residual data for SOI and 2OI are shown below location maps. Decay versus size feature plot is shown in bottom right. Dots are test data; stars are reference items. Numbered circles are models for this anomaly.

The Spencer Open Area MetalMapper Cued dataset comprised 1104 unique anomalies. Of the 3312 total models, 2623 were passed and used in the classification process; 689 were failed. Thirteen anomalies were classified as “cannot extract reliable parameters” due to poor inversion results. One of these (anomaly 308) corresponded to a TOI (37mm). 102 anomalies were classified as “high likelihood UXO” during QC; 83 of these (81%) correspond to actual TOI. The total number of unique TOI in the Spencer Open Area is 86.

A.1.2 Classification (URS, Open Area)

Training data selection

Figure 18 shows the distribution of passed models in decay versus size feature space.

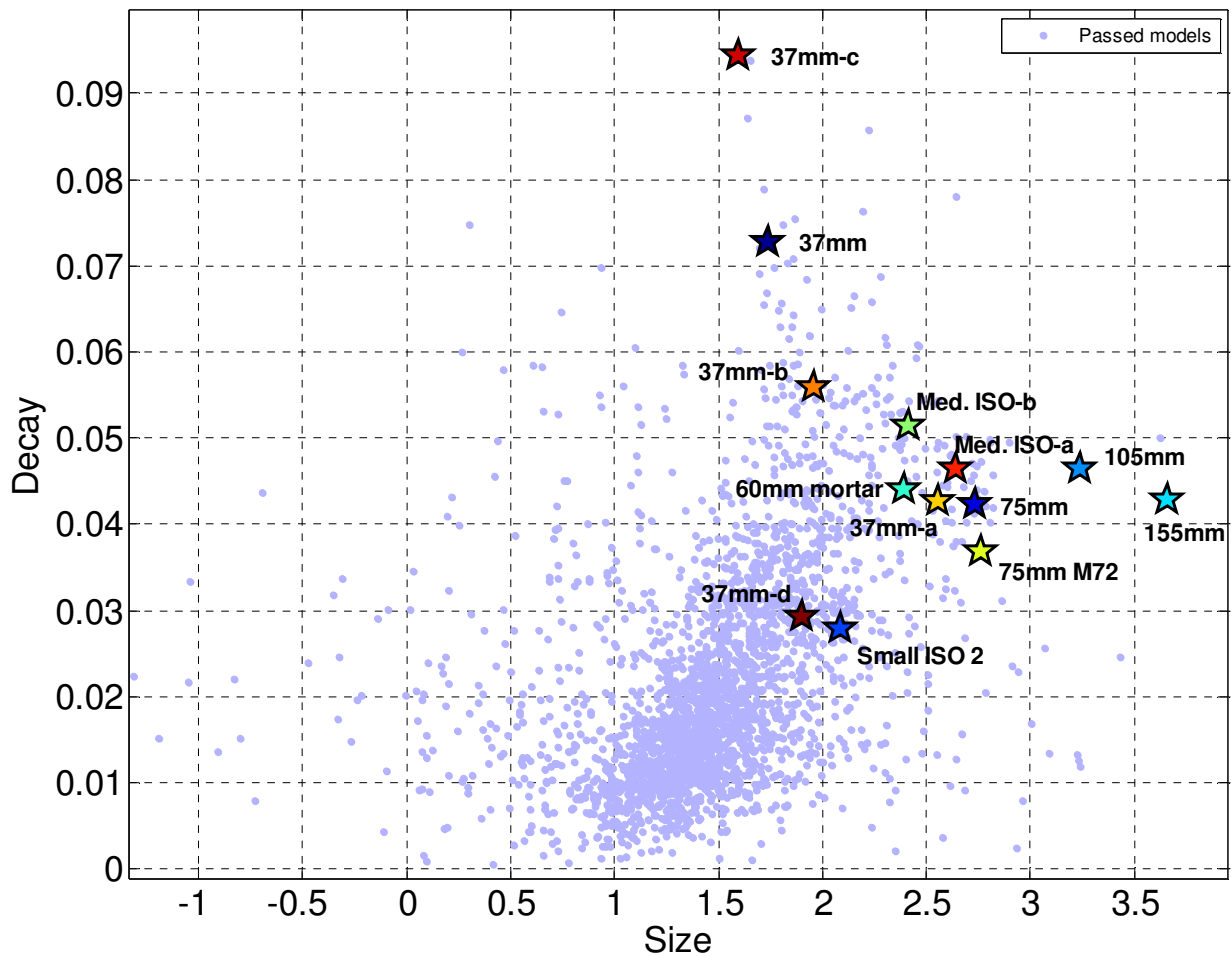


Figure 18: Distribution of passed models in decay(t_1, t_{29}) versus size(t_1) feature space, where size(t_1) is the total polarizability measured at the first time channel ($t_1=0.106\text{ms}$), and decay(t_1, t_{29}) is size(t_1)/size(t_{29}) where $t_{29}=2.006\text{ms}$. Some outliers are not shown. Labeled stars represent ordnance library reference items.

Our analysis method is based primarily on polarizability matching with respect to ordnance items in a reference library. For this approach to be successful it is important to determine the types of ordnance present at the site. During visual QC the analyst keeps track of suspicious, UXO-like items (i.e., items with modeled polarizabilities possessing UXO-like properties). Training data for some of these, particularly those with polarizabilities different from the items in the reference library, would be requested. In addition, we used our custom training data selection tool, *TrainZilla*, to explore feature space and automatically search for clusters of items with self-similar polarizabilities. In *TrainZilla*, the user selects a region in feature space by drawing a polygon, and the program automatically identify clusters of self-similar feature vectors by computing a misfit matrix \mathbf{M} with elements

$$M_{jk} = \sum_{i=1}^N (L^j_{total}(t_i) - L^k_{total}(t_i))^2$$

where L^j_{total} is the log-transformed total polarizability for the j^{th} feature vector. Feature vectors with mutual misfit less than a user-specified threshold define a cluster in polarizability space. This analysis helps to identify clusters that may not be readily evident in decay-size feature space: e.g., targets with consistent polarizabilities that may be hidden in the “cloud” of non-TOI features. A basic example of the use of *TrainZilla* is shown in Figure 19 and Figure 20.

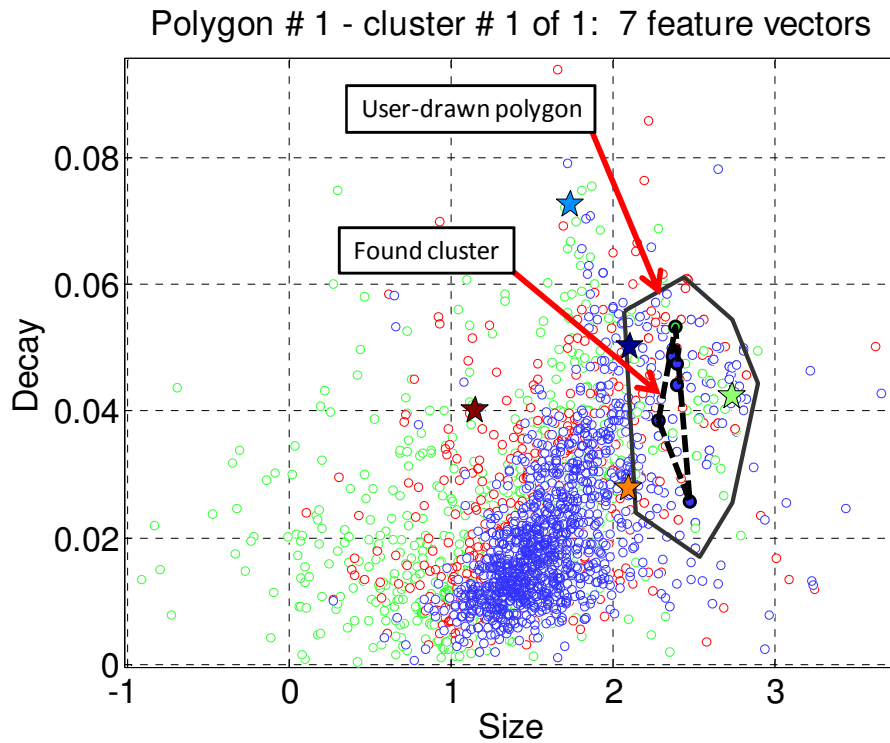


Figure 19: Example of use of the training data selection tool (*TrainZilla*). A polygon (solid black line) is drawn in feature space. Clusters of items with self-similar polarizabilities are automatically found based on the specified cluster search parameters. In this case a cluster comprising 7 features is visible (solid feature symbols encompassed by broken line). Polarizabilities for this cluster are shown in Figure 20.

Polygon 1 - Cluster 1 (7 pols)

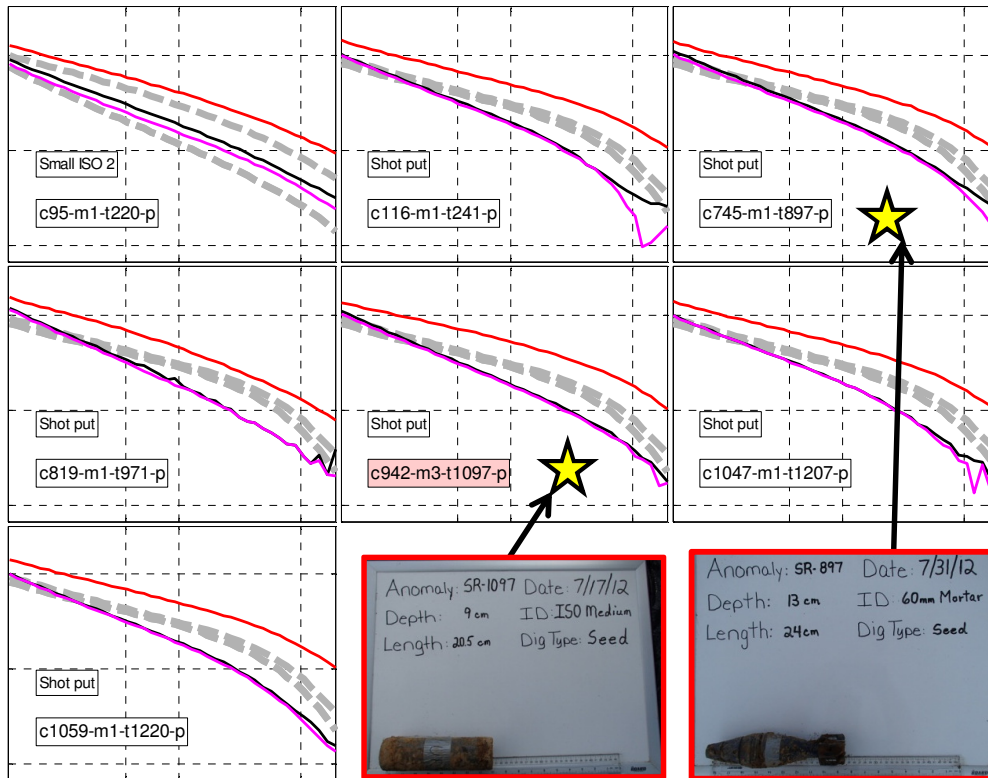


Figure 20: Polarizabilities for the cluster shown in Figure 19. Colored lines are predicted polarizabilities. Broken grey lines are best fitting reference polarizabilities. Training data were requested for Anomalies 897 and 1097 (stars); ground truth (photos) revealed that both of these anomalies are new TOI (relative to our starting ordnance reference library which comprised the four items from the test pit). Anomaly 897 is 60mm mortar; Anomaly 1097 is a medium ISO. These items were added to the reference library.

Our training data requests typically focused on: (1) items whose polarizabilities exhibited UXO-like properties distinct from those of items in our reference library; (2) items with polarizabilities similar to items in our reference library, but with degraded quality; and (3) one-off items. Figure 21 shows the location in decay-size feature space of all training requests. We paid particular attention to items with polarizabilities suggestive of small objects such as fuses and small caliber projectiles. All of these turned out to be non-TOI.

In our initial training request for 49 items, twelve of these were TOI, two of which were previously unknown ordnance items: 60mm mortar and medium ISO. We subsequently requested training on two more items, both of which proved to be non-TOI.

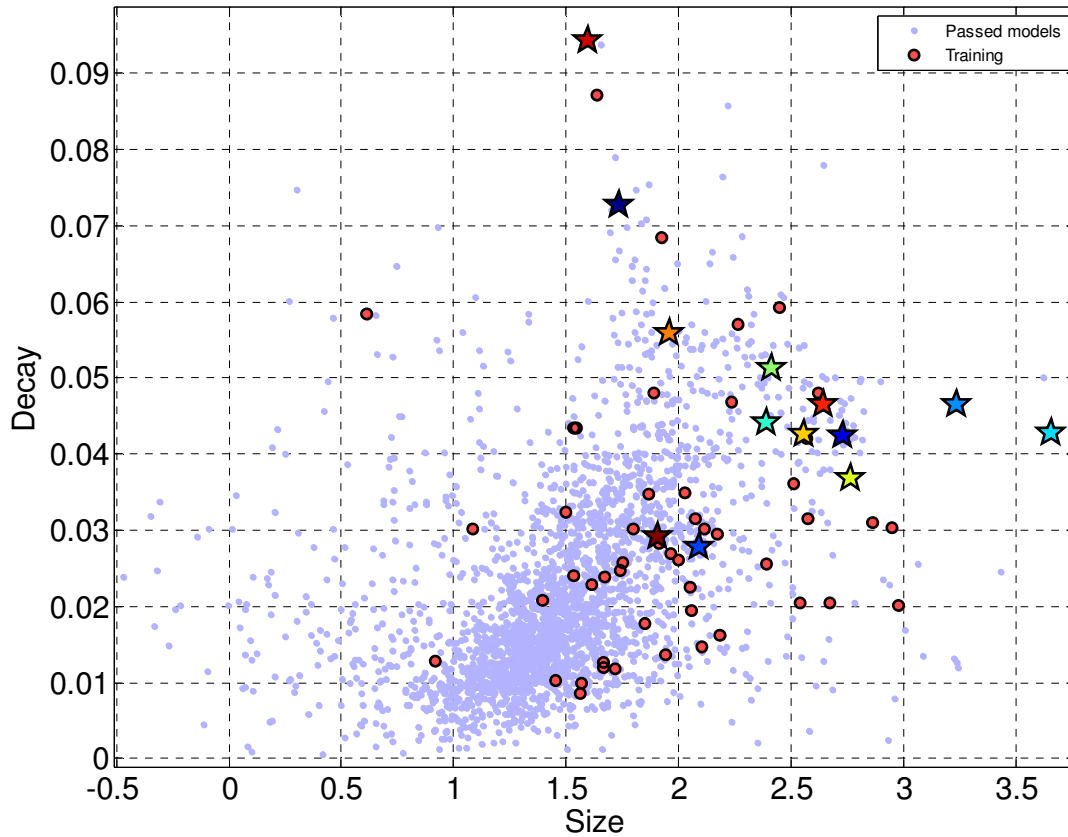


Figure 21: Decay versus size feature space plot showing passed models (blue dots) and the location of training data requests (red dots). Stars are library reference items.

A.1.3 Classification Method

Our dig lists were developed using the *DigZilla* module of UXOLab (Figure 22). *DigZilla* allows for the creation of multi-stage dig lists with minimal effort, and supports a number of classifiers.

Our initial dig list comprised two stages. For the early digs (1-201) the order was based on polarizability misfit using all three polarizabilities. The second stage (digs 202-1104) was based on polarizability misfit using only the primary polarizability. Figure 23 contains the polarizabilities used for classification.

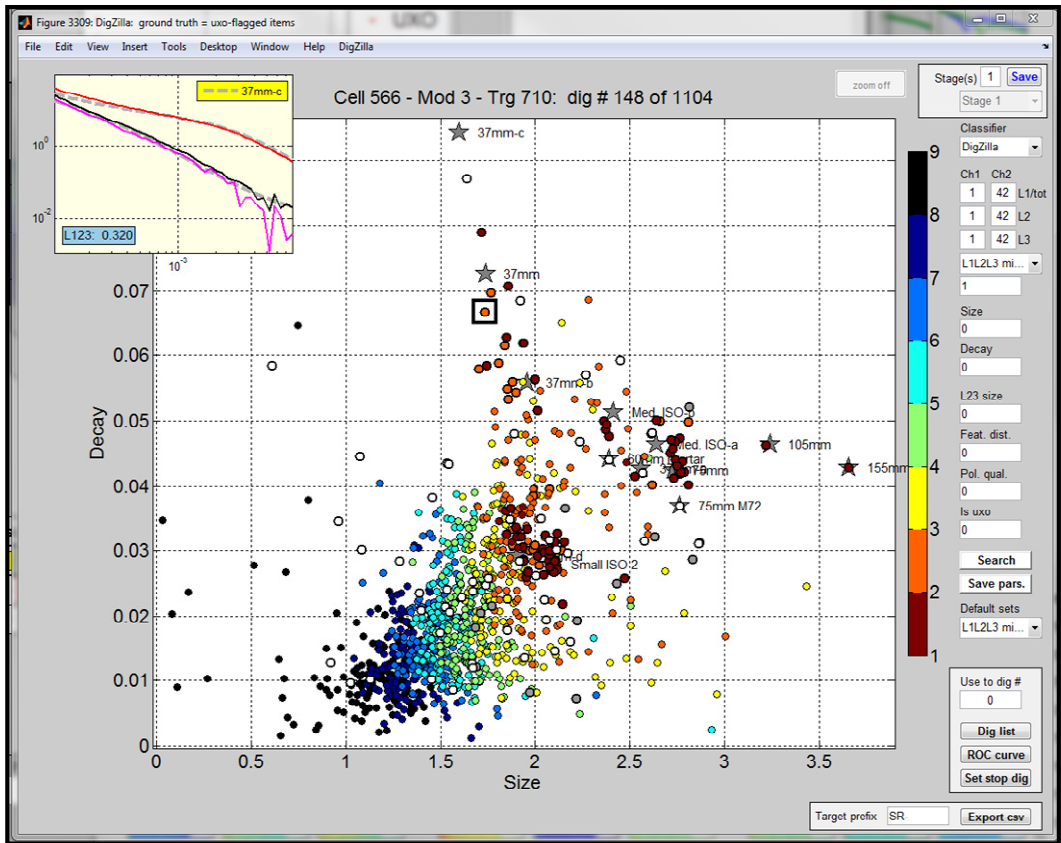


Figure 22: Screen shot of the *DigZilla* graphical user interface. Features in the decay versus size feature plot are color coded according to dig list order.

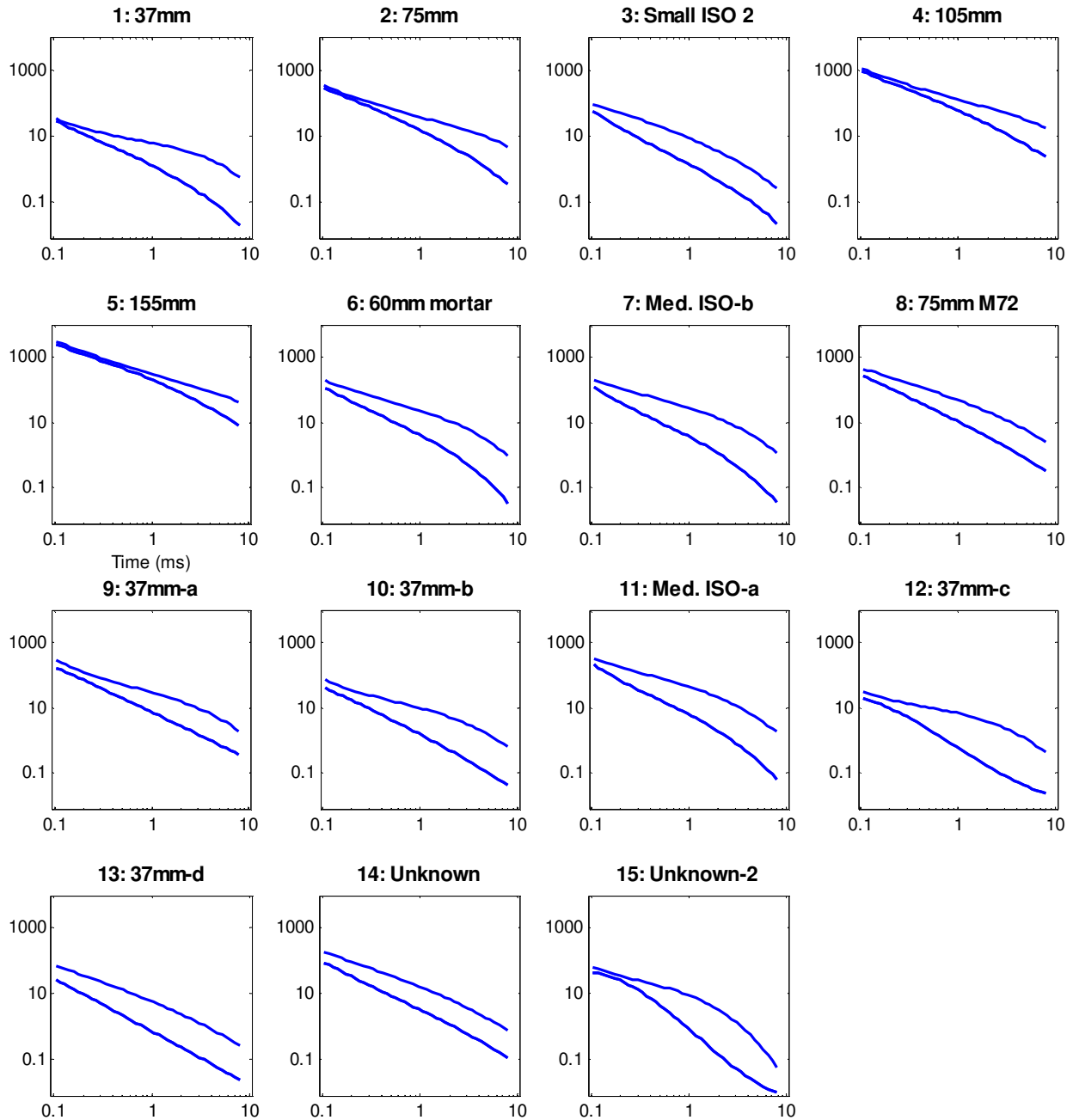


Figure 23: Ordnance library for the MetalMapper URS cued data. Polarizabilities 1 to 13 were used for the Open area. Polarizabilities 14 and 15 were added processing cued data acquired in the Dynamic area.

Additional details on our classification approach were provided in our Decision Memo, which is included below in its entirety.

Decision Memo

Site: Spencer URS

Analyst: Black Tusk Geophysics

Data: MM Cued

Date: Sept. 28, 2012

a. Criteria used to assign anomalies to the “can’t extract reliable parameters” class

Typically we classify an anomaly as “can’t extract reliable parameters” if either (1) the data misfit is large; and/or (2) the recovered model locations for all inversions are significantly distant from the center of the instrument. To identify anomalies in category (1) we use a measure of the data misfit (difference between observed and predicted data). Anomalies with misfit values for all inversions larger than 0.25 were flagged for follow-up visual inspection by an expert analyst. To identify anomalies in category (2) we look for anomalies with large offsets (>0.4m) for all models from all inversions. Anomalies meeting this criterion were flagged for follow-up visual inspection by an expert analyst. In the end, only one anomaly (SR-1063; Figure 24) was classified as cannot extract reliable parameters. [Subsequently, in later stages of the analysis, an additional twelve items were classified as cannot extract reliable parameters.]

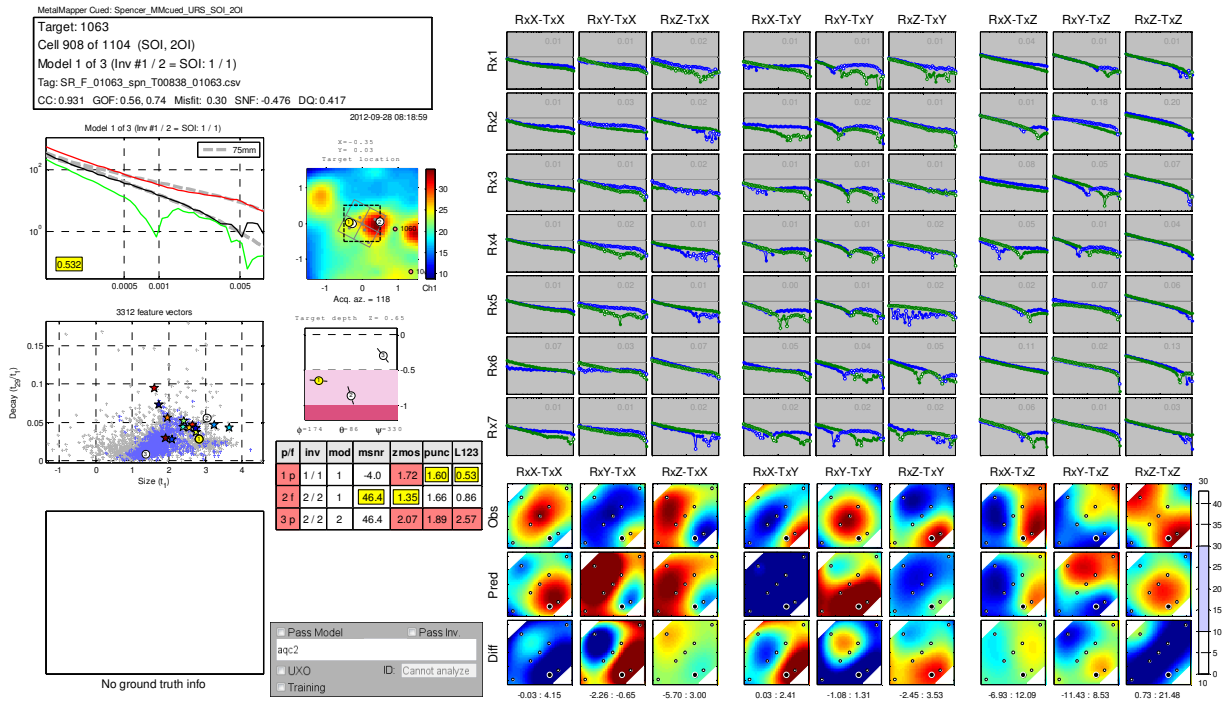


Figure 24: QC Tool display for Anomaly 1063. Large misfits between observed (blue lines in plots at top left) and predicted (green lines) data for most receiver-transmitter combinations for all inversions resulted in this anomaly being classified as cannot analyze.

b. Type of classification approach

We used a two-stage classifier based on matching of polarizabilities with reference UXO polarizabilities. Stage 1 was based on polarizability misfit to all three polarizabilities. Stage 2 was based on polarizability misfit to the primary polarizability.

c. List of features used for classification

Classification is based on polarizabilities. We used measures of polarizability misfits with respect to a library of reference UXO items.

d. Process used to select ground truth requests for training

We performed a semi-automated cluster analysis to search for clusters of items with self-similar polarizabilities. Clusters with polarizabilities that were judged to be UXO-like or even vaguely-UXO like were selected as clusters of interest. From these clusters of interest we typically selected a couple of example items for training data. In addition, anomalies lying on the edge of clusters of very likely UXO-like items would be selected for training data as a means of gauging both the potential variability of a cluster class, and the ability of the data to accurately recover the polarizabilities.

e. Values of all adjustable parameters and thresholds that were used in the final classification process

In the following table, wt = weight. L1L2L3 refers to polarizability matching with reference items using all three polarizabilities. L1 refers to polarizability matching with reference items using only the primary polarizability.

<p>STAGE 1: digs 1-201 L1L2L3 misfit (wt=1)</p>
<p>STAGE 2: digs 202-1104 L1 misfit (wt=1)</p>

f. Rationale used to specify the stop-dig point

Polarizabilities for each anomaly, arranged in dig list order, were visually inspected. The stop-dig point was chosen as the point at which the remaining polarizabilities were judged by an expert analyst to be unlikely to correspond to TOI.

The partial ROC curve for our stage 1, version 1 dig list is shown in Figure 25.

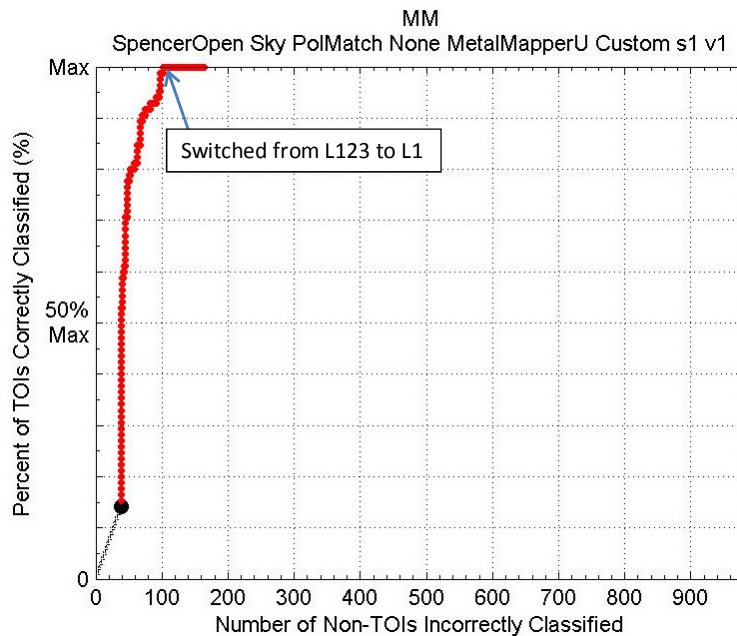


Figure 25: Partial ROC curve for the stage 1, version 1 dig list. The point at which the dig list switches between order based on matching all three polarizabilities to order based on only the primary polarizability is indicated.

The partial ground truth received with the scoring of the stage 1, version 1 dig list revealed two new TOI that were added to our reference library: 105mm and 155mm. Table 8. List of ordnance items in the reference library used in creating the final dig list. lists all of the ordnance items in reference library used when creating the final dig list.

Table 8. List of ordnance items in the reference library used in creating the final dig list.

Num	Name	Size (mm)
1	37mm	37
2	75mm	75
3	Small ISO 2	52
4	105mm	105
5	155mm	155
6	60mm mortar	60
7	Med. ISO-b	65
8	75mm M72	75
9	37mm-a	37
10	37mm-b	37
11	Med. ISO-a	65
12	37mm-c	37
13	37mm-d	37

Based on the results of the stage 1, version 1 dig list, we decided to make only one adjustment to the dig list: six additional anomalies were classified as “cannot analyze” due to poor data quality. The ROC curve for the stage 2, version 1 dig list looks very similar to Figure 25. The six extra digs were all non-TOI. Six additional anomalies (making a total of thirteen) were classified as “cannot analyze” due to poor data quality. Our stop dig point was increased by one dig. The classification parameters used in the final dig list are shown below.

Final (stage 3, version 1) dig list:

STAGE 1: digs 1-270
Same as S1 V1 dig list
STAGE 2: digs 271-1104
L1 misfit (wt=1)

The stop dig point was set at dig 271 (Anomaly 831). The partial ROC curve for this dig list is shown in Figure 26. No additional TOI were discovered relative to the stage 1 dig list.

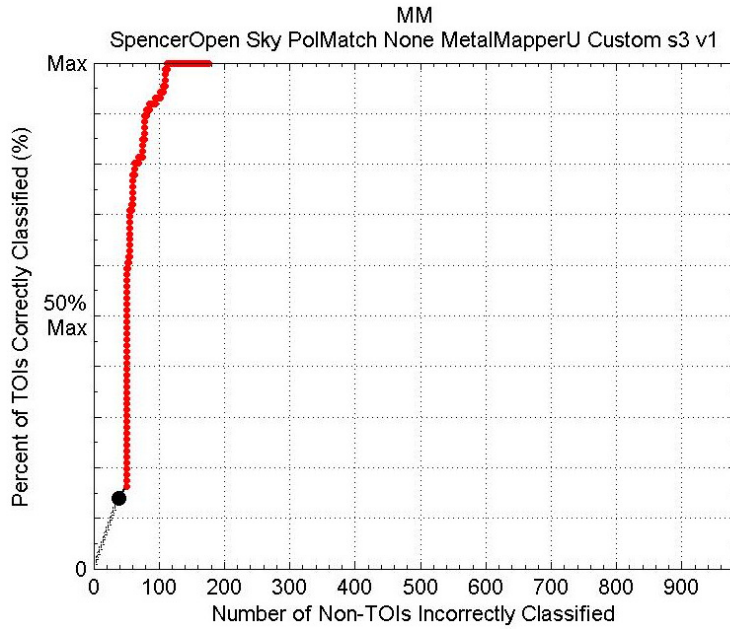


Figure 26: Partial ROC curve for the final (stage 3, version) 1 dig list.

The last TOI found was at dig 199, followed by 63 non-TOI digs. Based on these results, we considered it probable that all TOI had been dug.

The ROC curve for the final dig list is shown in Figure 27. There were no additional TOI beyond our stop dig point. We dug 262 items to find 86 TOI, giving a FAR of 2.05 non-TOI digs per TOI dig.

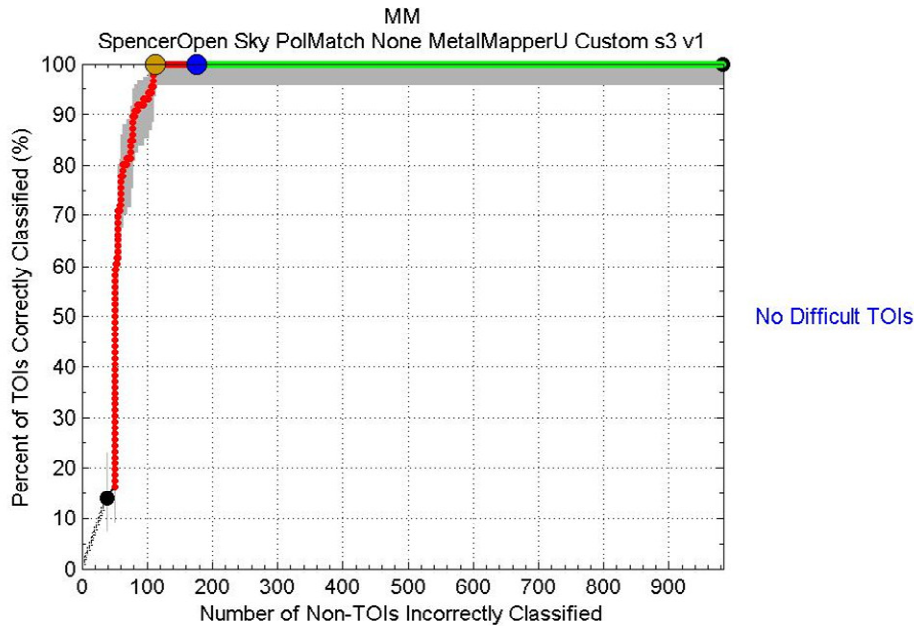


Figure 27: Final ROC curve for Spencer cued MetalMapper (URS) for the open area.

A.1.4 MetalMapper static retrospective analysis (open area)

Multi-object scenarios

The Spencer open area proved to be a relatively easy site. There were a limited number of TOI classes: 37mm, 60mm mortar, 75mm, small and medium ISOs, and two easy to detect large, one-off items (105mm and 155mm). There were no small unique items. Data quality was typically very good and there was minimal geologic noise.

At Spencer a number of the seeds were multi-object scenarios comprising one TOI and one piece of frag. In addition a number of other TOI seeds were found to be in close proximity to naturally occurring frag. This presents an opportunity to compare our two-object inversion (2OI) results with our single object inversion (SOI) results for the case of two objects within the field of view of the MetalMapper, and from this get a sense of the necessity for employing 2OI results in addition to SOI results when performing classification. Table 9 summarizes the results of the fifteen two-object scenarios. In half of the cases the SOI result was judged to be equally as good as the 2OI result. For the other half, the 2OI result (based on the similarity of the recovered polarizabilities to the relevant reference polarizabilities) are noticeably better.

Three examples (targets 194, 700 and 873) where the 2OI produces a noticeably better result than the SOI are shown in Figure 28. These results, and the other results listed in Table 9, show that, while a 2OI is not always necessary to get a good result in a two-object scenario, the 2OI is necessary in some cases to get the best possible result for classification.

Table 9: Summary of results from multi-object scenarios.

Target	Ground truth	TOI depth	Frag depth	Frag size rel. to TOI	Frag is seed	2OI better	Comment
194	ISO - Small+Other	22	13.5	similar	yes	yes	
207	ISO - Small+Frag	15	15	much smaller			SOI, 2OI both good
241	60mm mortar+Frag	12	24	similar	yes		
359	75mm projo+Frag	9	19.5	smaller	yes		2OI looks like 37mm
447	75mm projo+Frag	29	10.5	much smaller			SOI, 2OI both good
490	37mm projectile+Frag	26	3	much smaller		yes	SOI looks like small ISO
505	37mm projectile+Frag	8.5	27	similar			SOI, 2OI both good
700	ISO - Small+Other	6.5	10	similar		yes	
837	37mm projectile+Frag	27	28	similar	yes	yes	
873	ISO - Small+Frag	18	15	similar	yes	yes	SOI looks like 60mm
886	ISO - Small+Frag	20	45	similar	yes	yes	SOI looks like 60mm
950	75mm projectile body+240mm frag	7	10	smaller	yes		2OI looks like 37mm
971	ISO - Small+Frag	33	17	much smaller			SOI and 2OI look more like 60mm
1169	37mm projectile+Frag	10.5	3	much smaller			SOI, 2OI both good
1238	ISO - Small+Frag	21	24	similar	yes	yes	

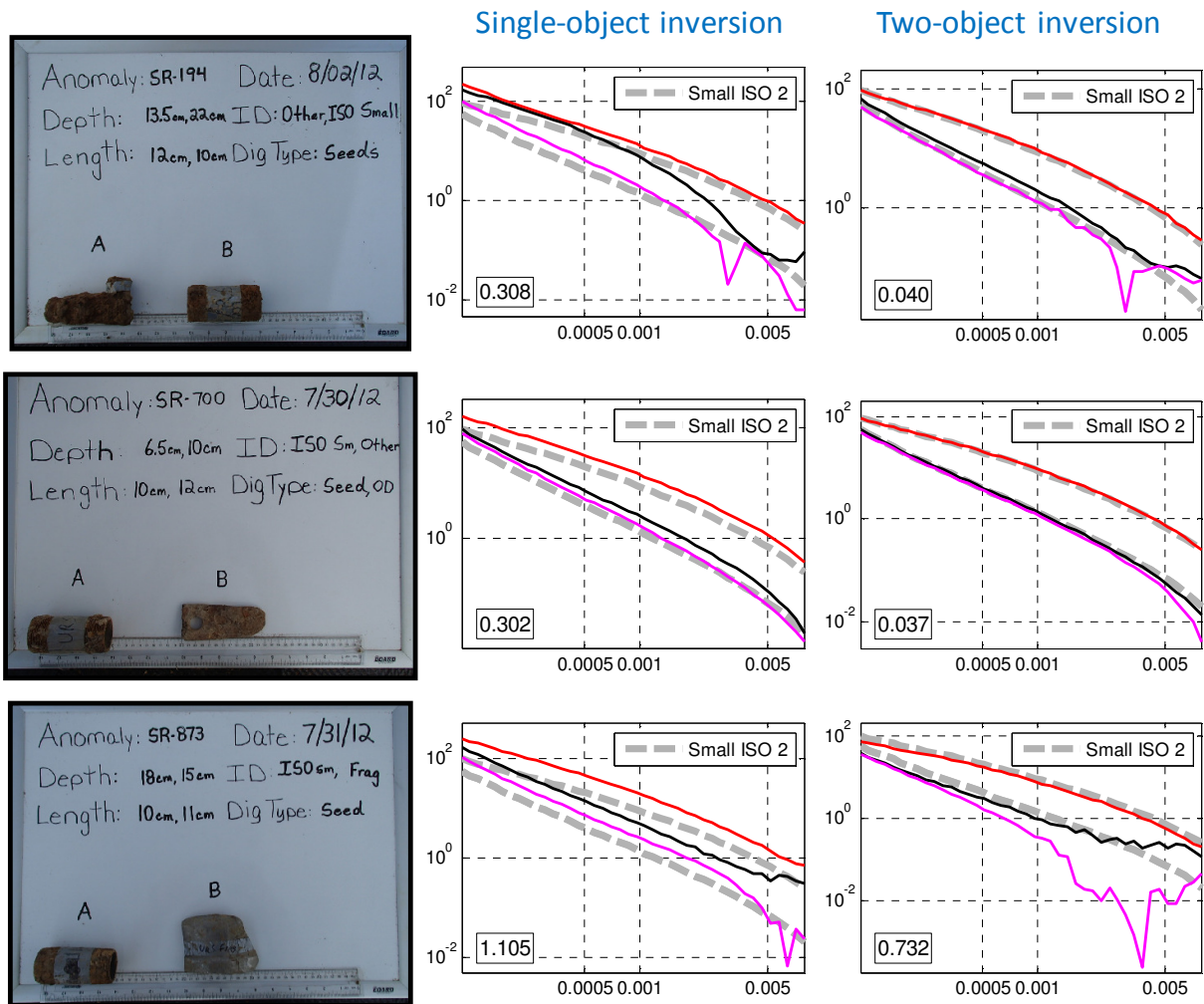


Figure 28: Comparison of SOI and 2OI inversion results for three two-object scenarios (targets 194, 700 and 873). In all three cases a piece of frag roughly equal in size to a small ISO was seeded with a small ISO. See Table 9 for details.

Small ISO consistency as measure of site difficulty

Small ISOs have been used as seed items at some of the recent Live Site demonstrations: Camp Beale (2011), Pole Mountain (2011) and Spencer (2012). The consistency of the recovered polarizabilities at each site can be viewed as a measure of the difficulty of each site for classification. Figure 29 shows the recovered polarizabilities for all small ISO anomalies in the Spencer open and dynamic areas. The overall consistency is quite good. Some of the more poorly recovered polarizabilities (e.g., Anomalies 1502 971, 873) are multi-object scenarios.

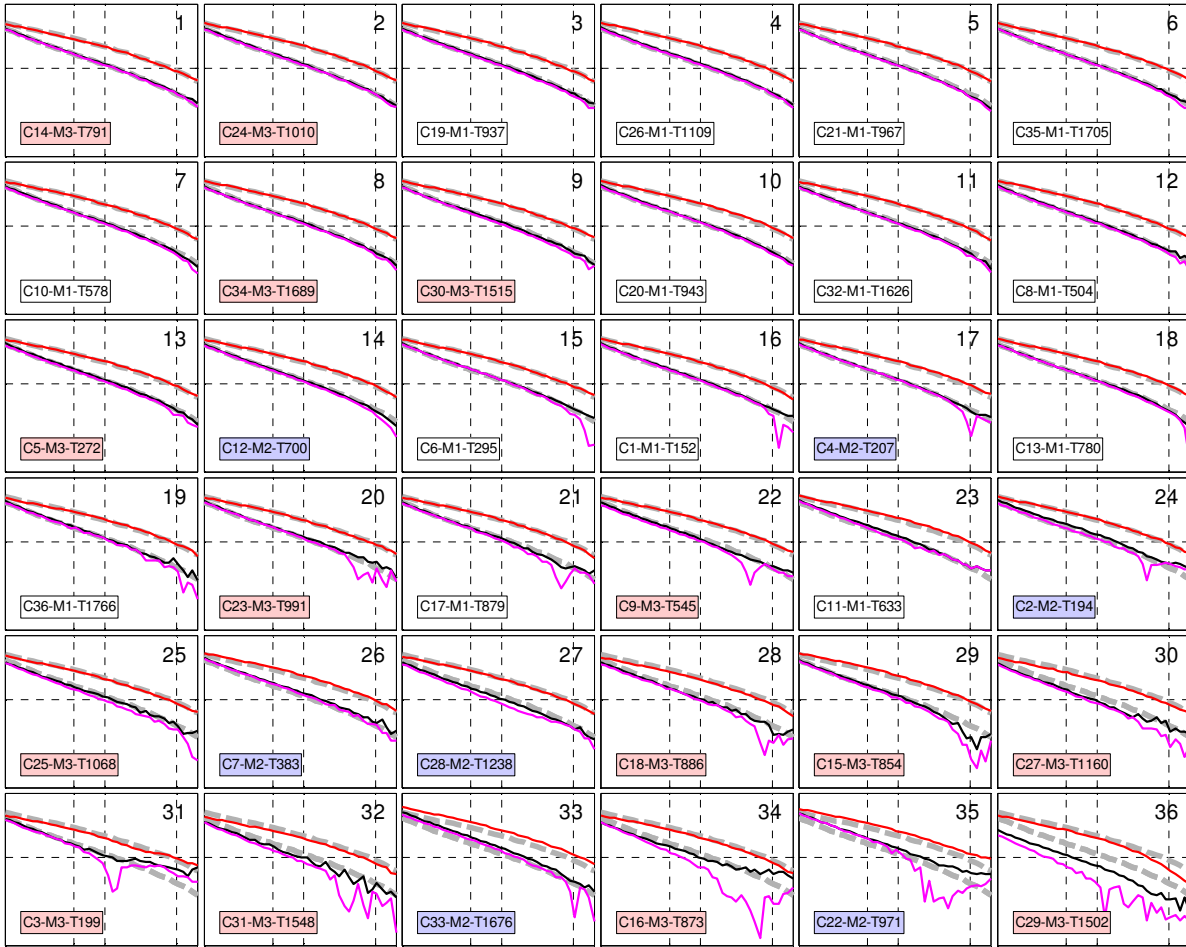


Figure 29: Polarizabilities for 36 small ISOs in the Spencer Open and Dynamic areas. Colored lines are predicted polarizabilities. Broken grey lines are small ISO reference polarizabilities taken from IVS measurements. Anomaly ID is the number after the “T” in each label. Polarizabilities are sorted by misfit (from best to worst) with respect to the small ISO reference model.

Figure 30 shows compilations of the polarizabilities for small ISOs at recent Live Site demonstrations. The mean misfit values, calculated with respect to the best fitting reference polarizability, is a good measure of site difficulty. It is clear that of the sites shown, Beale is the most challenging. The Beale Parsons and Beale CH2M Hill data sets comprise the same set of anomalies and the data were collected using the same MetalMapper instrument. For reasons that are not totally clear, but most likely related to differences in field practices, the Beale Parsons data resulted in more consistent ISO polarizabilities than the Beale CH2M Hill data. The excellent consistency of the Pole Mountain ISO polarizabilities reflects that site’s reputation as an easy site for classification. The Spencer URS ISO polarizabilities are slightly less consistent than the those from Pole Mountain, suggesting it is a slightly more challenging site. The consistency of the polarizabilities for the Spencer dataset collected by NAEVA is marginally better than that of the URS dataset (mean misfits of 0.22 and 0.26, respectively).

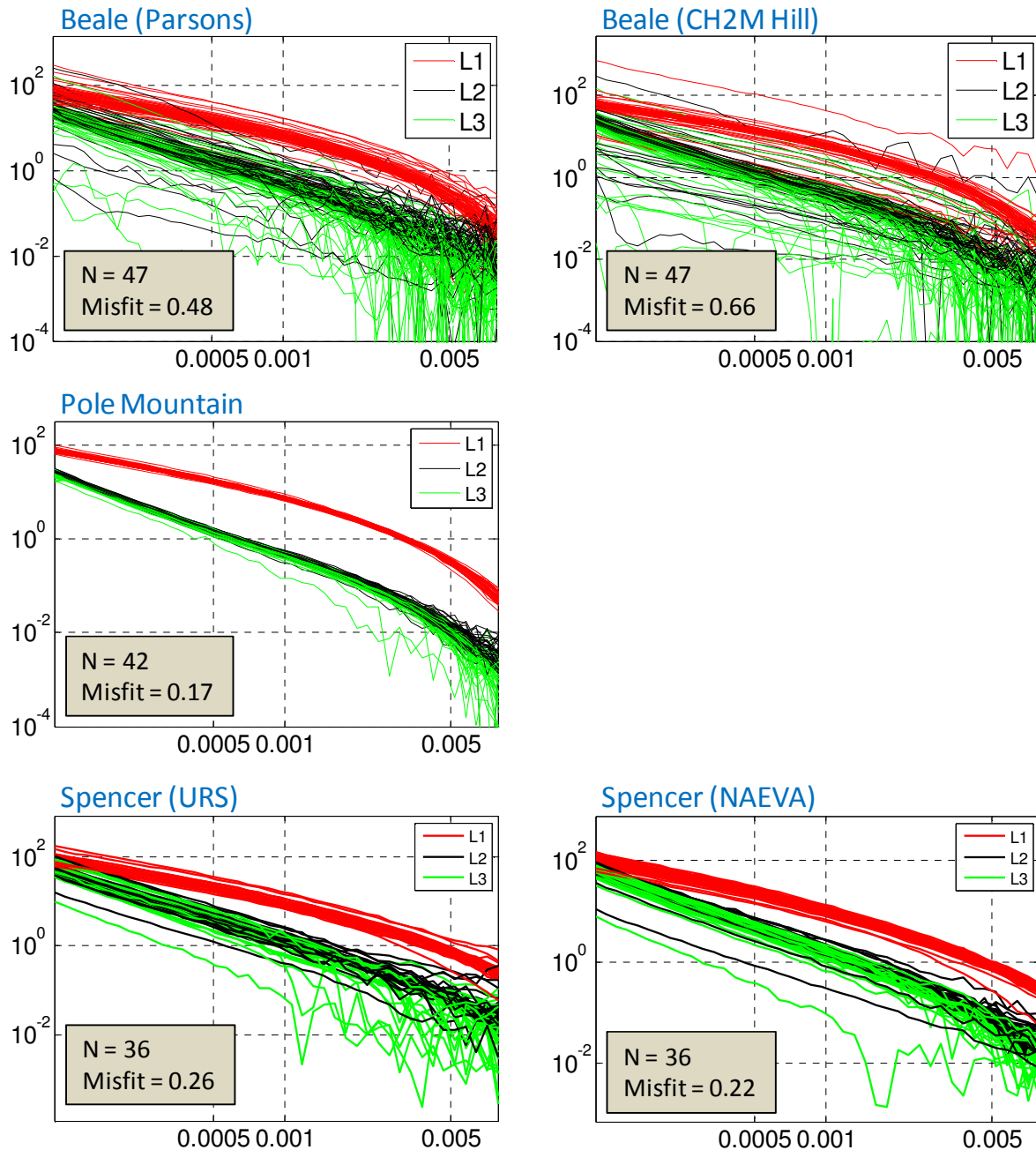


Figure 30: Compilations of polarizabilities for small ISOs from recent Live Site demonstrations. The two Beale and Spencer datasets each comprise the same set of anomalies but the data were collected by two different companies. The Spencer data include small ISOs from both the Open and Dynamic Areas. Misfit values are the mean misfits with respect to the reference polarizabilities calculated over all time channels using all three polarizabilities (L1, L2 and L3).

A.2 MetalMapper cued analysis (URS, Dynamic Area)

Cued MetalMapper data were also collected in the Dynamic Area. The Dynamic Area Cued dataset comprised 339 unique anomalies. Of the 1017 total (SOI and 2OI) models, 831 were passed and used in the classification process; 186 were failed. No anomalies were classified as "cannot extract reliable parameters" due to poor inversion results. 20 anomalies were classified as "high likelihood UXO" during QC; 18 of these (90%) correspond to actual TOI. The total number of unique TOI in the Spencer Dynamic Area is 23.

Analysis of the cued data in the dynamic area followed a very similar approach to the one used for the open area; only variations from the latter approach are noted here. We did not use any of the MM dynamic data to assist with the classification using the cued data. We did not request any training data for the dynamic area. We considered the ground truth that had been received (up to the stop dig point) for the open area to be sufficient training data. During visual QC of the data, a new class of suspicious, but unknown, TOI was added to the ordnance library based on the polarizabilities for Anomalies SR-1729 and SR-1550. Both of these turned out to be 37mm TOI. One of these (SR-1729) was a multi-object scenario (37mm with four medium to large pieces of frag). We also used our training data tool to look for other "hidden" clusters, but did not find any.

Our discrimination approach was similar to that used for the open area data. Our dig list comprised two stages. For the early digs (1-39) the order was based on polarizability misfit using all three polarizabilities. The second stage (digs 40-339) was based on polarizability misfit using only the primary polarizability. Our stop dig point was set at dig number 55.

Additional details on our classification approach were provided in our Decision Memo, which is included below in its entirety.

Decision Memo

Site: Spencer URS

Analyst: Black Tusk Geophysics

Data: MM Cued in Dynamic Area

Date: Jan. 2, 2013

a. Criteria used to assign anomalies to the "can't extract reliable parameters" class

Typically we classify an anomaly as "can't extract reliable parameters" if either (1) the data misfit is large; and/or (2) the recovered model locations for all inversions are significantly distant from the center of the instrument. To identify anomalies in category (1) we use a measure of the data misfit (difference between observed and predicted data). Anomalies with misfit values for all inversions larger than 0.25 were flagged for follow-up visual inspection by an expert analyst. To identify anomalies in category (2) we look for anomalies with large offsets (>0.4m) for all models

from all inversions. Anomalies meeting this criterion were flagged for follow-up visual inspection by an expert analyst. For the cued data in the Dynamic Area, no anomalies were classified as “can't extract reliable parameters” .

b. Type of classification approach

We used a two-stage classifier based on matching of polarizabilities with reference UXO polarizabilities. Stage 1 was based on polarizability misfit to all three polarizabilities. Stage 2 was based on polarizability misfit to the primary polarizability. We did not use any of the MM dynamic data to assist in the classification approach

c. List of features used for classification

Classification is based on polarizabilities. We used measures of polarizability misfits with respect to a library of reference UXO items.

d. Process used to select ground truth requests for training

We performed our usual semi-automated cluster analysis to search for clusters of items with self-similar polarizabilities. Not finding any new items of concern, we decided to not ask for additional training data. Effectively, we are using the data from the Open Area as training data.

e. Values of all adjustable parameters and thresholds that were used in the final classification process

In the following table, wt = weight. L1L2L3 refers to polarizability matching with reference items using all three polarizabilities. L1 refers to polarizability matching with reference items using only the primary polarizability.

STAGE 1: digs 1-39 L1L2L3 misfit (wt=1)
STAGE 2: digs 40-339 L1 misfit (wt=1)

f. Rationale used to specify the stop-dig point

Polarizabilities for each anomaly, arranged in dig list order, were visually inspected. The stop-dig point was chosen as the point at which the remaining polarizabilities were judged by an expert analyst to be unlikely to correspond to TOI.

The partial ROC curve for our stage 1, version 1 dig list is shown in Figure 31.

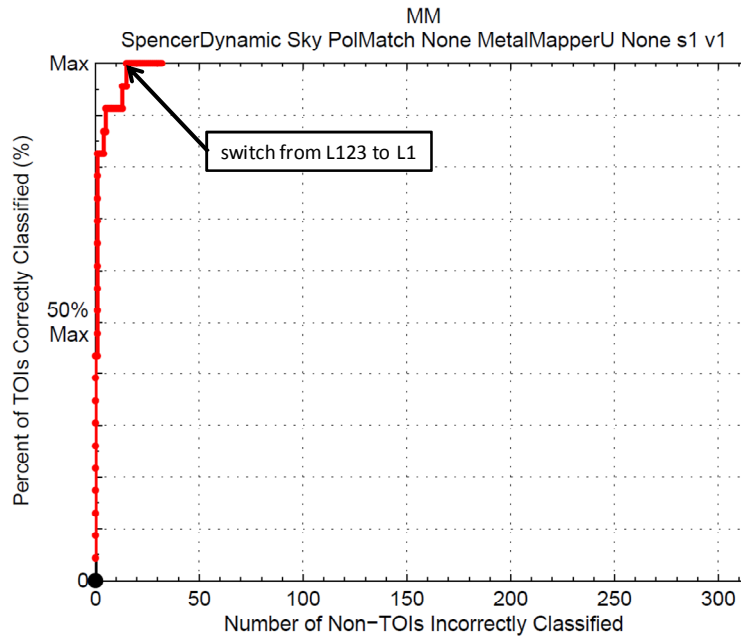


Figure 31: Partial ROC curve for the stage 1, version 1 dig list. The point at which the dig list switches between order based on matching all three polarizabilities to order based on only the primary polarizability is indicated.

The partial ground truth received with the scoring of the stage 1, version 1 dig list did not reveal any new TOI classes, or any other surprises. Based on the results of the stage 1, version 1 dig list, we decided to make only one minor adjustment to the dig list: the stop dig point was extended by three additional digs (58 total digs). The ROC curve for the stage 2, version 1 dig list looks very similar to Figure 31. The three extra digs were all non-TOI. The last TOI found was at dig 38, followed by 20 non-TOI digs. Based on these results, we considered it probable that all TOI had been dug.

The ROC curve for the final dig list is shown in Figure 32. There were no additional TOI beyond our stop dig point. We dug 58 items to find 23 TOI, giving a FAR of 1.52 non-TOI digs per TOI dig.

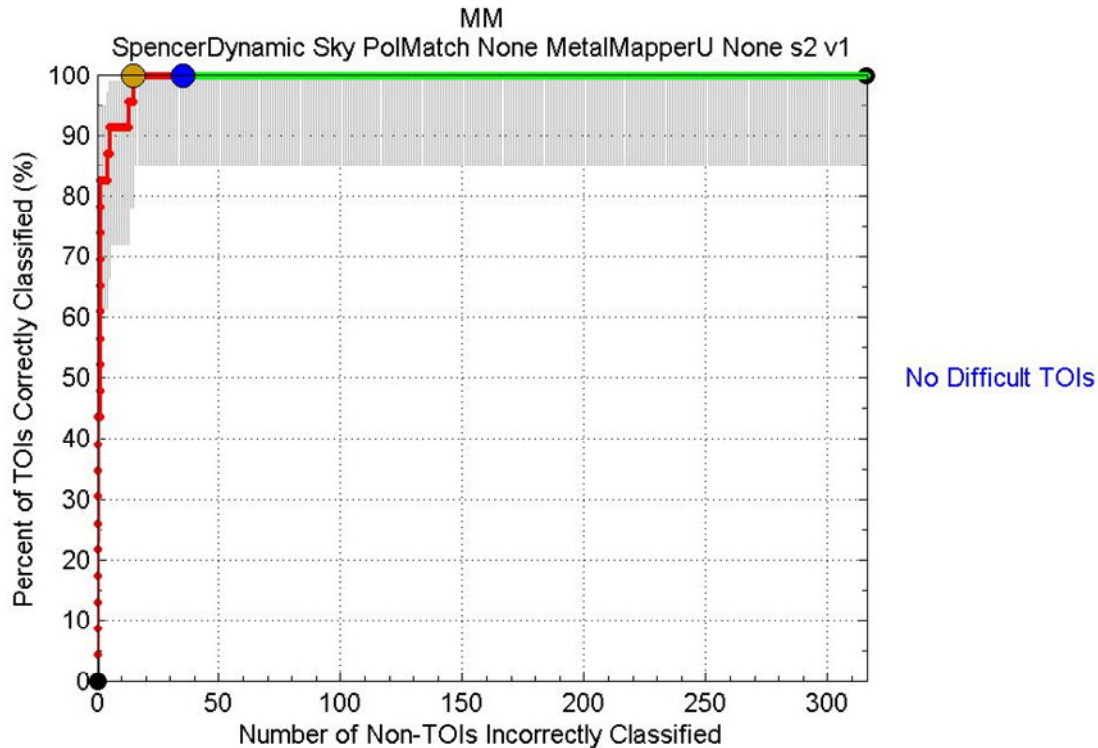


Figure 32: Final ROC curve for Spencer cued MetalMapper (URS) for the dynamic area.

Like the open area, the Spencer dynamic area proved to be a relatively easy site for classification with MetalMapper cued data. There were a limited number of TOI classes: 37mm, 60mm mortar, 75mm, small and medium ISOs, and one easy to detect large, one-off item (105mm). There were no small unique items. Data quality was typically very good and there was minimal geologic noise - ideal conditions for successful classification.

A.3 NAEVA MetalMapper Cued Feature Extraction and Discrimination

A.3.1 Feature extraction (Naeva, Open Area)

MetalMapper cued data for all anomalies were received as a set of raw TEM files and two sets of CSV files (with and without background corrections). Our analyses used the background-corrected data. Data import, inversion and model selection were performed exactly as described in Section A.1.1 Feature extraction (URS, Open Area) for the MetalMapper cued data collected by URS.

The Spencer Open Area MetalMapper Cued dataset comprised 1104 unique anomalies. The Naeva MetalMapper data also included a number of recollects which brought the total of cued data measurements to 1286. Single and 2 object inversions were performed for all measurements with a small subset of the measurements also having a 3 object inversion performed. In total the dataset contained 3917 models, with 2904 passed and used in the classification process; 1013 failed. Three anomalies were classified as “cannot extract reliable parameters”. Two of these (targets SR-571, SR-814) were a result of poor inversion results and one (target SR-512) because there was no data collected at the anomaly location. 161 anomalies were classified as “high likelihood UXO” during QC. The total number of unique TOI in the Spencer Open Area is 86. Of the false positives, the large majority were a result of small

pieces of frag which produced polarizabilities in excellent agreement with an item in the reference library as shown in Figure 1.

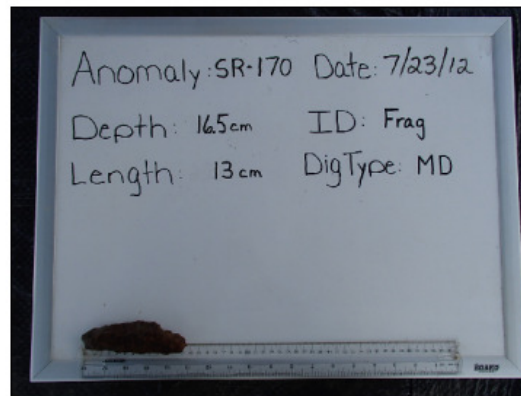
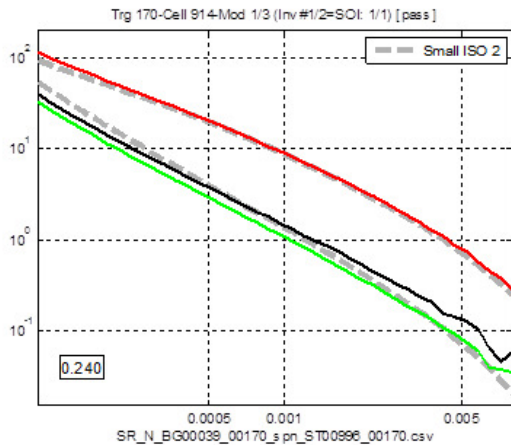
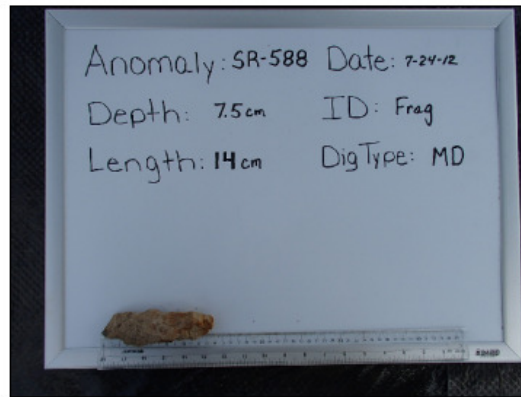
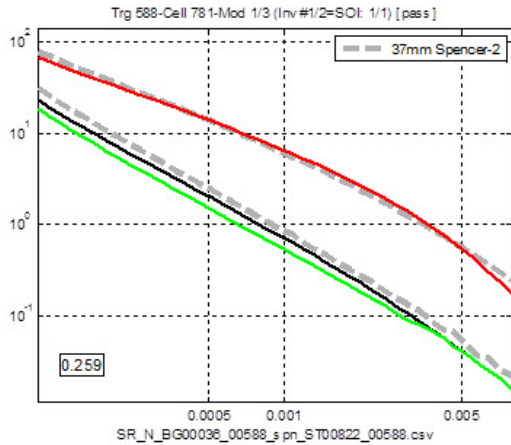


Figure 33: False positives where frag similar in size to a TOI in the reference library results in polarizabilities that are an excellent match to reference items. Reference polarizabilities are indicated by dashed grey line.

A.3.2 Classification (Naeva, Open Area)

Training data selection

Figure 34 shows the distribution of passed models in decay versus size feature space. Our analysis method is based primarily on polarizability matching with respect to ordnance items in a reference library. For this approach to be successful it is important to determine the types of ordnance present at the site. During visual QC the analyst keeps track of suspicious, UXO-like items (i.e., items with modeled polarizabilities possessing UXO-like properties). Training data for some of these, particularly those with polarizabilities different from the items in the reference library, would be requested. In addition, we used our custom training data selection tool, *TrainZilla*, to explore feature space and automatically search for clusters of items with self-similar polarizabilities. In *TrainZilla*, the user selects a region in feature space by drawing a polygon, and the program automatically identify clusters of self-similar feature vectors.

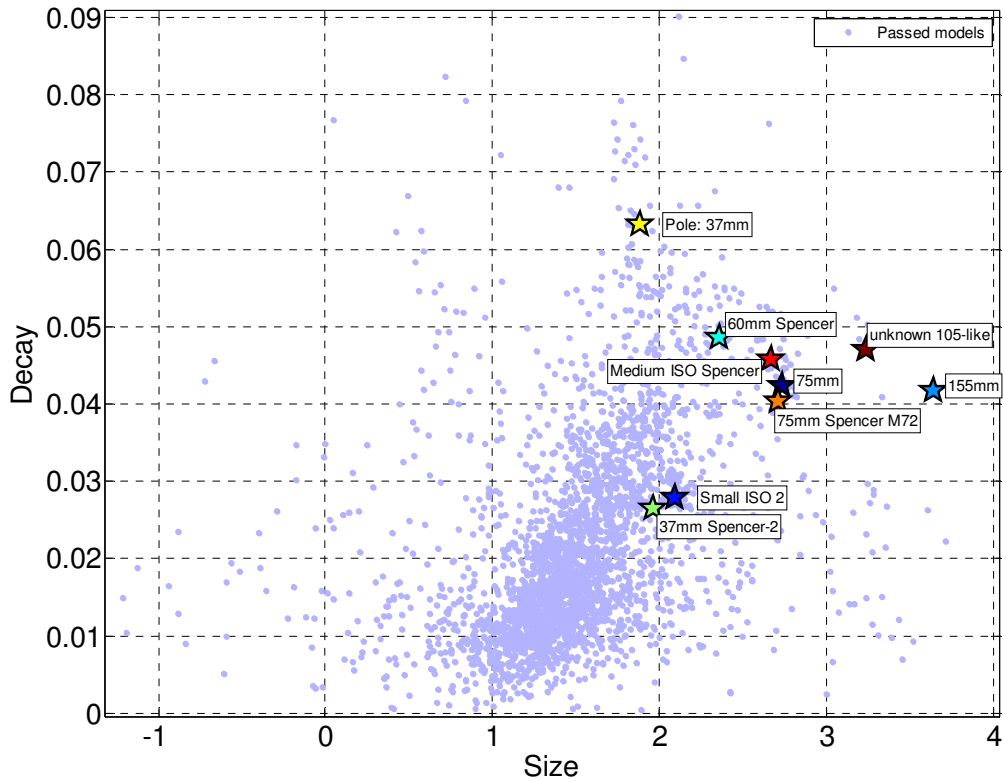


Figure 34: Distribution of passed models in decay(t1,t29) versus size(t1) feature space, where size(t1) is the total polarizability measured at the first time channel (t1=0.106ms), and decay(t1,t29) is size(t1)/size(t29) where t29=2.006ms. Labeled stars represent ordnance library reference items.

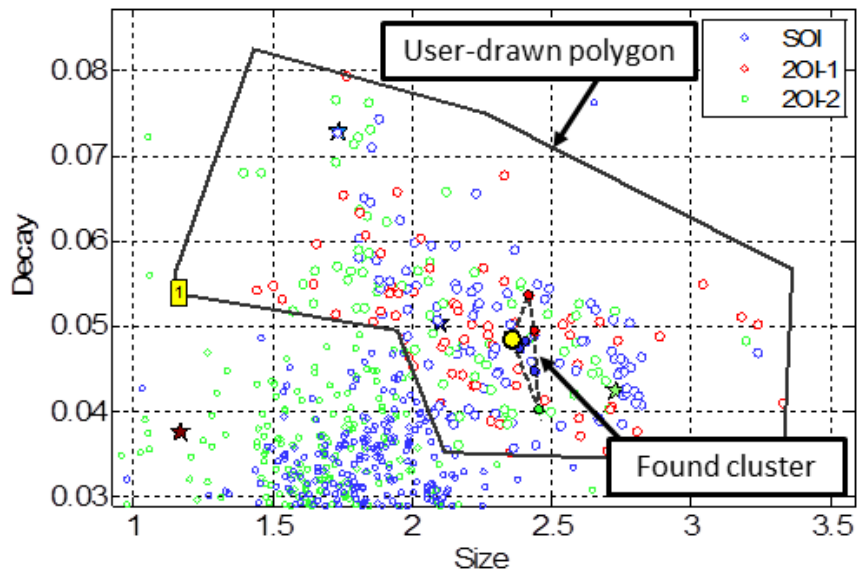


Figure 35: Example of use of the training data selection tool (*TrainZilla*). A polygon (solid black line) is drawn in feature space. Clusters of items with self-similar polarizabilities are automatically found based on the specified cluster search parameters. In this case a cluster comprising 7 features is visible (solid feature symbols encompassed by broken line). Polarizabilities for this cluster are shown in Figure 4.

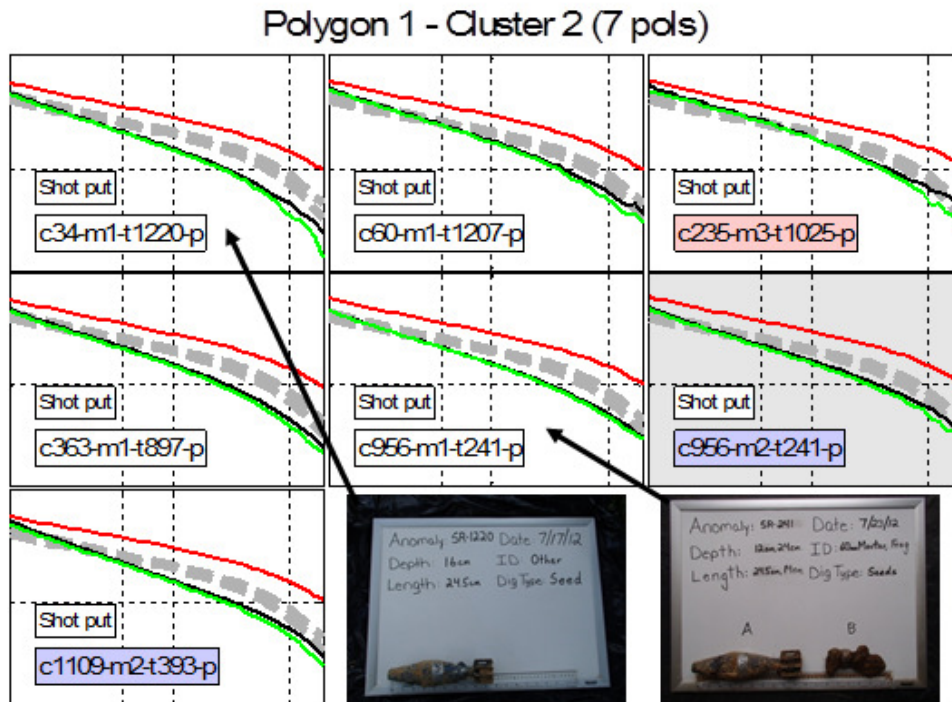


Figure 36: Polarizabilities for the cluster shown in Figure 3. Colored lines are predicted polarizabilities. Broken grey lines are best fitting reference polarizabilities. Training data were requested for Anomalies 1220 and 241; ground truth (photos) revealed that both of these anomalies were 60mm mortars, a new TOI (relative to our starting ordnance reference library which comprised the four items from the test pit). These items were added to the reference library.

Our training data requests typically focused on: (1) items whose polarizabilities exhibited UXO-like properties distinct from those of items in our reference library; (2) items with polarizabilities similar to items in our reference library, but with degraded quality; and (3) one-off items. Figure 21 shows the location in decay-size feature space of all training requests. We paid particular attention to items with polarizabilities suggestive of small objects such as fuzes and small caliber projectiles. All of these turned out to be non-TOI.

In our initial training request for 35 items, eight of these were TOI, two of which were previously unknown ordnance items: 60mm mortar and medium ISO. No additional training data was requested.

Classification method

Our dig lists were developed using *DigZilla* (Figure 22), which is fully integrated into UXOLab. *DigZilla* allows for the creation of multi-stage dig lists with minimal effort, and supports a number of classifiers. Our initial dig list comprised two stages. For the early digs (1-201) the order was based on polarizability misfit using all three polarizabilities. The second stage (digs 202-1104) was based on polarizability misfit using only the primary polarizability. Additional details on our classification approach were provided in our Decision Memo, which is included below in its entirety.

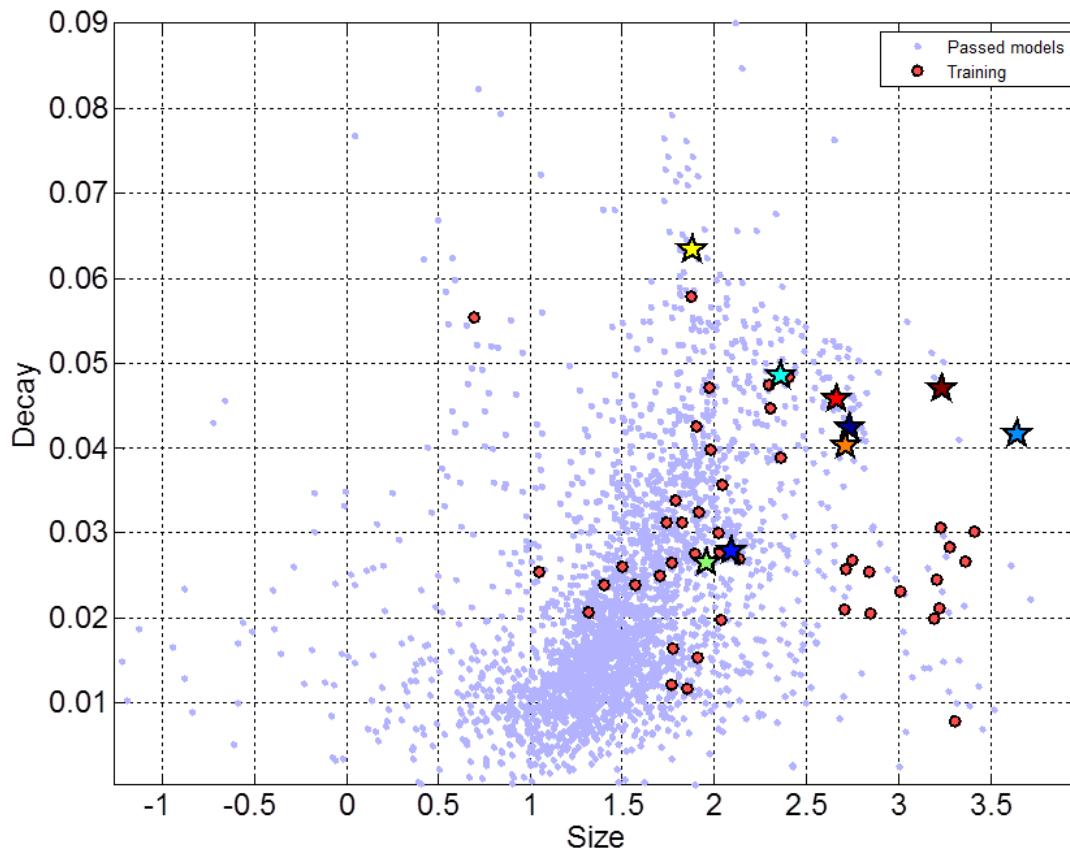


Figure 37: Decay versus size feature space plot showing passed models (blue dots) and the location of training data requests (red dots). Stars are library reference items.

Decision Memo

Site: Spencer NAEVA

Analyst: Black Tusk Geophysics

Data: MM Cued

Date: Dec. 20, 2012

a. Criteria used to assign anomalies to the “can’t extract reliable parameters” class

Typically we classify an anomaly as “can’t extract reliable parameters” if either (1) the data misfit is large; and/or (2) the recovered model locations for all inversions are significantly distant from the center of the instrument. To identify anomalies in category (1) we use a measure of the data misfit (difference between observed and predicted data). Anomalies with misfit values for all inversions larger than 0.25 were flagged for follow-up visual inspection by an expert analyst. To identify anomalies in category (2) we look for anomalies with large offsets (>0.4m) for all models from all inversions. Anomalies meeting this criterion were flagged for follow-up visual inspection by an expert analyst. In the end, only two anomalies (SR-571; Figure 24, SR-814) were classified as can’t extract reliable parameters. In addition, SR-512 was also placed into can’t extract reliable parameters because the raw data files were corrupt and could not be inverted.

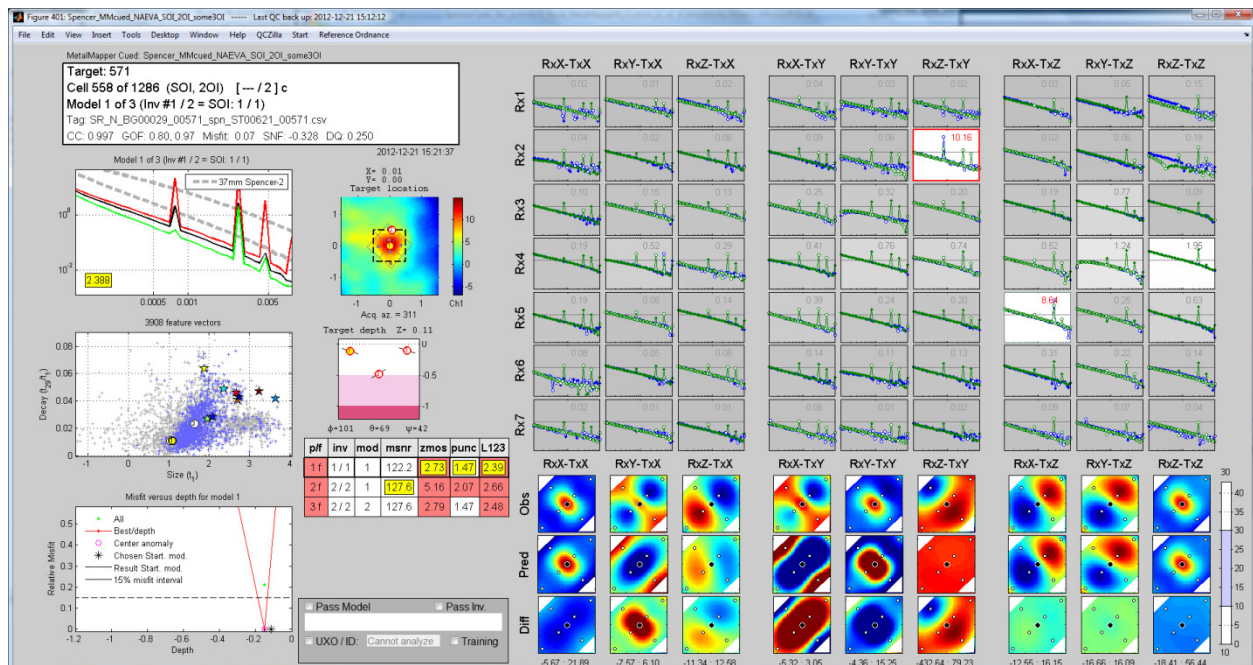


Figure 38: QC Tool display for Anomaly 571. Large misfits between observed (blue lines in plots at top left) and predicted (green lines) data for most receiver-transmitter combinations for all inversions resulted in this anomaly being classified as cannot analyze.

b. Type of classification approach

We used a classifier based on a combination of (1) matching polarizabilities with reference UXO polarizabilities and (2) decay rate. The specific weightings applied to polarizabilities and decay rate were automatically calculated via routines that sample the features of the dataset. There were no manual user manipulations performed on the automated diglist.

c. List of features used for classification

Classification is based on polarizabilities and decay. We used measures of polarizability misfits with respect to a library of reference UXO items. Decay was defined as the ratio of the 29th and the 1st time channels.

d. Process used to select ground truth requests for training

We performed a semi-automated cluster analysis to search for clusters of items with self-similar polarizabilities. Clusters with polarizabilities that were judged to be UXO-like or even vaguely-UXO like were selected as clusters of interest. From these clusters of interest we typically selected a couple of example items for training data. In addition, anomalies lying on the edge of clusters of very likely UXO-like items would be selected for training data as a means of gauging both the potential variability of a cluster class, and the ability of the data to accurately recover the polarizabilities.

e. Values of all adjustable parameters and thresholds that were used in the final classification process

In the following table, wt = weight. L1L2L3 refers to polarizability matching with reference items using all three polarizabilities. DR refers to decay ranked from slowest decaying to fastest decaying based on the ratio of the 29th and the 1st time channels.

STAGE 1: digs 1-1104 L1L2L3 misfit (wt=1), DR (wt=0.5)
--

f. Rationale used to specify the stop-dig point

Polarizabilities for each anomaly, arranged in dig list order, were visually inspected. The stop-dig point was chosen as the point at which the remaining polarizabilities were judged by an expert analyst to be unlikely to correspond to TOI.

The partial ROC curve for our stage 1, version 1 dig list is shown in Figure 39.

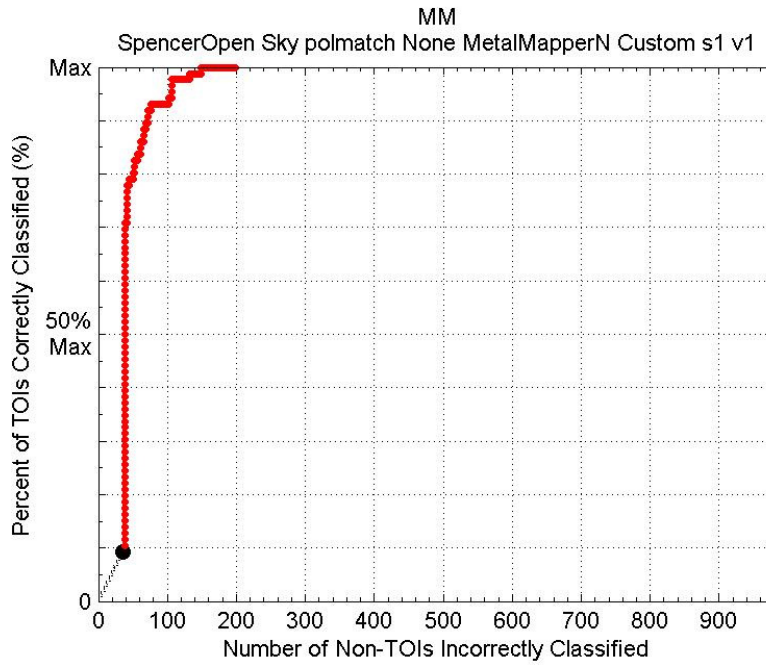


Figure 39: Partial ROC curve for the stage 1, version 1 dig list.

The partial ground truth received with the scoring of the stage 1, version 1 dig list did not reveal any new TOI. Table 8. List of ordnance items in the reference library used in creating the final dig list.

Table 10: List of ordnance items in the reference library used in creating the final dig list.

Num	Name	Size (mm)
1	75mm	75
2	Small ISO 2	52
3	155mm	155
4	60mm mortar	60
5	37mm	37
6	Pole: 37mm	37
7	75mm M72	75
8	Med. ISO-a	65
9	105mm	105

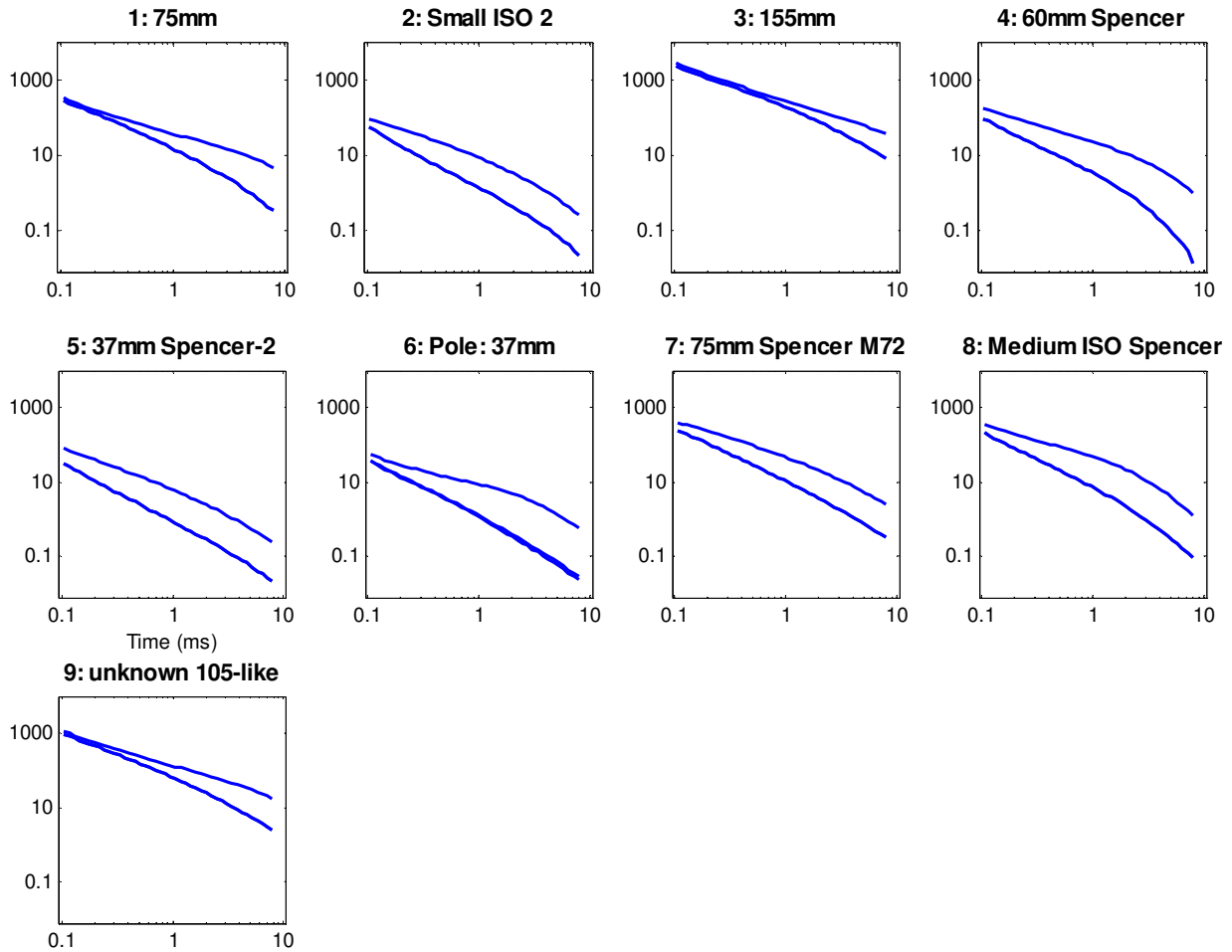


Figure 40: Ordnance library used when processing the MetalMapper Naeva cued data.

Based on the results of the stage 1, version 1 dig list, we decided to not make any adjustments to the dig list. The last TOI found was at dig 252, followed by 50 non-TOI digs. Based on these results, we considered it probable that all TOI had been dug. Our stop dig point was kept at dig 302 and the classification parameters used in the final dig list remained unchanged.

Final (stage 3, version 1) dig list:

STAGE 1: digs 1-1104
 L1L2L3 misfit (wt=1), DR (wt=0.5)

The ROC curve for the final dig list is shown in Figure 27. There were no additional TOI beyond our stop dig point. We dug 252 items to find 86 TOI, giving a FAR of 1.93 non-TOI digs per TOI dig.

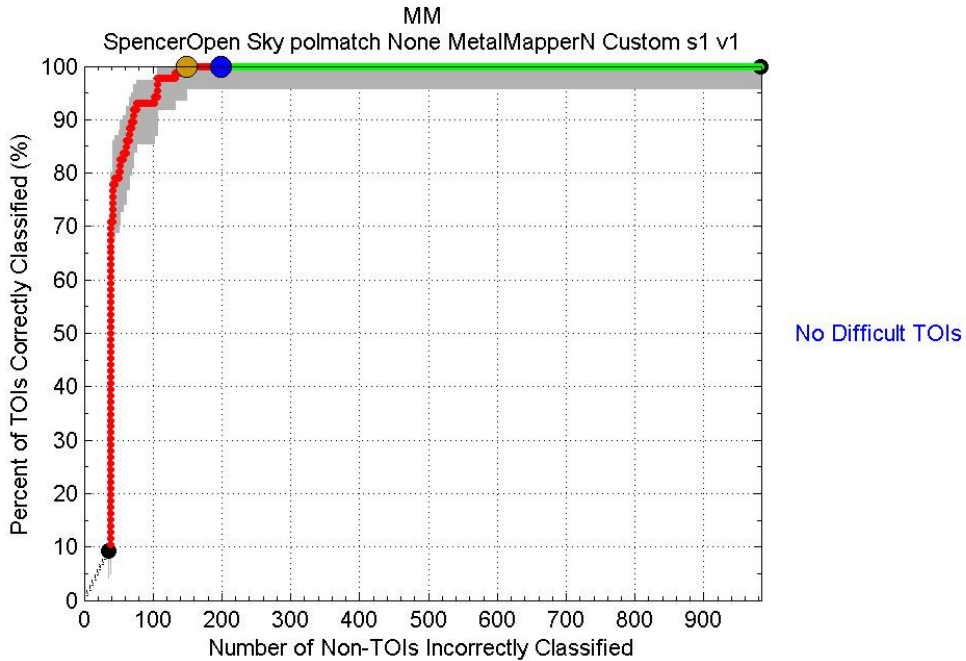


Figure 41: Final ROC curve for Spencer cued MetalMapper (NAEVA) for the open area.

A.3.3 MetalMapper static retrospective analysis (Naeva, Open Area)

Multi-object scenarios

The Spencer open area proved to be a relatively easy site. There were a limited number of TOI classes: 37mm, 60mm mortar, 75mm, small and medium ISOs, and two easy to detect large, one-off items (105mm and 155mm). There were no small unique items. Data quality was typically very good and there was minimal geologic noise.

At Spencer a number of the seeds were multi-object scenarios comprising one TOI and one piece of frag. In addition a number of other TOI seeds were found to be in close proximity to naturally occurring frag. This presents an opportunity to compare our two-object inversion (2OI) results with our single object inversion (SOI) results for the case of two objects within the field of view of the MetalMapper, and from this get a sense of the necessity for employing 2OI results in addition to SOI results when performing classification. Table 9 summarizes the results of the fifteen two-object scenarios. In half of the cases the SOI result was judged to be equally as good as the 2OI result. For the other half, the 2OI result (based on the similarity of the recovered polarizabilities to the relevant reference polarizabilities) are noticeably better.

Figure 42 shows three examples (targets 194, 700 and 873) where the 2OI produces a noticeably better result than the SOI. These results, and the other results listed in Table 9, show that, while a 2OI is not always necessary to get a good result in a two-object scenario, the 2OI is necessary in some cases to get the best possible result for classification.

Table 11: Summary of results from two-object inversion scenarios.

Target	Ground truth	TOI depth	Frag depth	Frag size rel. to TOI	Frag is seed	2OI better	Comment
194	ISO - Small+Other	22	13.5	similar	yes	yes	
207	ISO - Small+Frag	15	15	much smaller		yes	
241	60mm mortar+Frag	12	24	similar	yes		SOI, 2OI both good
359	75mm projo+Frag	9	19.5	smaller	yes	no	SOI better than both 2OI
447	75mm projo+Frag	29	10.5	much smaller		no	SOI better than both 2OI
490	37mm projectile+Frag	26	3	much smaller		yes	SOI looks like small ISO
505	37mm projectile+Frag	8.5	27	similar		no	SOI better than both 2OI
700	ISO - Small+Other	6.5	10	similar		yes	
837	37mm projectile+Frag	27	28	similar	yes		2OI looks like 60mm
873	ISO - Small+Frag	18	15	similar	yes	yes	SOI looks like 60mm
886	ISO - Small+Frag	20	45	similar	yes	yes	2OI looks like 37mm, 3OI best
950	75mm projectile body+240mm frag	7	10	smaller	yes		SOI, 2OI both good
971	ISO - Small+Frag	33	17	much smaller		yes	SOI looks like 60mm
1169	37mm projectile+Frag	10.5	3	much smaller			SOI, 2OI both good
1238	ISO - Small+Frag	21	24	similar	yes	yes	

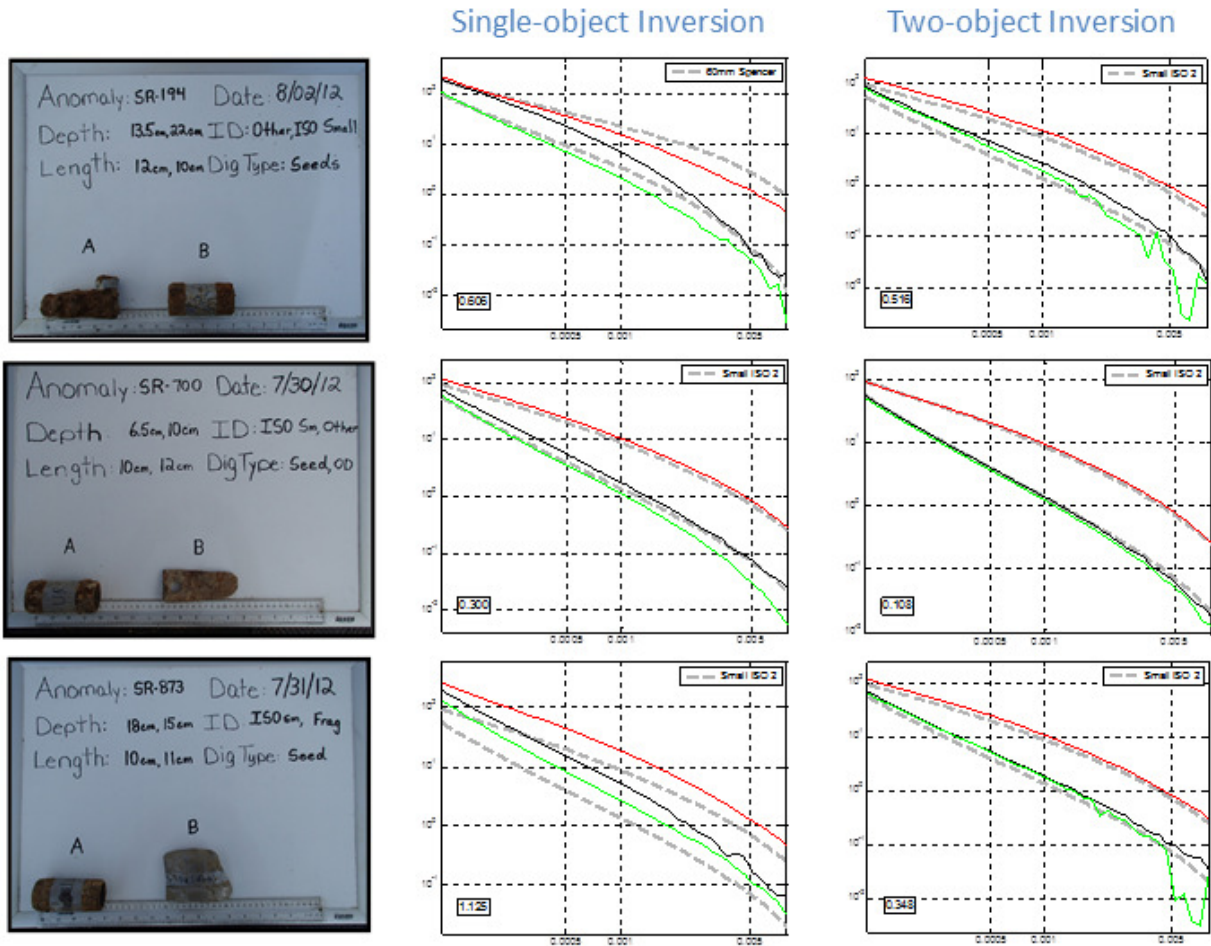


Figure 42: Comparison of SOI and 2OI inversion results for three two-object scenarios (targets 194, 700 and 873). In all three cases a piece of frag roughly equal in size to a small ISO was seeded with a small ISO. See Table 9 for details.

Three object inversions were also run on the entire dataset after initial analyst review of the single and two object inversion results. In order to determine where a three object inversion produced potential benefits without having to visually review all models produced by the three object inversions, a dig list comparison was undertaken. A separate dig list was created using the single and two object inversions for each item in the reference library shown in Table 10. A dig list for each of those targets in Table 10 were also created using the three object inversions (with no QC performed). The rankings of each target were then compared in the two dig lists to identify targets where the three object inversion produced a better polarizability match. This approach identified 19 targets where inclusion of the three object inversions resulted in a target moving significantly up the dig list. More than half of the targets identified were not multi object scenarios based on the ground truth. One of those items, target 308, was a confirmed TOI (37mm) and although there is a clear polarizability match in the three object inversion results, it would not likely have been dug based on the polarizabilities produced from the single and 2 object inversions.

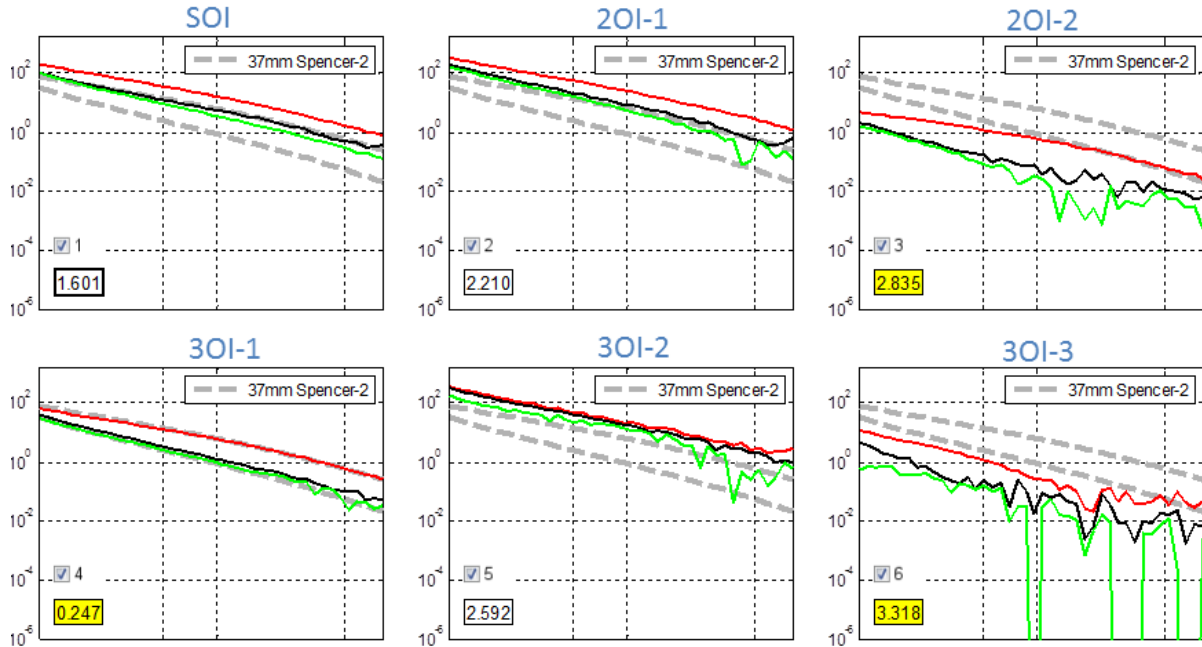


Figure 43: Recovered polarizabilities using SOI, 2OI and 3OI for target 308. Neither the SOI or either model of the 2OI produced polarizabilities that matched the 37mm projectile reference (shown as dashed grey). Ground truth revealed the target to be a 37mm projectile. The 3OI produces polarizabilities that match the 37mm reference in the 3OI-1 model.

Appendix B: Dynamic MetalMapper Feature Extraction and Classification

MetalMapper data acquired in a dynamic, full coverage mode were processed using UXOLab. The data were background corrected by identifying regions in the data that did not contain anomalies, and then using these anomaly free regions were used to estimate background levels which would subsequently be removed from the data.

We did not carry out any target picking or anomaly selection. An anomaly list was provided by the ESTCP program office. Data within a 1.5m square region surrounding each anomaly was extracted from the background corrected dataset, and a one and two dipole source inversion was used to provide location, orientation and dipole polarizability estimates.

B.1 Analysis of IVS data

Prior to applying a classification method to the field data, IVS data were processed. The IVS strip contained a Shot Put, 37 mm, 75 mm, and a small ISO positioned along a straight line. The 37 mm, 75 mm, and small ISO were oriented horizontally with the long axis of the target parallel to the across track direction.

Figure 44 compares the recovered polarizabilities for the four IVS targets when inverting the cued and dynamic MetalMapper data. When inverting cued MetalMapper data, the recovered polarizabilities are very consistent, with little variation in recovered parameters over multiple data collections. However, by plotting the recovered polarizabilities of the dynamic data, we see that the primary polarizability is poorly constrained by the dynamic data. The secondary polarizabilities are, relatively, well constrained by the data.

The inability for the dynamic data to constrain the primary polarizability is due the geometry of the MetalMapper transmitter loop and the target. The dynamic MetalMapper uses only the z-component transmitter loop. When the MetalMapper travels on a path directly above a target, the primary field does not have a component in the x-component (i.e. cross-track) direction at the location of the target. Since each target in the IVS is horizontal and cross-track, the primary polarizability will be poorly resolved.

Figure 45 plots the uncertainty of the L_{11} (or L_{xx}) component of the polarizability tensor when estimated by a dynamic, single pass of the MetalMapper. The red square indicates the location of the MetalMapper z-component transmitter. The blue line shows that if you follow a path directly over the target (i.e. $x=0$), the data will not be able to constrain the L_{11} component of the polarizability tensor. However, even a very small deviation in the x direction results in being able to constrain the polarizabilities.

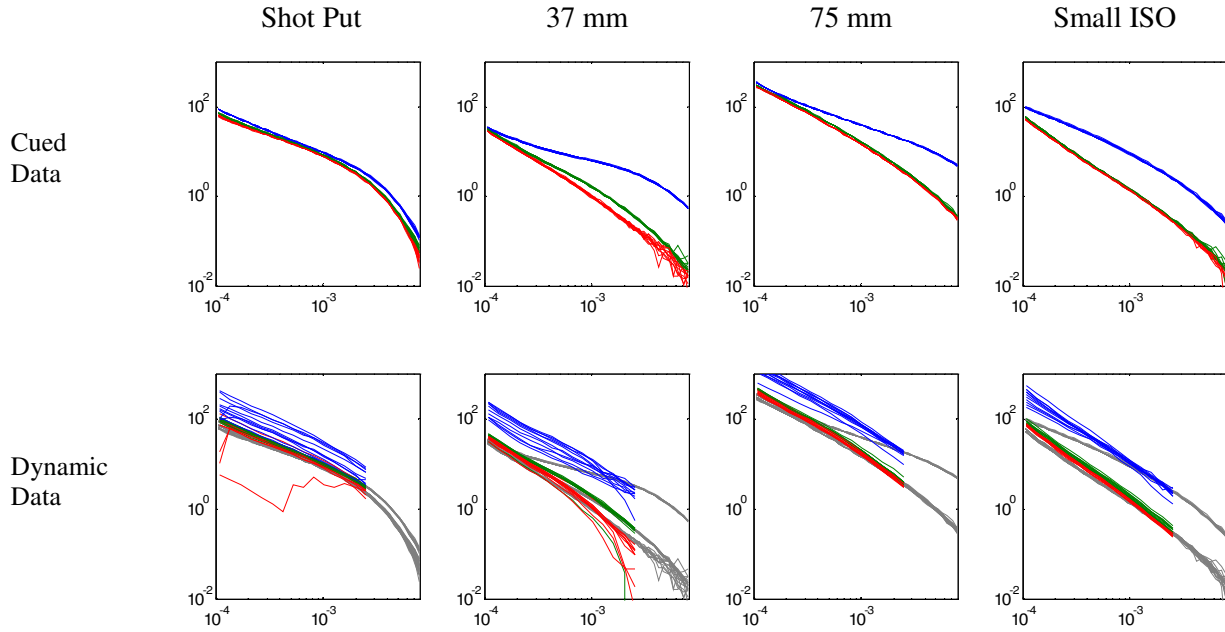


Figure 44: Analysis of Spencer Range dynamic MetalMapper IVS data. The top row show polarizabilities recovered from static, cued data. Multiple soundings acquired over each target, and the polarizabilities estimated from each sounding is plotted for each target. The bottom row plot the recovered polarizabilities when a single pass of dynamic data is collected over the targets. In contrast to operation in the cued mode, only the vertical transmitter is in operation when in dynamic mode. The primary polarizability of the target is poorly constrained for the IVS data, because each target is oriented with its long axis in an orientation that is poorly illuminated by the dynamic MetalMapper’s transmit field.

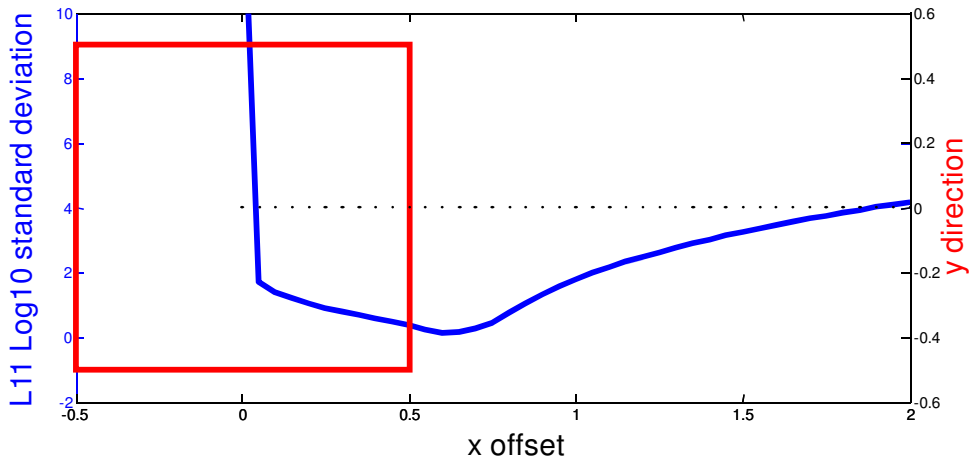


Figure 45: A covariance analysis of the L11 component of the polarizability matrix reveals that when passing directly over a target (i.e. x offset = 0), the primary polarizability will be poorly constrained by the data. Interestingly, on a few cms of across track offset from the target will allow for significant improvement in resolving the polarizabilities.

B.2 Analysis of Field data

Preprocessing

An anomaly was classified as “can’t extract reliable parameters” if either (1) the data misfit was large; or (2) data coverage was not sufficient.

For case (1) we calculated a measure of the data misfit (difference between observed and predicted data). We performed a single source and two source anomaly for each anomaly. Visual inspection resulted in two anomalies being classified as cannot analyze due to large misfit. There were numerous of low SNR anomalies that had a low relative misfit. However, in many cases the polarizabilities were considered to be smaller than the smallest expected item (based on training data). As such, the anomaly was not labelled can't analyze. Figure 46 contains an example of this type of anomaly.

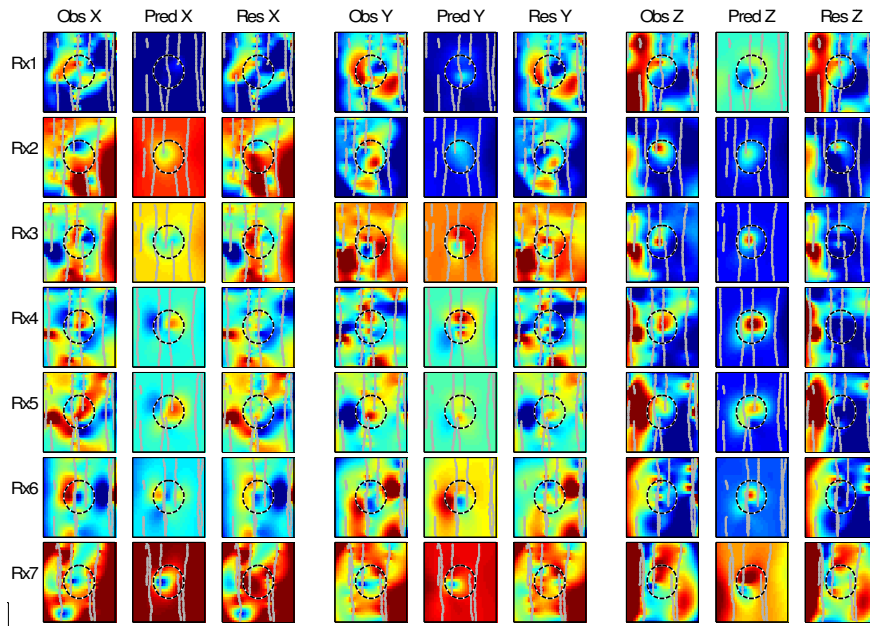
For the second case, there were numerous anomalies that had limited to no data coverage. These anomalies are located on the edge of the dynamic area. There were 13 anomalies that had no data coverage, and 12 anomalies that had limited data coverage. In both cases, the anomalies were labelled can't analyze. Figure 47 indicates anomalies that were listed as “can’t extract reliable parameters” due to poor data coverage.

Training Data Selection

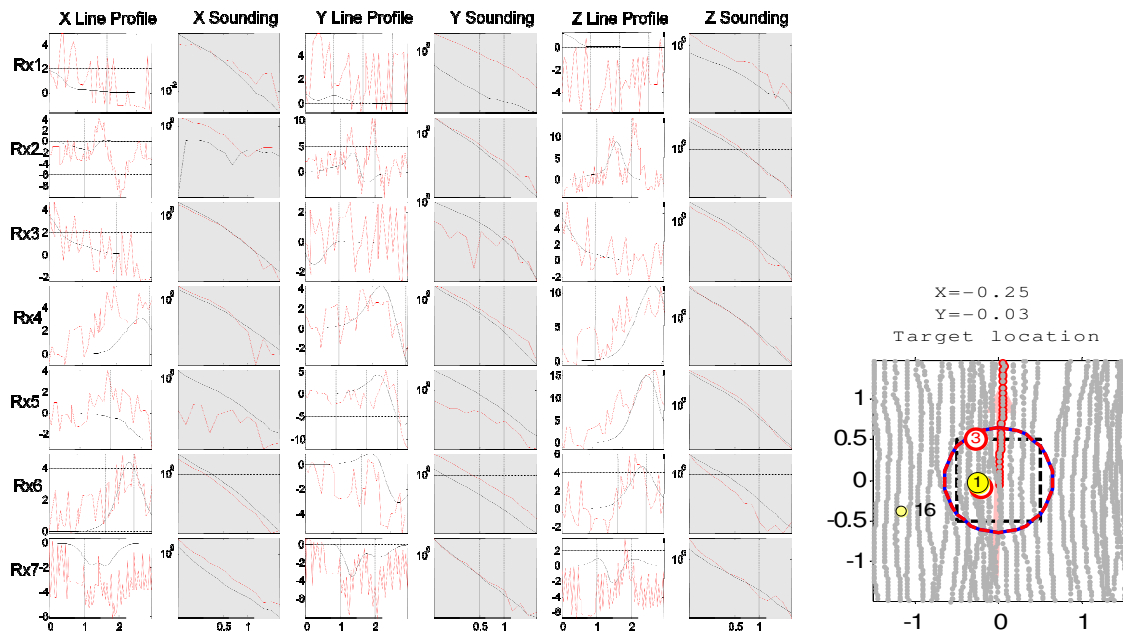
We performed a semi-automated cluster analysis to search for clusters of items with self-similar polarizabilities. Clusters were formed in three ways: (1) total polarizability, (2) primary polarizability, and (3) 1st and 2nd largest polarizabilities. Clusters that were judged to be UXO-like or vaguely-UXO like were selected as clusters of interest. From these clusters of interest we typically selected a couple of example items for training data. In addition, anomalies lying on the edge of clusters of very likely UXO-like items would be selected for training data as a means of gauging both the potential variability of a cluster class, and the quality of the data.

Figure 48 includes an example of a cluster automatically found using *TrainZilla*. Figure 48(a) shows the Size vs. Decay feature space. The stars represent items in the polarizability library. The solid black line indicates a polygon defined by the analyst, and the dashed line indicate a cluster of 5 models identified by comparing the similarity of the total polarizability. From this cluster, anomaly SR-1661 and SR-1502 were requested for training data. Figure 48(b) compares the estimated polarizabilities for the 5 models with polarizabilities from a 60 mm mortar. Although the total polarizability for SR-1502 matches a 60 mm very well, the principal polarizabilities do not have a good match. SR-1502 was due to a multi-target scenario with a small ISO. Choosing SR-1502 instead of one of the other anomalies in the cluster was very fortunate.

There was only a single training data request submitted to the program office. Table 12 summarizes the all the training data requests along the target information for each anomaly. The corresponding photos for the training requests are shown in Figure 49. A total of 17 anomalies were selected for training data, of which 9 were TOI. Based on this ground truth, a polarizability library was constructed (Figure 50).

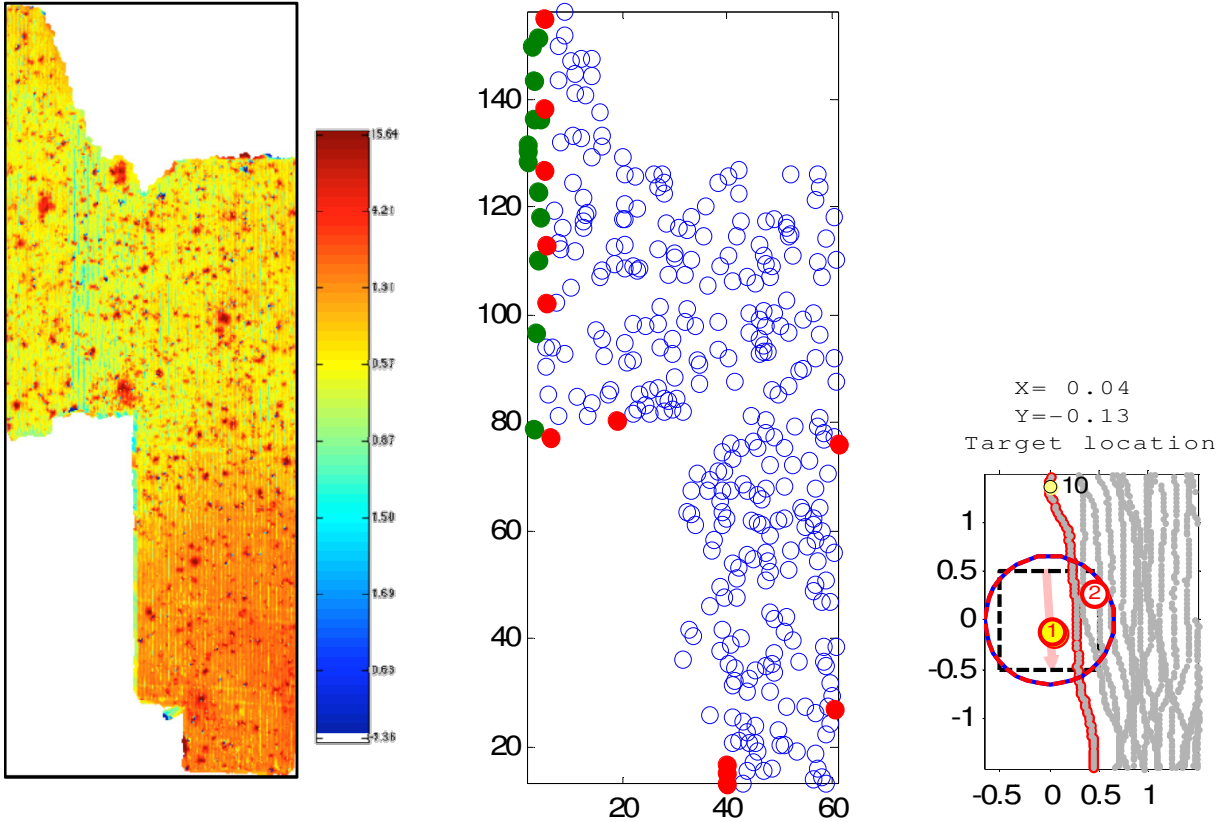


(a) Gridded image of the different Transmitter/Receiver combinations. Channel 5 is gridded.



(b) A profile view along a line over the anomaly. On the right is the location of the line. A time decay at the center of anomaly is also plotted (plots with grey background).

Figure 46: Anomaly SR-1520. For this target, the data had a relatively large data misfit, but the anomaly was passed because we considered the recovered polarizabilities to be smaller than the smallest target of interest on the site.



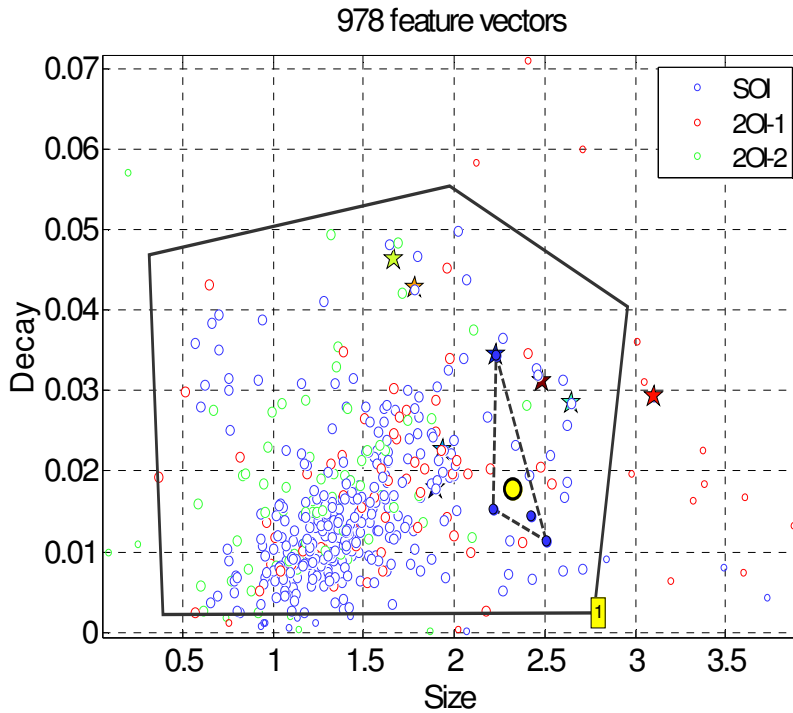
(a) Gridded image of Time channel 5 for the Z-component data of the Z transmitter. A normalized histogram is used to show the background variation in the data.

(b) Location of anomaly flags. Green circles indicate anomalies with no data, and red circles are anomalies with poor coverage such that reliable parameters can not be extracted from the data.

(c) An example of a target with insufficient coverage.

Figure 47: Anomalies categorized as “can’t extract reliable parameters” due to poor data coverage.

(a) Size vs. Decay feature space plot. The stars represent items in the polarizability library.



(b) Example of a cluster found by determining similar total polarizabilities.

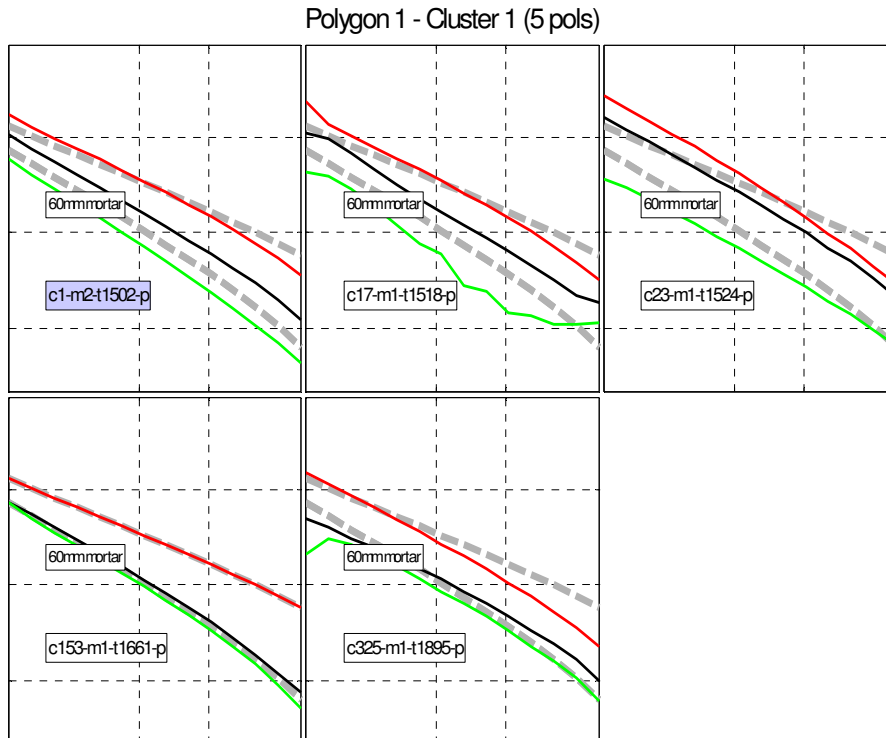


Figure 48: Example of an automatically identified cluster. In this case, the total polarizability was used to form a cluster. In this cluster, all the targets had similar total polarizabilities. From this cluster, training data was requested for SR-1502 and SR-1661. SR-1661 was a 60 mm mortar. Interestingly SR-1502 turned out to be a multi-target scenario that included an ISO.

Table 12: Ground truth request for the dynamically acquired MetalMapper data

Anomaly	Depth (cm, measured)	Identification	Length (cm, measured)	Dig Type
SR-1502	16	ISO - Small	10	TOI
SR-1502	28	Frag	17.5	MD
SR-1502	25	Frag	13.5	MD
SR-1508	15	Frag	13	MD
SR-1508	12	Frag	8.5	MD
SR-1508	11	Frag	6.5	MD
SR-1512	19	Other, bolt	9	OD
SR-1525	18	Frag	36	MD
SR-1534	16.5	Frag	17	MD
SR-1555	18	ISO - Medium	20	TOI
SR-1569	37	105mm projectile	47	TOI
SR-1576	9	37mm projectile	12	TOI
SR-1581	14	Small Arms	6	MD
SR-1606	15	37mm projectile	11	TOI
SR-1610	21	Frag	7	MD
SR-1610	8.5	Frag	12.5	MD
SR-1617	10	75mm projectile body	22.5	TOI
SR-1626	8	ISO - Small	10	TOI
SR-1661	17	60mm mortar	24.5	TOI
SR-1684	26	Frag	8	MD
SR-1684	16.5	Frag	11.5	MD
SR-1684	29	Frag	7	MD
SR-1684	29	Frag	4	MD
SR-1684	16.5	Frag	10	MD
SR-1781	12.5	37mm projectile	11.5	TOI
SR-1884	13	Frag	11	MD

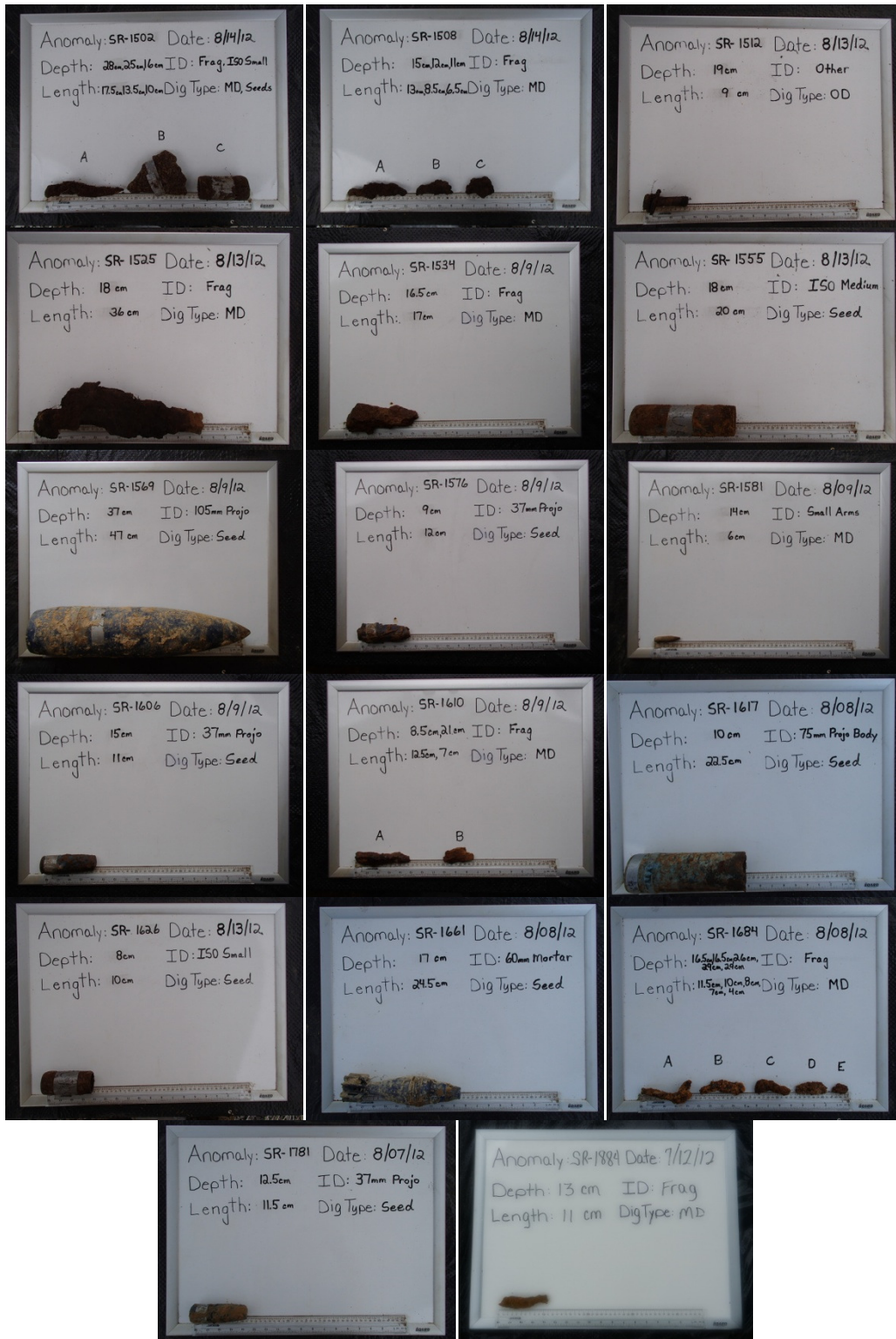


Figure 49: Ground truth photos from the training data request. The target information is summarized in Table 12

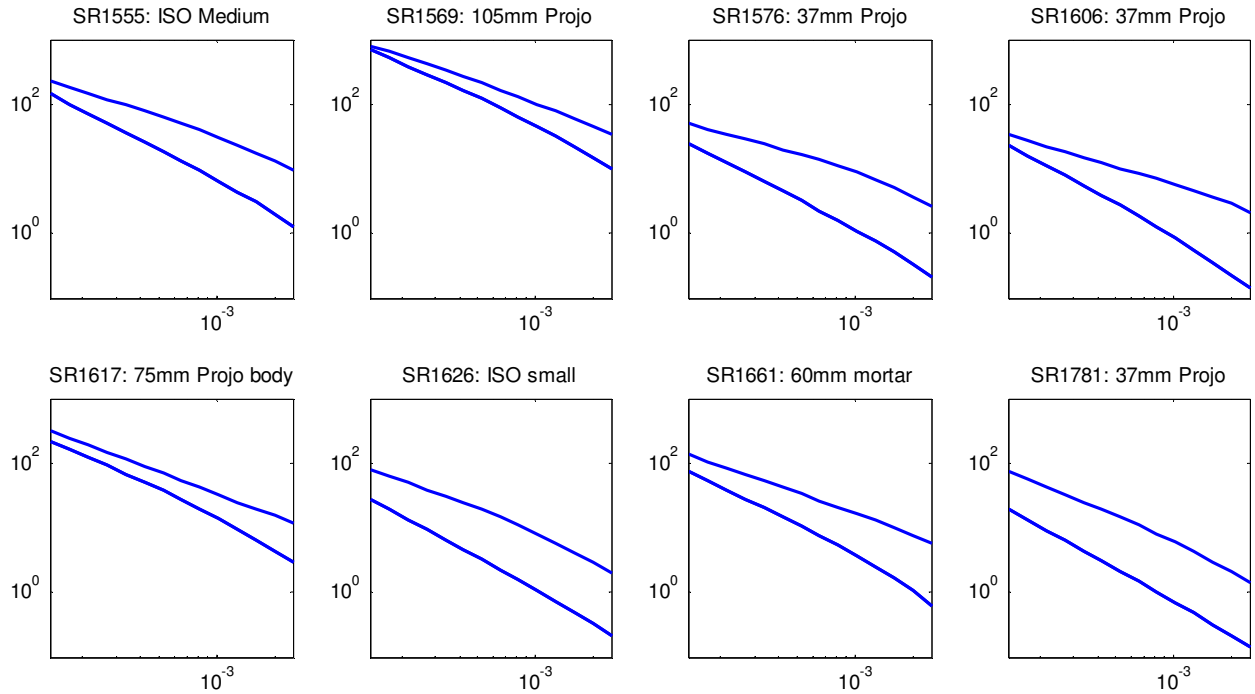


Figure 50: Ordnance library used during classification with the dynamic MetalMapper (URS) data.

Classification approach

For creating a ranked list, we use Combined Classifier Ranking (CCR) algorithm. The CCR is a simple classifier, requiring minimal or no input from the operator. Dig list order is based on four metrics: (1) best polarizability misfit relative to a library of reference ordnance items calculated using all three polarizabilities (L_1 , L_2 and L_3); (2) same as (1) but calculated using only the primary (L_1) polarizability; (3) polarizability size; and (4) polarizability decay. For each metric the anomalies are sorted according to the metric, creating four lists of ordinals for each anomaly: S_i^{L123} , S_i^{L1} , S_i^{size} and S_i^{decay} , where, for example, S_i^{L123} is the sort ordinal for the i^{th} anomaly. The final “score” for each anomaly is the sum of the ordinals:

$$S_i^{SUC} = k_1 S_i^{L123} + k_2 S_i^{L1} + k_3 S_i^{size} + k_4 S_i^{decay}.$$

For this data, we use the default weights k_i as defined by DigZilla. The anomaly with the lowest CCR score is dug first. The only parameters that could affect the result of the classifier are the time channels used to calculate the size, decay and polarizability misfits. For this dataset we use the first time channel to calculate size, channels 1 and 14 (of 14 time channels) to calculate decay, and channels 1 through 14 to calculate the polarizability misfits.

Determination of a Stop Dig Point

Polarizabilities for each anomaly, arranged in dig list order, were visually inspected. The stop-dig point was chosen as the point at which the remaining polarizabilities were judged by an expert analyst to be unlikely to correspond to TOI.

Results

A single dig list (Stage 1) was submitted to IDA for scoring. The ROC curve for the submitted list is shown in Figure 51. At the stop-dig point – excluding training data digs and “can’t analyze” digs – there were 90 total digs, of which 23 were TOI and 67 were non-TOI. At this operating point, 100% of the TOI were identified for excavation and 21.2% of the non-TOI anomalies were marked for excavation. The False Alarm Rate (FAR) was 0.165, with 52 of the 316 non-TOI excavated.

All performance metrics related to the accuracy of estimated target location were successfully met. The standard deviation of the depth estimate error is 0.03 m, and the Easting and Northing estimate error had standard deviations of 0.09 m and 0.06 m, respectively. A percent error was calculated to quantify the misfit between estimated polarizabilities and the library polarizability corresponding to the ground truth. The percent error is calculated using all three principal polarizabilities. Only 3 TOI exceeded the 20% threshold for the polarizability percent error metric. Of these 3 TOI, SR-1502 was identified in the training data stage of the classification, and the other two TOI (SR-1506 and SR-1729) had a good total polarizability match.

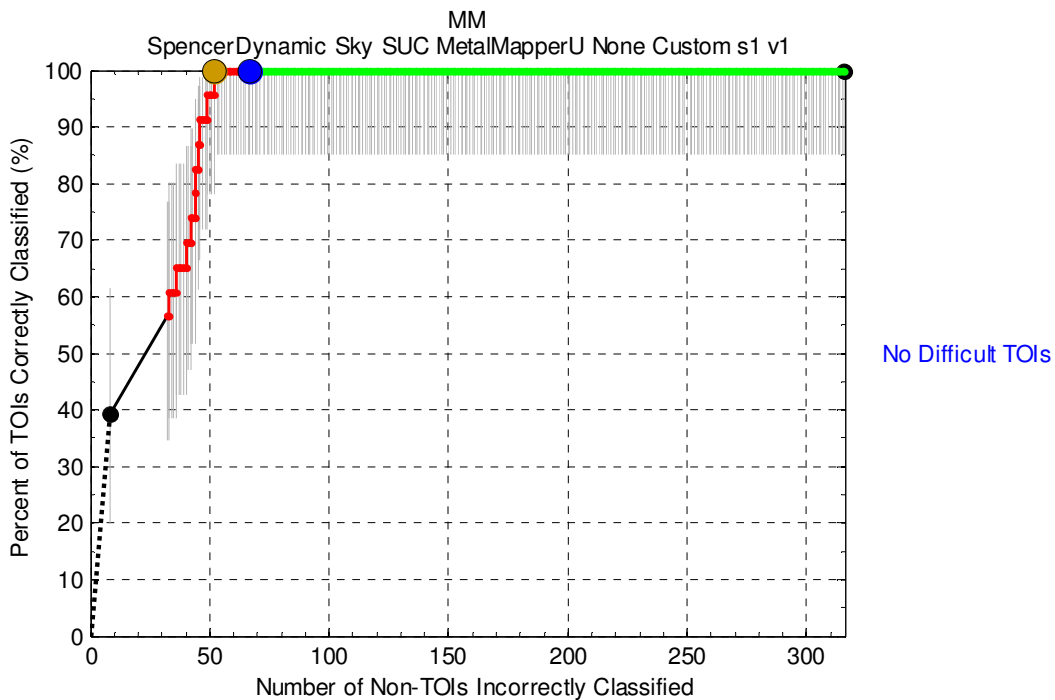


Figure 51: Dynamic MetalMapper scoring results from Institute of Defense analysis.

Appendix C: Processing and Classification Analysis of Cued TEMTADS Data

The Spencer Range demonstration had three sets of TEMTADS cued data available for classification: 692 TEMTADS 2x2 cued anomalies collected in the treed area; 339 TEMTADS 2x2 cued anomalies in the dynamic area; 1104 TEMTADS 5x5 anomalies at the open area. Each data anomaly was inverted using one-, two-, and three-source dipole models. A data and inversion QC review was carried out following the inversions. The QC process involved a visual review of each anomaly, aided by several metrics that included data misfit, data SNR, and properties of the recovered polarizabilities.

Classification was performed using a library matching method. The library method quantifies how well test polarizabilities agree with a set of reference TOI polarizabilities in the given library. All three principal polarizabilities (i.e. primary, secondary, and tertiary) were used to calculate the polarizability misfit (ϕ_m) to a reference (i.e. library) polarizability. The ϕ_m value is used to select which dipole model should be used for a particular anomaly, and the ϕ_m is used to rank all anomalies. For TEMTADS 2x2 and TEMTADS 5x5 data, ϕ_m values were calculated with time ranges of 0.179 ms to 7.462 ms and 0.095 ms to 4.943 ms, respectively.

C.1. TEMTADS 2x2 Classification at the Wooded Area

The library matching method consists of 4 parts:

- A. Building polarizability library.
- B. Assessment of matching level of test polarizabilities with respect to a set of reference polarizabilities.
- C. Request training data to refine polarizability library.
- D. Producing ranked anomaly list and classification.

A. Polarizability library

In the polarizability library, there are 8 reference classes: (1) 105-mm projectile; (2) 81-mm mortar; (3) 75 mm projectile; (4) 60mm mortar; (5) 37 mm projectile; (6) illumination round; (7) small ISO; (8) rod-tbi (to-be-identified). Target (8) "rod-tbi" was added for further query after an initial inspection found several similar polarizabilities were observed.

B. Assessment of polarizability matching level

Following the inversion of the data anomalies, an assessment of the polarizability match to the library is carried out. The anomalies are categorized into 5 classes ranging from high likely TOI (i.e. low ϕ_m) to low likelihood TOI (i.e. high ϕ_m). The different classes are defined in Table 13. The boundary between different classes is defined by visual inspection, with the corresponding range of polarizability misfit for each class listed in Table 1. By placing the anomalies into different classes, the analyst achieves a sense of the difficulty of the classification problem and a sense of the range of features such as size, decay rate, depth-range, and "skew-ness" of polarizabilities for this site. Skew-ness is a concept being developed in SERDP project MR2318 (See Appendix F for a short description).

HTOI anomalies make up about 6.8% of all anomalies. All 47 of the HTOI anomalies were dug. Figure 52 shows the polarizabilities of the last 11 anomalies in the HTOI set. Anomaly SR-2091 fits well with the reference polarizability ("rod-tbi") and was requested as one training anomaly to confirm/estimate the likelihood of being TOI for such a class of polarizability pattern. The anomalies in the remaining categories require additional investigation prior to assigning dig/no-dig labels. Training data are used to learn more about the targets that sit in these categories.

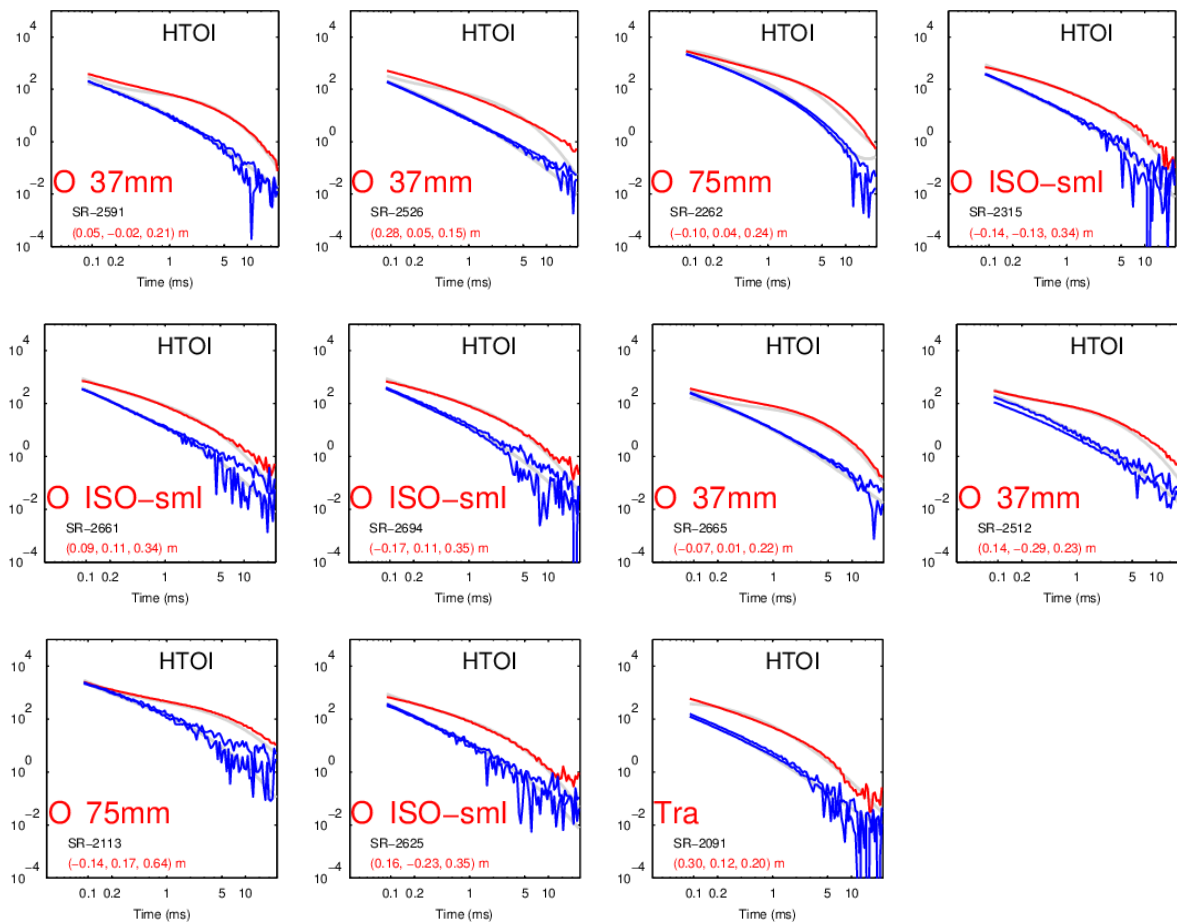


Figure 52: Polarizabilities of the last 11 anomalies in the HTOI set. Anomaly SR-2091 (related to the reference item, "rod-tbi") was requested as a training anomaly.

Table 13: TEMTADS 2x2 Evaluation at the wooded area.

Category		ϕ range	Total	Anomalies dug	Training	"Can't extract reliable parameters"	TOI	Non TOI
HTOI	High confidence TOI	$\phi \leq 0.255$	47	47	1	0	46	1
LTOI	Likely TOI	$0.255 < \phi \leq 0.483$	93	63	14	2	24	39
LLTOI	Low Likelihood TOI	$0.483 < \phi \leq 0.657$	94	41	28	2	1	40
LVLTOI	Very Low Likelihood TOI	$0.657 < \phi \leq 0.833$	142	12	8	1	0	12
LC	Likely Clutter	$\phi > 0.833$	316	15	13	0	0	15
Totals:			692	178	64	5	71	107

C. Training request

A number of approaches were used to select training data.

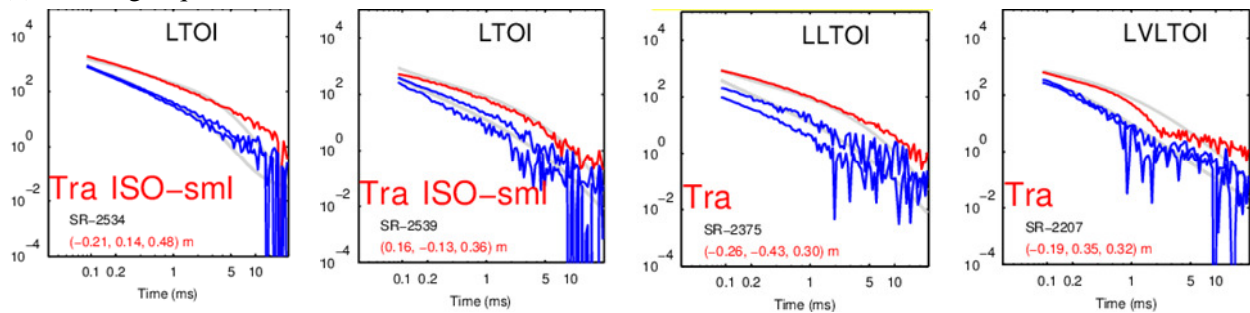
- A cluster analysis was performed to identify clusters that have distinct features from the current reference polarizability library.
- To understand the variability in recovered polarizabilities, anomalies were selected that only have a subset of polarizabilities match to a library target. That is, we identify anomalies with
 - a. primary and secondary polarizabilities that match, but not the tertiary
 - b. only the primary polarizability is close to a reference polarizability
 - c. only secondary and tertiary polarizabilities are close to those of reference polarizabilities.
- An examination of "skewness" of polarizabilities to find if there are some other "suspicious" spherical and rod-like objects that could be TOIs. See Appendix F for a description of the "skewness" metric.
- Some anomalies whose recovered polarizabilities behave noisy and oscillatory were also chosen for training data.

A total of 64 training anomalies were requested. Figure 53 shows some polarizabilities of these training anomalies. The top row shows the training anomalies related to small ISO; middle row 37mm, and bottom row "rod-tbi". For the small ISO and 37mm cluster classes, the training data suggests that there are likely TOI anomalies in the low matching level sets. However, for the "rod-tbi" reference class, I requested 18 related anomalies across all TOI likelihood categories. None of the requested items were TOI. A decision was made not to dig any related anomalies like "rod-tbi".

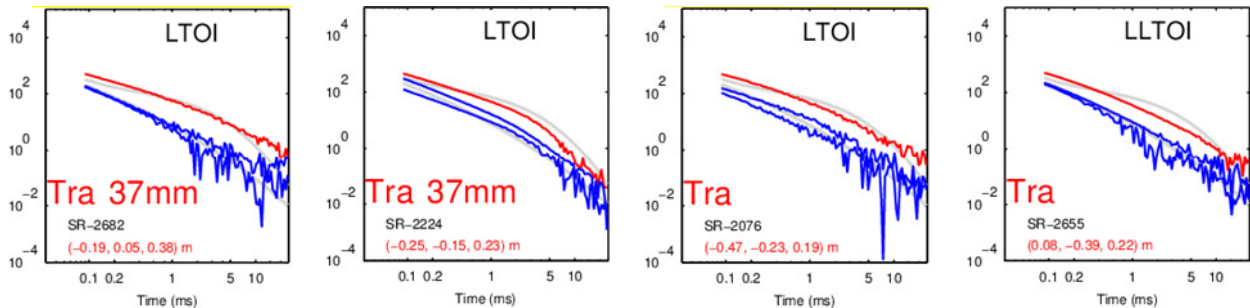
D. Ranked anomaly list and classification

There were two stages to the classification. Table 14 summarizes performance at each stage. In stage one, 106 anomalies were dug. Of these 106 anomalies, and 67 were TOIs. Based upon the ground truth of stage one, 3 additional anomalies were dug in stage two. These three anomalies were all due to non-TOI. There were 178 items dug. No QC seeds were missed in this classification. 5 items were assigned to the "Can't extract reliable parameters" class. As a result, all 71 TOIs are recovered. 514 anomalies were left in the ground and not dug. In other words, 82.8% of the non-TOI items were correctly labeled as non-TOI while identifying all of the TOI on the dig list. Figure 3 shows the ROC curve of stage 2. Figure 4 shows the polarizabilities of 21 TOI anomalies found in the LTOI and LLTOI sets in stage one at the expense of digging another 42 non-TOI anomalies whose polarizabilities resemble potential TOIs (refer to Table 1).

(a) Training requests related to small ISO



(b) Training requests related to 37 mm



(c) Training request related to "rod-tbi"

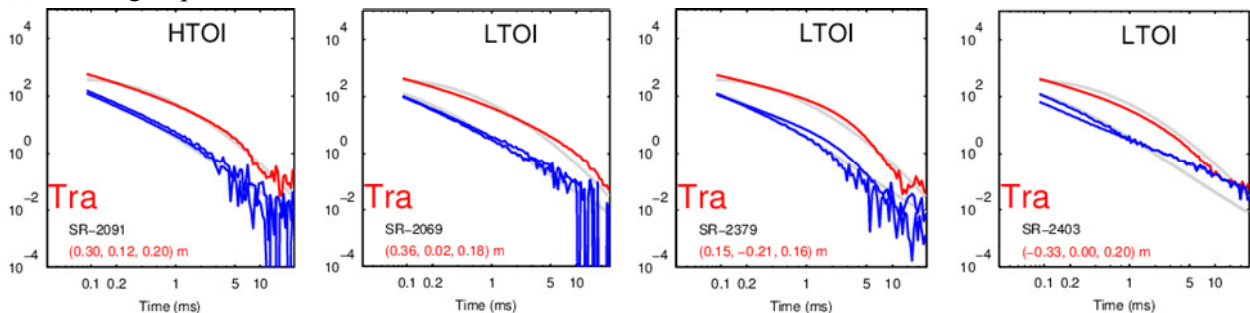


Figure 53: Examples of polarizabilities of 12 items from the training set. "Tra" indicates that the time was chose for training data, with the text after "Tra" indicating the ground truth label if the item was categorized as TOI

Table 14: Summary of TEMTADS 2x2 cued data classification in the Treed area

Category/Stage	Dug	TOI	Frag
Training	64	4	60
"Can't extract reliable parameters"	5	0	5
Stage One	106	67	39
Stage Two	3	0	3
Total	178	71	107

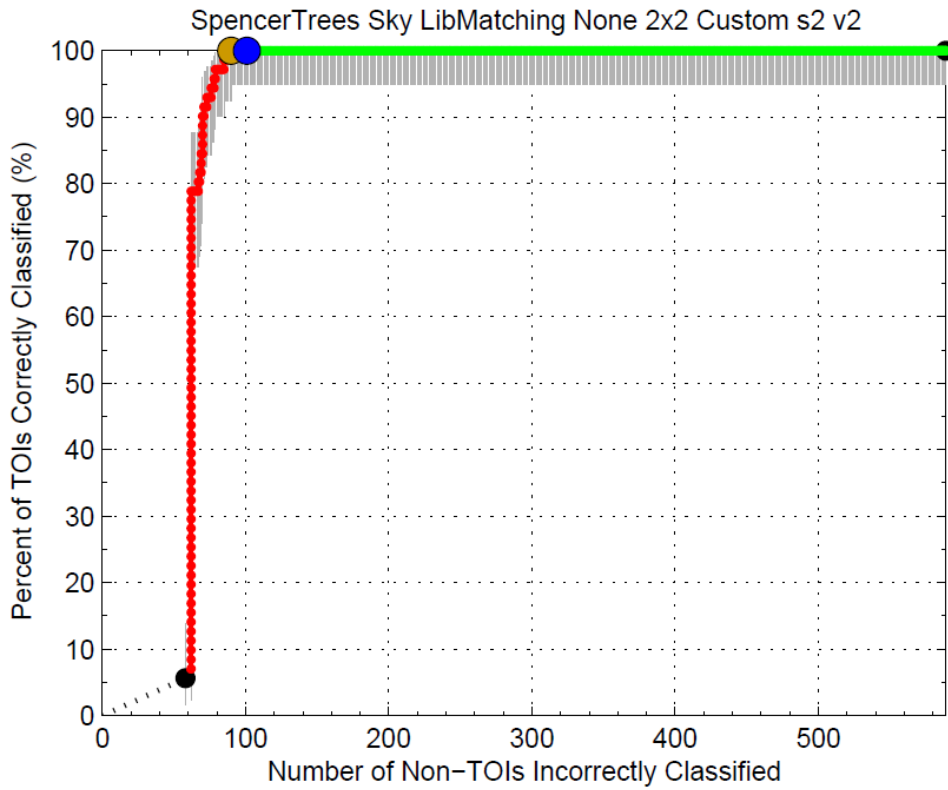


Figure 54: ROC curve for the stage 2 (and final) diglist submitted of the TEMTADS 2x2 cued data in the Treed area.

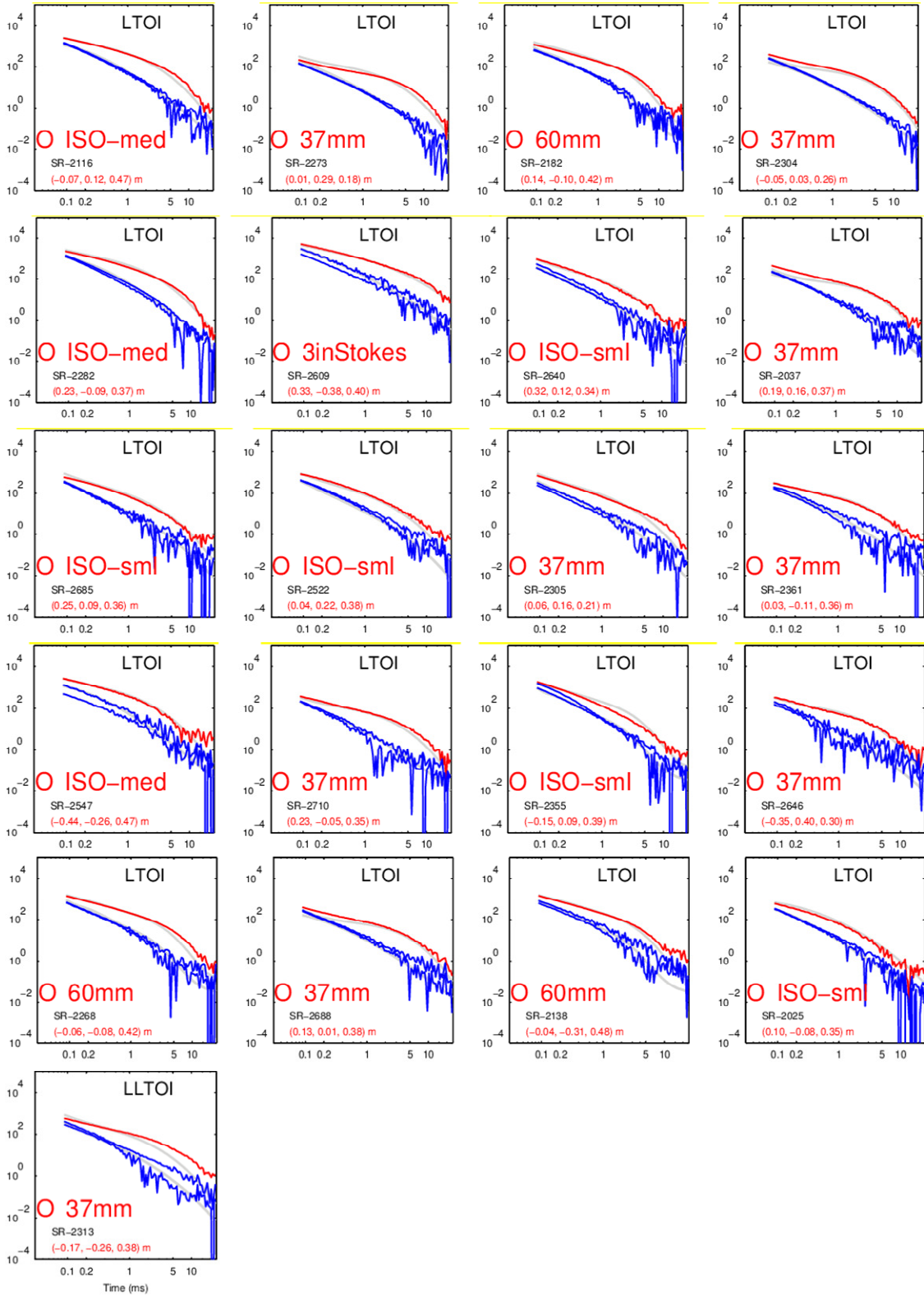


Figure 55: Polarizabilities of 21 TOI anomalies dug in the LTOI and LLTOI sets in stage 1.

C.2. TEMTADS 2x2 Classification at the Dynamic Area

Polarizability library

The polarizability library used in the Treed area was also used for the dynamic area.

Assessment of matching level

Table 3 lists the matching level of the 339 anomalies. HTOI anomalies represent 4.7% of all anomalies. Each of the 16 anomalies were assigned for digging, with only 1 HTOI anomaly being non-TOI. Figure 56 shows the polarizabilities of the 16 dug anomalies in the HTOI set. Although, anomaly SR-1525 is not a TOI target, its polarizabilities have a good match with a small ISO reference polarizability.

Training request

The similar training request rules in the Treed area was used for the Dynamic area, resulting in a total of 20 training anomalies. Figure 57 shows some polarizabilities of these training anomalies. Figure 57(a) and (b) shows training anomalies related to the small ISO and “rod-tbi”, respectively. For the cluster related to small ISO, the training data information suggested that other anomalies similar to SR-1706 and SR-1796 and with a fast primary decay after approximately 4 ms are likely non-TOIs. An additional 7 related anomalies related to “rod-tbi” were requested. Although, this set of training anomalies included a target of interest (SR-1502, small ISO), it was decided to not dig any more anomalies related to “rod-tbi”.

Ranked anomaly list and classification

A single classification diglist was submitted. Table 16 summarizes performance at this stage. No QC seeds were missed in this initial diglist. Of the 47 anomalies marked for digging, 22 were TOIs. After reviewing the ground truth information for these anomalies, it was determined that it was unlikely that there would be additional TOI in the remaining anomalies.

All 23 TOIs are were correctly marked for excavation. 86.9% of the non-TOI items were correctly labeled as non-TOI while retaining all of the TOI on the dig list. Figure 58 shows the polarizabilities of 7 TOI anomalies found in the LTOI set. In order to dig these anomalies, an additional 24 non-TOI anomalies were also included for digging. Figure 59 shows the final ROC curve provided by IDA.

All performance metrics related to classification of TOI and non-TOI satisfied the success criteria. Location estimates were not calculated, due to no IMU information being available for the survey. The standard deviation of the depth estimate error is 0.08 m. A percent error was calculated to quantify the misfit between estimated polarizabilities and the library polarizability corresponding to the ground truth. The percent error is calculated using all three principal polarizabilities. Only 4 TOI exceeded the 20% threshold for the polarizability percent error metric. Of these 4 TOI, SR-1502 was identified in the training data stage of the classification. Two of the 4 TOI (SR-1564 and SR-1576) had data recollected, for which the polarizability fit of the recollected data had a percent error that met the success criteria. Although anomaly SR-1609 had a poor fit to the library item, it was still dug just before the “stop-dig” point.

Table 15: TEMTADS 2x2 Evaluation at the dynamic area

Category		ϕ range	Total	Anomalies dug	Training	"Can't extract reliable parameters"	TOI	Non TOI
HTOI	High confidence TOI	$\phi \leq 0.255$	16	16	0	0	15	1
LTOI	Likely TOI	$0.255 < \phi \leq 0.483$	55	34	4	0	8	26
LLTOI	Low Likelihood TOI	$0.483 < \phi \leq 0.657$	49	12	11	0	0	12
LVLTOI	Very Low Likelihood TOI	$0.657 < \phi \leq 0.833$	54	1	1	0	0	1
LC	Likely Clutter	$\phi > 0.833$	165	4	4	0	0	4
Totals:			339	67	20	0	23	44

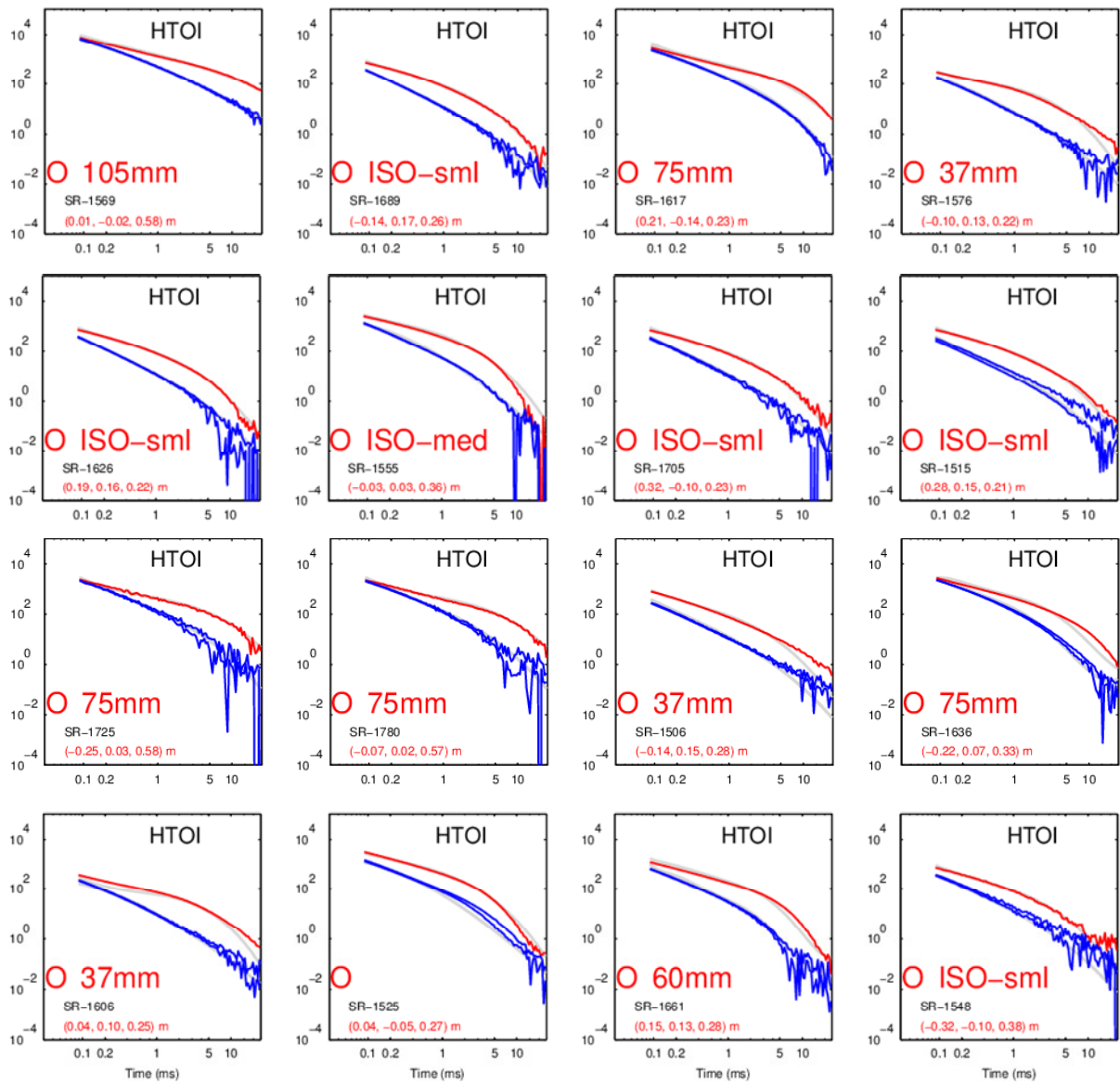
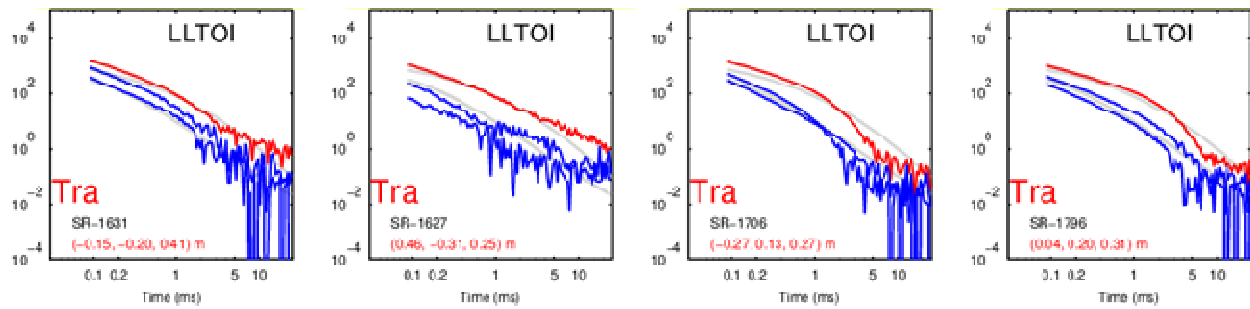


Figure 56: Polarizabilities of 16 anomalies dug in the HTOI set in stage 1. SR-1525 is a dug non-TOI.

(a) Training requests related to the small ISO



(b) Training requests related to "rod-tbi"

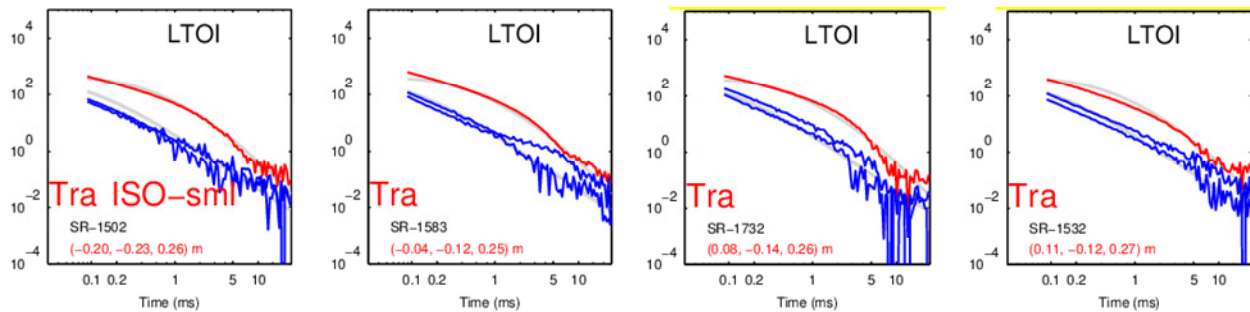


Figure 57: Polarizabilities of 8 anomalies in the training set for the dynamic area.

Table 16: Summary of TEMTADS 2x2 classification at the dynamic area

Category/Stage	Dug	TOI	Frag
Training	20	1	19
"Can't Extract Reliable parameters"	0	0	0
S1	47	22	25
Total	67	23	44
Non-dug	/	0	292 (86.9%)

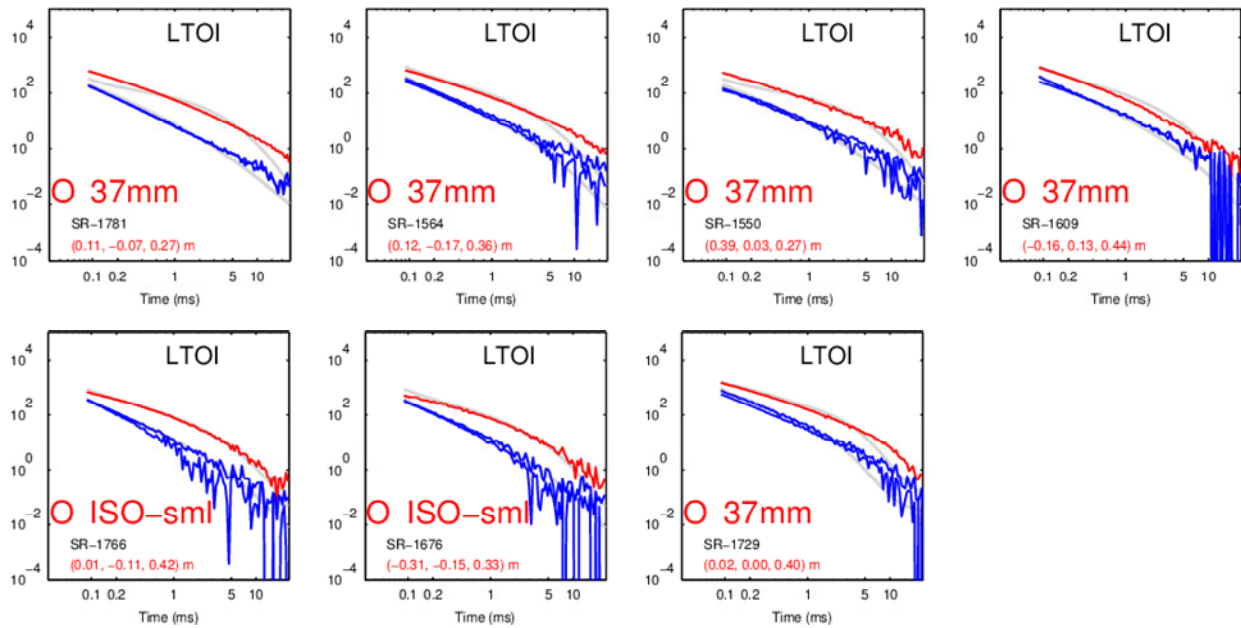


Figure 58: Polarizabilities of 7 TOI anomalies in the LTOI set for the dynamic area.

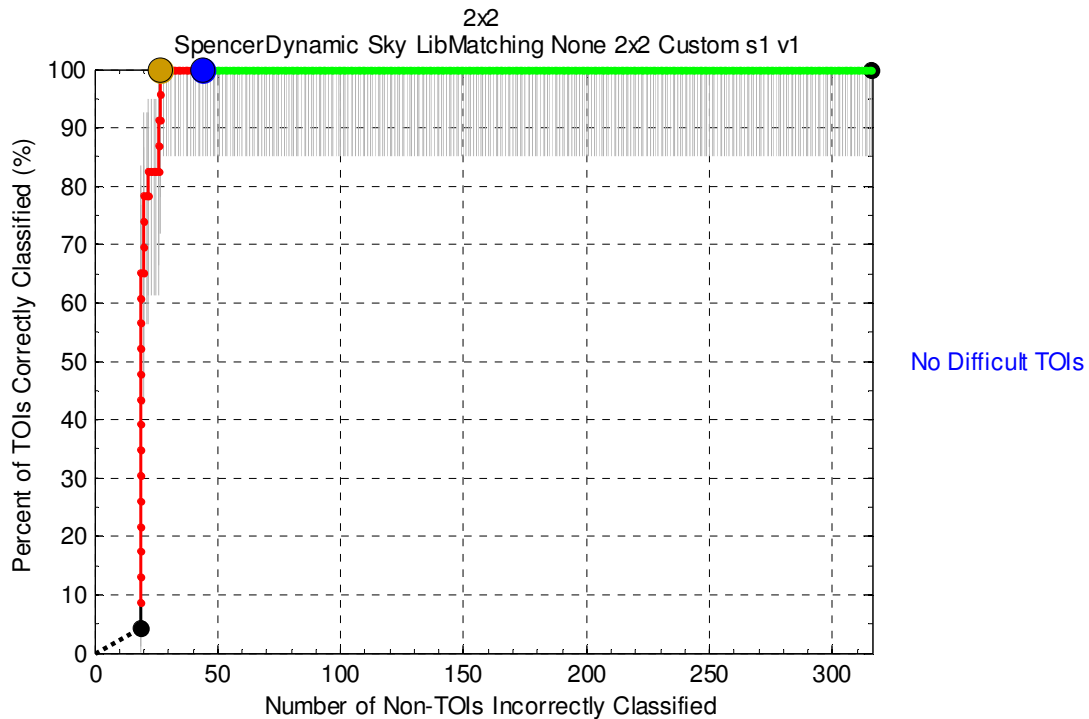


Figure 59: ROC curve at Stage 1 of TEMTADS 2x2 in the dynamic area.

C.3. TEMTADS 5x5 Classification at the Open Area

A. Polarizability library

In the polarizability library, there are 7 reference classes: (1) 105-mm projectile; (2) 81-mm mortar; (3) 75 mm projectile; (4) 60mm mortar; (5) 37 mm projectile; (6) small ISO; (7) "rod-tbi" (to-be-identified). The last item ("rod-tbi") was added for further query after an initial inspection where a large number of such similar rod-like polarizabilities were observed.

B. Assessment of matching level

HTOI set contains 108 anomalies, LTOI 218, LLTOI 184, LVLTOI 180, and LC 410 (Table 17). HTOI anomalies represent 9.8% of the total anomalies. An inspection of the HTOI set shows that 65 anomalies were related to the reference item of small ISO, the other 43 are related to reference classes of 105 mm, 75 mm, 60mm, and 37 mm. Note that there was no data collected over anomalies SR-688, SR-782, SR-912, and SR-1137. We were instructed by the program office to label these anomalies as "Can't extract reliable parameters".

C. Training request

A total of three training requests resulted in 91 anomalies with groundtruth. In the training set, 41 anomalies are related to small ISO, 13 are in the "rod-tbi", and 20 are related to 37mm. The remaining 17 are related to 60mm, 75mm, and 81mm. Figure 60 shows the polarizabilities of 16 training anomalies in the HTOI set related to small ISO and "rod-tbi" (SR-234).

Table 17: TEMTADS 5x5 classification in the Open area

Category		Total	Anomalies dug	Training	"Can't extract reliable parameters"	TOI	Non TOI
HTOI	High confidence TOI	108	78	16	0	57	21
LTOI	Likely TOI	218	118	40	0	28	90
LLTOI	Low Likelihood TOI	184	25	21	1	0	25
LVLTOI	Very Low Likelihood TOI	180	13	11	1	1	12
LC	Likely Clutter	410	12	5	7	0	12
Total		1100	246	93	9	86	160

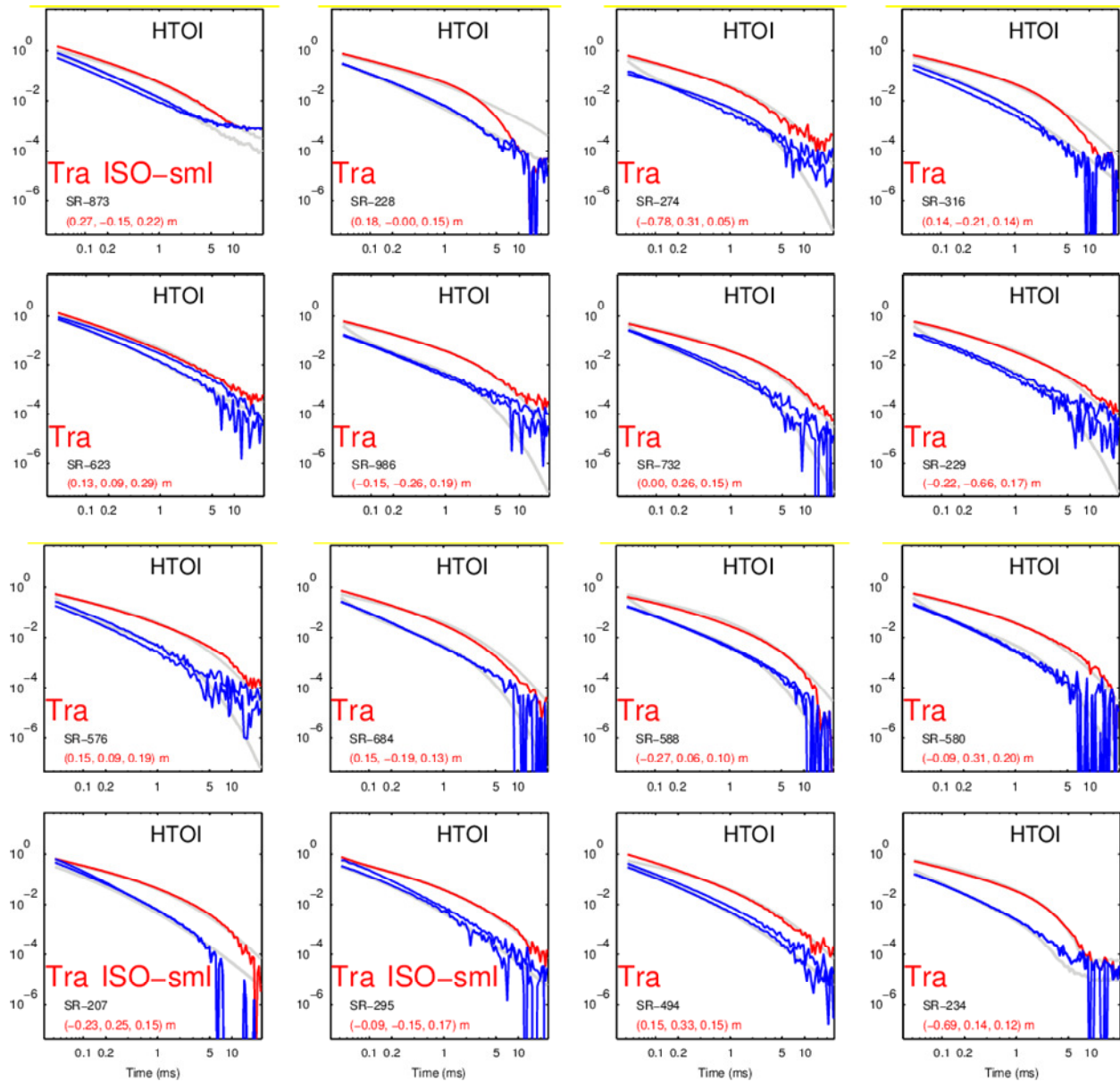


Figure 60: Polarizabilities of 16 training anomalies related to small ISO and rod-tbi (SR-234) in the HTOI set.

D. Analysis of missing QC seeds

In the first submitted ranked anomaly list, there were two QC seeds not marked for digging. The missed QC seeds are anomaly SR-572 and SR-1160 (Figure 61). The ground truth of SR-572 is an item of 37 mm projectile buried at the depth of 24 cm. The ground truth of SR-1160 is an item of small ISO buried at the depth of 22 cm. There was no information of how the object was oriented.

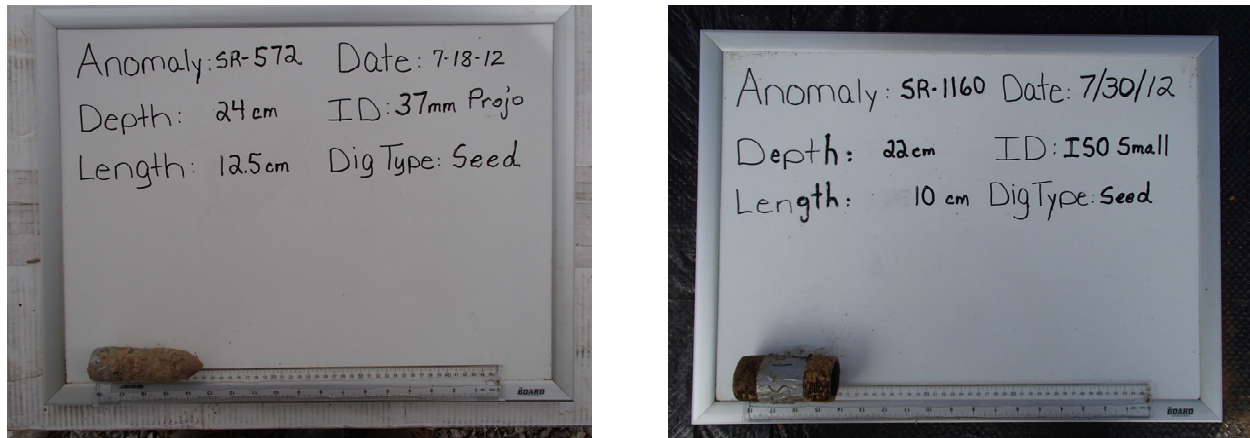


Figure 61: QC seeds SR-572 (left) and SR-1160 (right) that were missed in the initial ranked anomaly list.

Analysis of SR-572

Figure 62 presents the recovered polarizabilities of anomaly SR-572 (bottom right) and some similar non-TOI training anomalies. The library matching method found that this anomaly was close to a small ISO with a rank value of $\phi_m = 0.276$ and assigned to the Likely TOI (L-TOI) set. The LTOI set includes 218 anomalies that resemble a small ISO. In light of the large number of potential ISO-small anomalies, we investigated this cluster of targets via training requests.

Based on the IVS data, 4 sets of ISO polarizabilities (labeled iSO2A, iSO2B, iSO2C, iSO2D) were added to the ordnance library. The multiple polarizabilities were included to account for potential variability to the ISO cluster class. In the first training request, the polarizabilities of iSO2C and iSO2D were confirmed to be associated small ISO. Anomalies in the training request that were close to iSO2A or iSO2B resulted in being one or more pieces of munitions debris. To further investigate if iSO2A and iSO2B-like anomalies were likely non-TOI, 9 anomalies with a good match to the iSO2B polarizabilities were selected for training. The 9 anomalies in this second training request resulted to be all non-TOI.

A third training request was carried out to investigate iSO2A and iSO2B like targets. Three anomalies with a good match to iSO2A and three with a good match to iSO2B were submitted for ground truth. For iSO2B, the three anomalies are non-TOIs. For iSOA, the two of them are indeed small ISOs.

The three rounds of training requests suggested that anomalies close to iSO2B are unlikely to be TOI. Unfortunately, by not including ISO2B in the ordnance library, SR-572 was missed. For comparison, the polarizabilities of those training MD anomalies and missed QC seed SR-572 in Figure 62. The primary polarizability of the small 37mm projectile behaves with a slower decay after 5 ms than those MD items. To account for targets such as SR-572, polarizabilities of iSO2B are included in the polarizability library.

However, targets with polarizabilities that match iSO2b will be examined to determine if the late time decay after 5 ms is slower than in the reference polarizabilities..

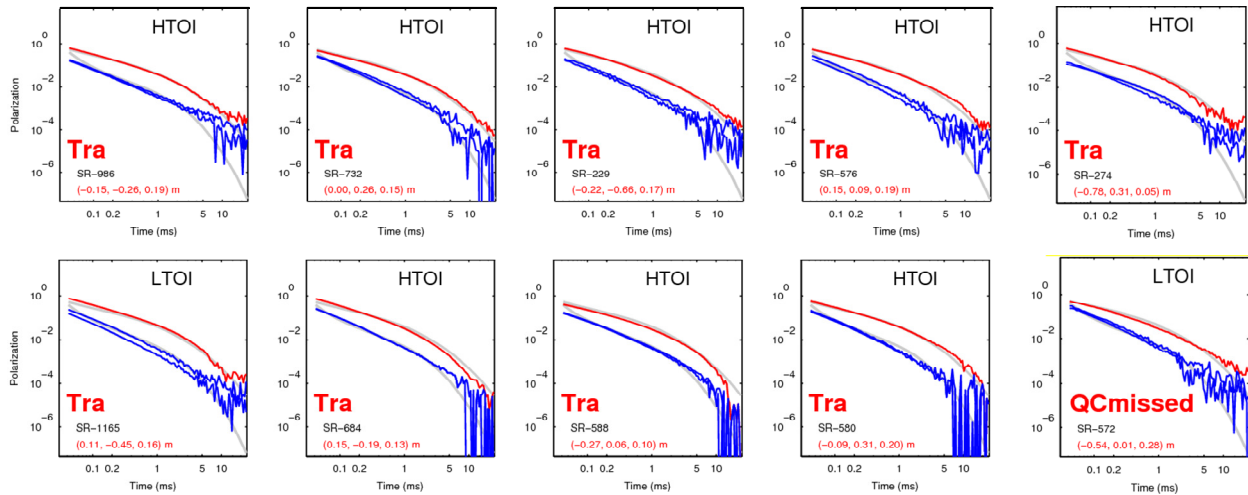


Figure 62: Recovered polarizabilities (red and blue curves) of the relevant training anomalies and the missed QC seed of SR-572, a 37mm projectile. The closest item to anomaly SR-572 is a small ISO (represented by the gray curves) with $\phi_m = 0.276$. In the initial classification stage, this anomaly was assigned into the Likely TOI (L-TOI) set but not marked to be dug.

Analysis of SR-1160

The ground truth of this anomaly is a small ISO (Figure 61, right). Figure 63 presents the recovered polarizabilities of anomaly SR-1160 (bottom right) and other related non-TOI training anomalies. The library matching method found that this anomaly was close to a suspicious rod-like object with a misfit value of $\phi_m = 0.741$ and assigned to the Likely Very Low TOI (LVL-TOI) set.

During the initial stage of obtaining training data, a suspicious rod-like object (a short name: "rod-tbi") was selected due to a large number anomalies having similar polarizabilities (some shown in Figure 63). To investigate what target "rod-tbi" could represent, 13 "rod-tbi"-like anomalies were selected. Each of the 13 chosen anomalies were due to pieces of munitions debris. Based on this training, a decision was made to not dig any anomalies with polarizabilities matching "rod-tbi". Unfortunately, SR-1160 would have been selected for digging based on its primary polarizability match to "rod-tbi".

We did not recover a set of polarizabilities for SR-1160 that resemble the small ISO references in our library. This may be due to the sensor being unable to capture sufficient signals for this small object buried at 22 cm. The inverted location (0.14, -0.87, 0.15) m is on the south edge of the instrument (Figure 64, right). It is possible that these factors contributed to the recovered polarizabilities that are more similar to "rod-tbi" than a small ISO.

Referring to Figure 12, we can observe that the primary polarizability of the QC seed decays somewhat slowly after 5 ms when compared to the rod-tbi. This might be a clue that can be used to guide a digging. This is similar to the case of SR-572.

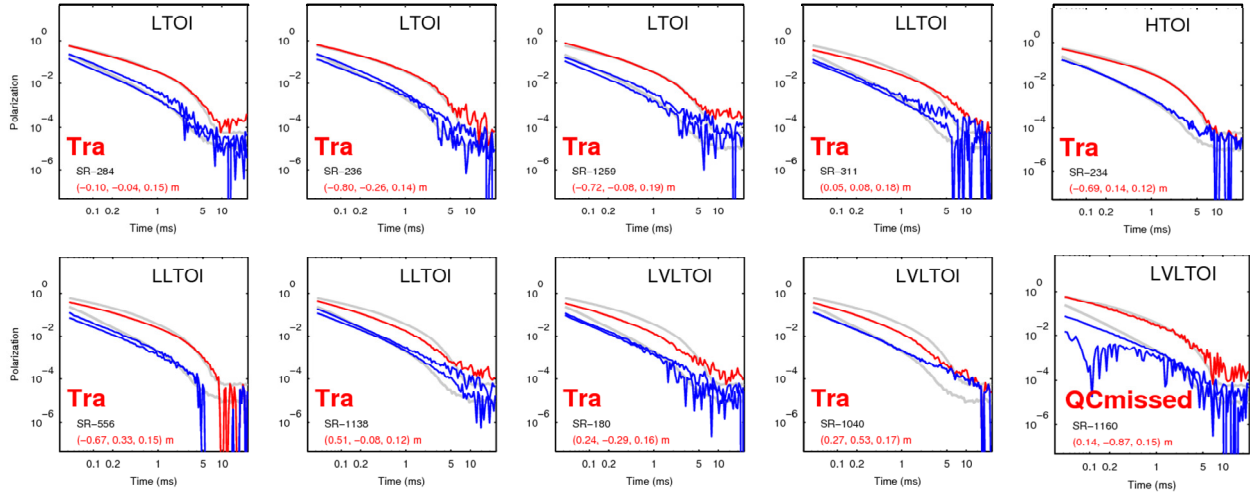


Figure 63: Recovered polarizabilities (red and blue curves) of the relevant Training anomalies and the missed QC seed of SR-1160, a small ISO. The closest item to anomaly SR-1160 is a suspicious rod-like object (represented by the gray curves) with $\phi_m = 0.741$. In the initial classification stage, this anomaly was assigned into the Likely Very Low TOI (LVL-TOI) set and not marked to be dug.

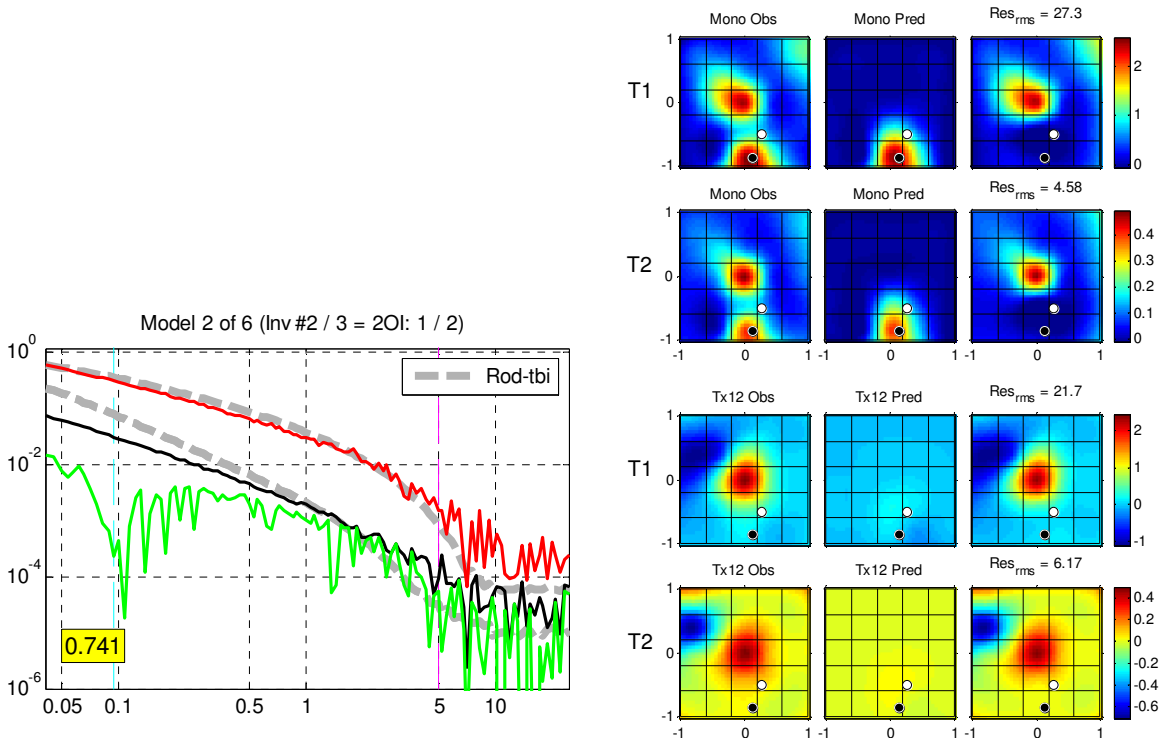


Figure 64: Anomaly 1160, the missed QC seed.

Modified analysis procedures based upon the missed QC seeds.

Due to the missing QC seeds, the polarizabilities for iSO2B and "rod-tbi" were added to the polarizability library. These polarizabilities are low in magnitude, and there are many non-TOI that would be labeled as "dig". In order to reduce the number of non-TOI, we included an additional step of looking at the decay rate of targets with anomalies that match iSO2B or "rod-tbi". Targets that match iSO2B and "rod-tbi" well, but have a faster decay rate after 5 ms, will not be considered TOI.

D. Ranked anomaly list and classification

Excavation results are listed in Table 18. As described above, the Stage 1 dig list missed a pair of QC seeds. Therefore, there was no partial ROC curve or ground truth information for the Stage 1 list. The Stage 2 dig list designated 144 anomalies for excavation, of which 78 were TOI. Including initial training digs, a stop-dig point was set at 246 digs. At this stop-dig point, 100% of the 86 TOI were identified for excavation. The majority of TOIs were in the HTOI and LTOI sets (Table 17). A total of 854 anomalies were chosen to leave in the ground. At this operating point, 84.2% of the non-TOI items were not dug. Figure 65 plots the polarizabilities of the last 24 TOI found in the LTOI class. In order to recover these 24 TOI, 54 non-TOI anomalies were excavated. Figure 66 show the ROC curve for the open area.

Table 18: Summary of TEMTADS 5x5 classification at the open area

Category/Stage	Dug	TOI	Frag
Training	93	8	85
CANT	9	0	9
Stage 1	No information due to missed seed		
Stage 2	144	78	66
Total	246	86	160
Non-dug	/	0	854 (84.2%)

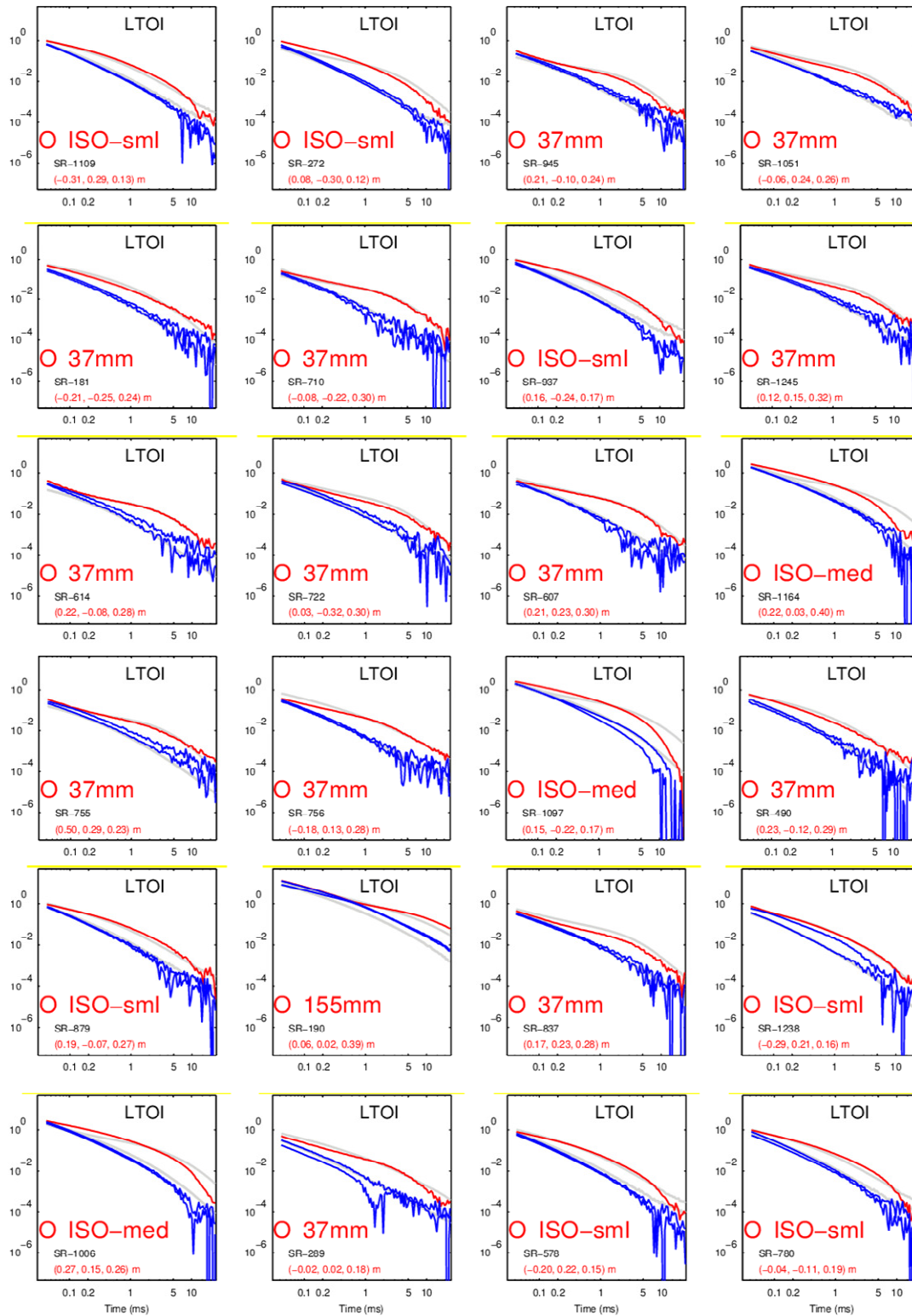


Figure 65: Polarizabilities of 24 TOI anomalies dug in the LTOI set

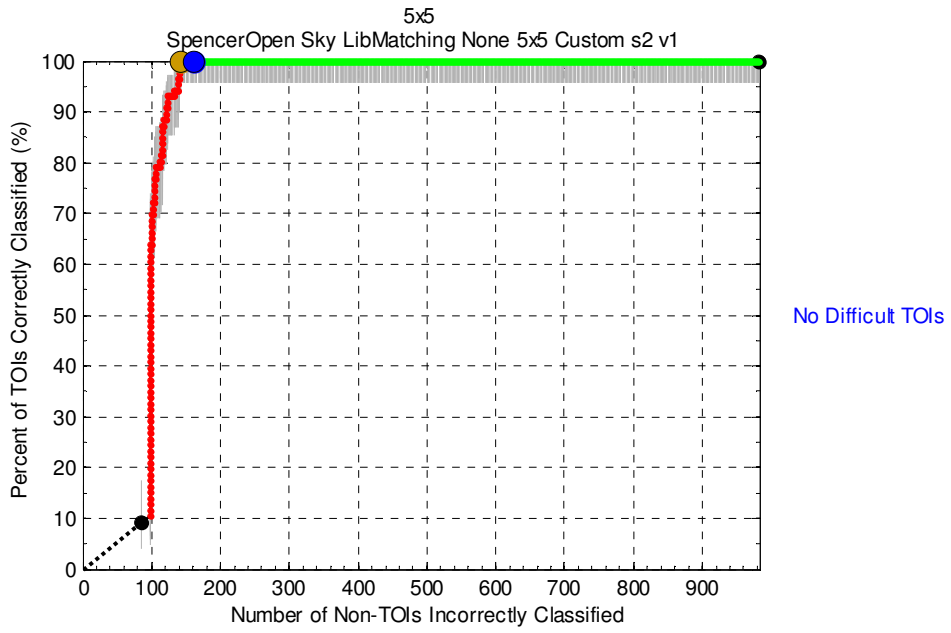


Figure 66: ROC curve for the Stage 2 dig list based on TEMTADS 5x5 Open Area data

Appendix D: PROCESSING AND CLASSIFICATION ANALYSIS OF DYNAMIC TEMTADS 2x2 DATA

D.1 Feature extraction

We processed the background corrected TEMTADS 2x2 dynamic data collected at the Spencer Range Dynamic area. The data were inverted in UXOLab using a sequential inversion approach to estimate target location, depth and primary polarizabilities. Instrument height above the ground was assumed to be 10 cm. Noise standard deviation estimates were not available, so a constant noise value of 1 over all time channels was used. Target location was constrained to lie between ± 0.5 m in both X and Y directions relative to the picked location. Target depth was constrained to lie between -1.2 and 0 m. The initial optimization for target location identified up to three starting models to input into the subsequent estimation of polarizabilities. We performed two single-object inversions per anomaly: (1) using all data within 75 cm of the picked target location; and (2) by inverting only the data along the transect that passed closest to the picked target location. Where necessary, the analyst adjusted masks and/or fit a two object inversion model to the data. The best fitting model for any of the inversions performed for a particular anomaly was used to make classification decisions.

Analysis of the data, including visual QC of data and model parameters, selection of training data, and dig list creation, was performed using the UXOLab software suite. Visual QC of the data was performed using *QCZilla*, which provides a thorough overview of the observed and predicted data, predicted model parameters, and measures of data/model quality (Figure 67). Predicted polarizabilities were compared to reference polarizabilities for various ordnance items initially derived from IVS measurements. The Spencer Artillery Range test pit contained four items: 75, 37mm, Small ISO, and Shot Put. The latter item was not used during the classification process. As the analysis proceeded, the library of reference items was augmented with additional items based on ground truth obtained through training data requests.

D.2 Classification

Training data selection

The TEMTADS 2x2 dynamic dataset at Spencer Range comprised 339 unique anomalies. Passed inversion models were obtained for all but four of the anomalies which were classified as “can’t extract reliable parameters”. Figure 68 shows the distribution of passed models in decay versus size feature space and the training data items that were selected. Ground-truth information was requested for twenty-one items spread across two training requests. The ground-truth requests focused on items with similar size and time-decay parameters to the known ordnance items and items that appeared to exhibit axial symmetry (Figure 69). Four of the ground-truth items were TOI, with most of the remaining items comprising rod-like pieces of shrapnel with comparable dimensions to the small ISO and 37 mm projectile. The ground-truth for one additional TOI (SR-1676 a small ISO seed) was revealed after the submission of the first dig-list.

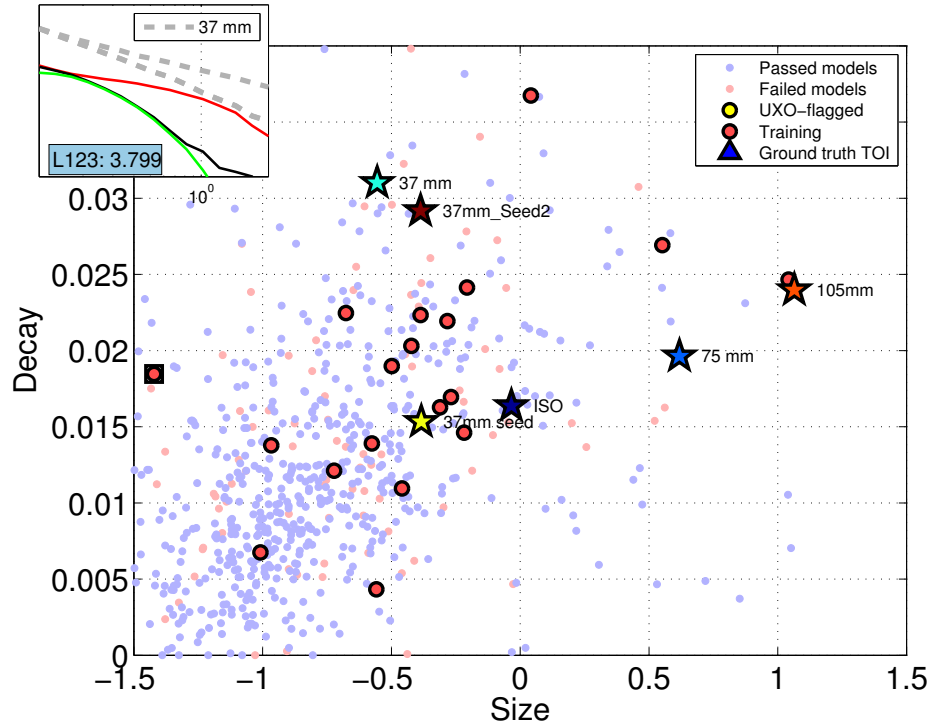


Figure 68: Distribution of passed (blue) and failed (red) models in decay(t_1, t_{15}) versus size(t_1) feature space, where size(t_1) is the total polarizability measured at the first time channel ($t_1=0.110$ ms), and decay(t_1, t_{25}) is size(t_1)/size(t_{29}) where $t_{29}=2.5$ ms. Some outliers are not shown. Labeled stars represent ordnance library reference items. The polarizability of the smallest training item selected (square symbol) is shown.

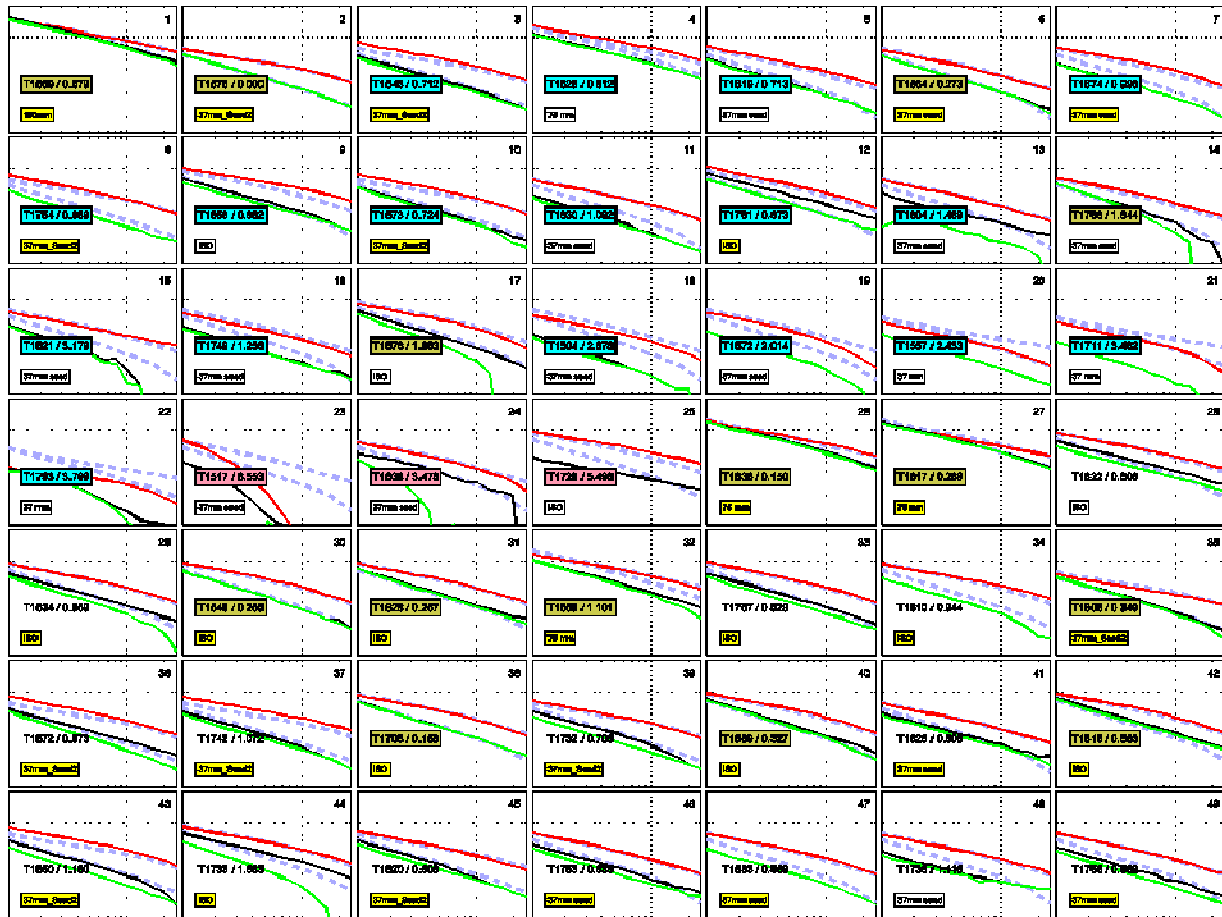


Figure 69: Polarizabilities of ground-truth items (first 22 plots) and the three “can’t extract reliable parameters” anomalies and the first 24 anomalies recommended for excavation.

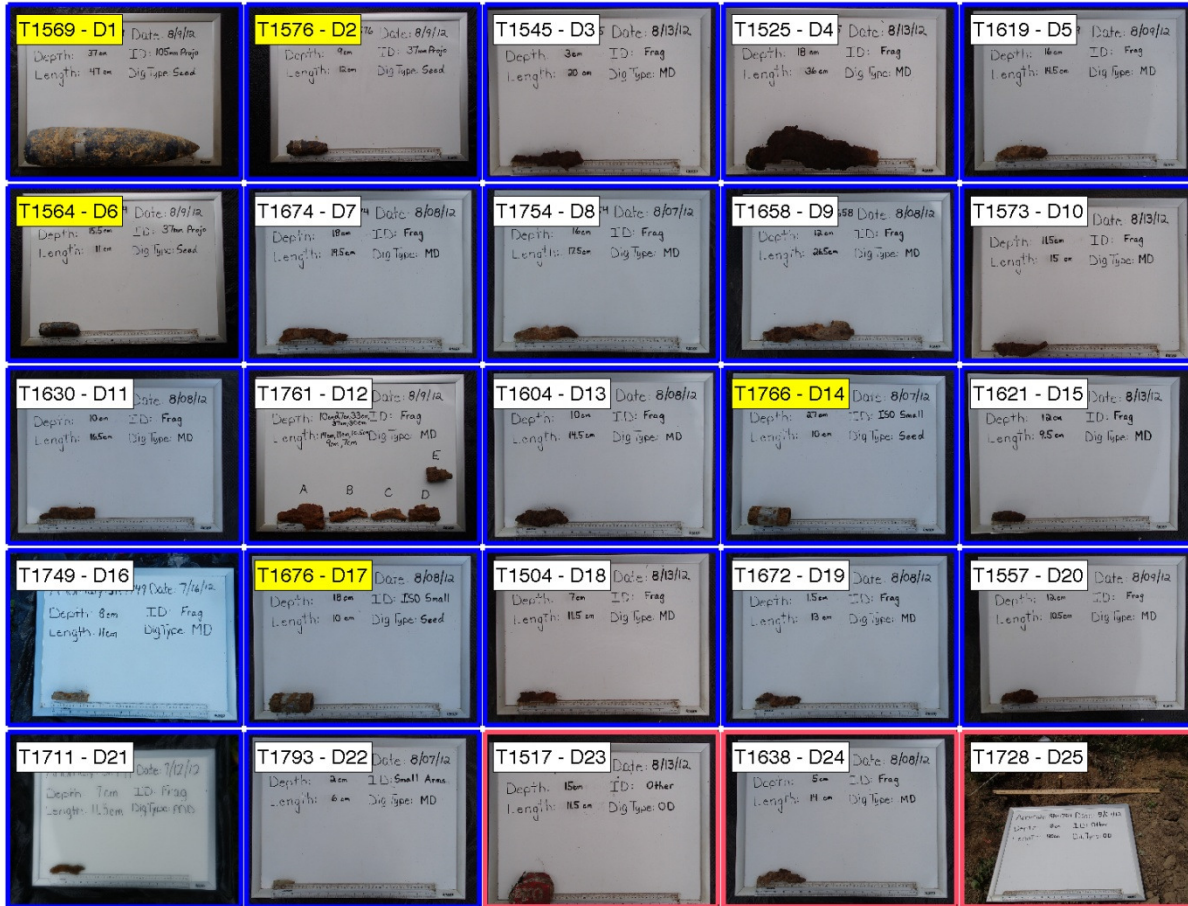


Figure 70: Photos of ground-truth items (first 22) and the three “can’t extract reliable parameters” anomalies. Item T1676 was a QC seed that was past the stop-dig point in the first dig-list submission. A yellow label indicates that the item is a TOI.

Classification method

The TEMTADS 2x2 dig order was developed using the *DigZilla* tool (Figure 22). *DigZilla* allows for the creation of multi-stage dig lists with minimal effort, and supports a number of classifiers. For the TEMTADS 2x2 dynamic we used the Combined Classifier Ranking (CCR) algorithm, with default weights. In the CCR algorithm we rank anomalies using feature vectors comprising (1) all polarizabilities; (2) primary polarizability; (3) Size and (4) Decay. Rankings for each of the four sets of feature vectors are obtained by comparison to the equivalent features in the reference library. The Combined Classifier Ranking is obtained by the weighted sum of the rankings in the four separate ranking schemes. Thus a feature vector that ranks high in more than one scheme will rank high in the CCR.

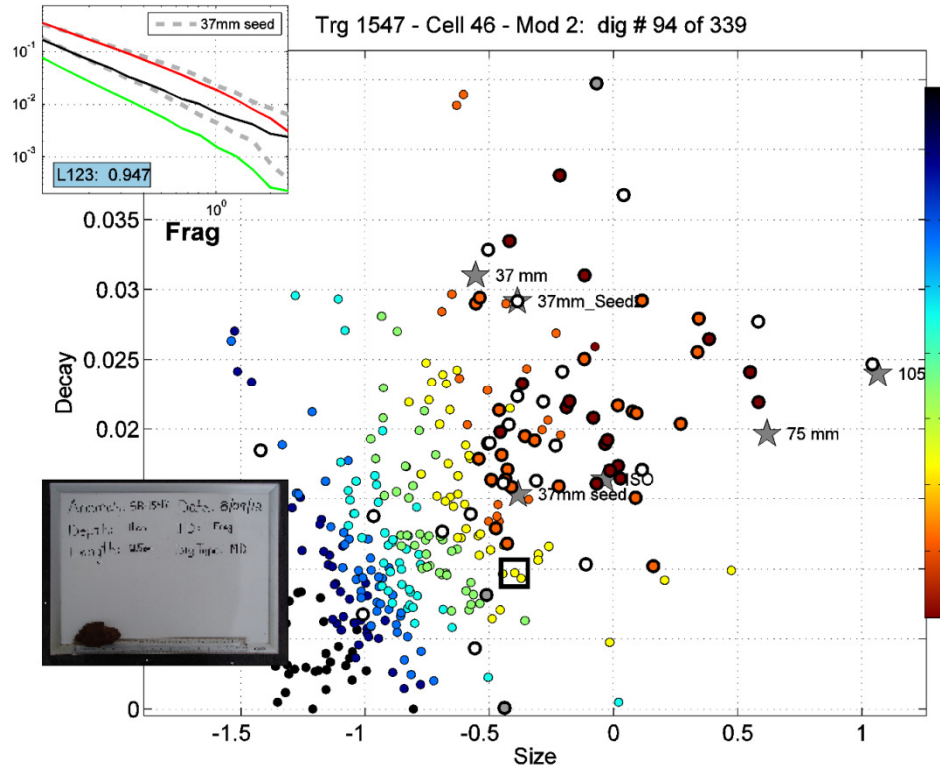


Figure 71: Screen shot of the *DigZilla* graphical user interface. Features in the decay versus size feature plot are color coded according to dig list order (warmer colors indicate items that are dug first). The first item after the stop-dig point is marked as a square and its feature plot and ground-truth photo are shown.

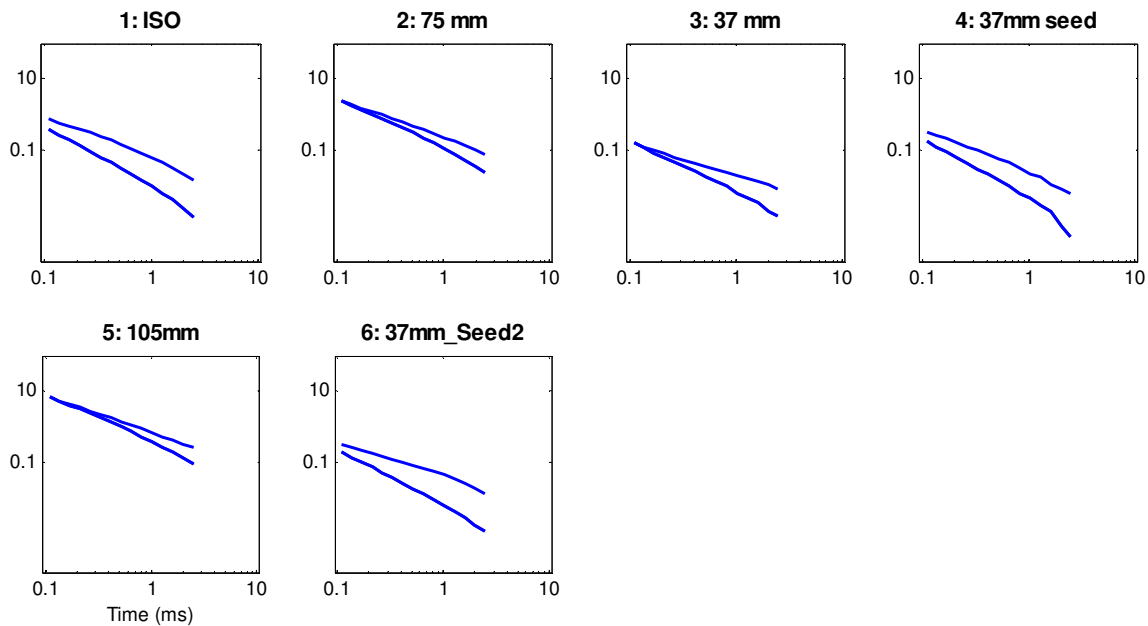


Figure 72: Polarizability library used for the TEMTADS 2x2 dynamic classification.

The stop dig-point was determined subjectively by the analyst: digging ceased after all items deemed to be high-priority TOI and/or low-confidence non-TOI items were dug. In the original dig-list submission one seed item (SR-1676) occurred past the stop-digging point. This item had a lower than expected time-decay parameter that placed it just past the stop-dig point. The CCR weights were adjusted so that items in the region of feature space below the ISO and 37 mm feature vectors were ranked higher.

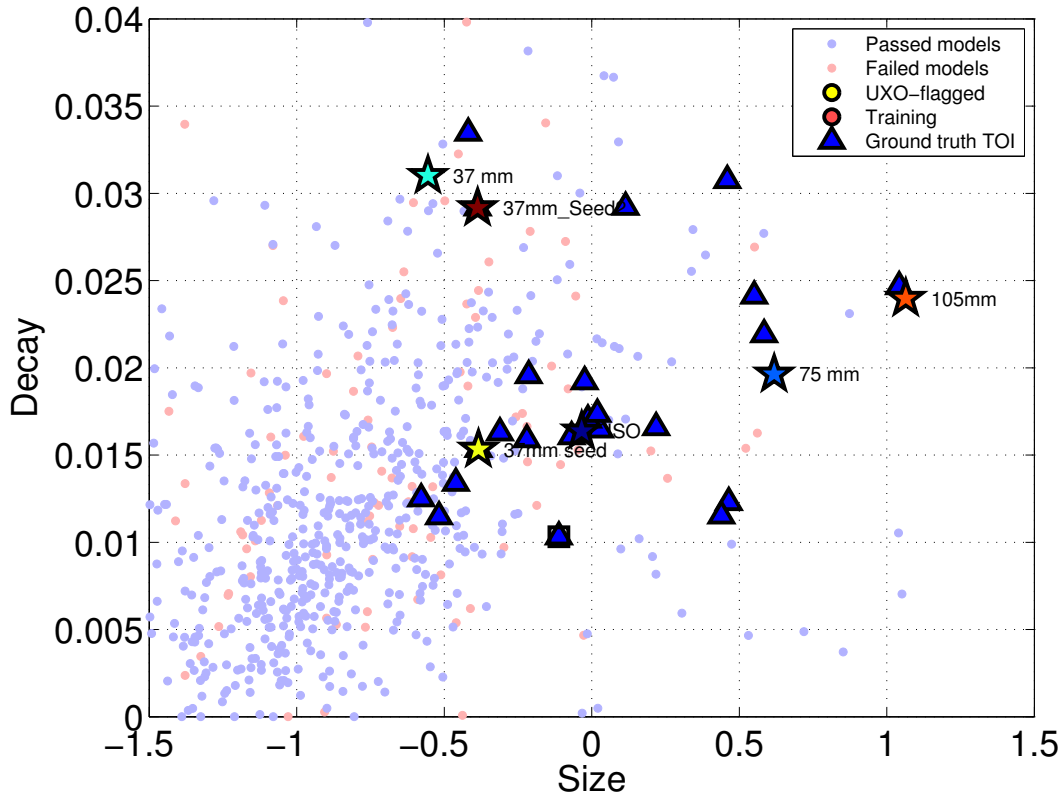


Figure 73: Size versus time-decay feature space plot with TOI items shown as blue-triangles. The one ISO seed item that occurred after the initial stop-dig point is marked with a square (on-top of the blue triangle).

A plot of the TOI and non-TOI feature vectors in the time-decay versus size space is shown in Figure 24. As expected the TOI cluster around the expected values for the reference library items. In some instances, the time-decay parameter exhibited a lower than expected value. This underestimation of the time-decay parameter appears to provides the highest risk exposure with dynamic TEMTADS 2x2 data.

The ROC curve for the final dig list is shown in Figure 27. There were no additional TOI beyond our stop dig point. We dug 115 items to find 18 TOI, giving a FAR of 5.4 non-TOI digs per TOI dig.

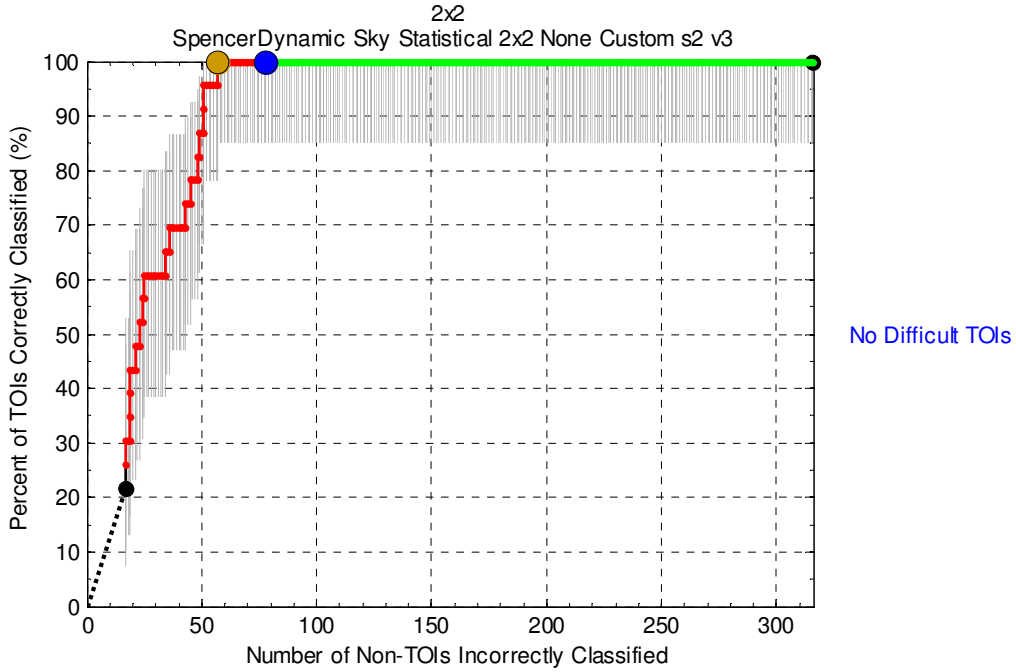


Figure 74: Final ROC curve for a dynamically deployed TEMTADS 2x2 data acquired in the Spencer Range Dynamic area.

Appendix E. Polarizability match to Targets of Interest

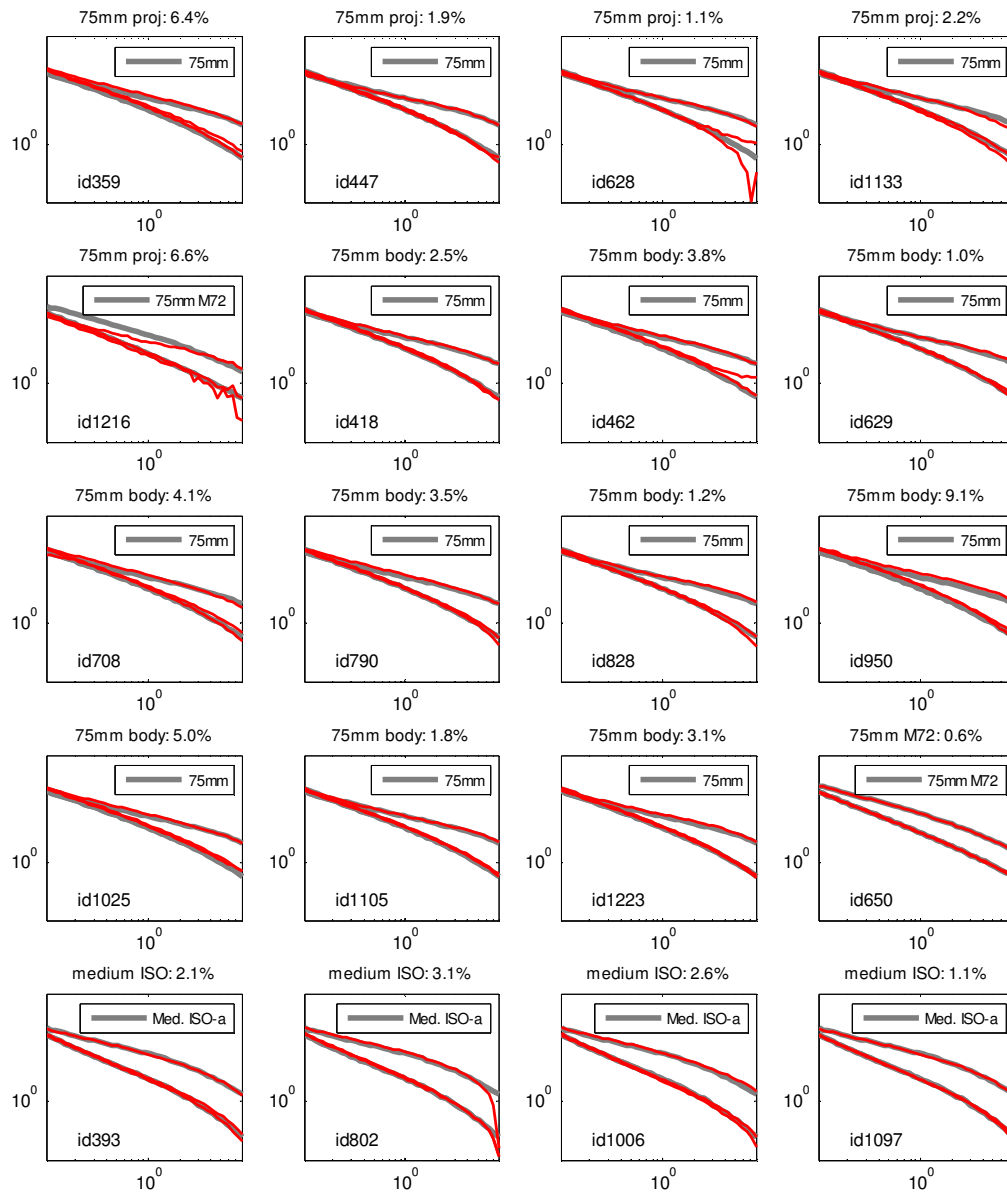


Figure 75: MetalMapper URS Cued data collected in the Open area (1/5).

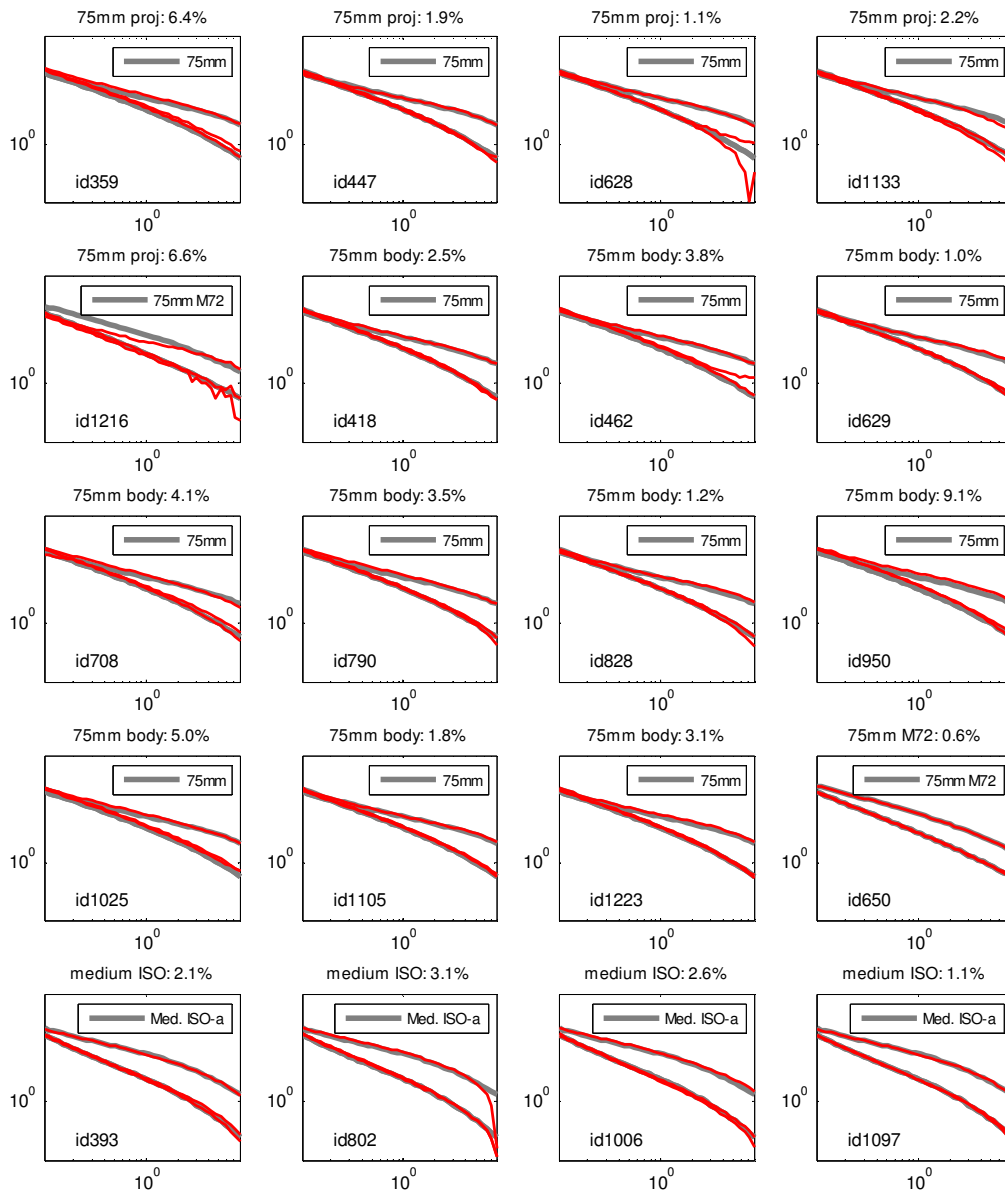


Figure 76: MetalMapper URS Cued data collected in the Open area (2/5).

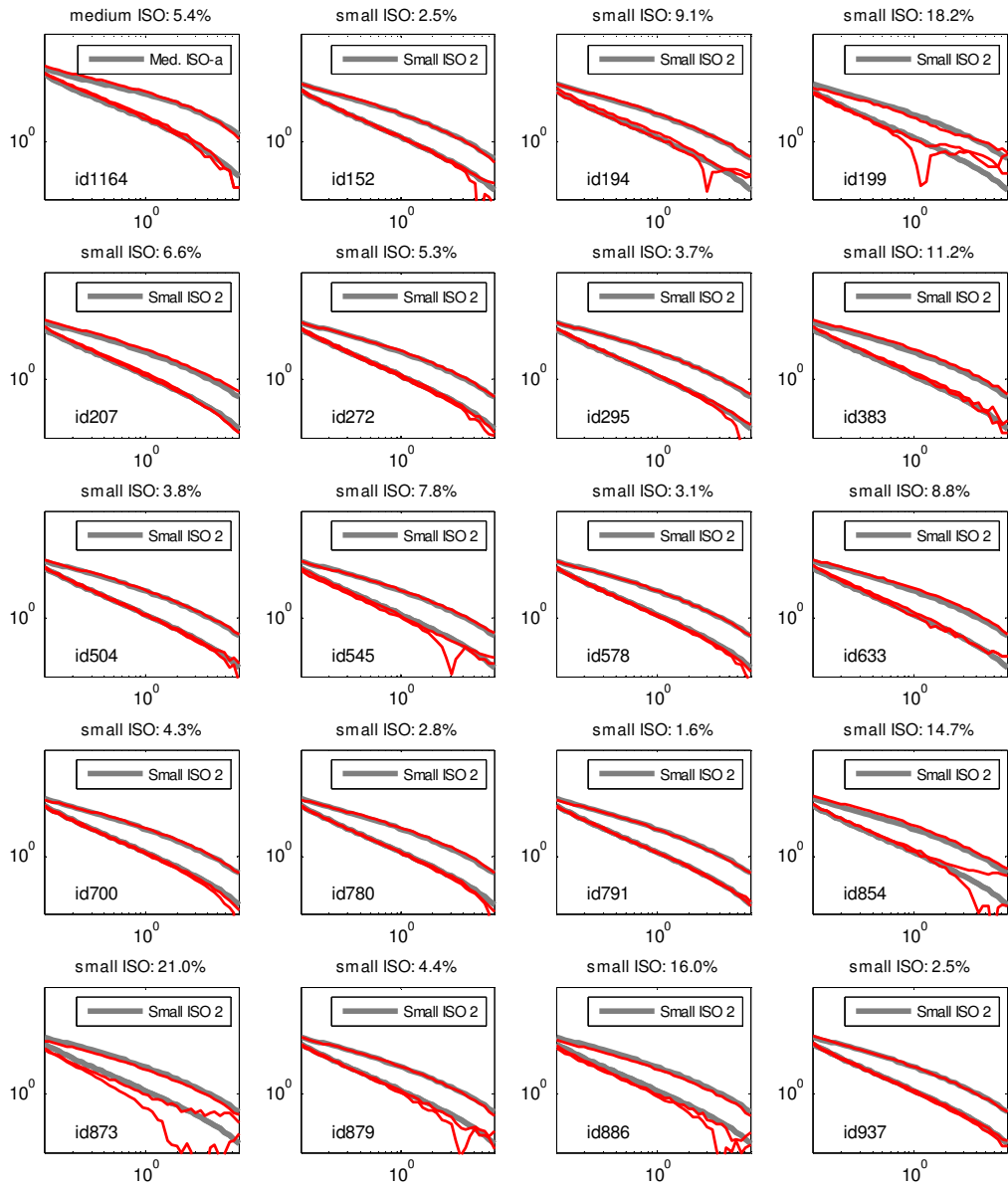


Figure 77: MetalMapper URS Cued data collected in the Open area (3/5).

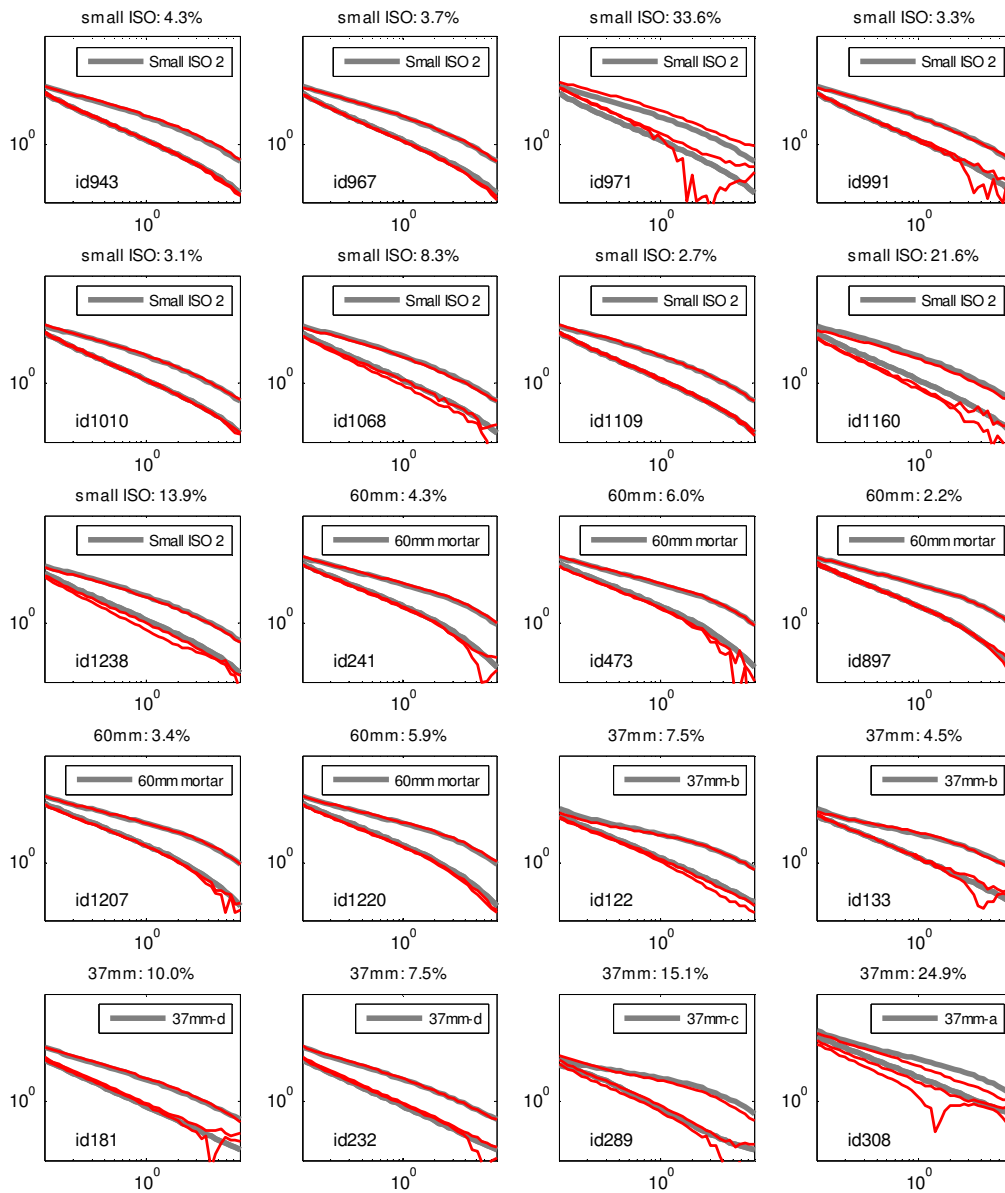


Figure 78: MetalMapper URS Cued data collected in the Open area (4/5).

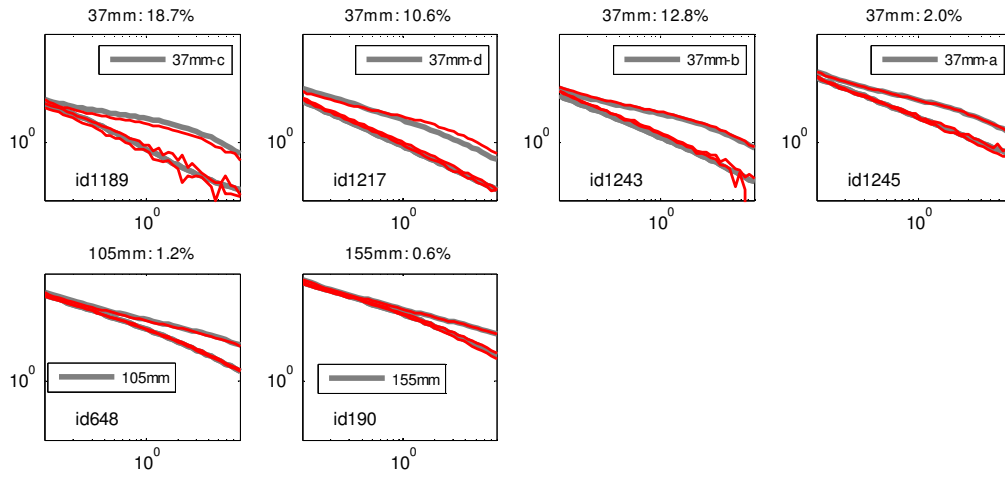


Figure 79: MetalMapper URS Cued data collected in the Open area (5/5).

Table 19: MetalMapper URS Cued data collected in the Open area.

Groud Truth	ID	%diff	Library reference
75mm proj	359	6.4	75mm
75mm proj	447	1.9	75mm
75mm proj	628	1.1	75mm
75mm proj	1133	2.2	75mm
75mm proj	1216	6.6	75mm M72
75mm body	418	2.5	75mm
75mm body	462	3.8	75mm
75mm body	629	1	75mm
75mm body	708	4.1	75mm
75mm body	790	3.5	75mm
75mm body	828	1.2	75mm
75mm body	950	9.1	75mm
75mm body	1025	5	75mm
75mm body	1105	1.8	75mm
75mm body	1223	3.1	75mm
75mm M72	650	0.6	75mm M72
medium ISO	393	2.1	Med. ISO-a
medium ISO	802	3.1	Med. ISO-a
medium ISO	1006	2.6	Med. ISO-a
medium ISO	1097	1.1	Med. ISO-a
medium ISO	1164	5.4	Med. ISO-a
small ISO	152	2.5	Small ISO 2
small ISO	194	9.1	Small ISO 2
small ISO	199	18.2	Small ISO 2
small ISO	207	6.6	Small ISO 2
small ISO	272	5.3	Small ISO 2
small ISO	295	3.7	Small ISO 2
small ISO	383	11.2	Small ISO 2
small ISO	504	3.8	Small ISO 2
small ISO	545	7.8	Small ISO 2
small ISO	578	3.1	Small ISO 2
small ISO	633	8.8	Small ISO 2
small ISO	700	4.3	Small ISO 2
small ISO	780	2.8	Small ISO 2
small ISO	791	1.6	Small ISO 2
small ISO	854	14.7	Small ISO 2
small ISO	873	21	Small ISO 2
small ISO	879	4.4	Small ISO 2
small ISO	886	16	Small ISO 2
small ISO	937	2.5	Small ISO 2
small ISO	943	4.3	Small ISO 2
small ISO	967	3.7	Small ISO 2
small ISO	971	33.6	Small ISO 2

Groud Truth	ID	%diff	Library reference
small ISO	991	3.3	Small ISO 2
small ISO	1010	3.1	Small ISO 2
small ISO	1068	8.3	Small ISO 2
small ISO	1109	2.7	Small ISO 2
small ISO	1160	21.6	Small ISO 2
small ISO	1238	13.9	Small ISO 2
60mm	241	4.3	60mm mortar
60mm	473	6	60mm mortar
60mm	897	2.2	60mm mortar
60mm	1207	3.4	60mm mortar
60mm	1220	5.9	60mm mortar
37mm	122	7.5	37mm-b
37mm	133	4.5	37mm-b
37mm	181	10	37mm-d
37mm	232	7.5	37mm-d
37mm	289	15.1	37mm-c
37mm	308	24.9	37mm-a
37mm	425	9.2	37mm-d
37mm	490	6.7	37mm-d
37mm	505	8.7	37mm-d
37mm	572	3.3	37mm-d
37mm	583	10.5	37mm-c
37mm	607	13.8	37mm
37mm	614	7.6	37mm
37mm	710	9.2	37mm-c
37mm	722	10.4	37mm
37mm	755	6.8	37mm-b
37mm	756	15.2	37mm-b
37mm	837	7.8	37mm-a
37mm	888	9.2	37mm-d
37mm	945	6	37mm-b
37mm	978	12.8	37mm
37mm	992	13.3	37mm
37mm	1051	3.9	37mm-c
37mm	1067	8.8	37mm-c
37mm	1083	5.7	37mm-d
37mm	1169	4.8	37mm-b
37mm	1189	18.7	37mm-c
37mm	1217	10.6	37mm-d
37mm	1243	12.8	37mm-b
37mm	1245	2	37mm-a
105mm	648	1.2	105mm
155mm	190	0.6	155mm

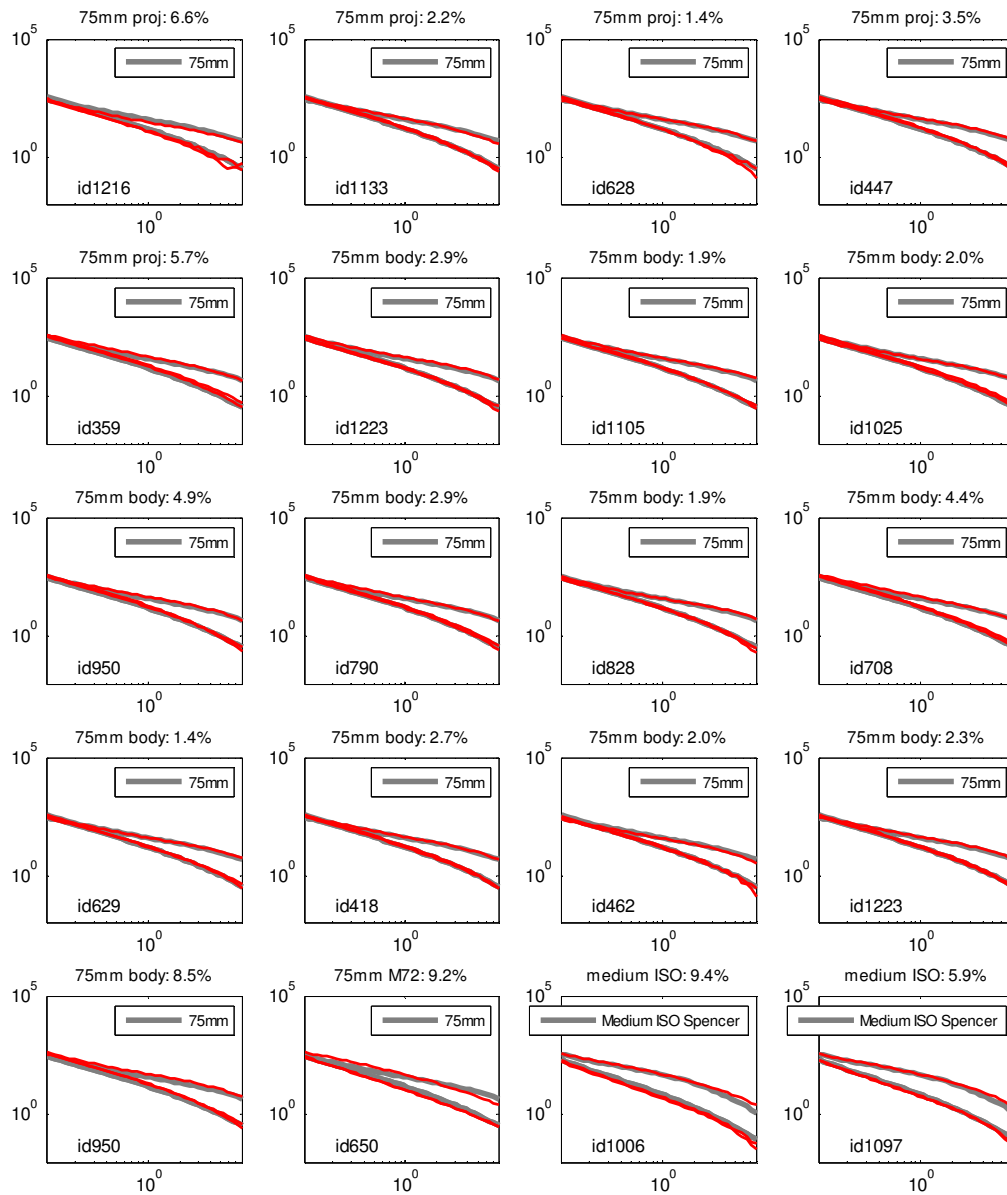


Figure 80: MetalMapper Naeva Cued data collected in the Open area (1/5).

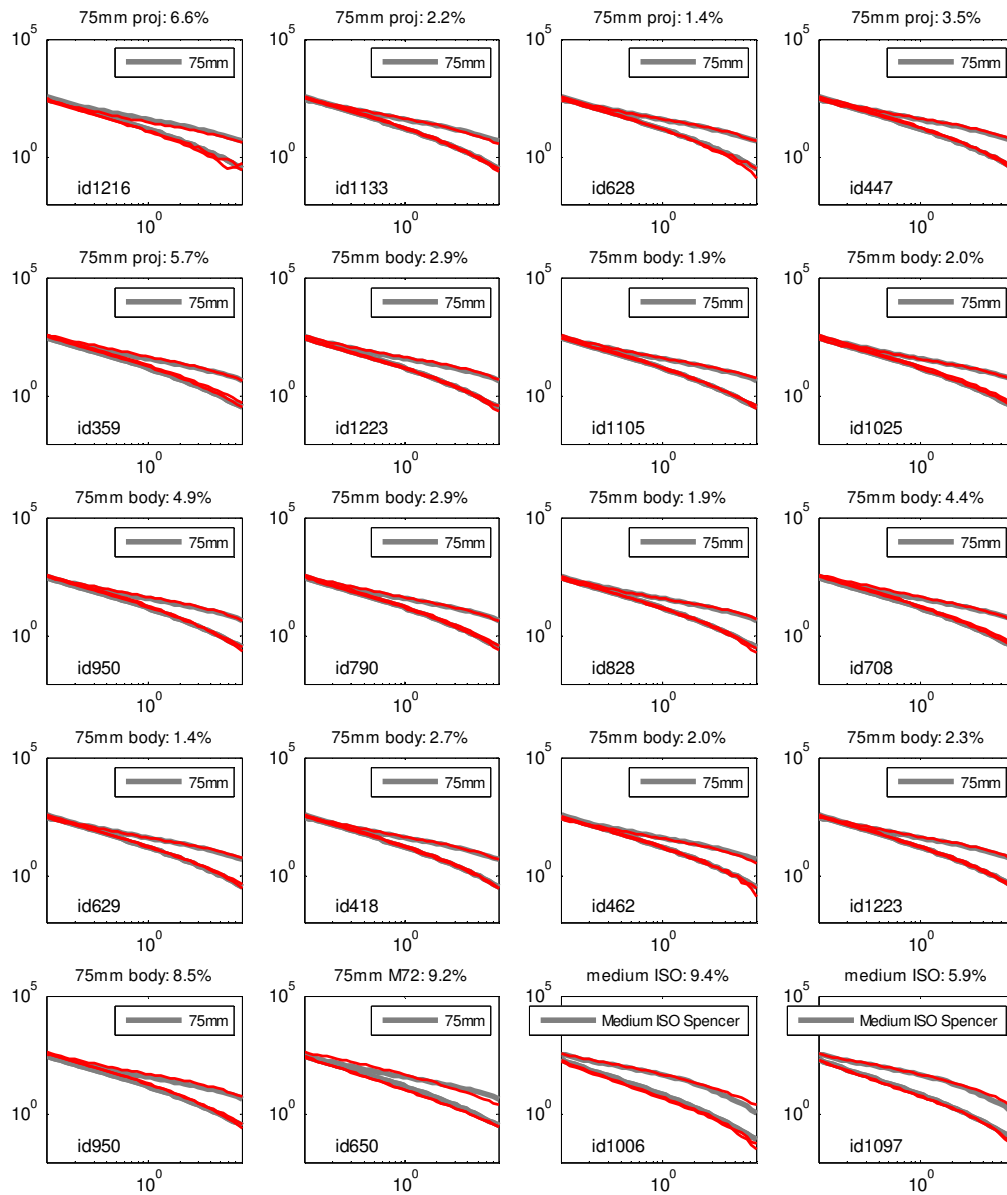


Figure 81: MetalMapper Naeva Cued data collected in the Open area (2/5).

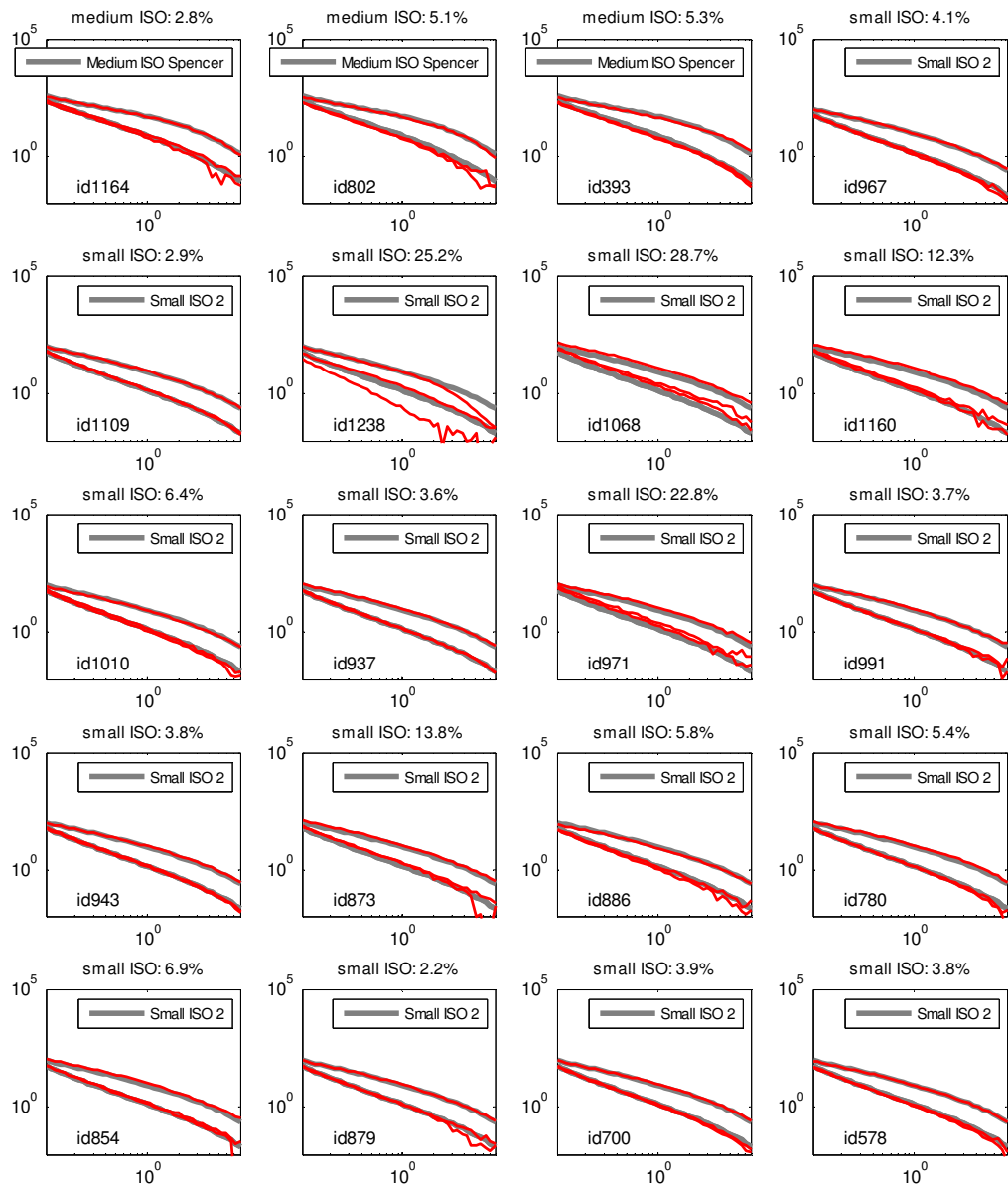


Figure 82: MetalMapper Naeva Cued data collected in the Open area (3/5).

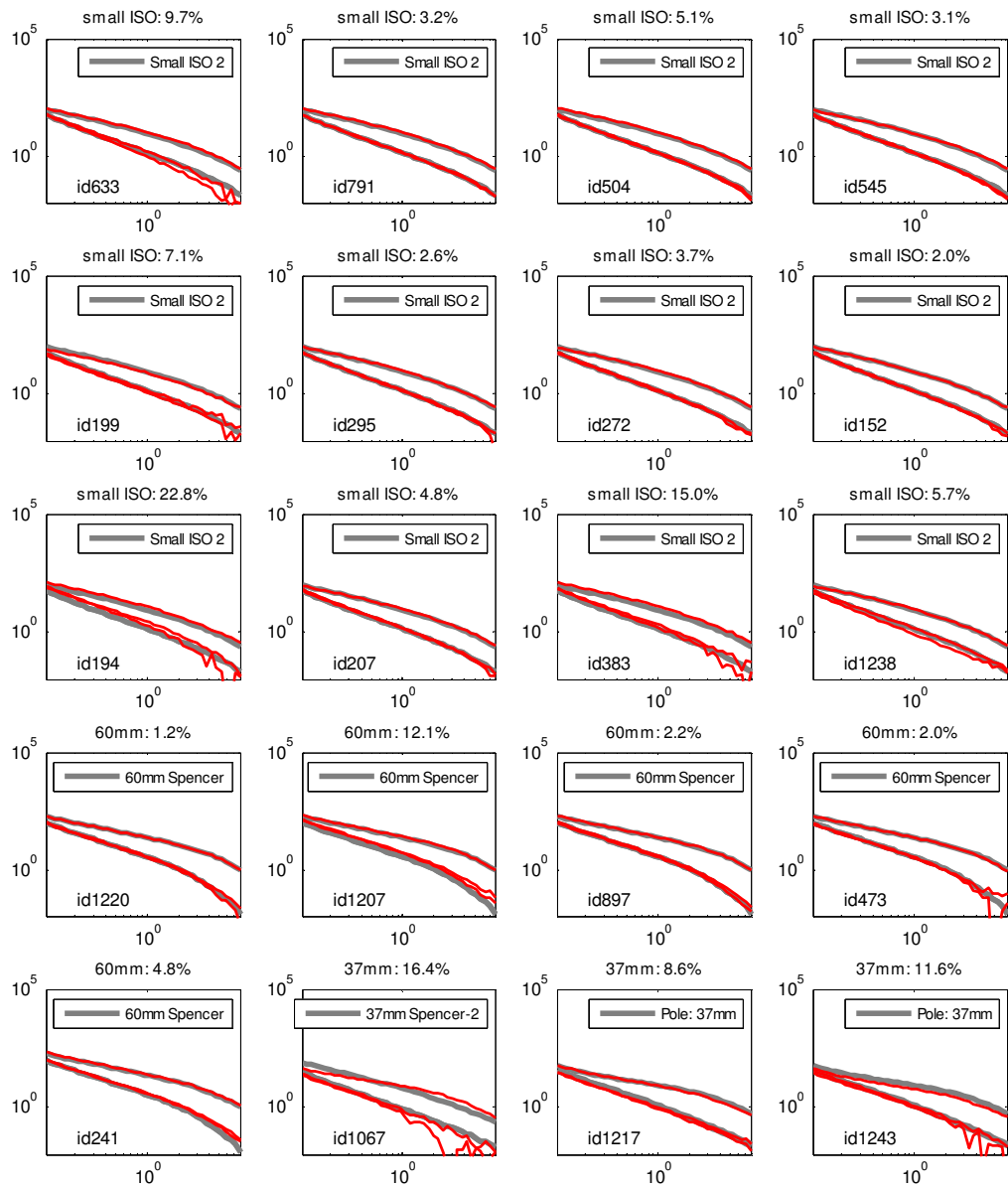


Figure 83: MetalMapper Naeva Cued data collected in the Open area (4/5).

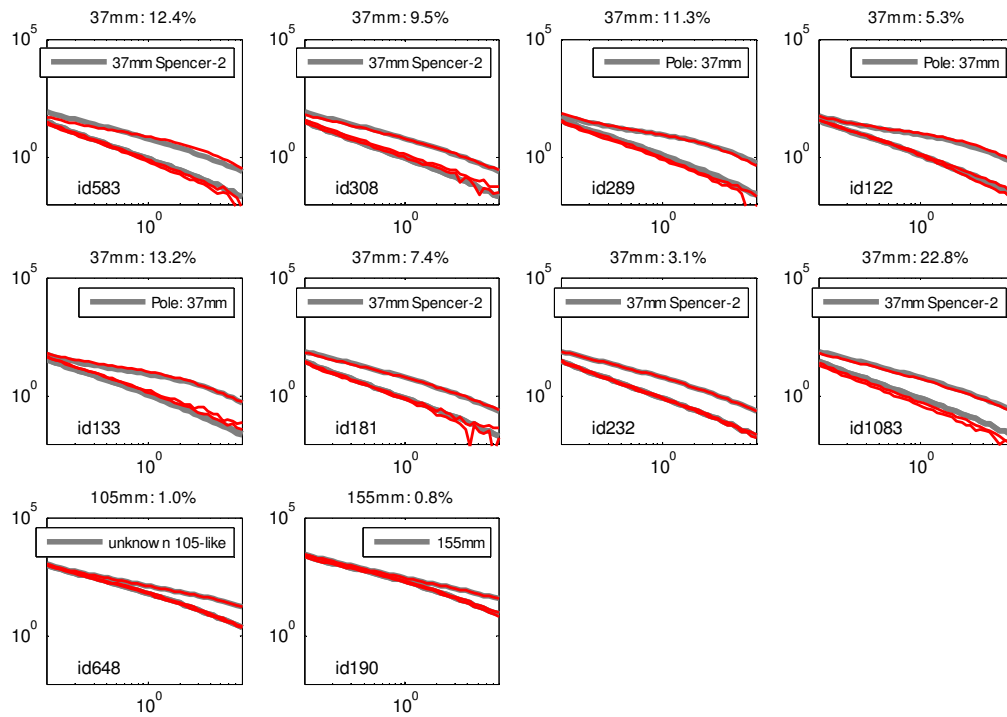


Figure 84: MetalMapper Naeva Cued data collected in the Open area (5/5).

Table 20: MetalMapper Naeva Cued data collected in the Open area.

Groud Truth	ID	% diff	Library reference
75mm proj	1216	6.6	75mm
75mm proj	1133	2.2	75mm
75mm proj	628	1.4	75mm
75mm proj	447	3.5	75mm
75mm proj	359	5.7	75mm
75mm body	1105	1.9	75mm
75mm body	1025	2	75mm
75mm body	950	4.9	75mm
75mm body	790	2.9	75mm
75mm body	828	1.9	75mm
75mm body	708	4.4	75mm
75mm body	629	1.4	75mm
75mm body	418	2.7	75mm
75mm body	462	2	75mm
75mm body	1223	2.3	75mm
75mm M72	650	9.2	75mm
medium ISO	1006	9.4	Medium ISO Spencer
medium ISO	1097	5.9	Medium ISO Spencer
medium ISO	1164	2.8	Medium ISO Spencer
medium ISO	802	5.1	Medium ISO Spencer
medium ISO	393	5.3	Medium ISO Spencer
small ISO	967	4.1	Small ISO 2
small ISO	1109	2.9	Small ISO 2
small ISO	1068	28.7	Small ISO 2
small ISO	1160	12.3	Small ISO 2
small ISO	1010	6.4	Small ISO 2
small ISO	937	3.6	Small ISO 2
small ISO	971	22.8	Small ISO 2
small ISO	991	3.7	Small ISO 2
small ISO	943	3.8	Small ISO 2
small ISO	873	13.8	Small ISO 2
small ISO	886	5.8	Small ISO 2
small ISO	780	5.4	Small ISO 2
small ISO	854	6.9	Small ISO 2
small ISO	879	2.2	Small ISO 2
small ISO	700	3.9	Small ISO 2
small ISO	578	3.8	Small ISO 2
small ISO	633	9.7	Small ISO 2
small ISO	791	3.2	Small ISO 2
small ISO	504	5.1	Small ISO 2
small ISO	545	3.1	Small ISO 2
small ISO	199	7.1	Small ISO 2
small ISO	295	2.6	Small ISO 2

Groud Truth	ID	% diff	Library reference
small ISO	272	3.7	Small ISO 2
small ISO	152	2	Small ISO 2
small ISO	194	22.8	Small ISO 2
small ISO	207	4.8	Small ISO 2
small ISO	383	15	Small ISO 2
small ISO	1238	5.7	Small ISO 2
60mm	1220	1.2	60mm Spencer
60mm	1207	12.1	60mm Spencer
60mm	897	2.2	60mm Spencer
60mm	473	2	60mm Spencer
60mm	241	4.8	60mm Spencer
37mm	1067	16.4	37mm Spencer-2
37mm	1217	8.6	Pole: 37mm
37mm	1243	11.6	Pole: 37mm
37mm	1245	18.9	Pole: 37mm
37mm	1051	5.6	Pole: 37mm
37mm	1083	7.7	37mm Spencer-2
37mm	1169	5.6	Pole: 37mm
37mm	1189	9.8	Pole: 37mm
37mm	978	3.2	Pole: 37mm
37mm	992	6.5	Pole: 37mm
37mm	888	5.9	37mm Spencer-2
37mm	945	6.7	Pole: 37mm
37mm	837	34.2	37mm Spencer-2
37mm	756	3.3	Pole: 37mm
37mm	710	14.7	37mm Spencer-2
37mm	572	13.8	37mm Spencer-2
37mm	614	7.5	Pole: 37mm
37mm	722	6.6	Pole: 37mm
37mm	755	8.3	Pole: 37mm
37mm	607	7	Pole: 37mm
37mm	425	10.5	Pole: 37mm
37mm	490	7.3	37mm Spencer-2
37mm	505	8.1	Pole: 37mm
37mm	583	12.4	37mm Spencer-2
37mm	308	9.5	37mm Spencer-2
37mm	289	11.3	Pole: 37mm
37mm	122	5.3	Pole: 37mm
37mm	133	13.2	Pole: 37mm
37mm	181	7.4	37mm Spencer-2
37mm	232	3.1	37mm Spencer-2
105mm	648	1	unknown 105-like
155mm	190	0.8	155mm

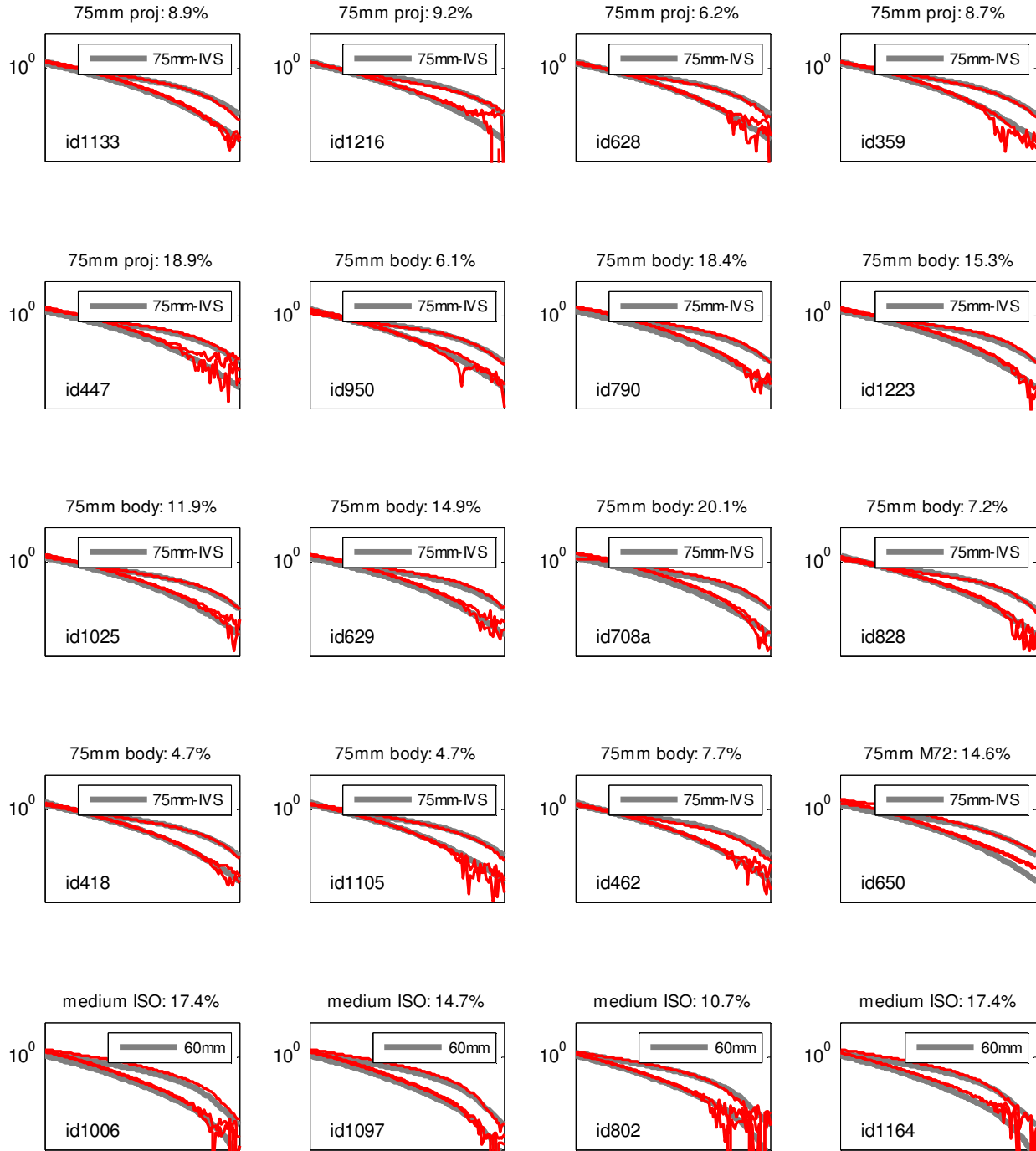


Figure 85: TEMTADS 5x5 cued data from the Open area (1/5).

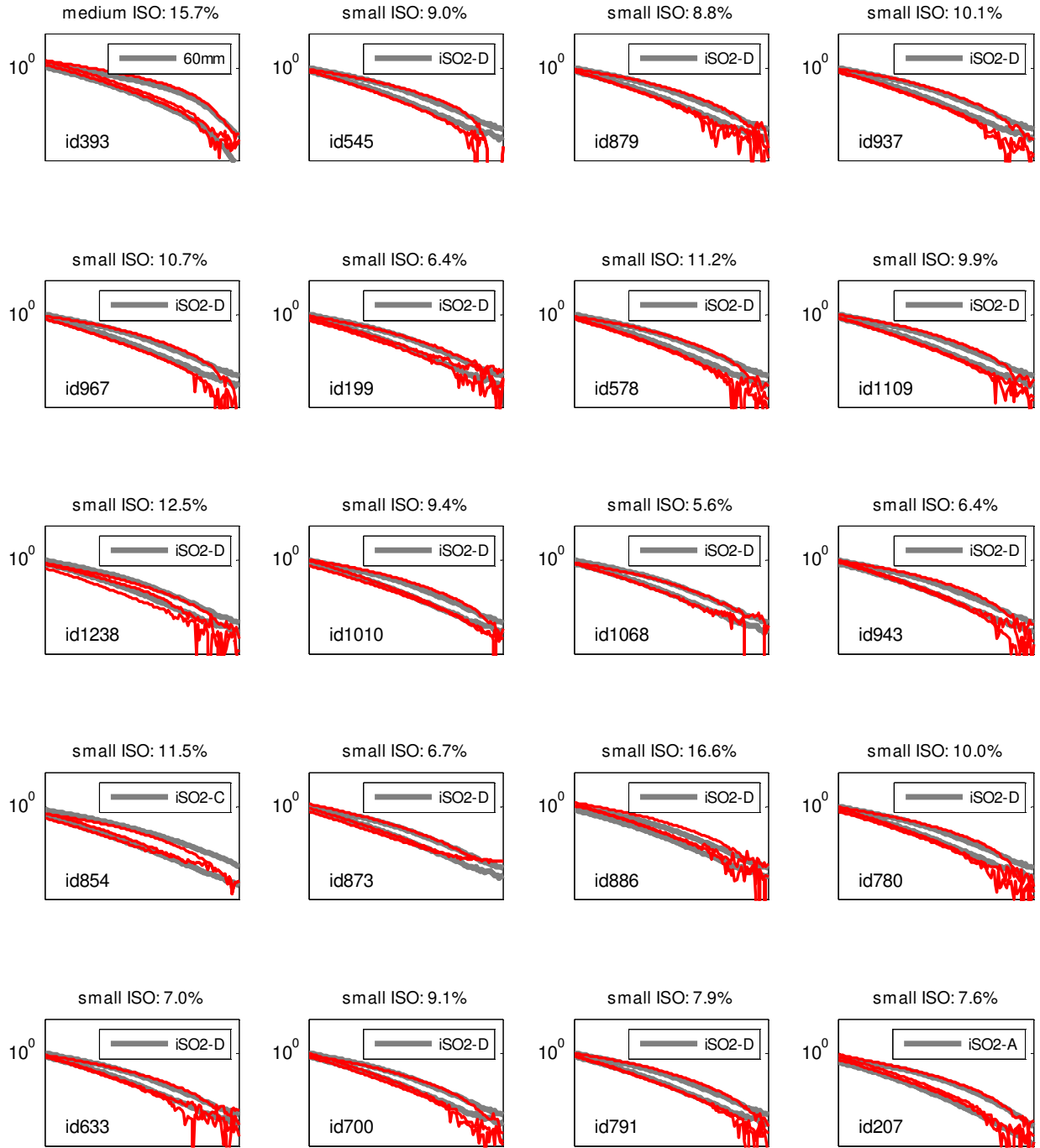


Figure 86: TEMTADS 5x5 cued data from the Open area (2/5).

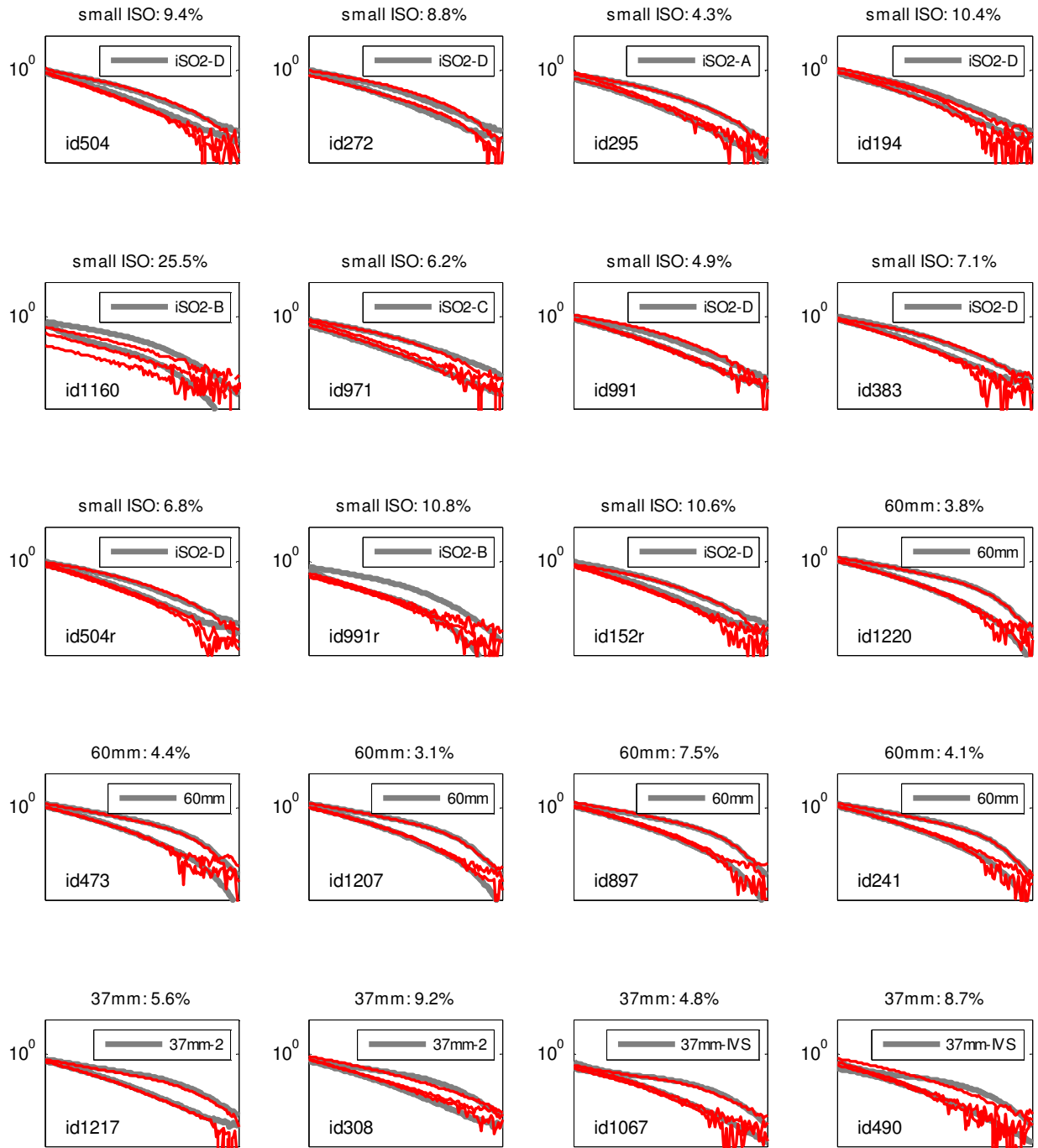


Figure 87: TEMTADS 5x5 cued data from the Open area (3/5).

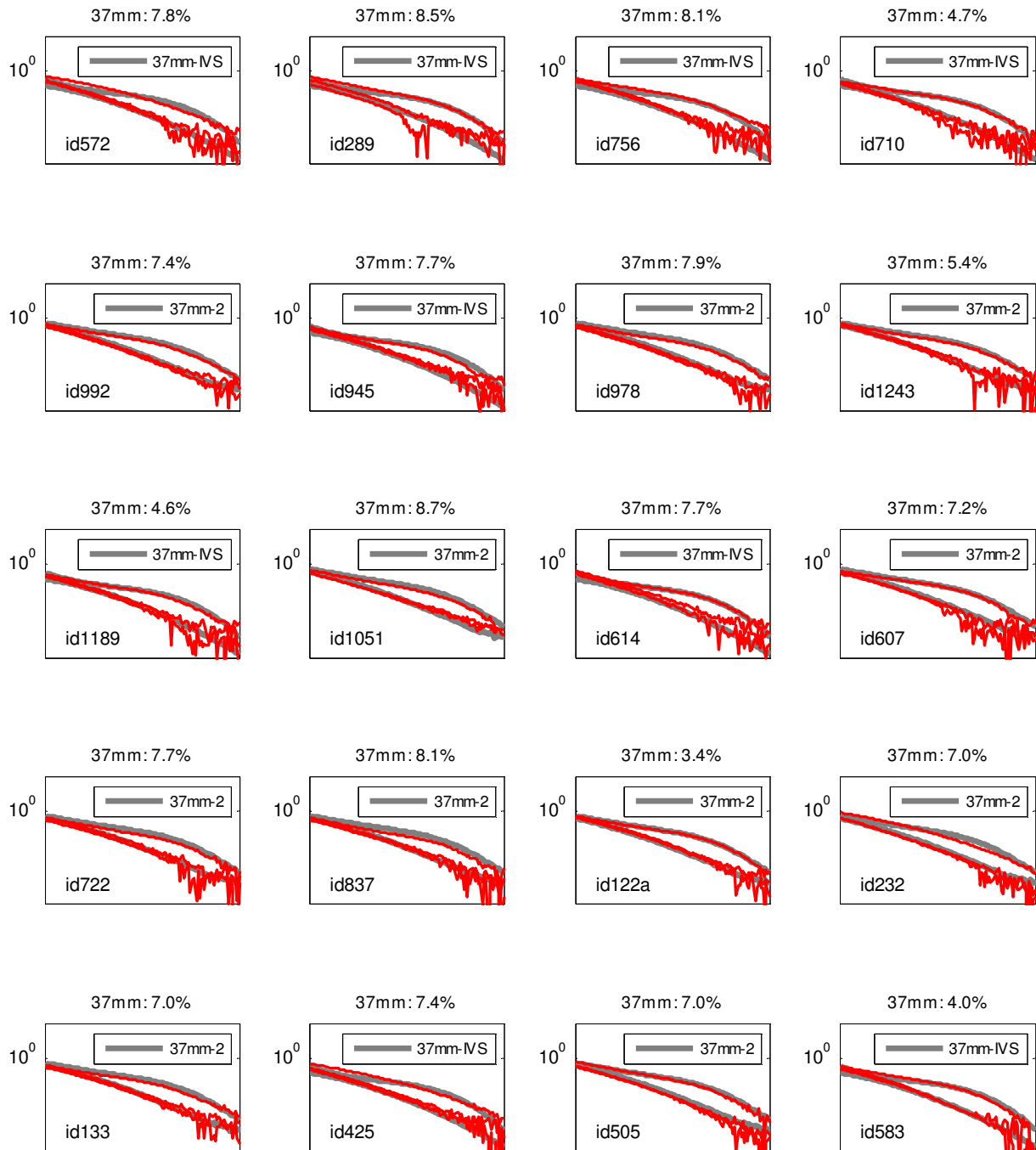


Figure 88: TEMTADS 5x5 cued data from the Open area (4/5).

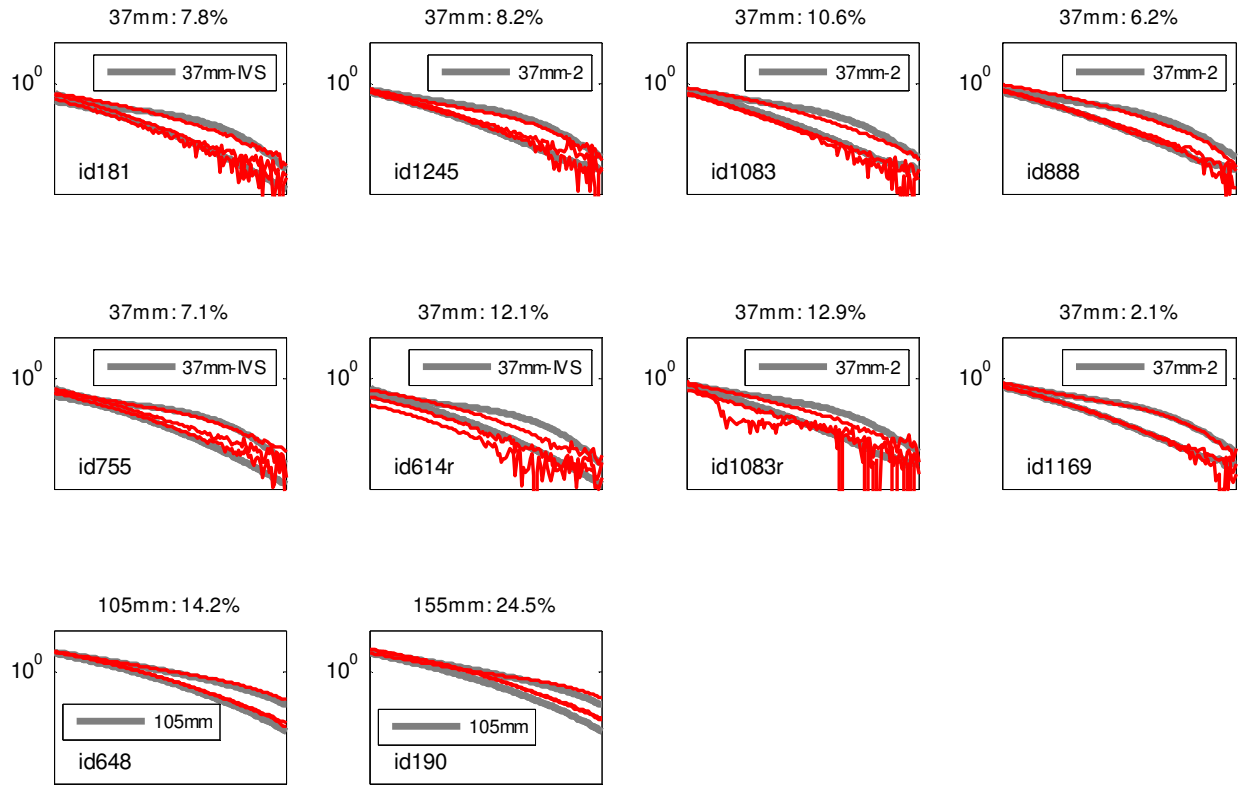


Figure 89: TEMTADS 5x5 cued data from the Open area

Table 21: TEMTADS 5x5 cued data from the Open area.

Groud Truth	ID	% diff	Library reference
75mm proj	1133	8.9	75mm-IVS
75mm proj	1216	9.2	75mm-IVS
75mm proj	628	6.2	75mm-IVS
75mm proj	359	8.7	75mm-IVS
75mm proj	447	18.9	75mm-IVS
75mm body	950	6.1	75mm-IVS
75mm body	790	18.4	75mm-IVS
75mm body	1223	15.3	75mm-IVS
75mm body	1025	11.9	75mm-IVS
75mm body	629	14.9	75mm-IVS
75mm body	708a	20.1	75mm-IVS
75mm body	828	7.2	75mm-IVS
75mm body	418	4.7	75mm-IVS
75mm body	1105	4.7	75mm-IVS
75mm body	462	7.7	75mm-IVS
75mm M72	650	14.6	75mm-IVS
medium ISO	1006	17.4	60mm
medium ISO	1097	14.7	60mm
medium ISO	802	10.7	60mm
medium ISO	1164	17.4	60mm
medium ISO	393	15.7	60mm
small ISO	545	9	iSO2-D
small ISO	879	8.8	iSO2-D
small ISO	937	10.1	iSO2-D
small ISO	967	10.7	iSO2-D
small ISO	199	6.4	iSO2-D
small ISO	578	11.2	iSO2-D
small ISO	1109	9.9	iSO2-D
small ISO	1238	12.5	iSO2-D
small ISO	1010	9.4	iSO2-D
small ISO	1068	5.6	iSO2-D
small ISO	943	6.4	iSO2-D
small ISO	854	11.5	iSO2-C
small ISO	873	6.7	iSO2-D
small ISO	886	16.6	iSO2-D
small ISO	780	10	iSO2-D
small ISO	633	7	iSO2-D
small ISO	700	9.1	iSO2-D
small ISO	791	7.9	iSO2-D
small ISO	207	7.6	iSO2-A
small ISO	504	9.4	iSO2-D
small ISO	272	8.8	iSO2-D
small ISO	295	4.3	iSO2-A
small ISO	194	10.4	iSO2-D
small ISO	1160	25.5	iSO2-B

Groud Truth	ID	% diff	Library reference
small ISO	971	6.2	iSO2-C
small ISO	991	4.9	iSO2-D
small ISO	383	7.1	iSO2-D
small ISO	504r	6.8	iSO2-D
small ISO	991r	10.8	iSO2-B
small ISO	152r	10.6	iSO2-D
60mm	1220	3.8	60mm
60mm	473	4.4	60mm
60mm	1207	3.1	60mm
60mm	897	7.5	60mm
60mm	241	4.1	60mm
37mm	1217	5.6	37mm-2
37mm	308	9.2	37mm-2
37mm	1067	4.8	37mm-IVS
37mm	490	8.7	37mm-IVS
37mm	572	7.8	37mm-IVS
37mm	289	8.5	37mm-IVS
37mm	756	8.1	37mm-IVS
37mm	710	4.7	37mm-IVS
37mm	992	7.4	37mm-2
37mm	945	7.7	37mm-IVS
37mm	978	7.9	37mm-2
37mm	1243	5.4	37mm-2
37mm	1189	4.6	37mm-IVS
37mm	1051	8.7	37mm-2
37mm	614	7.7	37mm-IVS
37mm	607	7.2	37mm-2
37mm	722	7.7	37mm-2
37mm	837	8.1	37mm-2
37mm	122a	3.4	37mm-2
37mm	232	7	37mm-2
37mm	133	7	37mm-2
37mm	425	7.4	37mm-IVS
37mm	505	7	37mm-2
37mm	583	4	37mm-IVS
37mm	181	7.8	37mm-IVS
37mm	1245	8.2	37mm-2
37mm	1083	10.6	37mm-2
37mm	888	6.2	37mm-2
37mm	755	7.1	37mm-IVS
37mm	614r	12.1	37mm-IVS
37mm	1083r	12.9	37mm-2
37mm	1169	2.1	37mm-2
105mm	648	14.2	105mm
155mm	190	24.5	105mm

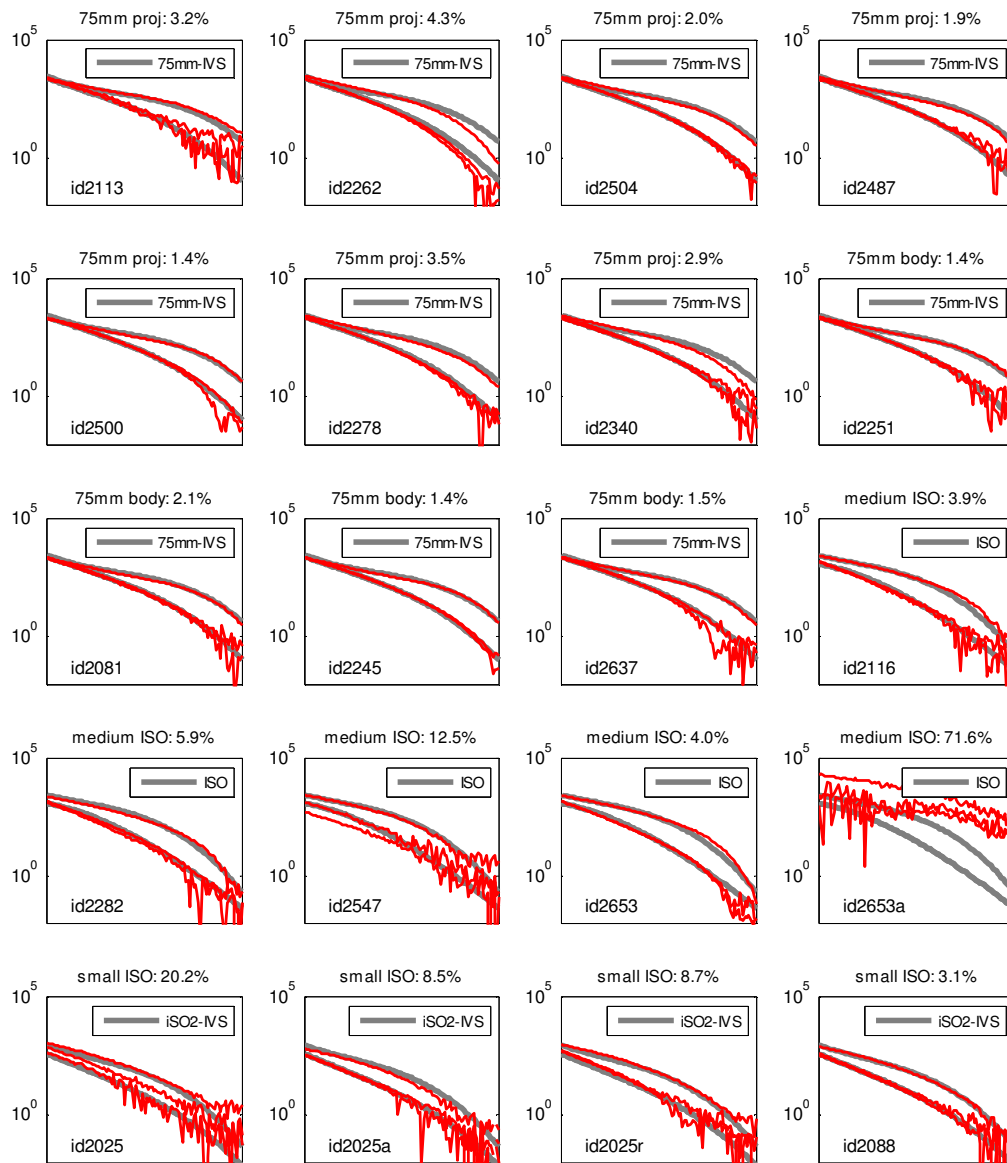


Figure 90: TEMTADS 2x2 cued data from the Treed area (1/4)

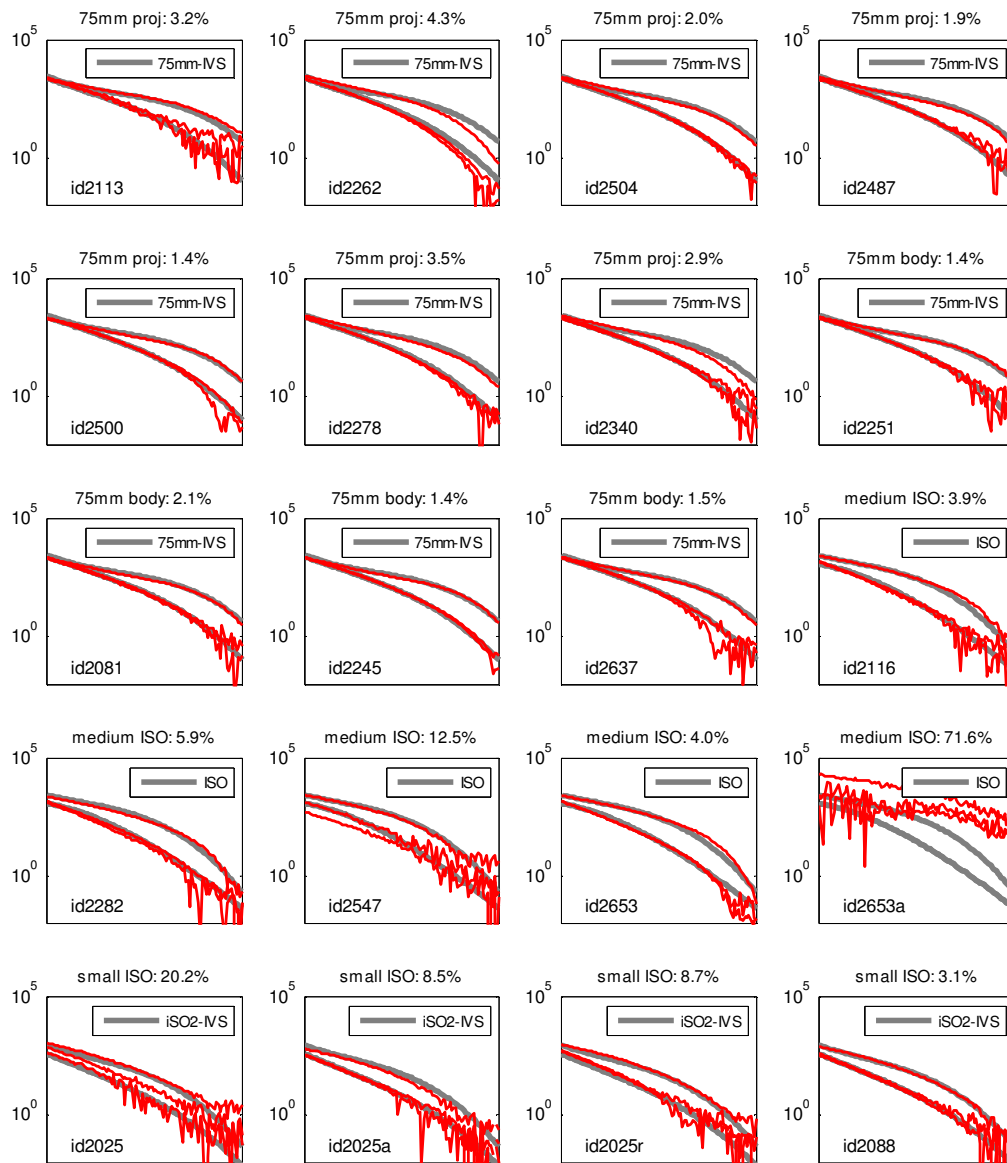


Figure 91: TEMTADS 2x2 cued data from the Treed area (2/4)

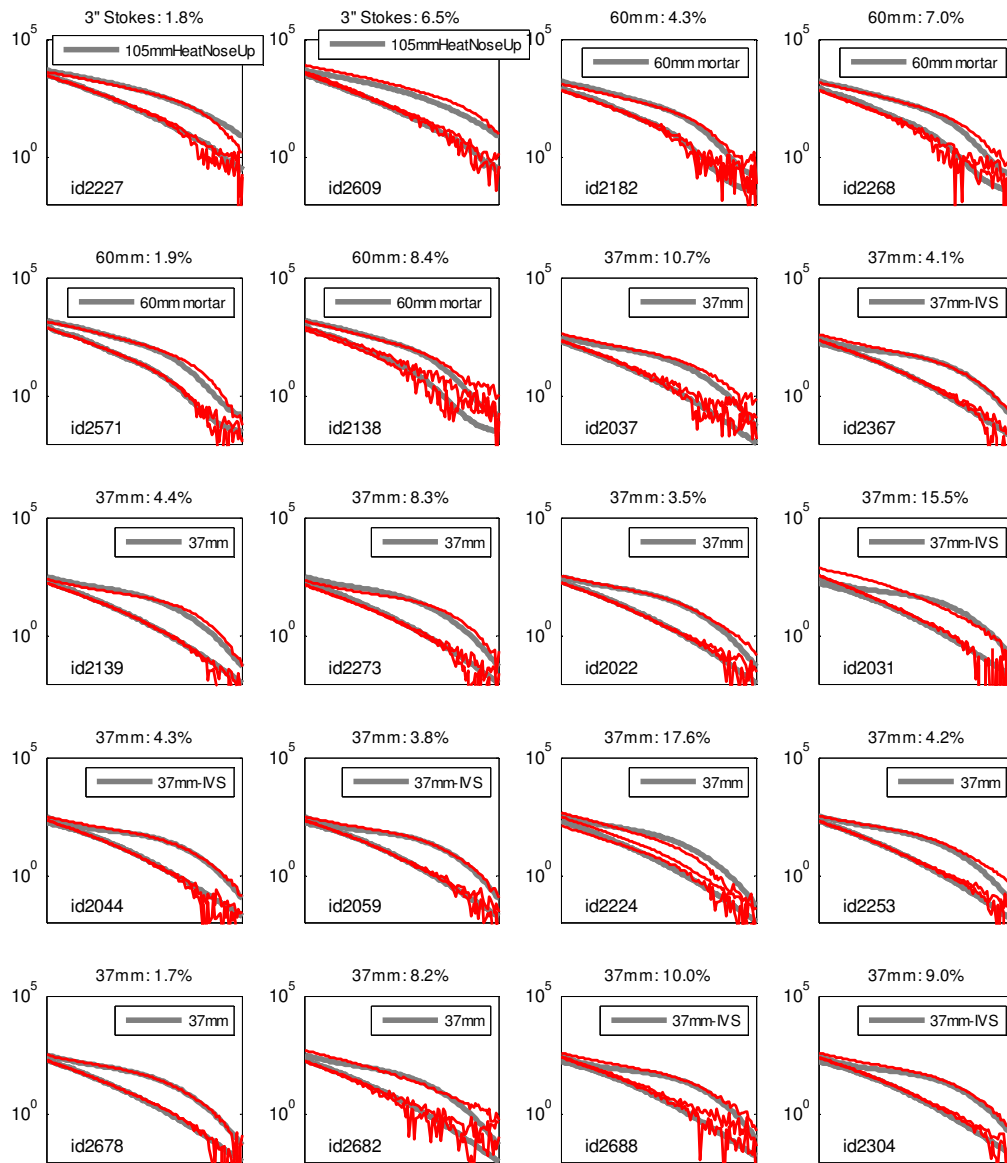


Figure 92: TEMTADS 2x2 cued data from the Treed area (3/4)

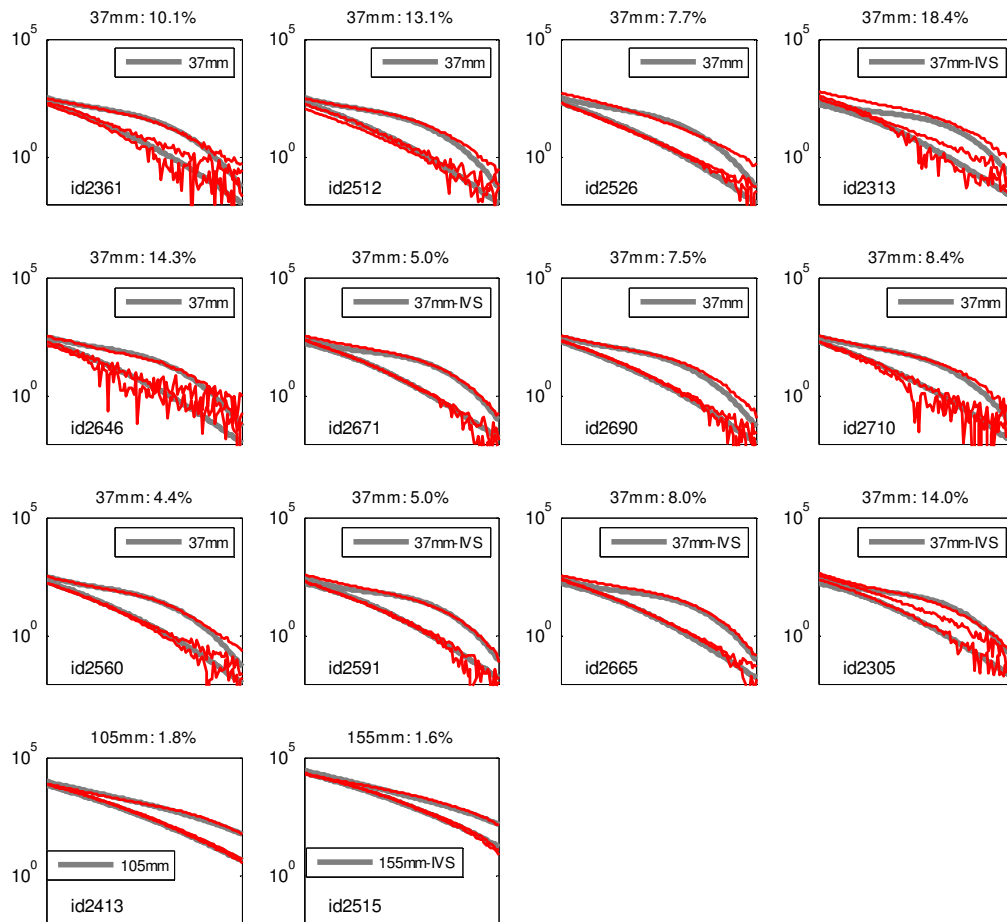


Figure 93: TEMTADS 2x2 cued data from the Treed area (4/4)

Table 22: TEMTADS 2x2 cued data from the Treed area.

Groud Truth	ID	% diff	Library reference
75mm proj	2113	3.2	75mm-IVS
75mm proj	2262	4.3	75mm-IVS
75mm proj	2504	2	75mm-IVS
75mm proj	2487	1.9	75mm-IVS
75mm proj	2500	1.4	75mm-IVS
75mm proj	2278	3.5	75mm-IVS
75mm proj	2340	2.9	75mm-IVS
75mm body	2251	1.4	75mm-IVS
75mm body	2081	2.1	75mm-IVS
75mm body	2245	1.4	75mm-IVS
75mm body	2637	1.5	75mm-IVS
medium ISO	2116	3.9	ISO
medium ISO	2282	5.9	ISO
medium ISO	2547	12.5	ISO
medium ISO	2653	4	ISO
medium ISO	2653a	71.6	ISO
small ISO	2025	20.2	iSO2-IVS
small ISO	2025a	8.5	iSO2-IVS
small ISO	2025r	8.7	iSO2-IVS
small ISO	2088	3.1	iSO2-IVS
small ISO	2196	4	iSO2-IVS
small ISO	2315	3.8	iSO2-IVS
small ISO	2373	2.1	iSO2-IVS
small ISO	2181	2.7	iSO2-IVS
small ISO	2084	3.6	iSO2-IVS
small ISO	2366	4.7	iSO2-IVS
small ISO	2625	4.3	iSO2-IVS
small ISO	2640	9.1	iSO2-IVS
small ISO	2661	3.2	iSO2-IVS
small ISO	2685	6.7	iSO2-IVS
small ISO	2534	27.1	iSO2-IVS
small ISO	2539	16	iSO2-IVS
small ISO	2564	5.8	iSO2-IVS
small ISO	2644	3	iSO2-IVS
small ISO	2355	22.8	iSO2-IVS
small ISO	2503	3.7	iSO2-IVS
small ISO	2577	2.1	iSO2-IVS
small ISO	2694	5.4	iSO2-IVS
small ISO	2713	4.9	iSO2-IVS
small ISO	2522	11.9	iSO2-IVS

Groud Truth	ID	% diff	Library reference
3" Stokes	2227	1.8	105mmHeatNoseUp
3" Stokes	2609	6.5	105mmHeatNoseUp
60mm	2182	4.3	60mm mortar
60mm	2268	7	60mm mortar
60mm	2571	1.9	60mm mortar
60mm	2138	8.4	60mm mortar
37mm	2037	10.7	37mm
37mm	2367	4.1	37mm-IVS
37mm	2139	4.4	37mm
37mm	2273	8.3	37mm
37mm	2022	3.5	37mm
37mm	2031	15.5	37mm-IVS
37mm	2044	4.3	37mm-IVS
37mm	2059	3.8	37mm-IVS
37mm	2224	17.6	37mm
37mm	2253	4.2	37mm
37mm	2678	1.7	37mm
37mm	2682	8.2	37mm
37mm	2688	10	37mm-IVS
37mm	2304	9	37mm-IVS
37mm	2361	10.1	37mm
37mm	2512	13.1	37mm
37mm	2526	7.7	37mm
37mm	2313	18.4	37mm-IVS
37mm	2646	14.3	37mm
37mm	2671	5	37mm-IVS
37mm	2690	7.5	37mm
37mm	2710	8.4	37mm
37mm	2560	4.4	37mm
37mm	2591	5	37mm-IVS
37mm	2665	8	37mm-IVS
37mm	2305	14	37mm-IVS
105mm	2413	1.8	105mm

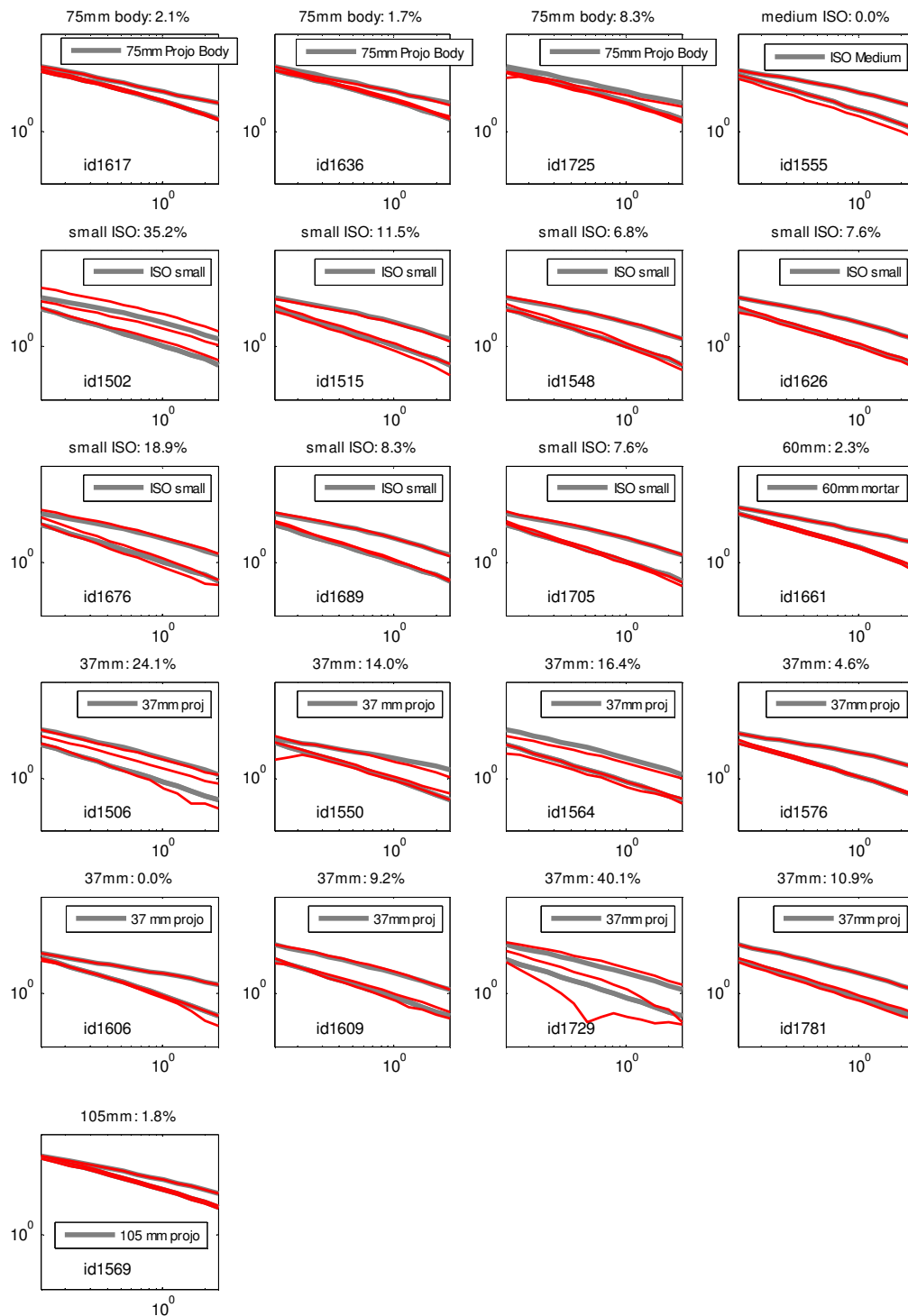


Figure 94: MetalMapper dynamic data acquired in the Dynamic area.

Table 23: MetalMapper dynamic data acquired in the Dynamic area.

Groud Truth	ID	% diff	Library reference
75mm body	1617	2.1	75mm Projo Body
75mm body	1636	1.7	75mm Projo Body
75mm body	1725	8.3	75mm Projo Body
medium ISO	1555	0	ISO Medium
small ISO	1502	35.2	ISO small
small ISO	1515	11.5	ISO small
small ISO	1548	6.8	ISO small
small ISO	1626	7.6	ISO small
small ISO	1676	18.9	ISO small
small ISO	1689	8.3	ISO small
small ISO	1705	7.6	ISO small
60mm	1661	2.3	60mm mortar
37mm	1506	24.1	37mm proj
37mm	1550	14	37 mm projo
37mm	1564	16.4	37mm proj
37mm	1576	4.6	37mm projo
37mm	1606	0	37 mm projo
37mm	1609	9.2	37mm proj
37mm	1729	40.1	37mm proj
37mm	1781	10.9	37mm proj
105mm	1569	1.8	105 mm projo

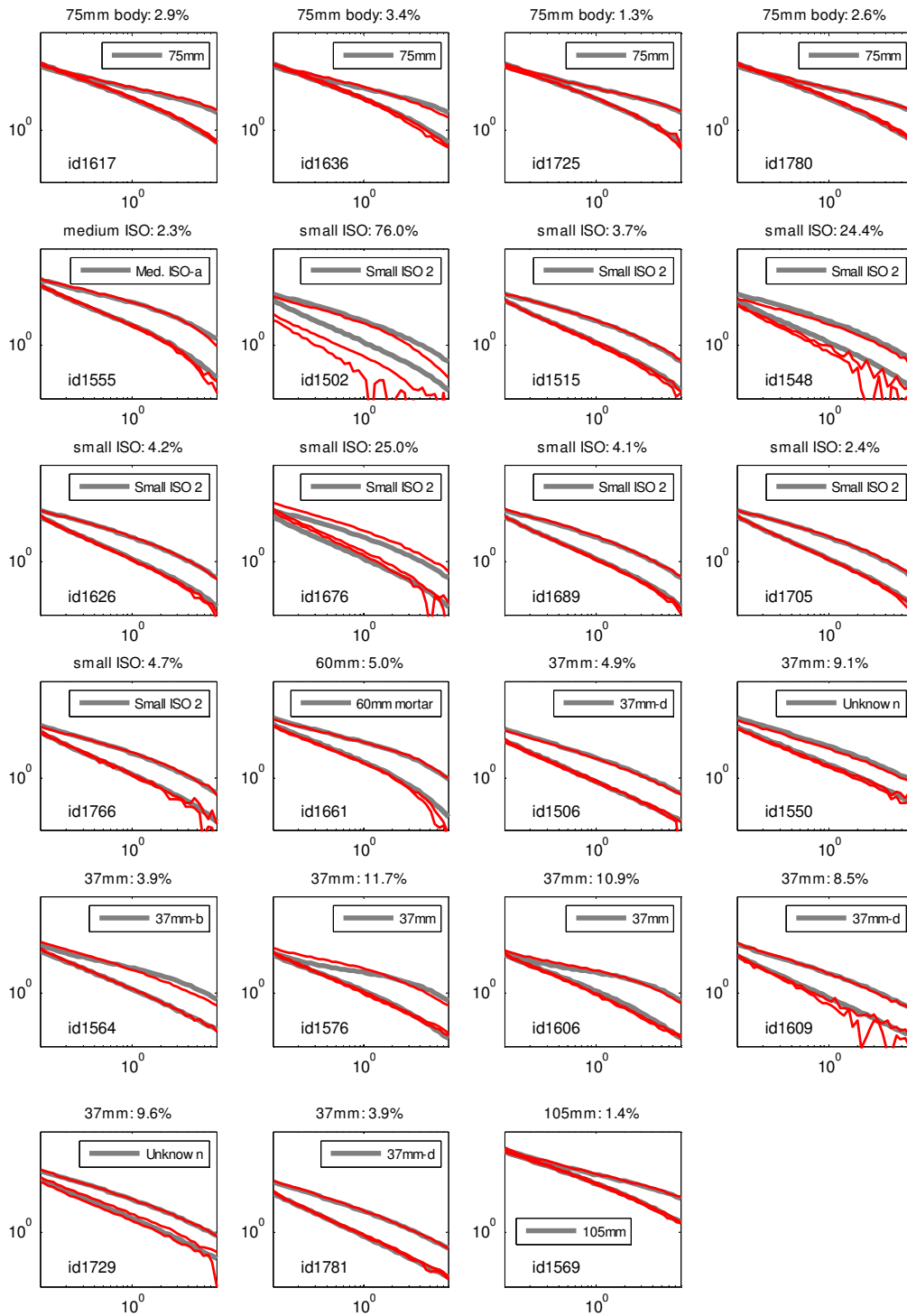


Figure 95: MetalMapper URS cued data acquired in the Dynamic area.

Table 24: MetalMapper URS cued data acquired in the Dynamic area.

Groud Truth	ID	% diff	Library reference
75mm body	1617	2.9	75mm
75mm body	1636	3.4	75mm
75mm body	1725	1.3	75mm
75mm body	1780	2.6	75mm
medium ISO	1555	2.3	Med. ISO-a
small ISO	1502	76	Small ISO 2
small ISO	1515	3.7	Small ISO 2
small ISO	1548	24.4	Small ISO 2
small ISO	1626	4.2	Small ISO 2
small ISO	1676	25	Small ISO 2
small ISO	1689	4.1	Small ISO 2
small ISO	1705	2.4	Small ISO 2
small ISO	1766	4.7	Small ISO 2
60mm	1661	5	60mm mortar
37mm	1506	4.9	37mm-d
37mm	1550	9.1	Unknown
37mm	1564	3.9	37mm-b
37mm	1576	11.7	37mm
37mm	1606	10.9	37mm
37mm	1609	8.5	37mm-d
37mm	1729	9.6	Unknown
37mm	1781	3.9	37mm-d
105mm	1569	1.4	105mm

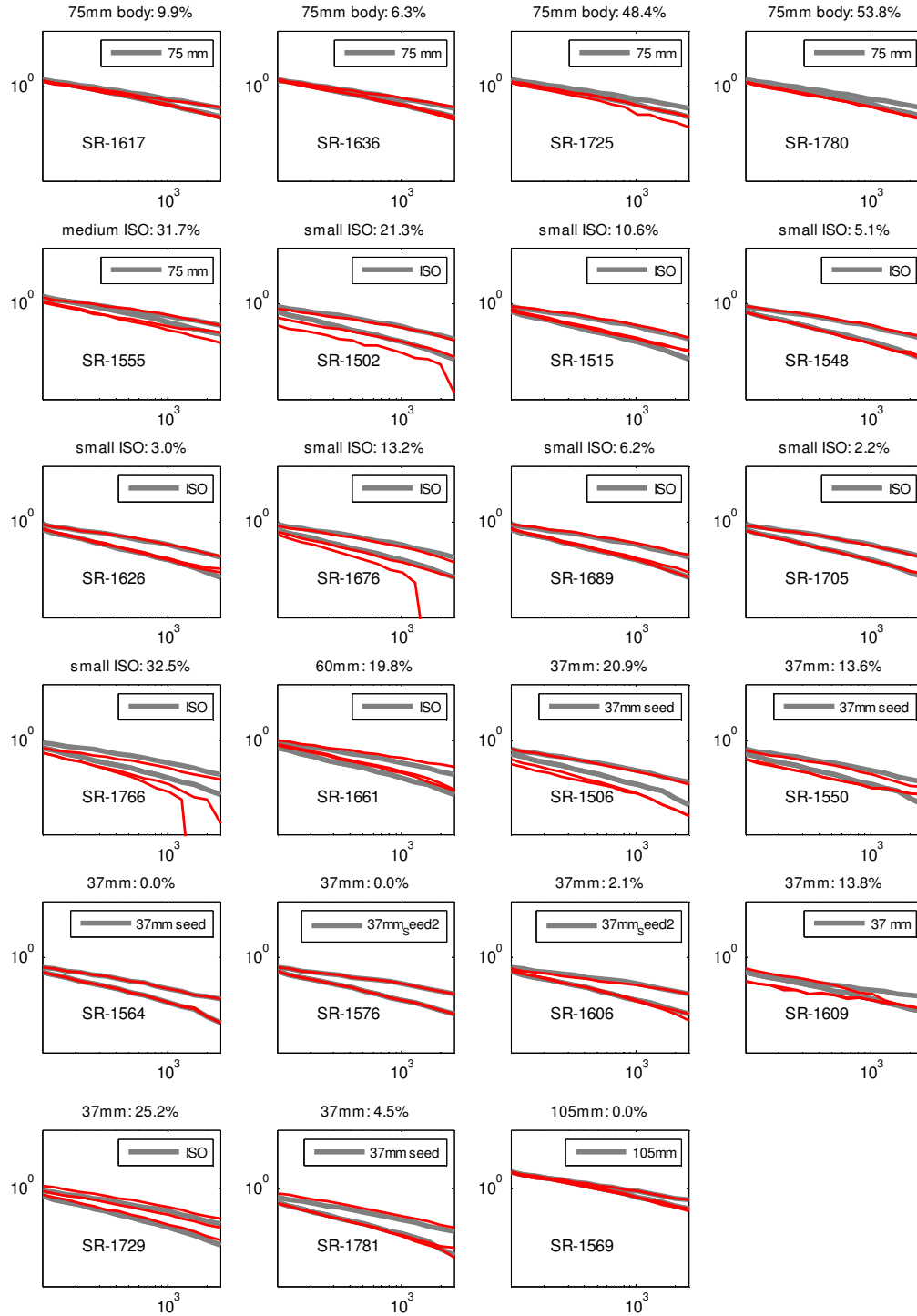


Figure 96: TEMTADS 2x2 dynamic data acquired in the Dynamic area.

Table 25: TEMTADS 2x2 dynamic data acquired in the Dynamic area.

Groud Truth	ID	% diff	Library reference
75mm body	1617	9.9	75 mm
75mm body	1636	6.3	75 mm
75mm body	1725	48.4	75 mm
75mm body	1780	53.8	75 mm
medium ISO	1555	31.7	75 mm
small ISO	1502	21.3	ISO
small ISO	1515	10.6	ISO
small ISO	1548	5.1	ISO
small ISO	1626	3	ISO
small ISO	1676	13.2	ISO
small ISO	1689	6.2	ISO
small ISO	1705	2.2	ISO
small ISO	1766	32.5	ISO
60mm	1661	19.8	ISO
37mm	1506	20.9	37mm seed
37mm	1550	13.6	37mm seed
37mm	1564	0	37mm seed
37mm	1576	0	37mm_Seed2
37mm	1606	2.1	37mm_Seed2
37mm	1609	13.8	37 mm
37mm	1729	25.2	ISO
37mm	1781	4.5	37mm seed
105mm	1569	0	105mm

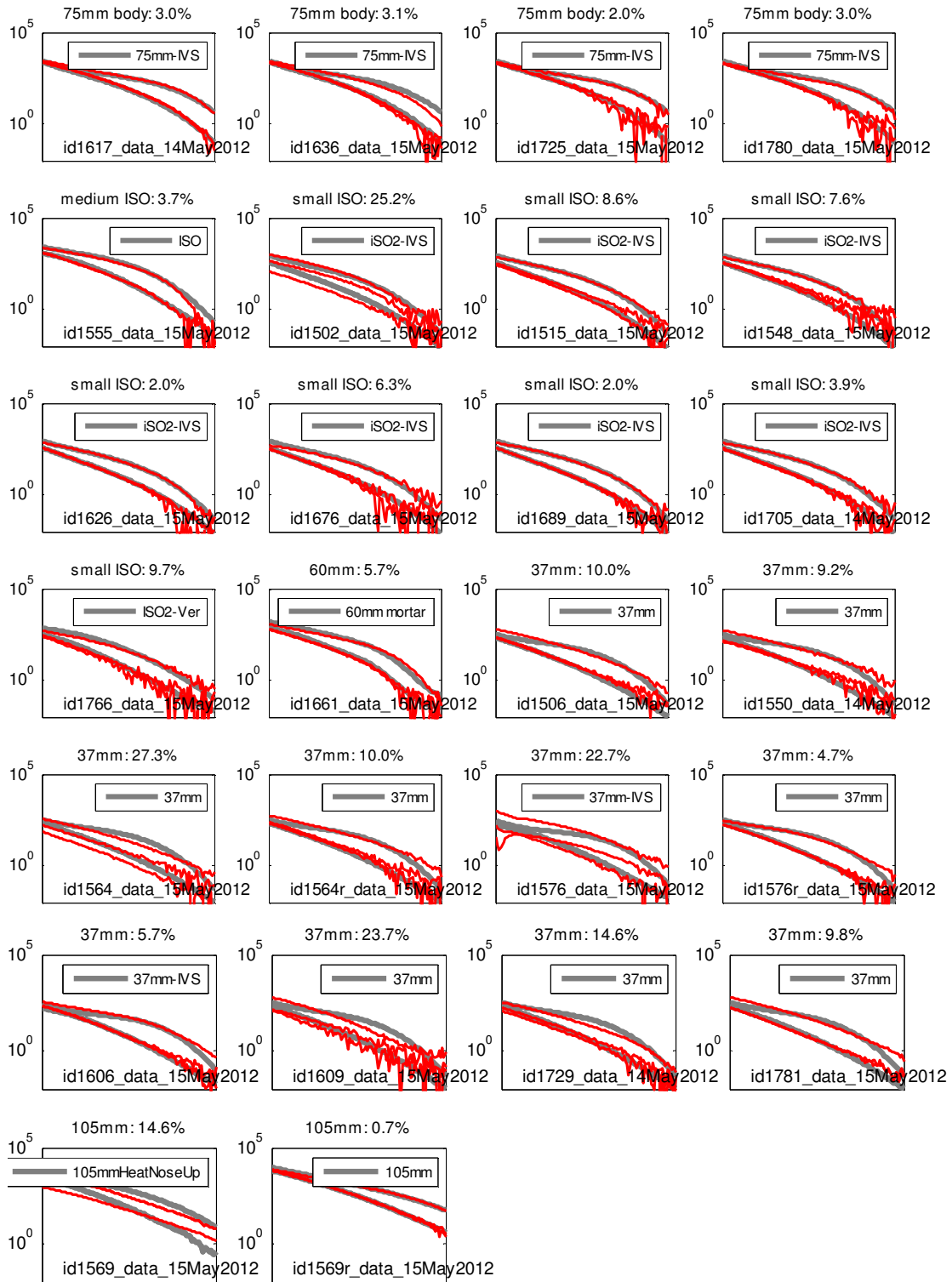


Figure 97: TEMTADS 2x2 cued data acquired in the Dynamic area.

Table 26: TEMTADS 2x2 Cued data acquired in the Dynamic area

Groud Truth	ID	% diff	Library reference
75mm body	1617_data_14May2012	3	75mm-IVS
75mm body	1636_data_15May2012	3.1	75mm-IVS
75mm body	1725_data_15May2012	2	75mm-IVS
75mm body	1780_data_15May2012	3	75mm-IVS
medium ISO	1555_data_15May2012	3.7	ISO
small ISO	1502_data_15May2012	25.2	iSO2-IVS
small ISO	1515_data_15May2012	8.6	iSO2-IVS
small ISO	1548_data_15May2012	7.6	iSO2-IVS
small ISO	1626_data_15May2012	2	iSO2-IVS
small ISO	1676_data_15May2012	6.3	iSO2-IVS
small ISO	1689_data_15May2012	2	iSO2-IVS
small ISO	1705_data_14May2012	3.9	iSO2-IVS
small ISO	1766_data_15May2012	9.7	ISO2-Ver
60mm	1661_data_15May2012	5.7	60mm mortar
37mm	1506_data_15May2012	10	37mm
37mm	1550_data_14May2012	9.2	37mm
37mm	1564_data_15May2012	27.3	37mm
37mm	1564r_data_15May2012	10	37mm
37mm	1576_data_15May2012	22.7	37mm-IVS
37mm	1576r_data_15May2012	4.7	37mm
37mm	1606_data_15May2012	5.7	37mm-IVS
37mm	1609_data_15May2012	23.7	37mm
37mm	1729_data_14May2012	14.6	37mm
37mm	1781_data_15May2012	9.8	37mm
105mm	1569_data_15May2012	14.6	105mmHeatNoseUp
105mm	1569r_data_15May2012	0.7	105mm

Appendix F: Definition of "Skew-ness"

"Skew-ness" is a property of recovered of the recovered polarizabilities that was used in the TEMTADS analysis to help identify potential TOI and training data targets.

The diagonalized polarizability matrix L can be written as the following sum:

$$L = \begin{bmatrix} L_{11} & 0 & 0 \\ 0 & L_{22} & 0 \\ 0 & 0 & L_{33} \end{bmatrix} = \bar{L}I + \alpha \begin{bmatrix} -1 & 0 & 0 \\ 0 & -1 & 0 \\ 0 & 0 & 2 \end{bmatrix} + \beta \begin{bmatrix} 1 & 0 & 0 \\ 0 & -1 & 0 \\ 0 & 0 & 0 \end{bmatrix}$$

where the second and third terms correspond to "non-spherical" components, and the coefficients α and β are defined as

$$\alpha = \frac{1}{3} \left(L_{33} - \frac{L_{11} + L_{22}}{2} \right) \quad \text{and} \quad \beta = \frac{1}{2} (L_{22} - L_{11}).$$

The "skew" is then defined as

$$Skew(L) = \frac{1}{3} tr \left[(L - \bar{L}I)^3 \right] = 2\alpha(\alpha^2 - \beta^2)$$

A single number for "skew" is defined as the sum of Skew(L) over all time channels

$$\overline{Skew} = \sum_t Skew(L(t))$$

Figure 98 gives some examples of skew for a number of targets. A target with one major polarizability and two smaller, equal polarizabilities will have a positive skew. A target with three equal polarizabilities have zero skew. Three distinct polarizabilities will result in negative skewness. Rod-like objects will sit along the $\alpha = skew^{1/2}$ "edge", and should be considered for training data.

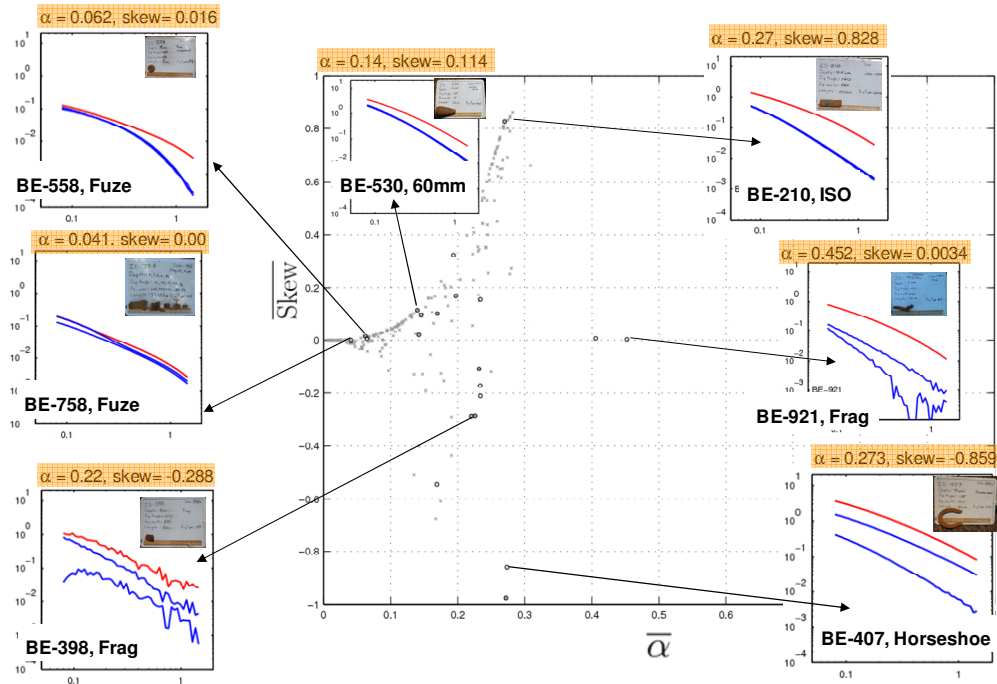


Figure 98: Examples of the "Skew" metric using Camp Beale data.

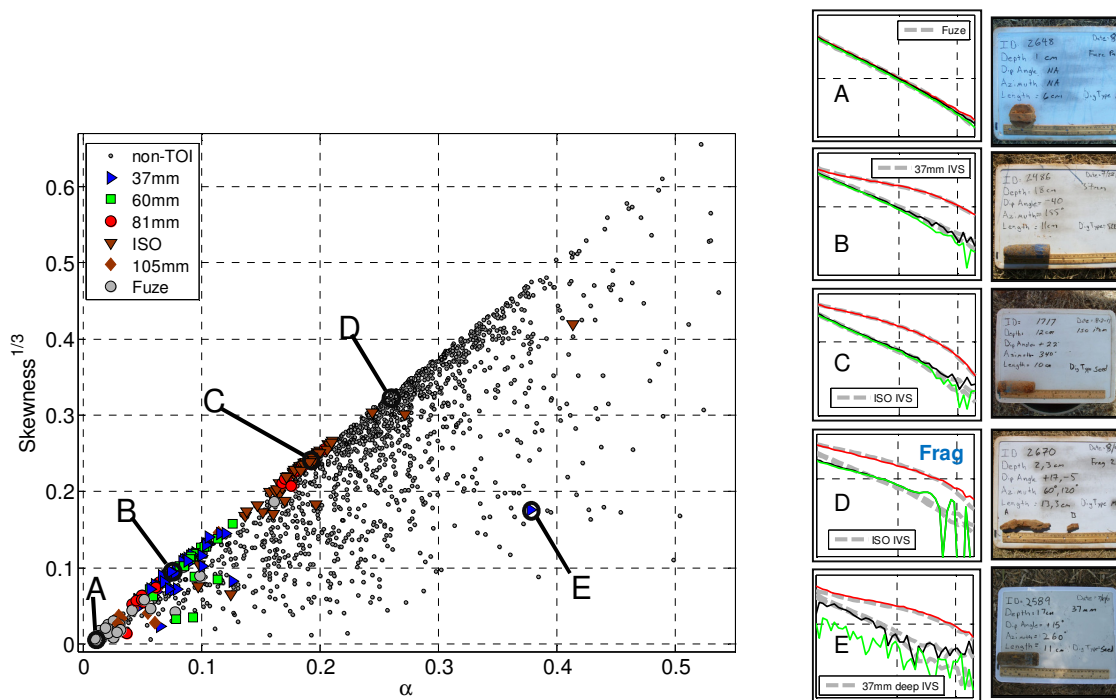


Figure 99: Example of the "Skew" metric using Camp Beale data.

Appendix G: Location and depth estimate error distributions

In this section, we present location and depth estimate error distributions calculated for targets of interest. All data soundings were considered in this analysis. That is, if an anomaly flag has multiple data anomalies acquired, depth and location estimates from all the data inversions are included in the statistics. The TETMADS did not have IMU information, and therefore we do not calculate position errors for the cued TETMADS surveys.

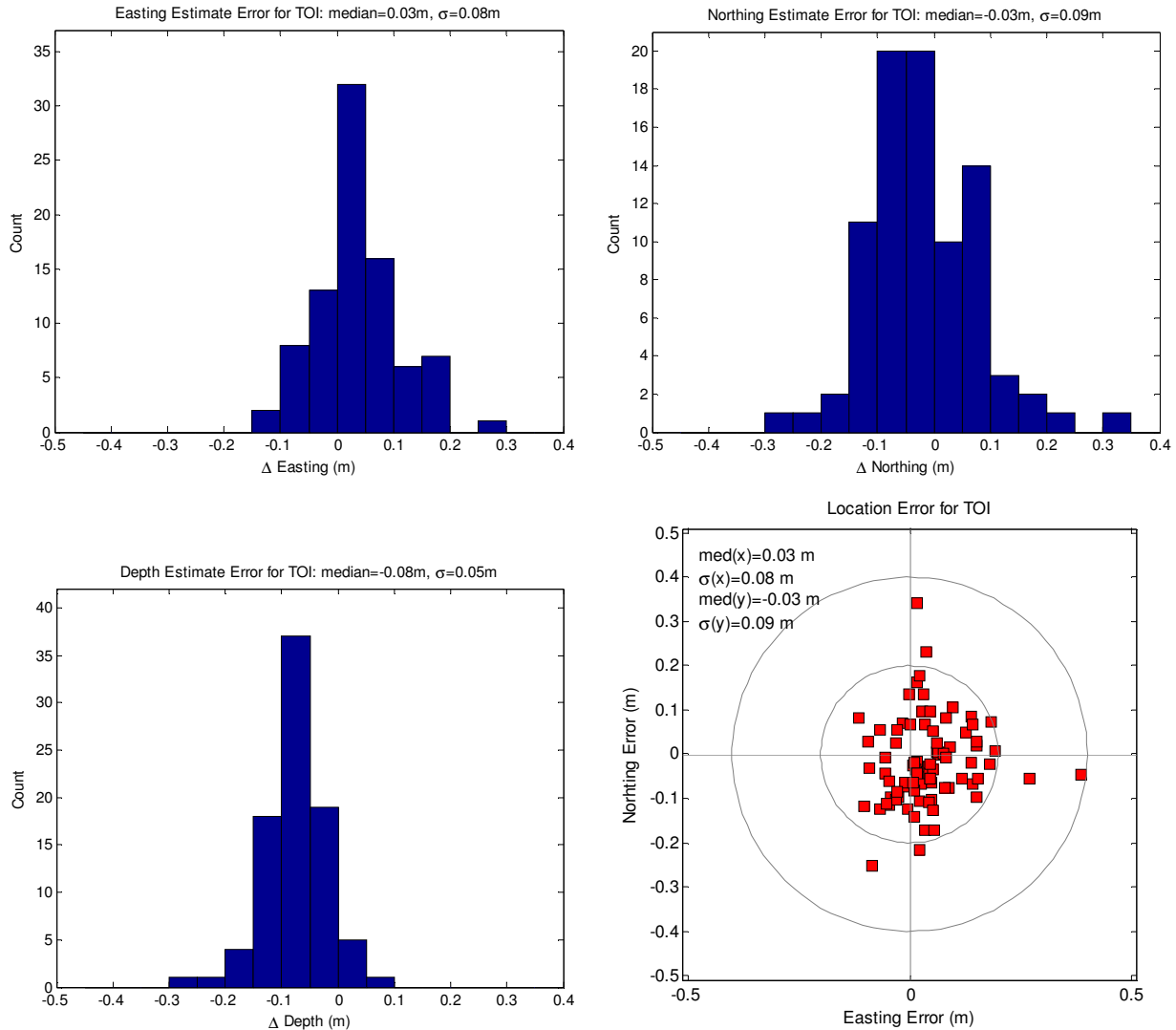


Figure 100: Location and depth error distributions for the MetalMapper (URS) cued data collected in the Open area.

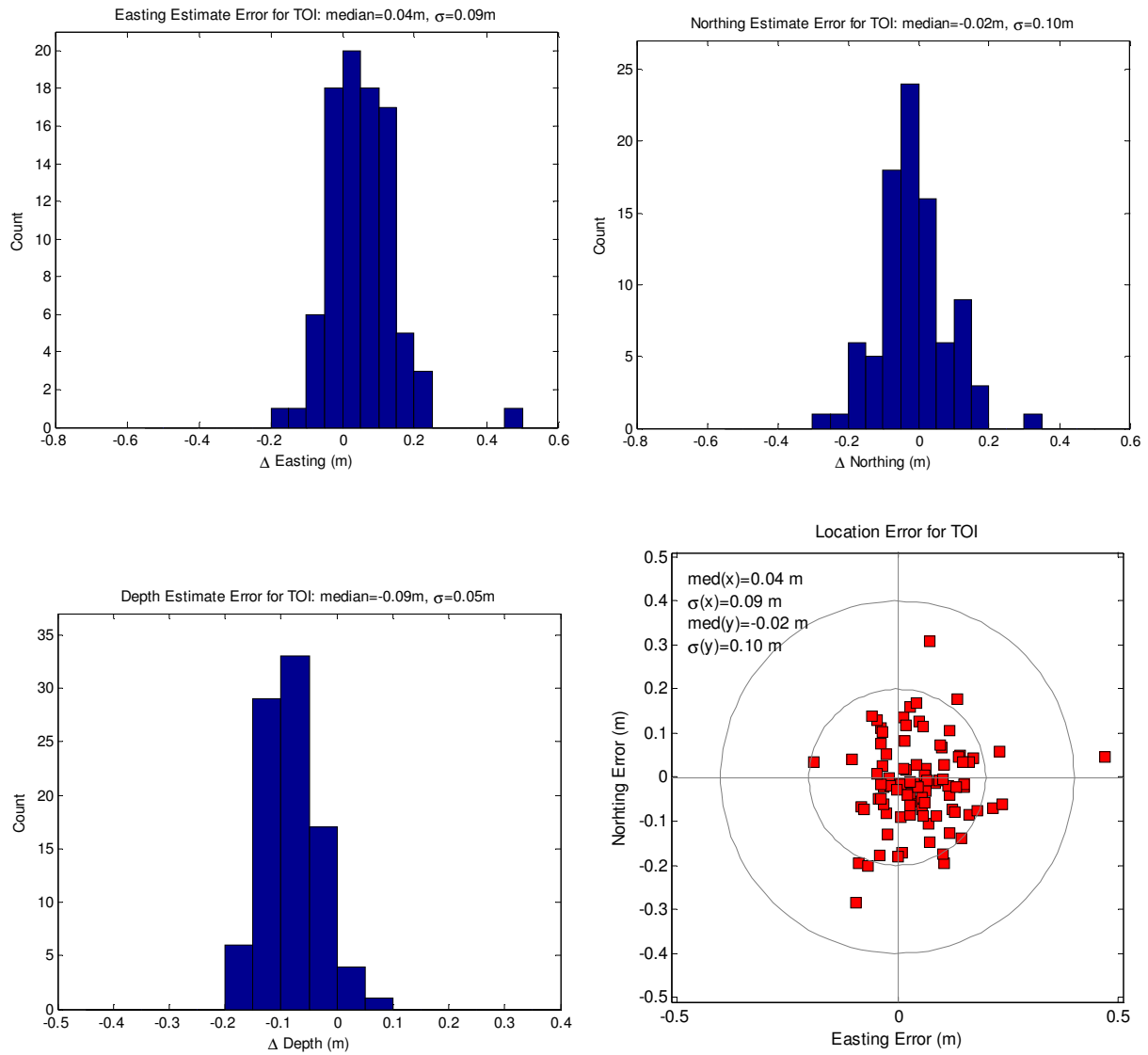
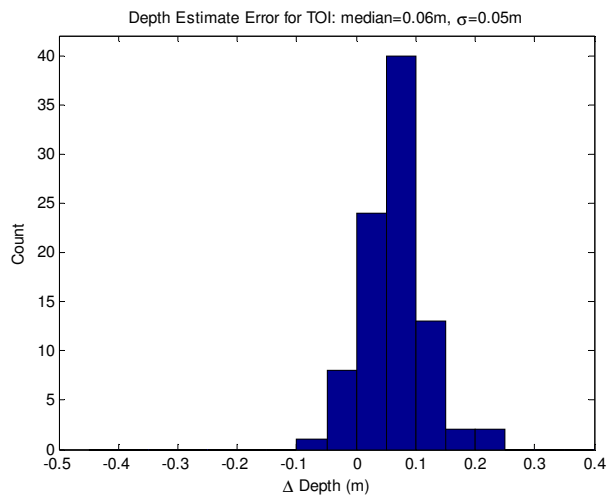
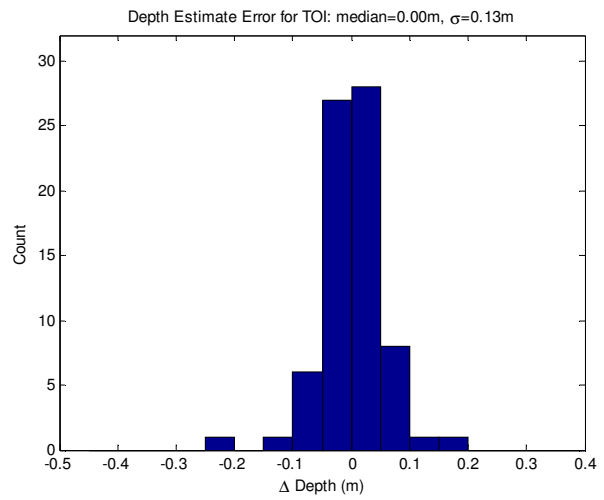


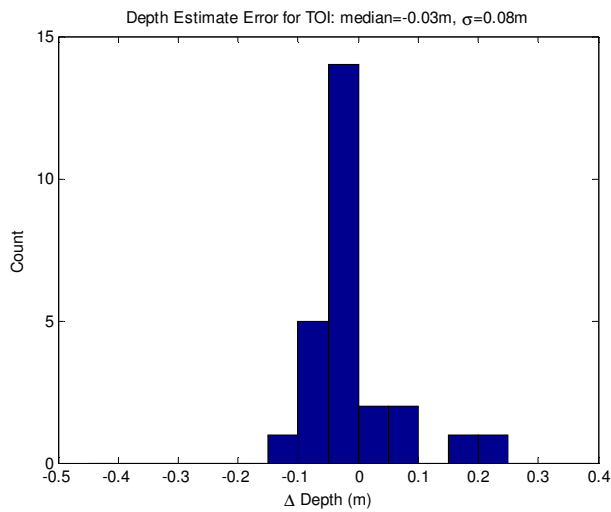
Figure 101: Location and depth error distributions for the MetalMapper (NAEVA) cued data collected in the Open area.



(a) TEMTADS 5x5, Open Area



(b) TEMTADS 2x2 cued, Treed Area



(c) TEMTADS 2x2 cued, Dynamic Area

Figure 102: Depth error distributions for the different cued TEMTADS surveys. Location error information was not calculated due to no IMU information being available.

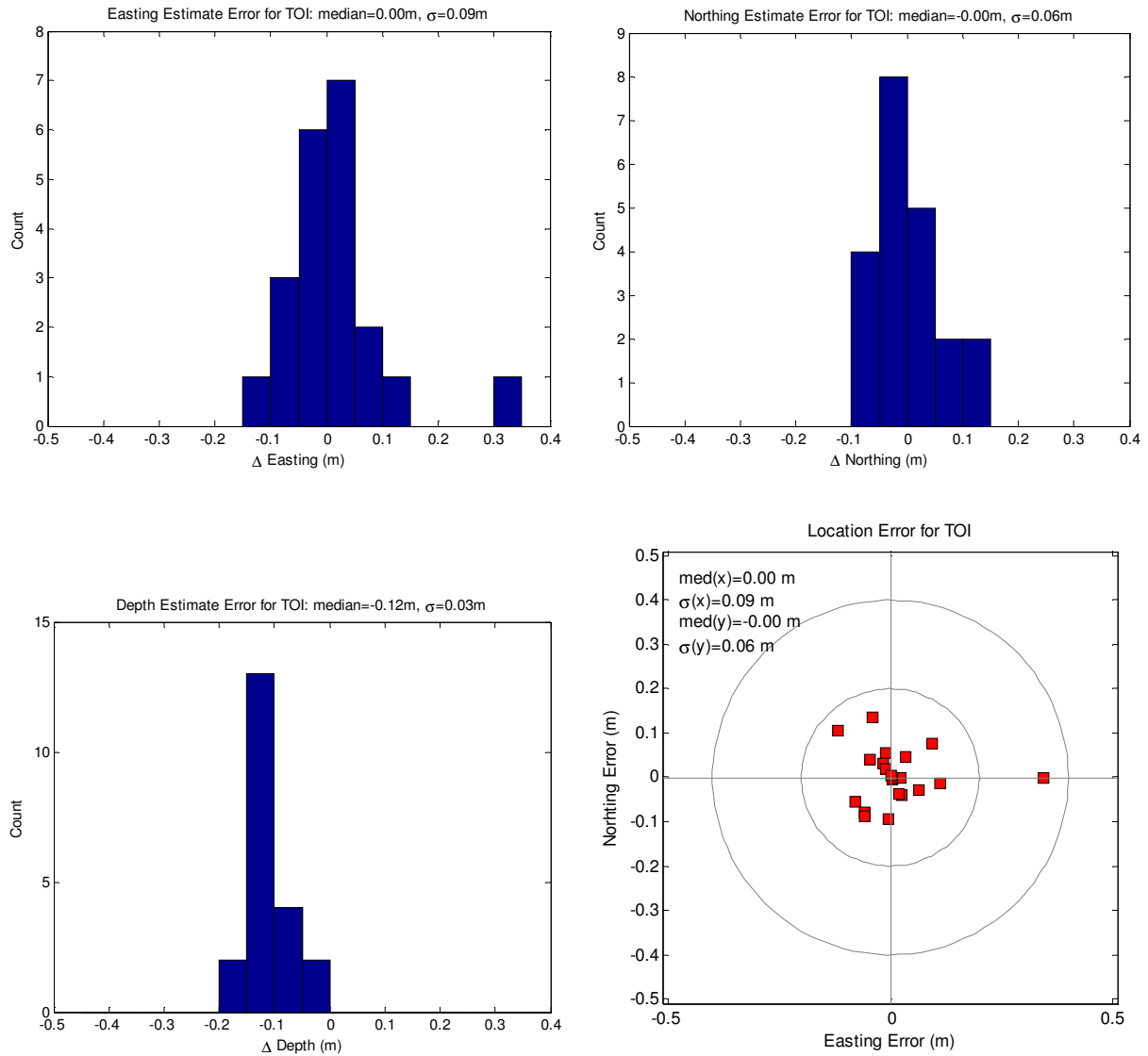


Figure 103: Location and depth error distributions for the MetalMapper (URS) Dynamic data collected in the Dynamic area.

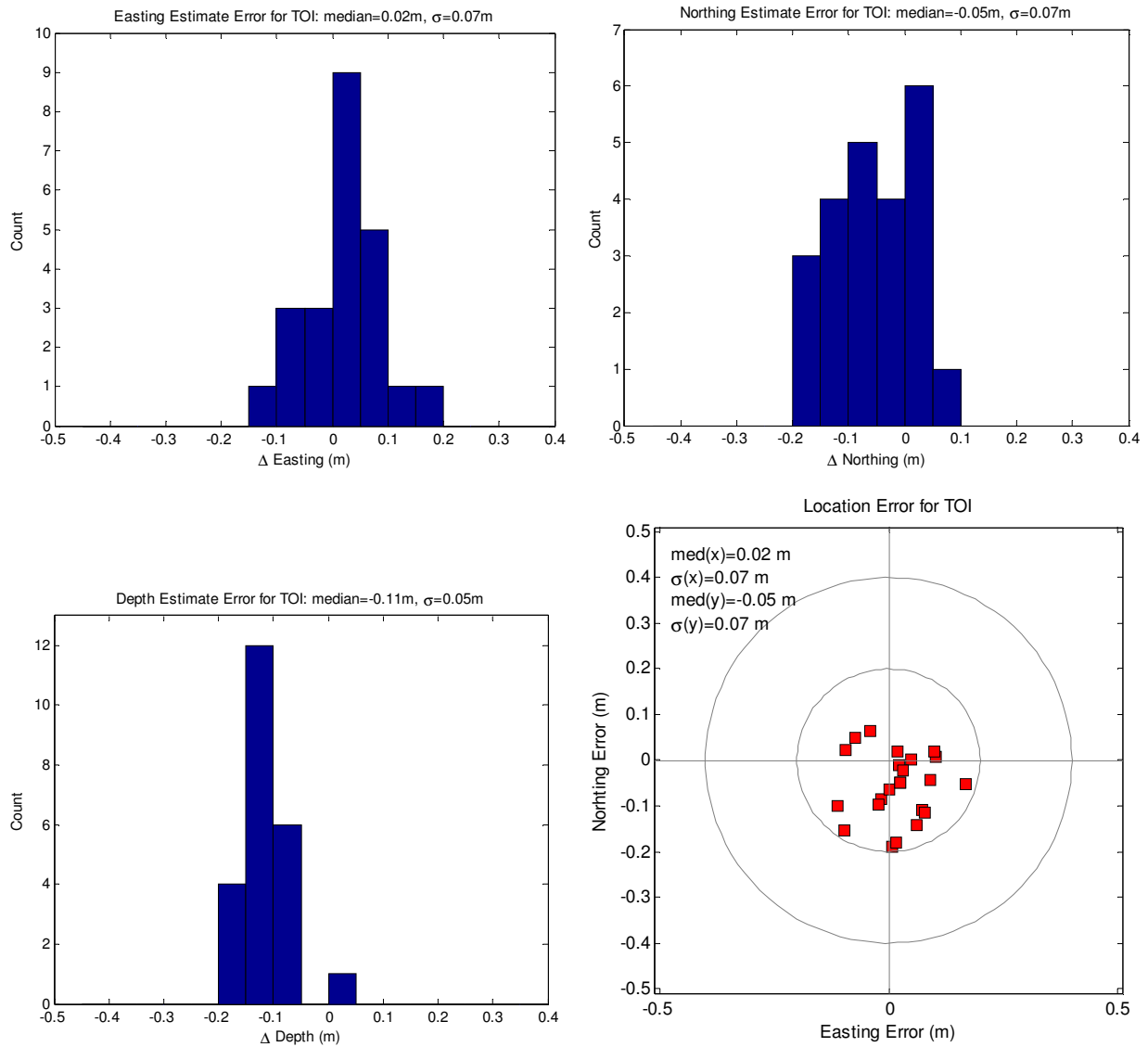


Figure 104: Location and depth error distributions for the MetalMapper (URS) cued data collected in the Dynamic area.

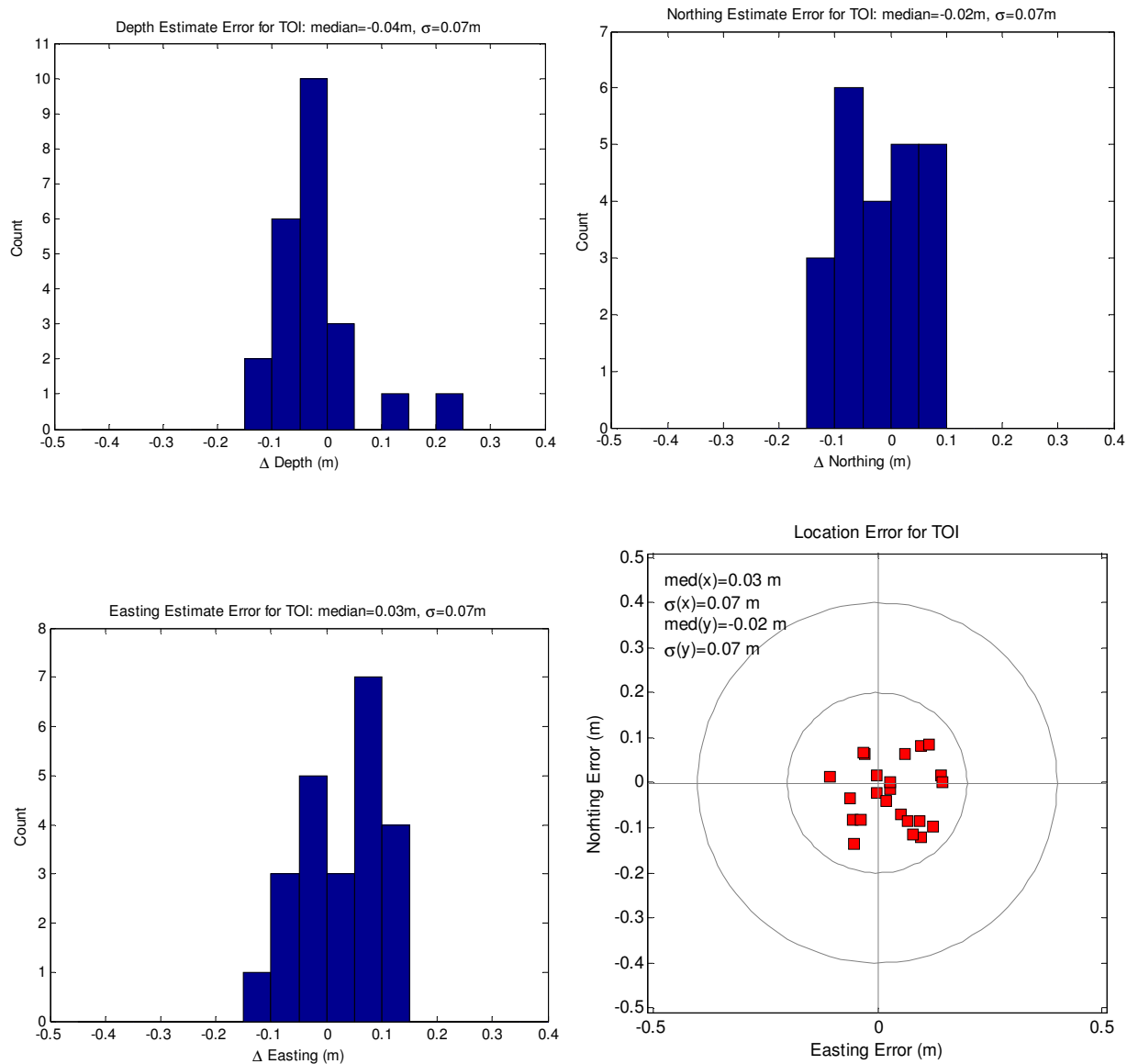
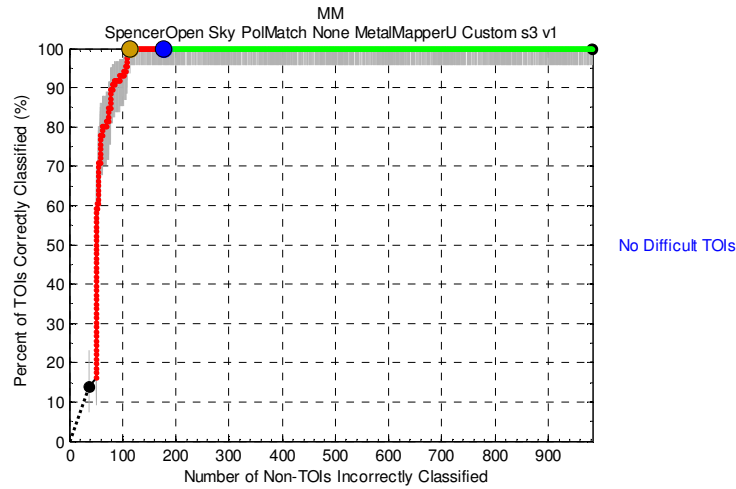


Figure 105: Location and depth error distributions for the TEMTADS 2x2 dynamic data collected in the Dynamic area.

Appendix H: Summary of Scoring from the Institute of Defense Analysis



MM
SpencerOpen Sky PolMatch None MetalMapperU Custom s3 v1

Analyst's Type (caliber/diameter in mm)

	0	37	48	52	60	61	65	75	105	155	Total
0	807	65	0	44	14	0	2	1	0	0	933
37	0	22	0	1	0	0	0	0	0	0	23
48	0	2	0	21	2	0	0	0	0	0	25
52	0	0	0	0	0	0	0	0	0	0	0
60	0	0	0	0	4	0	0	0	0	0	4
61	0	0	0	0	0	0	3	1	0	0	4
65	0	0	0	0	0	0	0	0	0	0	0
75	0	2	0	0	0	0	1	12	0	0	15
105	0	0	0	0	0	0	0	0	1	0	1
155	0	0	0	0	0	0	0	0	0	1	1
Total	807	91	0	66	20	0	6	14	1	1	1006

0 = Non-TOI
37 = 37mm
48 = Small ISO
52 = 52mm
60 = 60mm
61 = Medium ISO
65 = 65mm
75 = 75mm
105 = 105mm
155 = 155mm

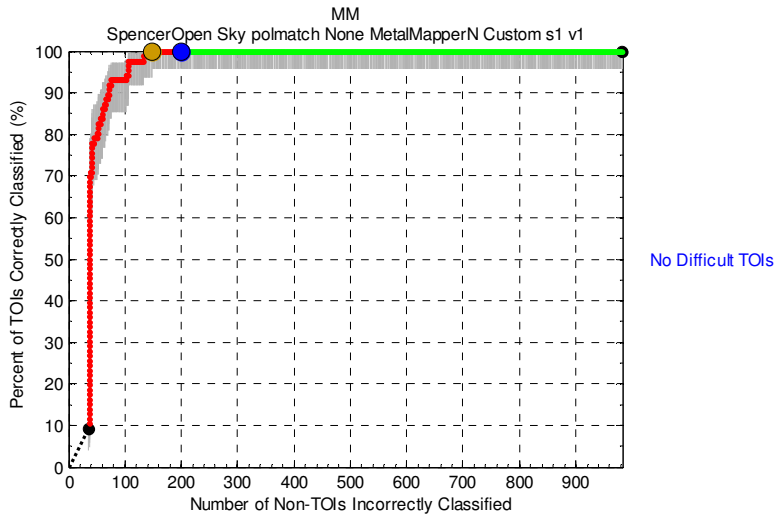
MM
SpencerOpen Sky PolMatch None MetalMapperU Custom s3 v1

Analyst's Type

	Non-TOI	Small TOI	Medium TOI	Large TOI	Total
Non-TOI	807	109	17	0	933
Small TOI	0	46	2	0	48
Medium TOI	0	2	21	0	23
Large TOI	0	0	0	2	2
Total	807	157	40	2	1006

Small TOI: 20 - 53
Medium TOI: 55 - 89
Large TOI: 102 - 155

Figure 106: Scoring results for the MetalMapper URS data acquired in cued mode, in the Open area.



MM
SpencerOpen Sky polmatch None MetalMapperN Custom s1 v1

Analyst's Type (caliber/diameter in mm)

	0	37	48	52	60	61	65	75	105	155	Total
0	784	74	0	57	19	0	6	4	1	0	945
37	0	25	0	1	2	0	0	0	0	0	28
48	0	2	0	23	1	0	0	0	0	0	26
52	0	0	0	0	0	0	0	0	0	0	0
60	0	0	0	0	3	0	0	0	0	0	3
61	0	0	0	0	0	0	2	2	0	0	4
65	0	0	0	0	0	0	0	0	0	0	0
75	0	0	0	0	0	0	0	15	0	0	15
105	0	0	0	0	0	0	0	0	1	0	1
155	0	0	0	0	0	0	0	0	0	1	1
Total	784	101	0	81	25	0	8	21	2	1	1023

0 = Non-TOI
37 = 37mm
48 = Small ISO
52 = 52mm
60 = 60mm
61 = Medium ISO
65 = 65mm
75 = 75mm
105 = 105mm
155 = 155mm

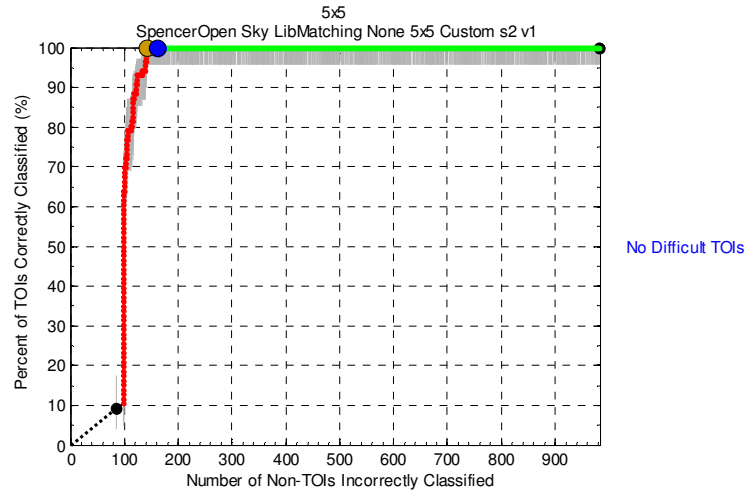
MM
SpencerOpen Sky polmatch None MetalMapperN Custom s1 v1

Analyst's Type

	Non-TOI	Small TOI	Medium TOI	Large TOI	Total
Non-TOI	784	131	29	1	945
Small TOI	0	51	3	0	54
Medium TOI	0	0	22	0	22
Large TOI	0	0	0	2	2
Total	784	182	54	3	1023

Small TOI: 20 - 53
Medium TOI: 55 - 89
Large TOI: 102 - 155

Figure 107: Scoring results for the MetalMapper – Naeva cued data acquired in the Open area.



5x5
SpencerOpen Sky LibMatching None 5x5 Custom s2 v1

Analyst's Type (caliber/diameter in mm)

	0	31	37	45	48	60	61	75	81	105	155	Total
0	821	4	12	24	0	15	0	3	6	0	0	885
31	0	0	0	0	0	0	0	0	0	0	0	0
37	0	0	20	9	0	0	0	0	0	0	0	29
45	0	0	0	0	0	0	0	0	0	0	0	0
48	0	0	2	18	0	2	0	0	0	0	0	22
60	0	0	0	0	0	5	0	0	0	0	0	5
61	0	0	0	0	0	1	0	3	0	0	0	4
75	0	0	0	0	0	0	0	9	7	0	0	16
81	0	0	0	0	0	0	0	0	0	0	0	0
105	0	0	0	0	0	0	0	0	0	1	0	1
155	0	0	0	0	0	0	0	0	0	1	0	1
Total	821	4	34	51	0	23	0	15	13	2	0	963

Ground Truth (caliber/diameter in mm)

0 = Non-TOI
31 = 31mm
37 = 37mm
45 = 45mm
48 = Small ISO
60 = 60mm
61 = Medium ISO
75 = 75mm
81 = 81mm
105 = 105mm
155 = 155mm

5x5
SpencerOpen Sky LibMatching None 5x5 Custom s2 v1

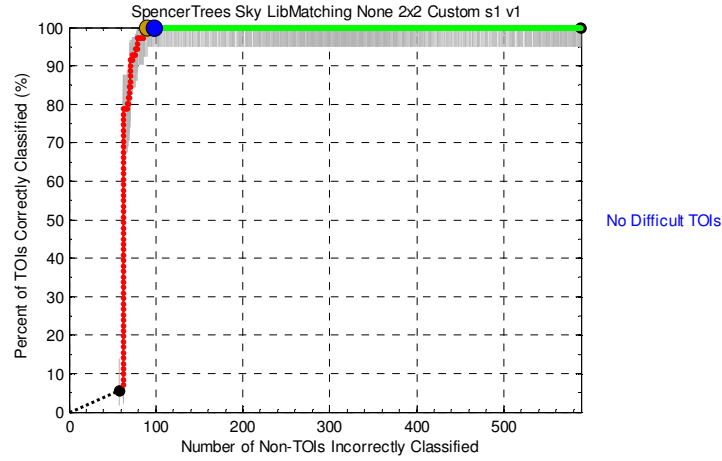
Analyst's Type

	Non-TOI	Small TOI	Medium TOI	Large TOI	Total
Non-TOI	821	40	24	0	885
Small TOI	0	49	2	0	51
Medium TOI	0	0	25	0	25
Large TOI	0	0	0	2	2
Total	821	89	51	2	963

Ground Truth

Small TOI: 20 - 53
Medium TOI: 55 - 89
Large TOI: 102 - 155

Figure 108: IDA scoring summary for TEMTADS 5x5 cued data



SpencerTrees Sky LibMatching None 2x2 Custom s1 v1

Analyst's Type (caliber/diameter in mm)

	0	37	45	48	60	61	75	76	81	105	155	Total
0	491	18	13	0	5	0	0	0	0	0	0	527
37	0	21	3	0	0	0	0	0	0	0	0	24
45	0	0	0	0	0	0	0	0	0	0	0	0
48	0	0	19	0	1	0	0	0	0	0	0	20
60	0	0	0	0	4	0	0	0	0	0	0	4
61	0	0	0	0	4	0	0	0	0	0	0	4
75	0	0	0	0	0	0	10	0	1	0	0	11
76	0	0	0	0	0	0	0	0	0	2	0	2
81	0	0	0	0	0	0	0	0	0	0	0	0
105	0	0	0	0	0	0	0	0	0	1	0	1
155	0	0	0	0	0	0	0	0	0	0	1	1
Total	491	39	35	0	14	0	10	0	1	3	1	594

0 = Non-TOI
 37 = 37mm
 45 = 45mm
 48 = Small ISO
 60 = 60mm
 61 = Medium ISO
 75 = 75mm
 76 = 3in
 81 = 81mm
 105 = 105mm
 155 = 155mm

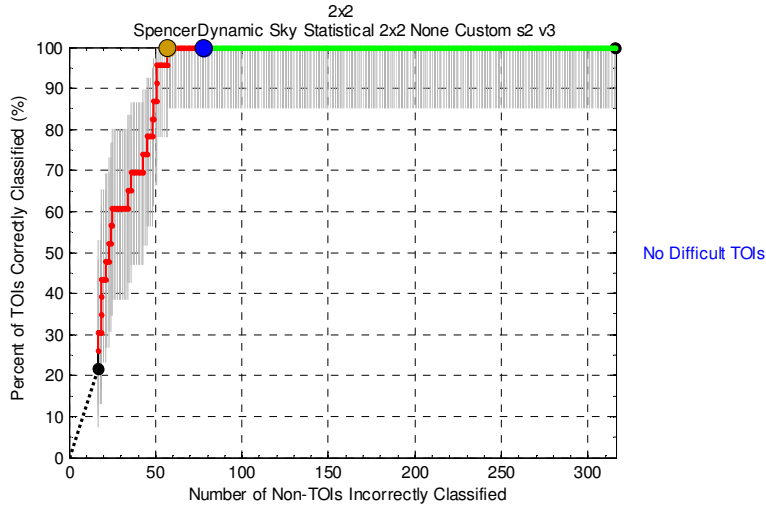
SpencerTrees Sky LibMatching None 2x2 Custom s1 v1

Analyst's Type

	Non-TOI	Small TOI	Medium TOI	Large TOI	Total
Non-TOI	491	31	5	0	527
Small TOI	0	43	1	0	44
Medium TOI	0	0	19	2	21
Large TOI	0	0	0	2	2
Total	491	74	25	4	594

Small TOI: 37 - 52
 Medium TOI: 60 - 81
 Large TOI: 105 - 155

Figure 109: IDA scoring summary for TEMTADS 2x2 data collected in the Treed area



2x2
SpencerDynamic Sky Statistical 2x2 None Custom s2 v3

Analyst's Type (caliber/diameter in mm)

	0	30	37	48	60	61	75	155	Total
0	238	17	41	0	0	0	0	3	299
30	0	0	0	0	0	0	0	0	0
37	0	0	5	0	0	0	1	0	6
48	0	6	0	0	0	0	0	0	6
60	0	1	0	0	0	0	0	0	1
61	0	0	0	0	0	0	1	0	1
75	0	0	0	0	0	0	4	0	4
155	0	0	0	0	0	0	0	0	0
Total	238	24	46	0	0	0	6	3	317

0 = Non-TOI
30 = 30mm
37 = 37mm
48 = Small ISO
60 = 60mm
61 = Medium ISO
75 = 75mm
155 = 155mm

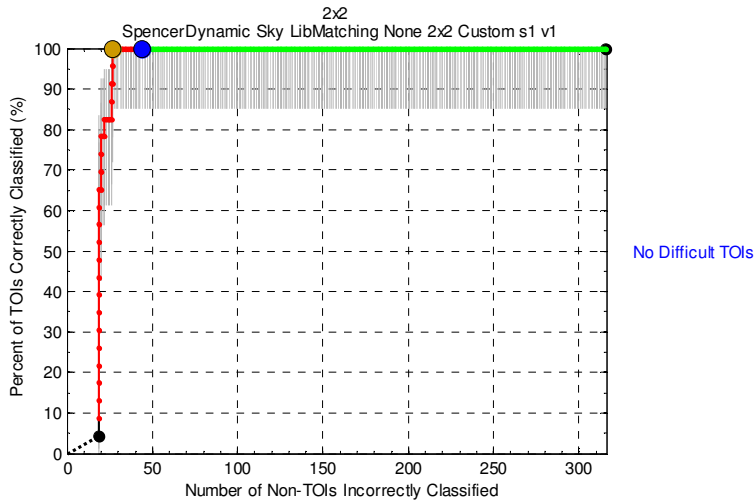
2x2
SpencerDynamic Sky Statistical 2x2 None Custom s2 v3

Analyst's Type

	Non-TOI	Small TOI	Medium TOI	Large TOI	Total
Non-TOI	238	58	0	3	299
Small TOI	0	11	1	0	12
Medium TOI	0	1	5	0	6
Large TOI	0	0	0	0	0
Total	238	70	6	3	317

Small TOI: 20 - 52
Medium TOI: 55 - 89
Large TOI: 105 - 155

Figure 110: IDA scoring summary for TEMTADS 2x2 data collected in dynamic mode in the Dynamic area



2x2
SpencerDynamic Sky LibMatching None 2x2 Custom s1 v1

Analyst's Type (caliber/diameter in mm)

	0	37	45	48	60	61	75	76	81	105	Total
0	272	7	14	0	3	0	0	1	0	0	297
37	0	4	3	0	1	0	0	0	0	0	8
45	0	0	0	0	0	0	0	0	0	0	0
48	0	0	7	0	0	0	0	0	0	0	7
60	0	0	0	0	1	0	0	0	0	0	1
61	0	0	0	0	1	0	0	0	0	0	1
75	0	0	0	0	0	0	3	0	1	0	4
76	0	0	0	0	0	0	0	0	0	0	0
81	0	0	0	0	0	0	0	0	0	0	0
105	0	0	0	0	0	0	0	0	0	1	1
Total	272	11	24	0	6	0	3	1	1	1	319

0 = Non-TOI
37 = 37mm
45 = 45mm
48 = Small ISO
60 = 60mm
61 = Medium ISO
75 = 75mm
76 = 3in
81 = 81mm
105 = 105mm

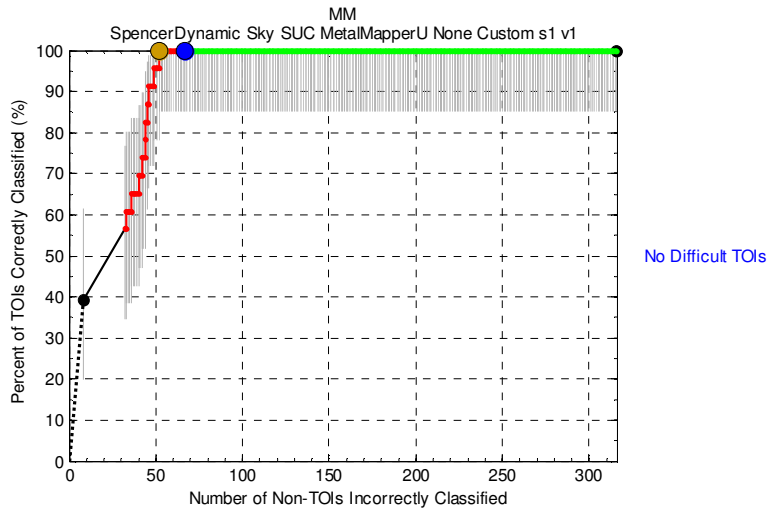
2x2
SpencerDynamic Sky LibMatching None 2x2 Custom s1 v1

Analyst's Type

	Non-TOI	Small TOI	Medium TOI	Large TOI	Total
Non-TOI	272	21	4	0	297
Small TOI	0	14	1	0	15
Medium TOI	0	0	6	0	6
Large TOI	0	0	0	1	1
Total	272	35	11	1	319

Small TOI: 20 - 52
Medium TOI: 55 - 89
Large TOI: 105 - 155

Figure 111: IDA scoring summary for analysis of TEMTADS 2x2 cued data acquired in the Dynamic area



MM
SpencerDynamic Sky SUC MetalMapperU None Custom s1 v1

Analyst's Type (caliber/diameter in mm)

	0	37	40	48	60	65	75	105	Total
0	249	16	6	0	6	1	2	4	284
37	0	2	2	0	0	0	0	0	4
40	0	0	0	0	0	0	0	0	0
48	0	0	5	0	0	0	0	0	5
60	0	0	0	0	0	0	0	0	0
65	0	0	0	0	0	0	0	0	0
75	0	0	0	0	0	2	0	0	2
105	0	0	0	0	0	0	0	0	0
Total	249	18	13	0	6	3	2	4	295

0 = Non-TOI
37 = 37mm
40 = 40mm
48 = Small ISO
60 = 60mm
65 = 65mm
75 = 75mm
105 = 105mm

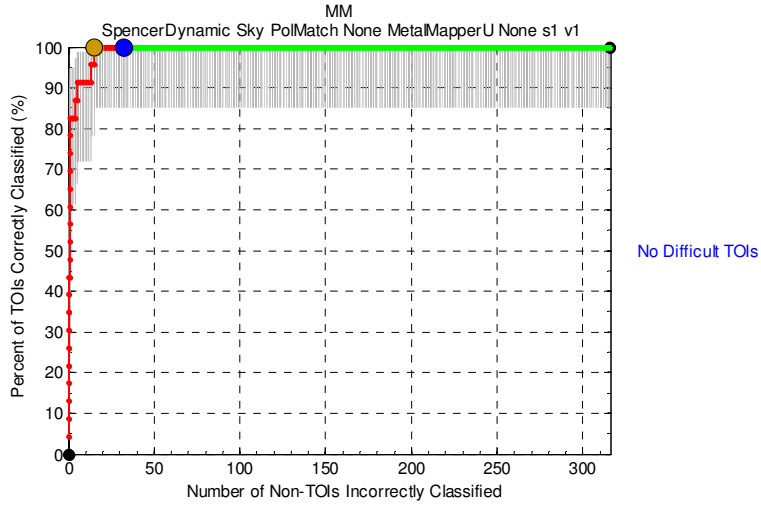
MM
SpencerDynamic Sky SUC MetalMapperU None Custom s1 v1

Analyst's Type

	Non-TOI	Small TOI	Medium TOI	Large TOI	Total
Non-TOI	249	22	9	4	284
Small TOI	0	9	0	0	9
Medium TOI	0	0	2	0	2
Large TOI	0	0	0	0	0
Total	249	31	11	4	295

Small TOI: 20 - 52
Medium TOI: 55 - 89
Large TOI: 105 - 155

Figure 112: IDA scoring summary for MetalMapper (URS) data collected in dynamic mode in the Dynamic area



MM
SpencerDynamic Sky PolMatch None MetaMapperU None s1 v1

Analyst's Type (caliber/diameter in mm)

	0	37	48	52	60	61	65	75	105	Total
0	284	17	0	10	3	0	1	1	0	316
37	0	5	0	1	2	0	0	0	0	8
48	0	0	0	5	3	0	0	0	0	8
52	0	0	0	0	0	0	0	0	0	0
60	0	0	0	0	1	0	0	0	0	1
61	0	0	0	0	0	0	1	0	0	1
65	0	0	0	0	0	0	0	0	0	0
75	0	0	0	0	0	0	1	3	0	4
105	0	0	0	0	0	0	0	0	1	1
Total	284	22	0	16	9	0	3	4	1	339

0 = Non-TOI
37 = 37mm
48 = Small ISO
52 = 52mm
60 = 60mm
61 = Medium ISO
65 = 65mm
75 = 75mm
105 = 105mm

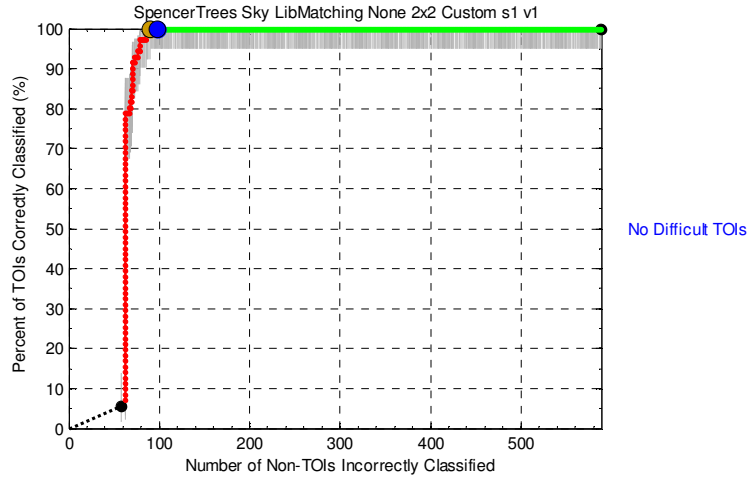
MM
SpencerDynamic Sky PolMatch None MetaMapperU None s1 v1

Analyst's Type

	Non-TOI	Small TOI	Medium TOI	Large TOI	Total
Non-TOI	284	27	5	0	316
Small TOI	0	11	5	0	16
Medium TOI	0	0	6	0	6
Large TOI	0	0	0	1	1
Total	284	38	16	1	339

Small TOI: 20 - 52
Medium TOI: 55 - 89
Large TOI: 105 - 155

Figure 113: IDA scoring summary for MetalMapper (URS) data collected in cued mode in the Dynamic area



SpencerTrees Sky LibMatching None 2x2 Custom s1 v1

Ground Truth (caliber/diameter in mm)	Analyst's Type (caliber/diameter in mm)										Total	
	0	37	45	48	60	61	75	76	81	105		155
0	491	18	13	0	5	0	0	0	0	0	0	527
37	0	21	3	0	0	0	0	0	0	0	0	24
45	0	0	0	0	0	0	0	0	0	0	0	0
48	0	0	19	0	1	0	0	0	0	0	0	20
60	0	0	0	0	4	0	0	0	0	0	0	4
61	0	0	0	0	4	0	0	0	0	0	0	4
75	0	0	0	0	0	0	10	0	1	0	0	11
76	0	0	0	0	0	0	0	0	0	2	0	2
81	0	0	0	0	0	0	0	0	0	0	0	0
105	0	0	0	0	0	0	0	0	0	1	0	1
155	0	0	0	0	0	0	0	0	0	0	1	1
Total	491	39	35	0	14	0	10	0	1	3	1	594

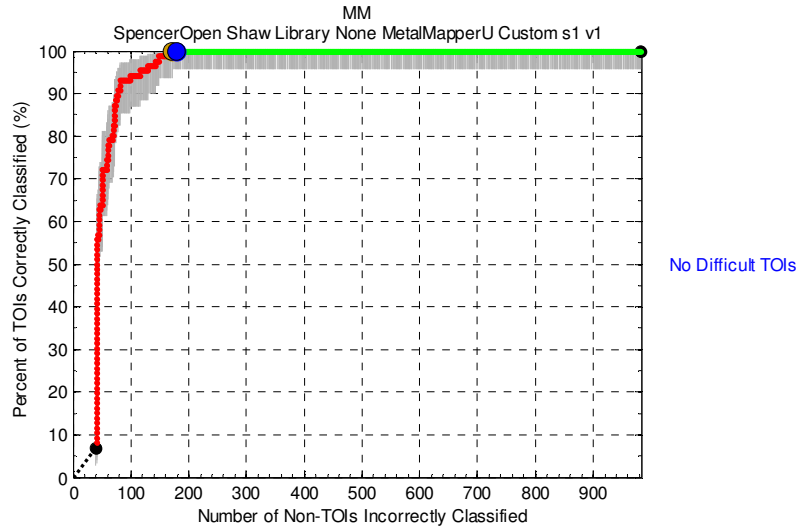
0 = Non-TOI
 37 = 37mm
 45 = 45mm
 48 = Small ISO
 60 = 60mm
 61 = Medium ISO
 75 = 75mm
 76 = 3in
 81 = 81mm
 105 = 105mm
 155 = 155mm

SpencerTrees Sky LibMatching None 2x2 Custom s1 v1

Ground Truth	Analyst's Type				Total
	Non-TOI	Small TOI	Medium TOI	Large TOI	
Non-TOI	491	31	5	0	527
Small TOI	0	43	1	0	44
Medium TOI	0	0	19	2	21
Large TOI	0	0	0	2	2
Total	491	74	25	4	594

Small TOI: 37 - 52
 Medium TOI: 60 - 81
 Large TOI: 105 - 155

Figure 114: IDA scoring summary for the TETMADS 2x2 cued data acquired in the Treed area



MM
SpencerOpen Shaw Library None MetalMapperU Custom s1 v1

Analyst's Type (caliber/diameter in mm)

	0	37	48	52	60	61	75	105	155	Total
0	805	10	0	81	31	0	15	0	0	942
37	0	19	0	7	1	0	0	0	0	27
48	0	0	0	25	3	0	0	0	0	28
52	0	0	0	0	0	0	0	0	0	0
60	0	1	0	0	3	0	0	0	0	4
61	0	0	0	0	4	0	0	0	0	4
75	0	0	0	0	2	0	13	0	0	15
105	0	0	0	0	0	0	1	0	0	1
155	0	0	0	0	0	0	1	0	0	1
Total	805	30	0	113	44	0	30	0	0	1022

0 = Non-TOI
37 = 37mm
48 = Small ISO
52 = 52mm
60 = 60mm
61 = Medium ISO
75 = 75mm
105 = 105mm
155 = 155mm

MM
SpencerOpen Shaw Library None MetalMapperU Custom s1 v1

Analyst's Type

	Non-TOI	Small TOI	Medium TOI	Large TOI	Total
Non-TOI	805	91	46	0	942
Small TOI	0	51	4	0	55
Medium TOI	0	1	22	0	23
Large TOI	0	0	2	0	2
Total	805	143	74	0	1022

Small TOI: 20 - 53
Medium TOI: 55 - 89
Large TOI: 102 - 155

Figure 115: IDA scoring summary for the MetalMapper (URS) cued data acquired in the Open area. This summary is based on analysis performed by Shaw geophysicists with UXOLab.

Appendix I: Technology Transfer

Applying Dipole-Based Advanced Discrimination

Spencer Range Demonstration Site, 2011

Shaw Environmental

The objective of the project was to transition mature data analysis and evaluation techniques and specialized knowledge base regarding dipole-based advanced discrimination from Sky Research (Sky) to Shaw's production team through a one week training session with Sky's technology developers in Vancouver, Canada.

The geophysical datasets used for the training consisted of dynamic EM61-MK2 measurements with integrated GPS and static MetalMapper records for 1104 anomalies at the Spencer Range Mountain Demonstration Site located in TN.

Sky provided background information and general training on their UXO Lab software routines and data inversion and classification techniques. Shaw used the UXO Lab software routines and Sky information presented during training to analyze 1104 anomalies and output a diglist of suspected target off interest (TOI).

Initial Data Screening and QC

MetalMapper records for 1104 locations were imported into UXOLab and an inversion was performed to generate information on the x-y-z location and polarizabilities for each record. Both single and multi-target models were fitted during the inversion process and these data were subsequently analyzed using the *QC Tool Flex* routine in UXOLab. The initial evaluation allowed the analyst to review MetalMapper polarizability profiles for each record in conjunction with the amplitude and spatial attributes of each EM61-MK2 anomaly, inversion model fit statistics (signal to noise ratios, general model uncertainty, uncertainty of recovered polarizability, color-coded images of the polarizabilities for all 9 transmitter-receiver combinations) and predicted depth for each model fit. Of particular importance were the polarizability curves from the TOI from the library reference items that were superimposed on polarizability profile of each MetalMapper record, which allowed a direct comparison of the similarity of the polarizabilities. A decay-size feature plot was also useful for evaluating the current model's attributes compared to the entire dataset and library of reference items.

Each model and inversion result was passed or failed by the data analyst. Additionally, notes regarding whether the anomaly was a suspected TOI for the project based on the library of reference items or an elongated, UXO-like object were made in order to facilitate final ranking during diglist development.

Data Analysis and Selection of Training Data

The models passed by the analyst from the inversion process were displayed on a feature plot with the decay on the y-axis and relative size on the x-axis along with the library reference items (37 mm, Shot put, 75mm, and small ISO). Anomalies that clustered close to the library reference items were evaluated further in terms of the similarity of their polarizabilities to those of the known TOI. During the analysis and evaluation process, other clusters (or populations) of anomalies were identified, some of which exhibited UXO-like polarizabilities, signal amplitude, and decay properties upon examination. Examples are 1) one large cluster with “subclusters” of smaller relative sizes than library reference items, variable decay rates, and UXO-like polarizabilities, 2) relative size larger than a small ISO and smaller than a 57mm with UXO-like polarizabilities and decay properties, and 3) non-clustered but having interesting combinations of polarizability, decay, or relative size characteristics. Shaw utilized these populations to select training data using Sky’s *QC Training* module.

A total of 46 anomalies were selected for training. The first round of training data included 36 anomalies. The results included the identification of a medium ISO, three 37mm projectiles, one 60mm mortar, and one 75mm projectile. A second request for training data included 10 anomalies which resulted in the identification of two 0.50 caliber projectiles. The non-TOI items selected as part of the training process resulted in elongated, UXO-like items that were either MD, CD, and three anomalies were labeled as ‘No Contact’. The medium ISO, the 60mm mortar and the 0.5 caliber projectiles were not included in the reference library for the Spencer demonstration.

During this phase of the project the 60mm mortar and medium ISO polarizability information were added to the UXOLab TOI library for use in the automated development of the final diglist.

Initial Diglist Development

Initial diglist development was accomplished using the Sky *Digzilla* tool, which is designed to automate the prioritization of the diglist. Using this tool, the analyst is able to interactively prioritize anomalies using various parameters such as polarizability misfit and quality, decay, relative size, analyst notes (e.g., “UXO-like”) and other related attributes. Shaw used the minimum polarizability misfit compared to the library of reference items and analyst notes (e.g., “UXO-like”) as the primary attributes to refine the initial diglist.

The prioritized diglist output from *Digzilla* was reported in MatLab and transferred into an Excel spreadsheet for final prioritization.

“Stop Dig” Point Selection and Final Diglist Prioritization

This project required that anomalies on the diglist be categorized as “likely UXO”, “can’t decide”, “likely clutter” or “can’t extract reliable parameters”. Since the overall data quality was

considered to be very good with regards to the inversion results for the field data and library of reference items, Shaw classified all of the anomalies on the diglist as either “likely UXO” or “likely clutter”. Each anomaly was then marked as “dig” or “no dig”.

The *QC Training* tool was employed to automate the selection of the “stop dig” point by defining the confidence level, the anomalies selected as “dig” and the total number of anomalies. Shaw used the number of anomalies specified by the *QC Training* tool as a guide and manually reviewed the anomalies surrounding the recommended stop dig point with the *QC Flex tool*. This procedure was performed to ensure the classification was optimized for each anomaly based primarily on the polarizabilities, decay, depth, and relative size.

A portion of the anomalies reviewed were characterized by inversion results that had one or more parameter estimates thought to be unrealistic for the specified model (e.g., large depth estimate, predicted location at edge of search window, or relatively noisy polarizability curves). Because the data analyst was uncertain and wanted to err on the side of conservatism, some of these anomalies were reclassified as “likely clutter”, “dig”. Based on the results sent to SERDP, no TOIs were present in the additional selections and no new information was gained and it was decided to stop “digging”.

The attached ROC exhibits the overall results of the dig selection process.

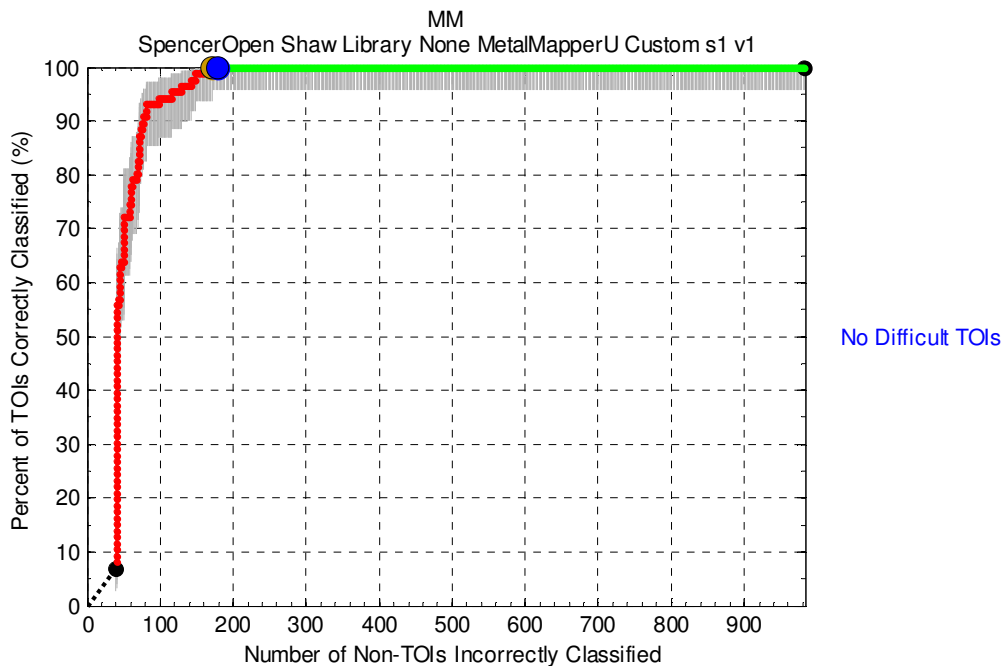


Figure 116: ROC curve for Shaw processing of MetalMapper (URS) cued data in the Open area.

Summary

Shaw geophysicists were trained in the use of Sky's discrimination and classification methods using several UXOLab modules (*QCFlex*, *QCTraining*, and diglist prioritization using *Digzilla*).

Of the 46 targets selected as training data 6 were TOI, including a medium ISO and a 60mm mortar that were not present in the original library of reference items.

Initially, 226 of the 1104 anomalies were selected for investigation. The information attained from the training data and *QC Training* module resulted in an additional 46 selections for a total of 272 anomalies to investigate (20% of the total number of anomalies).

All 87 UXO (excluding training data) and ISOs were identified with the 272 anomaly selections.

Very few non-TOI are present amongst the high priority anomalies. The frequency of non-TOI increases with decreasing rank on the diglist.

Appendix J: Points of Contact

POINT OF CONTACT	ORGANIZATION	Phone E-mail	Role in Project
Leonard Pasion	Black Tusk Geophysic Inc, #401, 1755 W Broadway Vancouver, BC, V6J 4S5	604 428 3380 leonard.pasion@btgeophysics.com	Principal Investigator (PI)
Kevin Kingdon	Black Tusk Geophysics Inc, #401, 1755 W Broadway Vancouver, BC, V6J 4S5	604 428 3382 kevin.kingdon@btgeophysics.com	Project management and personnel coordination
Barry Zelt	Black Tusk Geophysics Inc, #401, 1755 W Broadway Vancouver, BC, V6J 4S5	604 428 3382 barry.zelt@btgeophysics.com	Data analyst and UXOLab programming
Stephen Billings	Black Tusk Geophysics Inc, 131 Ernest Street, Manly, QLD, 4179, Australia	+1 720 306 1165 stephen.billings @btgeophysics.com	Data analyst
Laurens Beran	Black Tusk Geophysics Inc, #401, 1755 W Broadway Vancouver, BC, V6J 4S5	604 428 3382 laurens.beran@btgeophysics.com	Data analyst, classification theory